Investigation of Metal-Catalyzed Epoxide Polymerisation and Phosphanyl Transition-Metal Complexes by Electron Paramagnetic Resonance

Dissertation

zur

Erlangung des Doktorgrades (Dr. rer. Nat.)

der

Mathematisch-Naturwissenschaftlichen Fakultät

der

Rheinischen Friedrich-Wilhelms-Universität Bonn

vorgelegt von

Asli Cangönül

aus

Malatya (Türkei)

Bonn 2012

Angefertigt mit Genehmigung der Mathematisch-Naturwissenschaftlichen Fakültät
der Rheinischen Friedrich-Wilhelms-Universität Bonn

1. Gutachter: Prof. Dr. Andreas Gansäuer

2. Gutachter: PD. Dr. Maurice van Gastel

Tag der Promotion: 25. 02. 2013

Erscheinungsjahr: 2013

Abstract

The first part of this thesis is concerned with the reaction mechanism of activation of H_2O by titanocene(III) chloride. Two important aspects of $Cp_2TiCl(H_2O)$ complexes are investigated: (1) does the oxygen from water directly bind to titanium? and (2) is there a hydrogen bond between water and chloride?

Experimental and computational studies have been carried out to describe the correct structures and revised mechanism of water binding. In the computational study, calculations of the bond dissociation energies for each molecules and the complexation of $Cp_2TiCl(H_2O)$ with THF and without THF are performed. In the experimental study, the EPR and CV measurements provide direct evidence for the cationic species as elucidated from the magnetic properties of the Ti center. The calculations are in a good agreement with the experimental observations.

The second part of the thesis concentrates on the reaction mechanism of reductive epoxide opening. This part is composed of two sections that deal with the binding of epoxide to titanocene(III) chloride with and without spin trapping. During epoxide ring opening, the spin trapping method has been carried out to detect the presence of a carbon radical.

The calculations on the formation of the Cp_2TiCl-epoxide show that, in the presence of chloride, epoxide does not coordinate to titanium. In agreement with the calculations, the EPR spectra of this complex reveal rhombic symmetry and show dissociation of chloride ligand.

With respect to the spin trapping experiments, DFT studies of Cp_2TiCl(DMPO)-Epoxide indicate that the epoxide opens reductively upon the binding to Ti(III). Further EPR measurements show a signal coming from a DMPO radical.

The third part of the thesis focuses on the characterization of the paramagnetic Ti species in terms of electronic, structural, chemical and magnetic features. A novel concept for catalytic radical 4-*exo* cyclizations is studied, which does not require the assistance of the *gem*-dialkyl effect. The computational study shows that the formation of the corresponding *cis*-products is thermodynamically unfavorable and hence their ring opening is too fast to allow the pivotal radical reduction.

The last part of the thesis concerns the oxidation of a Li/X ($X = Cl^-, F^-$) phosphinidenoid complex. To obtain insight into the mechanistic aspects of this oxidation reaction, the reactivity of a Li/X phosphinidenoid complex is investigated by using the two tritylium salts $[Ph_3C]BF_4$ and $[(p\text{-Tol})_3C]BF_4$. The EPR investigations of this reaction show that the unpaired electron occupies a pure 3p orbital at P without admixture of the 3s orbital.

Zusammenfassung

Der erste Teil der vorliegenden Arbeit beschäftigt sich mit dem Reaktionsmechanismus der Aktivierung von H_2O mit Titanocen(III)chlorid und konzentriert sich hierbei auf zwei wichtige Aspekte des $Cp_2TiCl(H_2O)$ Komplexes. (1) Bindet der Sauerstoff des Wasserliganden direkt an das Titanzentrum? (2) Kommt es zur Ausbildung von Wasserstoffbrücken zwischen Wasser und Chlorid im Titanocen Komplex?

Hierzu wurden experimentelle und theoretische Studien durchgeführt, um korrekte Strukturvorschläge zu machen und den Mechanismus neu vorherzusagen. In der computerchemischen Studie wurden Berechnungen zu Bindungsdissoziationsenergien der verschiedenen Moleküle und die Komplexierung von $Cp_2TiCl(H_2O)$ mit THF und ohne THF durchgeführt. Die experimentellen EPR spektroskopischen und elektrochemischen (CV) Messungen liefern einen direkten Beweis für die Beteiligung einer kationischen Spezies, wie aus den magnetischen Eigenschaften des Ti Zentrums hervorgeht. Die theoretischen Ergebnisse stimmen gut mit den entsprechenden experimentellen Daten überein.

Der zweite Teil der Arbeit konzentriert sich auf den Reaktionsmechanismus der reduktiven Epoxidöffnung. Dieser Teil besteht aus zwei Abschnitten, die sich mit der Bindung des Epoxids an Titanocen(III)chlorid befassen, wobei die Experimente hier sowohl mit oder ohne Spin-trapping durchgeführt wurden. Während der Epoxidringöffnung muss das Spin-trapping Verfahren angewandte werden, um das Vorhandensein eines radiklischen Kohlenstoffzentrums nachweisen zu können.

Berechnungen zum weiteren Verlauf der Reaktion zeigen, dass die Bildung von Cp_2TiCl-Epoxid Komplexen die Dissoziation von Chlorid bedingt. Sofern ein Chloridligand an den Titanocen komplex koordiniert, kann das Epoxid nicht an das Titan atom binden. In Übereinstimmung mit den Berechnungen zeigen die EPR-spektroskopischen Ergebnisse eine rhombische Symmetrie der Komplexe und die Dissoziation von Chlorid.

In Bezug auf die Spin-trapping-Experimente zeigen die DFT Studien der Cp_2TiCl(DMPO)-Epoxid Komplexe, dass das Epoxid reduktiv geöffnet wird sobald Koordination an das Titan(III) Ion erfolgt. Weitere EPR Messungen zeigen ein eindeutiges Signal, welches einem DMPO Radikal zugeordnet werden kann.

Der dritte Teil fokussiert sich auf die Charakterisierung von paramagnetischen Ti-Spezies in welches keine Hilfe des *gem*-dialkyl Effekts erfordert. Die theoretische Studie zeigt, dass die Bildung des entsprechenden *cis*-Intermediates thermodynamisch ungünstig ist und damit seine Ringöffnung zu schnell verläuft, um die entscheidenden radikale Reduktion zu ermöglichen.

Der letzte Teil der Arbeit befasst sich mit der Oxidation von Li/X ($X = Cl^-, F^-$) Phosphinidenoid Komplexen. Um einen Einblick in die mechanistischen Aspekte der Oxidationsreaktion zu erhalten, wurde die Reaktivität der Li/X Phosphinidenoid Komplexe bezüglich der beiden Tritylium Salze $[Ph_3C]BF_4$ und $[(p\text{-}Tol)_3C]BF_4$ untersucht. Die EPR-spektroskopische Analyse dieser Reaktionen zeigen, dass das ungepaarte Elektron ein reines 3p-Orbital am P Atom ohne Beimischung der 3s-Orbital besetzt.

LIST OF PUBLICATIONS

PUBLICATIONS RELATED TO THE THESIS

- **Chapter 4**

A. Gansäuer, A. Cangönül, M. Behlendorf, C. Kube, J. M. Cuerva, J. Friedrich and M. van Gastel. H_2O-Activation for HAT: Correct Structures and Revised Mechanism. *Angew. Chem. Int. Ed.* 2012, 51, 3266-3270.

In this work synthetic, electrochemical, experimental (a variety of EPR techniques), and computational approaches were combined to study the reaction mechanism of activation of water by titanocene(III) chloride. I was involved with the development and implementation of the EPR methodology used in this work.

- **Chapter 5**

A. Cangönül, M. Behlendorf, A. Gansäuer, and M. van Gastel. Trapping Radicals in Reductive Epoxide Opening. (To be submitted)

In this work the reaction mechanism of the reductive epoxide opening was studied in a combined experimental (a variety of EPR techniques) and computational (DFT calculations of the EPR parameters and the spin density) approach. I carried out the entire study.

- **Chapter 6**

A. Gansäuer, K. Knebel, C. Kube, A. Cangönül, M. van Gastel, K. Daasbjerg, T. Hangele, M. Hülsen, M. Dolg, and J. Friedrich. Radical 4-*exo* Cyclizations via Template Catalysis. *Chem. Eur. J.* 2012, 18, 2591-2599.

In this work a novel concept for catalytic radical 4-*exo* cyclizations was studied, which does not require the assistance of the *gem*-dialkyl effect. A combined synthetic, electrochemical, spectroscopic, and computational approach was used. My contribution to this project was the entire spectroscopic study.

- **Chapter 7**

V. Nesterov, A. Özbolat-Schön, G. Schnakenburg, L. Shi, A. Cangönül, M. van Gastel, F. Neese, and R. Streubel. An Unusual Case of Facile Non-Degenerate P-C Bond Making and Breaking. *Chem. Asian J.* 2012, 7, 1708-1712.

In this work the oxidation of Li/X phosphinidenoid complex was studied with a combined synthetic, experimental (a variety of EPR techniques), and computational approach. My

contribution to this work was the implementation and analysis of the EPR experiments and the calculation of the spin density of investigated molecule, which was used to perform the DFT calculations.

Acknowledgements

I would like to thank everyone who contributed to my PhD thesis over the last years. There are various academics who helped me during my PhD and from whom I had the opportunity to learn a lot.

First and foremost, I would like to present my deep gratitude to my supervisor PD Dr. Maurice van Gastel, who introduced me with patience into the fields of EPR and theoretical chemistry and who taught me his perspective on many topics related to EPR investigations and beyond. I am very grateful for his warm support, thoughtful guidance and encouragement to perform different techniques and to present our activities on numerous conferences, workshops and seminars.

I wish to thank to all EPR group members, especially Gudrun Klihm and Dr. Edward J. Reijerse for helping me with technical problems.

I would like to thank all who collaborated in this study

- Prof. Dr. Andreas Gansäuer and Maike Behlendorf for the preparing of the sample and fruitful discussions.
- Prof. Dr. Reiner Streubel, Carolin Albrecht, J.M. Perez and Vitaly Nesterov for the preparing of the sample and discussions.

Many other People in the institute in Bonn and in Max Planck Institute for chemical energy conversion contributed to a pleasant atmosphere over the last years. I thank to Mrs. Christina Reuter who helped me for all the administration and official jobs. The support by mechanical, the electronically and the glassblower works is kindly acknowledged.

A very special thanks to Itana Krivokapic for critically reading and correcting several parts of my thesis.

My warm thanks go to friends who supported me during that time. Yüsra, Tuba and Aysegül, it was a lot of fun and an unforgettable days in Eifel.

I am most grateful to my parents and my brother for everything that they have done for me. They supported me through my entire life.

My special thanks go to my dear friend Fatma and her family for being kind, helpful everytime and for contributing a pleasant living environment in Cologne. Without their helping, support and encouragement, this work would not have been completed.

Finally I want to thank the SFB 813 and the University of Bonn for financial support.

Contents

List of Tables

List of Schemes

List of Figures

Abbreviations

2D	Two-Dimension
AIBN	Azobisisobutyronitril
BDE	Bond Dissociation Energy
Coll	Collidine
COSMO	Conductor like Screening Model
cp	cyclopentadienyl anion
CV	Cyclic Voltammetry
cw	Continuous Wave
DFT	Density Functional Theory
DMPO	5,5-dimethyl-1-pyrroline-N-oxide
dr	diastereomeric ratio
DT	Degenerate Transfer
ee	enantiomeric excess
ENDOR	Electron Nuclear Double Resonance
EPR	Electron Paramagnetic Resonance
ESE	Electron Spin Echo
ESEEM	Electron Spin Echo Envelope Modulation
FID	Free Induction Decay
FS	Field Swept
FT	Fourier Transformed
HAT	Hydrogen Atom Transfer
HMPA	Hexamethylphosphoramid
HOMO	Highest Occupied Molecular Orbital
HTA	High Tuning Angle

HYSCORE	Hyperfine Sublevel Correlation
IR	Infrared spectrum
LDA	Lithiumdiisopropylamid
LUMO	Lowest Unoccupied Molecular Orbital
MAO	Methlyaluminoxane
Me	Methyl
MeOH	Methanol
MW	Microwave
NMR	Nuclear Magnetic Resonance
NQR	Nuclear Quadrupole Frequency
PAS	Principal Axis System
PBN	N-*tert*-butyl-α-phenylnitrone
POBN	α-(4-Pyridyl-1-oxide)-N-*tert*-butylnitrone
RF	Radio Frequency
RRO	Radical Ring Opening
RT	Room Temperature
SET	Single Electron Transfer
SMART	Single Pulse Matched Resonance Transfer
SOC	Spin Orbit Coupling
SOMO	Singly Occupied Molecular Orbital
TBP	2,2´-thiobis(6-*tert*-butyl-4-methylphenol)
tert.	tertiary
THF	Tetrahydrofuran
Tol	Toluol
trityl*	tris(*p* methylphenyl)methyl
TWT	Travelling Wave Tube
ZFS	Zero Field Splitting

ZORA	Zeroth Order Regular Approximation
ZPE	Zero Point Energy
ZPVE	Zero Point Vibrational Energy

1 Introduction

1.1 Organic Synthesis in Chemistry

In synthetic chemistry, the synthesis of substances should ideally be safe and environmentally friendly. It is also advantageous to optimize the synthesis with respect to energy consumption and costs through the use of efficient procedures. Preferably, selective reactions are performed, for which knowledge of the chemistry of the educts is required. Furthermore, the use of protecting groups should be avoided, if possible. In the context of this concept, the requirements for an ideal synthesis were described in 1989 by *E.J. Corey*.[1] *Corey* also described the requirements for an ideal asymmetric synthesis, which is presently commonly used in modern organic synthesis. An asymmetric synthesis is a reaction in which a chiral moiety is generated from a prochiral center such that the asymmetric products, either enantiomers or diastereomers, are formed in different amounts. Ideally, only one isomer is formed.[2]

In pharmacology, asymmetric synthesis should be optimized to produce active isomers analogous to the natural products. The natural products have clearly defined stereo-centers, and it was recognized early that the isomers are different in their reactivity.[3] Zopiclone, a pharmaceutical substance that is used to treat insomnia, is an example. The (S)-enantiomer, which is known as eszopiclon (Figure 1.1) has a higher binding affinity to specific benzodiazepine receptors in the human brain than the (R)-enantiomer.

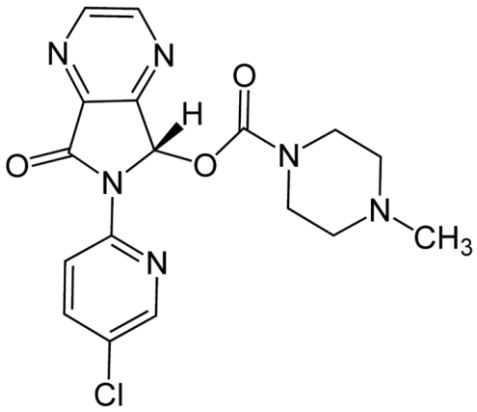

Figure 1.1. Eszopiclon.

Stereo centers also play a role in sensory impressions such as smell. As a result, there is presently a great deal of interest in stereoselective synthesis for aromatic substances. The growing demand for stereoselective methods makes it essential to improve upon existing synthesis methods and to develop and establish new processes.

Over the past three decades, the knowledge of stereoselectivity has improved tremendously. New reactions have been especially established in radical chemistry and catalysis. The range of reactions extends up to highly selective catalytic processes with transition metals. In addition to the application of these methods, the continued development of known reactions and methods is a focal point of researchers.

1.2 Epoxides

Among all substances used as educts in organic and synthetic chemistry, epoxides are one of the most commonly used substrates. This is because of their high reactivity and their ease of preparation from available precursors such as olefins or carbonyl compounds. Many natural substances possess epoxide units, which play a decisive role for their specific biological activity. Examples are triptolide, epothilones and cryptophycin (Figure 1.2a). These molecules are key intermediates in the biosynthesis of many natural products such as brevetoxin-B, monensin and glabrescol (Figure 1.2b).

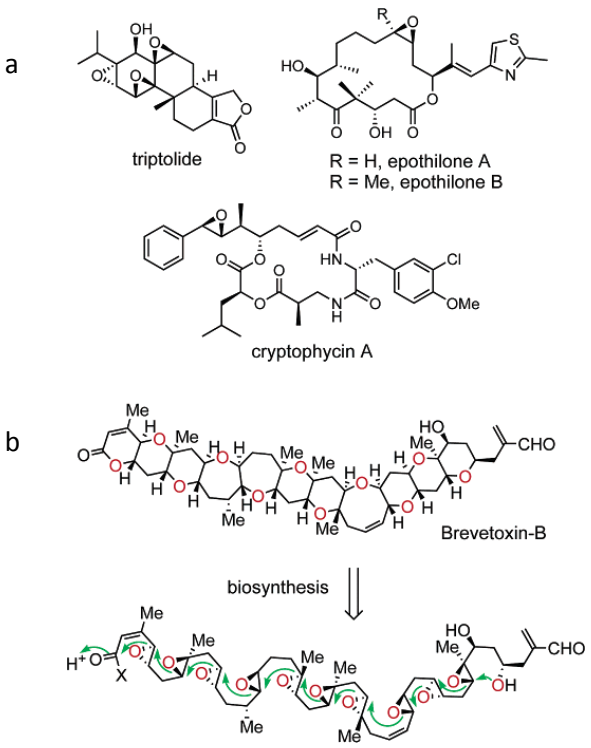

Figure 1.2. Examples of natural products containing epoxide units.[4]

The opening of epoxides, which is based on titanocene(III)-promoted epoxide deoxygenation, has been used in the synthesis of a wide array of natural products. Methods for synthesizing complex natural products require selectivity, mild experimental conditions and wide functional group tolerance. Because the requirement of this condition can be provided by titanocene(III) complexes, the method has been used in the synthesis of about natural products and advanced synthons. *Cuerva J. M., Oltra J. E.*[5,6] and coworkers have demonstrated that titanocene(III)-catalyzed radical cascade cyclizations has been used successfully in the synthesis of terpenoids. Another example is the work of *Roy et al.*,[7,8] which has been intensively exploited for the total synthesis of antibiotic butyrolactones, and the works of *Ziegler* and *Sarpong*,[9] who used a titanocene-promoted cyclization for the synthesis of a protected carbocyclic core of BMS200475 (entecavir), a nucleoside active at the nanomolar level against the hepatitis B virus. Consequently, in these fields the method has already largely proved its synthetic usefulness. This titanocene(III)-based transformation is exhaustively explained in chapter 1.2.

The origin of the high reactivity of epoxides is based on the inherent strain of approximately 27 kcal/mol in the three-membered ring, which provides a sufficient driving force for the ring opening event. Their facile nucleophilic ring opening has been very useful in S_N2 reactions, which conserve the configuration at the reacted carbon atoms. Among the most useful of the epoxide openings in S_N2 reactions are the transition-metal-catalyzed desymmetrizations of *meso*-epoxides and the production of monosubstituted and 1,1-disubstituted epoxides.[10-13] Thus, a broad range of 1,2-difunctionalized compounds have been obtained with high enantio- and stereo-selectivity, both of which possess two contiguous chiral centers. In this respect, epoxides, especially when prepared in enantiomeric excess, have furnished a number of highly useful procedures.

Probably the first asymmetric epoxidation using a synthetic catalyst was achieved by *Katsuki* and *Scharpless*[14] in 1980, for which Barry Scharpless was awarded the 2001 Nobel Prize for his work in the field of asymmetric epoxidation. His awarded study has been expanded greatly for the preparation of pharmaceutical products such as antibiotics, anti-inflammatory drugs and other medicines. In 1990, *Jacobsen* and *Katsuki*[15,16] discovered a system for catalytic asymmetric epoxidation that contains unfunctionalized alkenes by using manganese salen complexes.

However, in spite of the successful applications, there are also limitations to this approach.[17,18] Enantioselectivity is controlled by some of alkene classes via the available epoxidation procedure. Interestingly, achiral meso-epoxides (symmetric) give rise to chiral ring opening, which these protocols do not perform. In order to synthesize the enantiomeric ring-opened products, a conceptually different approach has been developed. This approach is not based on enantioselective epoxides. (Scheme 1.1)

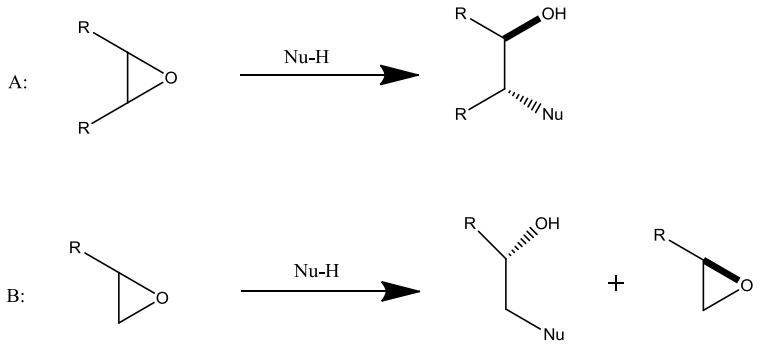

Scheme 1.1. Enantioselective ring-opening of a meso-epoxide (A) and racemic epoxide (B).

An alternative approach to exploit the high reactivity of the strained epoxide is constituted by ring opening reactions through electron transfer from low-valent metal complexes. The general idea of this concept was achieved by *Nugent* and *RajanBabu* in 1988-1994.[19-22] In this scenario, a suitable chiral catalyst is used, typically a chiral Lewis acid that coordinates to the oxygen and activates the epoxide toward electron transfer by complexation with the metal and its ligands. Titanocenes have emerged as the most powerful compounds in these transformations, which reductively open the epoxide either with or without deoxygenation. This is achieved by epoxide binding to the titanocene followed by cleavage of the C-O bond through a homolytic substitution reaction and overcoming the activation energy of the latter process.[23] Even the oxygen rebound step, a homolytic substitution reaction has been also discussed for the hydroxylation reaction of hydrocarbons either by

organometallic complexes or by enyzmes as such the P450 enzymes.[24] The mechanistic aspect is shown in Scheme 1.2, which includes a ring opening, ring closure and hydroxylation reaction.

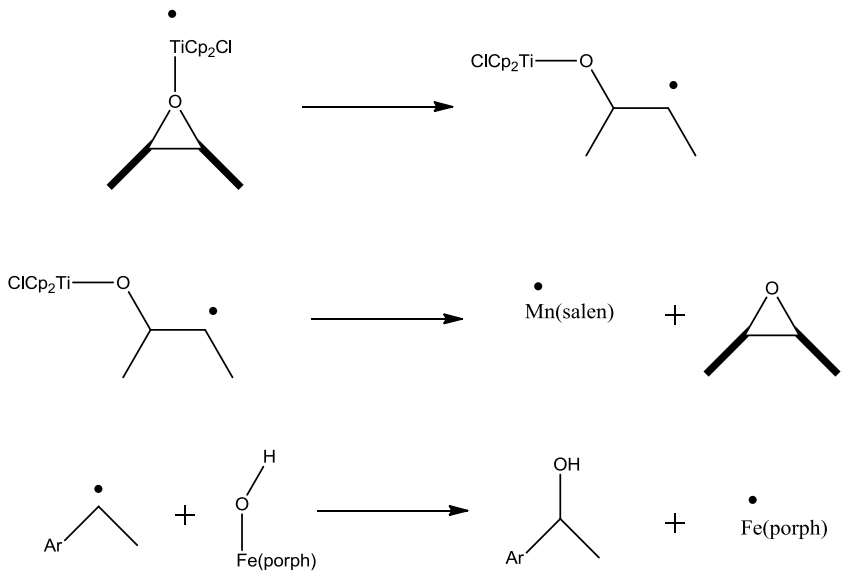

Scheme 1.2. Reaction featuring a homolytic substitution reaction with a metal oxygen bond.

1.2.1 Examples of Epoxide Ring Opening Reactions

Probably the first example of epoxide opening via electron transfer was reported in 1950. *Brown* and coworkers reported that the various labile norbornyl epoxides would be reduced by using lithium-ethylamine to corresponding alcohols.[25] This reaction was processed under strongly protic Birch conditions, in which norbornanol (**4**) was generated from norbornene oxide (**1**) in 87 % yield (Figure 1.3).

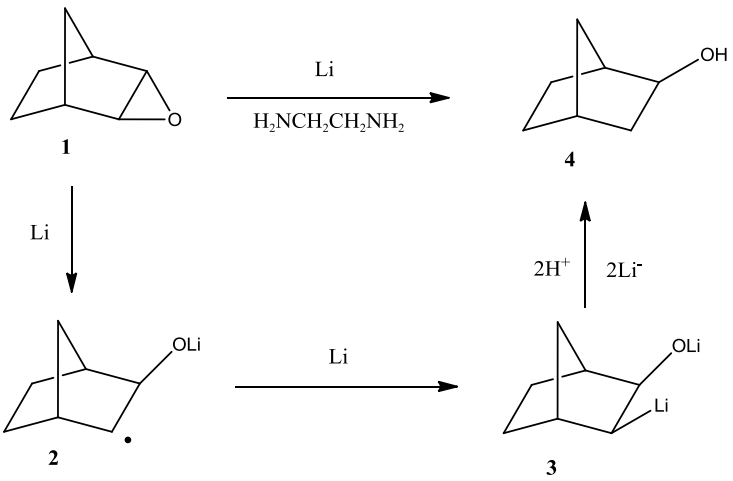

Figure 1.3. The reduction of narbornene oxide by Brown.

In this reaction, first the α-metal-oxy radical (**2**) is formed by an electron the transfer to epoxide. This radical is converted in a subsequent step by a second reduction into corresponding organolithium compound (**3**). Finally, the abstraction of lithium-carbon and lithium-oxygen bonds results in alcohols (**4**). Additionally, the protic birch conditions ensure that no organolithium compound is formed, which interferes with other electrophiles in the intermediate stage.[26,27] However, the calcium reagent can be also reduced epoxide to alcohols in etylenamine in higher yields, which is the possibility of choosing large-scale reductions of epoxides.[28]

In this respect, an important reaction was discovered by *Bartmann*[29] in 1986. He demonstrated that epoxides could be opened by aromatic radical anions such as biphenyl at low temperature via electron transfer under aprotic Birch conditions (Figure 1.4).

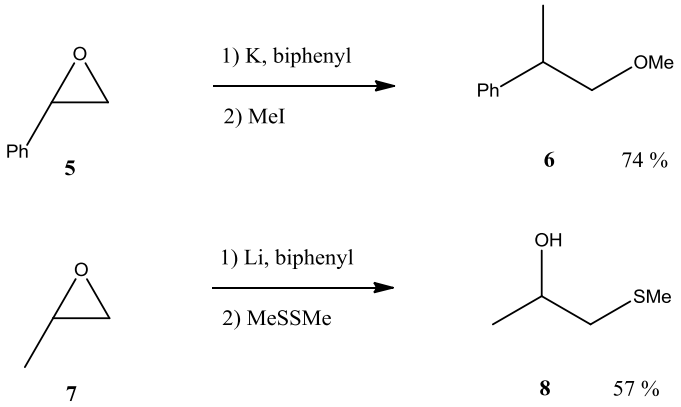

Figure 1.4. Epoxide opening with aromatic radical anions by Bartmann.

The regioselectivity of ring opening depends on the substituents of the oxirane. If the substituent is a phenyl or an ester group (**5**), the neighboring carbon-carbon bond is only cleaved and includes enalotes and benzylic organometallic compounds (**6**). But if the substituent is an alkyl group (**7**), the more distant carbon-oxygen will be cleaved, which lead to the less-substituted organolithium compounds (**8**). The intermediate β-lithioalkoxides can be successfully trapped at a low temperature (-90 °C) by using very reactive electrophiles, for example, H_2O, D_2O, CO_2, MeI or disulfides.[30]

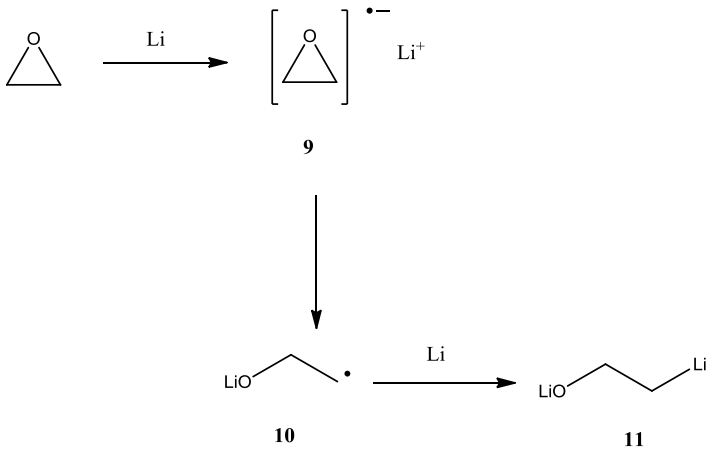

Figure 1.5. Calculation of epoxide opening by Cohen and Houk.

The mechanism of this oxirane opening has been explored by *Cohen* and *Houk*. (Figure 1.5) The comprehensive calculations show that the lithiated radical anion (**9**) is a decisive intermediate. This study also predicted that the intermediate opening of epoxide was exothermic (-100 kJ/mol) and that radical (**10**) was obtained, which was further reduced to (**11**). [31]

Two years later, *Bartmann*, *Nugent* and *Rajanbabu* introduced a new concept, in which the titanocene(III) chloride can be used as a stoichiometric reagent for the reductive opening of epoxide with or without deoxygenation. Their hypothesis is based on a σ-complex of epoxide with a transition metal, which possesses a half-filled d-orbital. The carbon-centered β-metaloxyradical is formed after the carbon-oxygen bond is cleaved. Their study has striking an analogy to the cyclopropylmethyl radical for which the opening of the epoxide proceeds through electron transfer[19-21] (See Figure 1.6).

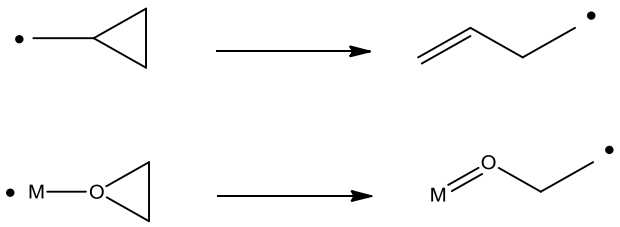

Figure 1.6. Opening of cyclopropylmethyl radical with the strategy of Nugent and Rajanbabu.

These unprecedented features of epoxide make them attractive reactants for radical chemistry.

1.3 Radicals in Organic Chemistry

Free radicals are paramagnetic reactive intermediates of considerable importance in the organic chemistry.[32,33] A detailed picture of the reactivity, selectivity and stability of many types of organic radical has emerged[34-36] and free radical reactions in organic synthesis are highly desirable. A review by *Hart*[37] in 1984 has provided a summary of accomplishments prior to the period of rapid growth. In another review, *Giese et al.*[38] have provided in-depth coverage of important concepts and applications, in particular the mildness of radical generation, the wide applicability to many functional groups and the high predictability of C-C bond-forming reactions.

Because of the advantages of radical reactions, the research groups have become increasingly interested in radical chemistry. The drive to accurately understand the mechanism of radical reactions derives from the desire of new developments that contain radical-based stereoselective reactions and synthesis.

1.3.1 History of Radical Chemistry

Radicals in organic synthesis were discovered long ago. The first stable radical in organic chemistry was observed in 1900 by *Gomberg*[39]. He developed the synthesis and investigated the reactivity of the triphenylmethyl radical, which is in equilibrium with its dimer (Figure 1.7). In his work, Gomberg was actually looking for tetramethylmethane and hexaphenylethane but found the radicals instead. Nevertheless, he established a low yield of the desired products. Moreover, he realized that the synthesized product includes an unpaired electron. Another example is aromatic *p*-diamine or so-called Wurster's salt, which is a radical-cation or a ketyl radical anion from benzophenone and which may polymerize in a sufficiently concentrated solution[40]. These radicals are, in general, much more stable than the corresponding quinone diimines. The absorption spectra of these radicals are given by *Piccard* and display a very distinct pattern of bands according to substitutions at the amino groups or at the rings.[41] The exact description of the electronic structure of these radicals was given by Rutherford after first presentation of the radical a century earlier.

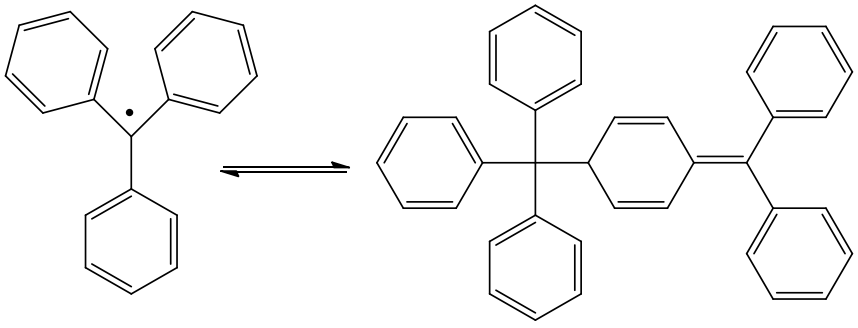

Figure 1.7. Gomberg's triphenylmethyl radical and its dimer in equilibrium.

Another key radical reaction was discovered by *Kharasch*[42,43] for the *anti-Markonikov*-addition in 1940, in which organohalide compounds such as carbon tetrachloride or chloroform add to alkenes. This reaction is very important for industry, especially for olefin polymerization,[44] which is considered a first step in atom transfer radical polymerization. A further development in radical chemistry was the production of cyclic systems through the intramolecular addition of radicals. This requires the precise knowledge of their selectivities and their reactivities. In this context, *Houk*[45] and *Beckwith*[46] have been investigated these intramolecular addition reactions by means of theory and kinetic assays. In this respect, *Porter*[47] and *Storck,*[48] who have used radicals for macrocyclization or for complex synthesis can be given as a good example. Substituted macrocyclic ketones or lactones have been used to cyclize by using bromide precursor. As an example of an electron transfer agent in radical chemistry, samarium diiodide has been used by *Kagan et al*.[49]

Radicals generally play a prominent role in the synthesis of complex natural products and are widespread in many biological processes. Radical reactions are more selective and predictable than ionic reactions, which can occur in additions and cyclizations in the syntheses of simple or complex nature products. The radical processes show numerous advantages over their ionic counterparts, which has only recently been recognized. They have greater functional-group tolerance, and thus the reaction conditions are more flexible. Furthermore, radicals can be generated under pH-neutral conditions, and thus strong acidic or basic conditions are not necessary. In addition, radicals are usually stable under protic conditions. There are many examples of radical reactions that can be performed in alcohols or even in water. Therefore, radical chemistry is amenable to “green” chemistry. Consequently, protic functional groups such as hydroxyl or amino functions do not need protection because they behave inertly. Otherwise, radical processes also show the ability to be incorporated into elaborate reaction cascades that rapidly increase molecular complexity. Considering all of these advantages, the synthesis of natural products is more attractive by using free radical reactions.

For a deeper understanding of the reactivity or stereoselectivity of radicals, a physico-chemical analysis by spectroscopic or microscopic methods is required. In addition, with computational methods the courses of many radical reactions can be understood in detail.

1.3.2 Examples of Radical Reactions

1.3.2.1 Samarium(II) diiodide based Reactions

In the following section, a few examples of radical reactions are given. Samarium diiodide as an electron transfer reagent in organic synthesis was used by Kagan[50] in 1980. The high oxophilicity of samarium allows the addition reactions of ketyl radicals to olefins. In this manner, an important class of ketyl coupling is obtained through cyclization, in which bicyclic products can be obtained with a simple substrate. (Figure 1.8) Other applications of ketyl cyclization are the addition hydrazones, nitriles and oximes.[51-53]

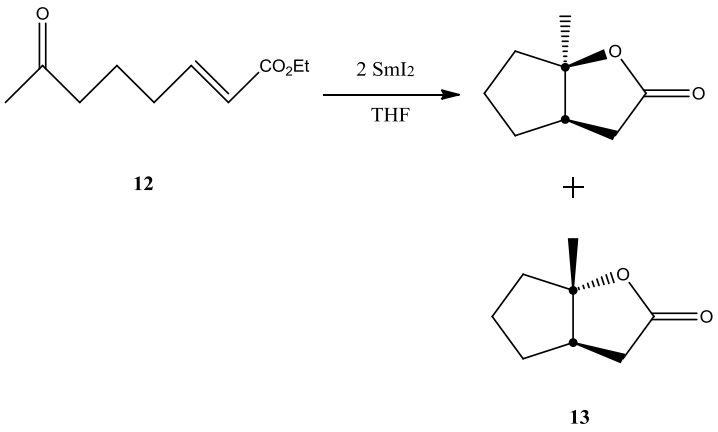

Figure 1.8. Samarium(II) iodide cyclization. [54]

Another set of reactions in radical chemistry comprises single electron transfer (SET), which is well-established in organometallic reactions. Aldehydes or ketones are usually used as radical precursors. SET reagents can initiate radical reactions either by the donation of a single electron from the metal to the substrate via reduction or by an electron transfer from the substrate to the reagent via oxidation. For this purpose, samarium diiodide, which is a strong electron donor, provides the key intermediate for the synthesis of Hypnophilin. (**16**) Here, samarium diiodide added to a suitable aldehyde homolytically cleaves the carbon-oxygen bond (Figure 1.9).

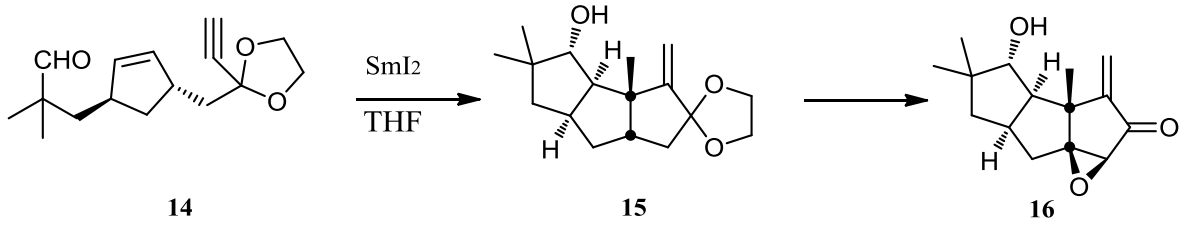

Figure 1.9. Preparation of the Hypnophilin. [55,56]

Samarium diiodide has been established as a major reagent in most forms of radical reactions, which include ketyl-alkene couplings, conjugate additions, pinacol coupling reactions, deoxygenation, dehalogenation or other many reduction reactions[57]. The basic reactions induced by SmI_2 concern intermolecular or intramolecular reactions and reductions of various functional groups, which are called Barbier reaction[58,59]. *Suginome* and *Yamada*[60] have applied the Barbier procedure to synthesize exaltone or (±)-muscone. They have achieved this by intramolecular cyclization as shown in Figure 1.10. The SmI_2-mediated Barbier type reactions can be carried out between aldehydes or ketones and a variety of organic halides.(**17**) In the absence of organic halides or protic conditions, pinacol can easily be reduced by reductive coupling of aldehydes whereas the formation of pinocol is slow by ketones under the same conditions. Otherwise, samarium diiodide plays a key role in several Reformatzky-type protocols, which allows hemolytic carbon-halogen bond cleavage and cyclization of carbon-carbon multiple bonds.

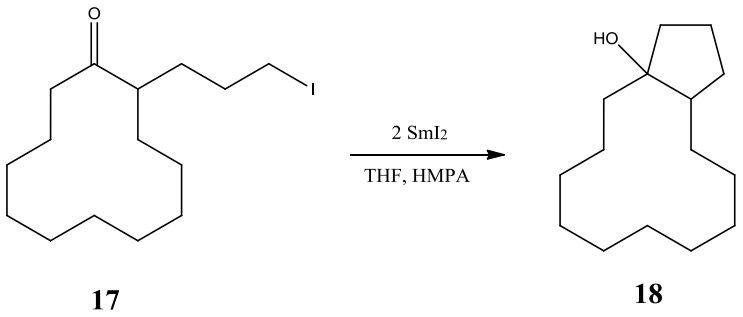

17 18

Figure 1.10. SmI_2-mediated intramolecular Barbier reaction.

1.3.2.2 Organotin based Reaction

As mentioned above, radical reactions have gained importance in the synthesis of natural products. Nature is highly selective and very efficient and often uses sequential transformations, which contain a series of reaction steps. In these reaction steps, several bonds are formed or broken without isolation of the intermediate. In this field, alkaloids, terpenes and especially steroids, which possess five or six ring systems, are important examples. In radical reactions, a novel radical is generated after cyclization or any other radical translocation. Because of this feature, a secondary carbon bond formation can be extended even further. These reactions are often referred to as tandem reactions. A tandem reaction is a process involving two or more consecutive reactions in which subsequent reactions result as a consequence of the functionality formed by bond formation or fragmentation in the previous step. The resulting tandem reactions can be used for the efficient preparation of polycyclic compounds from simple starting materials. This method was used successfully by *Stork et al.*[61] for the synthesis of prostaglandins in which rapid intramolecular cyclization is followed by a slow intermolecular addition. Another example for a radical tandem cyclization was reported by *Curran et al.*[62-65] for the synthesis of (±)-Hirsutene, which involves halogen compounds. This reaction is based on two steps and finally creates a tricyclic system[65] (Figure 1.11).

Because free radical reactions tolerate oxygen functionally well, more triquinanes have been prepared such as (±)-coriolin or (±)-hypnophilin by the same synthetic strategy. In general, an illustration of this synthetic strategy consists of the direct condensation toward linear cyclopentanoids and sequential constructions of each ring in the tricyclic system. In the remainder of the paragraph, the production of (±)-Hirsutene is described. In the presence of catalytic amounts of the azo-bis-isobutyronitril (AIBN) radical initiator, the tributylstannyl radical is generated. Treatment of an appropriate precursor such as bromide or iodide **19** with tri-n-butyltin hydride should produce the transient radical **20**. This carbon radical (**20**) undergoes two successive cyclizations to produce two five-member rings. This results in the production of vinyl radical **22**. Finally, in a slower step, the vinyl radical (**22**) abstracts hydrogen from tri-n-butyltin hydride in which the terminal double bond is formed and the tricyclic product Hirsutene (**23**) is generated. These reactions would produce hirsutene (**23**) from **19** in a single step synthesis.

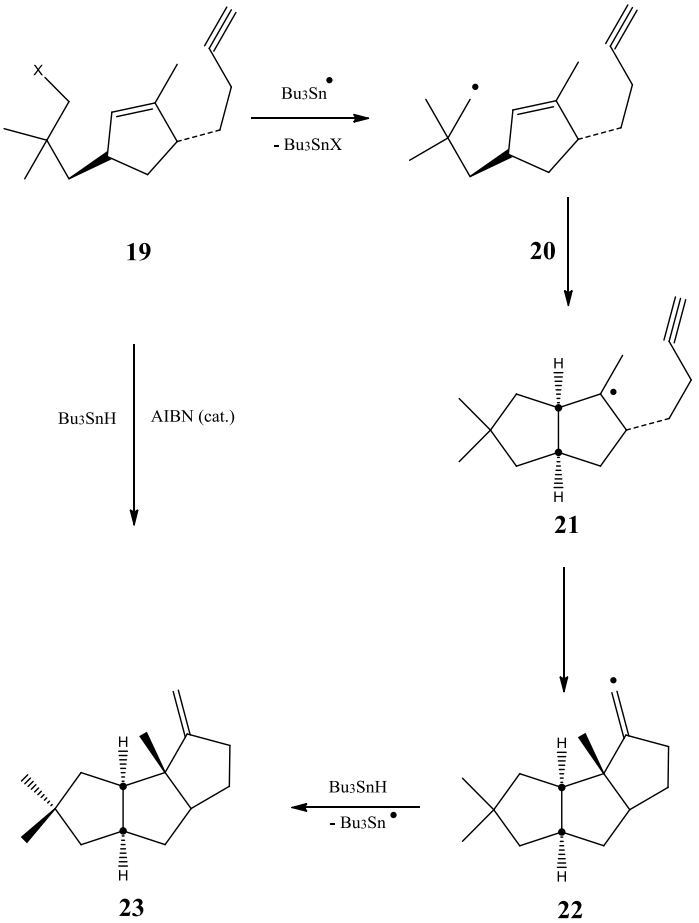

Figure 1.11. Preparation of (±)-Hirsutene. (X = Br, I, etc.).

Organotin compounds such as tributylstannane offer the possibility of a mediated radical addition for the reductive formation of carbon-carbon bonds, including many additions that are difficult to carry out through standard methods. Most radicals are generated using tin hydrides, and they have proven their merit for the substitutions of hydrogen in place of halogen, amino, nitro, carboxylate, Xanthate or other functional groups.[66] However, there are some drawbacks for tin-based radical chemistry. Trialkyl tin hydride is very toxic. Furthermore, it is difficult to remove from the desired end products, which are intended for human consumption such as drugs or medicines. Due to the toxicity of organic tin compounds, many alternatives have been introduced, of which silicon-based radical reducing reagents are the best alternatives. Phosphorous-based radical reducing reagents or even transition metal based hydrides are major alternatives to the tin hydrides in which the risk of toxicity in some cases is reduced to a minimum.[67-69]

1.3.3 Reagent Controlled Radical Chemistry

Most free radicals are highly reactive species. Unlike anions and cations, they react with themselves, for example by disproportionation. The free radical reaction can be classified by addition-, fragmentation- or cyclization-reaction types. To be useful in synthesis, these radicals must have sufficient lifetimes. However, there are also disadvantages to this type of radical reaction. The reaction cannot usually be controlled and the ligand sphere on the reagent generating the radical, which plays a key role on the selectivities of the reactions, cannot be influenced.[70,71]

An interesting alternative is represented by reagent controlled transformations.[72,73] The benefit of this kind of reaction concerns a wider application because the reactivity of the substrate on the chemo- and stereoselectivity can ideally be controlled. This can be performed with a chiral Lewis acid, a chiral catalyst or a chiral environment, and thus the route of reaction can be straightforwardly controlled.

In this approach, electron transfer from low-valent metal complexes to available radical precursors such as aldehydes or ketones occurs. The reagent control is achieved by varying these metals and their ligands. In this respect, the samarium diiodide mediated reactions with carbonyl compounds have led to activity. But because of the high nucleophilicity of the iodide the iodohydrin can be formed, which is further reduced by samarium. However, owing to the high costs and the large molecular weight of the metal, these reactions are unattractive. Other reagents such as chromium or vanadium have not been successful for these prospects. The radicals resulting from electron transfer of the vanadium cannot be trapped in the reaction, which included carbon-carbon forming reactions. The reason for the unexpected result can be explained by the fact that the dimeric structure of the vanadium in solution gives rise to an intramolecular second electron transfer. Chromium demonstrates low reactivity in this manner.

Another attractive method has been developed by *Nugent* and *Rajanbabu*. They have used titanocene chloride, which provides an efficient alternative for the exploitation of carbon-carbon bond forming reactions. In this strategy, epoxides can be used as radical precursors because they are conveniently prepared from various functional groups. The reductive epoxide opening is achieved by a single electron transfer reaction from titanocene(III) monochloride. This allows a mild conditions and highly chemoselective access to radical chemistry, which in this case includes a β-titanoxy radical. Titanocene dichloride is usually reduced by zinc or manganese powder, in order to form the titanocene(III) monochloride catalyst. The titanocene monochloride reagent features an unprecedented cleavage of the titanium-oxygen bond in reductive epoxide opening. The weak Ti-O bond arises from a combination of the low Lewis acidity and low reducing power of titanocene(III) monochloride, which prevents epoxide opening by an S_N2 mechanism. Rather, the epoxide opening reaction proceeds by a β-metal-oxy radical intermediate. The reducing agent and titanocene are employed in stoichiometric quantities. This provides a better reagent control than with non-stoichiometric amounts of titanocene. In stoichiometric quantity, the titanocene alkoxide intermediate is converted into a derivate of the alcohol or the alcohol itself and titanocene dichloride. An acid regenerates the titanocene(III) complex by protonation of the titanium-bound oxygen. However, there is some limitation for choosing the acid. The acid must be strong enough for the protonation, but it may not oxidize the metal powder and it may not deactivate the reaction by complexation of the resulting base to the catalyst. (See chapter 1.4) Because of the pKa value, pyridinium hydrochloride is appropriate for these requirements.

1.3.4 Radical Polymerization

The most important industrial application of free radical chemistry in organic synthesis is radical-induced polymerization, for example, ethylene polymerization.

In order to develop new polymers the control of stereoregularity is important. The discovery of a metallocene catalyst made this important step possible in practical applications, which permits

stereochemical control in polymerization.[74-78] Consequently, studies including a metallocene catalyst have been extended with the desired successful results. *Kaminsky*[79] *et al*. have developed this using a high active catalyst Ti and metylaluminoxane (MAO) as a co-catalyst, which acts as a Lewis acid in order to abstract a hydride anion and to facilitate the formation of electron-deficient unsaturated cationic titanocene species. However, *Jordan*[80] *et al.* have demonstrated that some of the dicyclopentadienyl zirconium alkyl complexes carry out ethylene polymerization in the absence of a co-catalyst. Recently, in 1994, *Kim* has reported that a mixture of zirconocene modified with $Si(CH_3)_3OH$ and trialkylaluminums as a co-catalyst gives polyethylene in a high yield.[81] Furthermore, the dicyclopentadienyl titanium(III) complexes are known to be of considerable interest as Ziegler-type catalysts, e.g., in the polymerization of ethylene or propylene.[79,82-84] Two classes of Ziegler type catalysts are known. The first class consists of catalysts, which are called heterogeneous catalysts. This class contains e.g. titanium based catalysts such as $TiCl_4$ and $TiCl_3$, which are highly active in alkene polymerization. The second class comprises two subclasses, comsisting of metallocene and non-metallocene catalysts, which are called homogeneous catalysts. Among them, the ansa-bridged metallocene catalysts, particularly titanocene compounds can produce isotactic or syndiotactic polymers of propylene.

Hopefully, the metallocene catalytic system might improve the copolymerization of ethylene and styrene in which many technical problems cannot be resolved with traditional Ziegler-Natta catalysts. The metallocene catalyst can serve to control of the properties of the polymer products. The syntheses of ethylene-styrene copolymers can be performed by using metallocene catalysts, which are activated by metlyaluminoxane (MAO). The produced poly(ethylene-styrene) can be further used to produce polyolefin blends and composites. The copolymerization process depends on the catalyst performance and the ligand modification of the catalyst, which plays a decisive role for the copolymer properties such as tacticity, microstructure or the level of the incorporation of a comonomer. The construction of the ligand structure, which is chosen based on the desired steric and electronic properties of the copolymer, constitutes an important part of the investigation of the copolymerization of ethylene-styrene. As an example for the influence of the ligand structure on the performance of the catalyst, inclusion of a bridging unit between two ligands shows an increased activity owing to increased Lewis acidity of the catalyst. In this area, *Bercaw* and *Okuta*[75,85] have firstly reported a new type of metallocene catalyst that functions without producing amounts of homopolymer impurities. *Kakugo et al.*[86] have discovered that a bidentate 2,2´-thiobis(6-*tert*-butyl-4-methylphenol) (TBP) is extremely active toward olefin and styrene and produces ethylene-styrene copolymers together with syndiotactic polystyrene. In contrast to this result, *Mulhaupt*[87] has found by using the identical catalyst, that only a random ethylene-styrene copolymer was formed without an isotactic structure.

Polymerization of styrene can also be achieved by using zirconium- and titanium half-sandwich complexes. The zirconium compounds are less active than the titanium compounds and show lower syndiospecifity and lower molecular masses of the polymers. In contrast, the half-sandwich titanocene catalysts, which contain cyclopentadienyl, substituted cyclopentadienyl, indenyl or substituted derivatives, are highly active, highly syndiospecific and give rise to a broader molecular weight distribution of the styrene polymers.[88-96]

The synthesis of macromolecular structure has benefited from living radical polymerization, which can be controlled by the molecular weight (M_n) and polydispersity (M_w/M_n) by the reversible

termination of the growing chains with persistent radicals or degenerate transfer (DT) agents.[97] In general, living polymerization occurs by atom transfer, dissociation-combination or degenerate transfer, which is catalyzed using a transition metal. The studies in the field of living radical polymerization focused on the titanocene-catalyzed radical ring opening (RRO) of epoxides, which are reduced by Ti(III) species. This reaction can be successfully carried out in the initiation of a radical polymerization, which is mediated by Ti in a living fashion. In the presence of the epoxide, one equivalent of Ti(III) opens the ring of epoxide, and this radical adds to styrene, which initiates the polymerization. Another equivalent of Ti(III) controls the polymerization. Some advantages of this method are because the epoxide can serve as a convenient substance for the synthesis of complex polymer architectures by transformation epoxide-generated alcohol groups. Moreover, this method is started by an inexpensive homogeneous catalyst, which does not need extra ligands, additives or activators. Furthermore, the most important point of this method is the selection of the steric and electronic nature of the titanocene complexes; additionally, the most titanocene structures used in coordination polymerizations may also be successful in living polymerization in conjunction with zinc, epoxides or another initiator.[97-99]

1.4 Titanocene in Organic Chemistry

1.4.1 History of Titanocene and Fundamental Properties

After the discovery of titanium by William Gregor in 1791, knowledge of its chemistry has remained relatively limited as compared to that of many other metals, although titanium has a natural abundance (the nineth-most abundant) of about 0.63 % in the earth's crust. The most common oxidation state of titanium is 4+, which is called titania. However, the 2+ and 3+ oxidation states are also readily accessible. The 3+ oxidation state is much better known than the 2+ oxidation state and has an unprecedented function as a reducing agent in organic chemistry. As examples for the usefulness of titanium as a reducing agent, *Knecht and Hibbert*[100,101] have shown that aqueous solution of $TiCl_3$ reduces nitro-arene to amino-arene. A short time later they also reported the reduction of quinones to hydroquinones by $TiCl_3$. In 1922, *Macbeth*[102] demonstrated that Ti(III) was capable of one-electron reduction of N-Br and N-Cl bonds in a variety of substrates. *Van Temelen* and *Schwartz*[103] in 1965 have reported the reduction of allylic and benzylic alcohols to dimeric symmetrical hydrocarbons by titanium, in which the valence is changed from 4+ to 2+. As can be seen from the examples, low-valence titanium reagents are undoubtedly important for organic chemistry. Many more examples can be found in literature that illustrate the usefulness Ti(III) in organic and radical chemistry.

Nevertheless, with the discovery of metallocenes, a new area opened up for the chemistry of titanium. Titanocene and analogues of other transition metals show a wide range of properties. Among these, the most important property is the 18-electron rule, which describes metallocenes with a total of 18 valence electrons. The metallocenes that comply with this rule are stable and have sandwich-structure. For example, ferrocene, which is the most stable of the metallocenes, has a sandwich structure, because of having the ideal number of the electrons. On the other hand, Cobaltocene, a d^7-19 electron complex and nickelocene, a d^8-20 electron are easily oxidized.[104] On the other hand, complexes such as titanocene (d^2-14 electron) or vanadocene (d^3-15 electron) are electron deficient, having fewer than 6 d electrons. One way the electron-deficient complexes can achieve the desired 18-electron configuration is to add additional ligands, which can contribute additional electrons. When the additional ligands coordinate to the metal, the cyclopentadienyl ligands bend back and in this structure, the cyclopentadienyl ligands are almost free to rotate with respect to each other. The simplest examples of bent cyclopentadienyl-metal complexes are the compounds in which the metal atom has two cyclopentadienyl and one hydride ligand. There are also molecules with a variety of ligands, including halides and alkyl groups.[105] Examples of these complexes are Cp_2MX_2 complexes. They all generally have the same geometry and have non-bonding d^1 electron configuration. *Petersen, Dahl* and *Fenske*[106-108] have spectroscopically investigated these complexes and calculated the molecular orbitals. For example, the electronic g values a few vanadium complexes and related Cp_2TiCl_2 complexes are in excellent agreement with EPR results. The EPR spectra provide information that the unpaired electron is in a_1 orbital of high metal character, primarily $3d_{z2}$ with only a very small amount of $3d_{x2-y2}$ and virtually no s or p character.

1.4.2 Examples of Monomeric, Dimeric and Trimeric Catalysts Based on Titanocene

A variety of titanocene complexes has chirality in the ligand or at the titanium center. They have been used as enantioselective catalysts. Especially, complexes with chiral ligands have been used with success in catalytic enantioselective opening of meso-epoxides.[109] The chirality in the cyclopentadienyl-ligand can have different origins which have been categorized in three types. Their chirality depends on how the two faces of the Cp ligands are oriented to each other. Homotopic faces of cyclopentadienyl ligands are equivalent because of the existence of a C_2 symmetry axis between the two faces. Enantiotopic faces of cyclopentadienyl ligands evidence a mirror plane and give enantiomeric compounds, when metalated with an achiral metal fragment. Diastereotopic faces of cyclopentadienyl ligands give a mixture of diastereomers because of their asymmetric property, when metalated. A first example of chiral cyclopentadiene is menthyl-derived cyclopentadiene, which was described by *Kagan* and collaborators[110] in 1978. They have been prepared from the inexpensive, enantiomerically pure natural product menthol. The ansa-metallocenes, which *Brintzinger et al.*[111,112] have described, possess an interannular connection and are another example of chiral cyclopentadienyl-metal complexes containing prochiral cyclopentadiene ligands. Chiral cyclopentadienyl- and prochiral cyclopentadienyl-metal complexes have been applied in three main areas.[113] First, they are used as catalysts in asymmetric hydrogenation reactions, reactions involving ketones, aldol reactions, epoxidations and alkene isomerizations. In this area, *Kagan* and collaborators[114,115] have used bis(cyclopentadienyl) titanium dichloride with menthyl or neomenthyl-substituted cyclopentadienyl ligands in hydrogenation of 2-phenyl-butane. As another example in the same area, *Colletti* and *Halterman* reported that bis[1-indenyl]titanium dichloride can function as a catalyst for the asymmetric epoxidation of unfunctionalized alkenes[116]; second, as stoichiometric reagents for stereoselective cobalt-mediated cyclizations and zirconium-mediated aminations; third, as catalysts in stereoregular polymerizations of alkenes. Additionally, the allylmetal reagents have been successfully used for synthetically interesting transformations that have led to the development of allyl complexes of chiral titanocene. For example, *Collins* has reported an enantioselective allylation of aldehydes using a chiral allytitanium reagent.[117]

The allydicyclopentadienyl titanium complexes can be also given as examples for monomeric structures of titanocene derivatives. In these compounds, the allylic groups act as bidentate ligands. Unlike the other structures of titanocene, which are able to polymerize ethylene, solutions of allylic complexes are not an active towards ethylene polymerization. IR measurements showed that allylic ligands are π-backbonded to the metal in analogy to cyclopentadienyl ligands.[118]

Several carboxylate derivatives of bis(cyclopentadienyl) titanium compounds have been prepared by *Coutts* and *Wailes*.[119] These compounds have mono- or di- carboxylate ligands. Their study has shown that the carboxylate ligands are bidentate and exhibit a covalent bond to the metal. The complex is symmetric with respect to both monomer halves.

Nöth *et al.*[120,121] have reported the magnetic properties of these trivalent cyclopentadienyl titanium derivatives. In the case of titanium trichloride, the susceptibility does not follow a Curie-Weiss law. If one cyclopentadienyl group is present, it behaves as a magnetically dilute compound, so its susceptibility does follow the Curie-Weiss law and the structure of mono-cyclopentadienyl titanocene dichloride is a dimeric. With two cyclopentadienyl groups, the spin-spin interaction

becomes stronger. In the absence of the halogen, tris(cyclopentadienyl) titanium(III) shows no spin-spin interaction and is only present in monomeric form.

The hydride derivatives of titanocene, which may be present as a dimeric or monomeric structure, are of considerable interest because of their activity in low-pressure ethylene polymerization. Some complexes of group (IV-VII) transitions metals have been found, in which a hydride ligand acts as a bridge between two metal centers of a binuclear species. This hydride bridge behaves chemically most like an embedded proton in the electron density of a metal-metal bond. In some cases, the hydrogen bridge can be formed by insertion of a proton into a neutral metal-metal bonded species. In other instances, the hydrogen complex is easily deprotonated and the remaining electrons form the corresponding metal-metal bond in the anionic complex in alkaline media. However, the metal boron hydrides [Cp_2TiBH_4] have a monomeric structure, in which the titanium and boron atoms are linked by two hydrogen bridges. According to the IR and EPR spectra, this compound exhibits tetrahedral symmetry.[120-122]

According to a recent report[123], the [Cp_2TiCl] compound is dimeric in the crystalline state and in benzene solution. The dimer form involves pairs of Titanium atoms that are grouped together by bridging chloride ligands. Magnetic measurements of this complex showed that the compound has one unpaired electron per titanium atom and exhibits an antiferromagnetic interaction between the two Titanium centers. The spin-spin interaction between the titanium atoms causes singlet and triplet states in thermal equilibrium. As the temperature is lowered, the singlet state becomes more populated at the expense of the triplet state and the susceptibility and magnetic moment decrease. From IR measurements, it became clear that the dimeric species are tetrahedral, and the overall symmetry is not cubic.[124] In contrast to the case in the benzene solution, the complex is present as a monomer in ether or tetrahydrofuran solution, because coordination of an ether molecule to the vacant coordination site of [Cp_2TiCl] is strong enough to compete with the formation of the dimer. The dipole moment and electron diffraction of the monomeric compound of Cp_2TiCl indicated that this complex can be described as a “wedge-shaped sandwich” of tetrahedral structure.[125,126] The aromatic rings are usually not parallel but an unrestricted rotation of the rings about the bond axis through the metal atom is possible. The unpaired electron magnetically interacts with each of the ten ring hydrogen atoms.

The dimetallic complexes, in which the coordinated bridging ligands are chloride ions, are other interesting examples of cyclopentadienyl titanium halide complexes. These compounds do not easily decompose.[127] Unlike the dimeric formation of other titanium halide compounds, the titanocene halide complexes exhibit a weak magnetic interaction between the titanium atoms. The cyclopentadienyl rings are weakly σ bound to titanium. Although dimetallic and trimetallic complexes have identical bonds between cyclopendienyl and titanium, *Reid*, *Scaife* and *Wailes et al.*[128] have demonstrated that the characteristic vibration for the π-systems in the IR spectrum is not completely identical for the dimetallic and trimetallic systems. As for the symmetry, Titanium-Zinc-Titanium trinuclear complexes and cyclopentadienyl titanium dimeric complexes must have the same symmetry due to identic splitting of the d-d transitions of the each complex. For the trinuclear complex, it was shown that two titanocene units are linked by $ZnCl_4$ through chloride ligands. The local symmetry of each titanium is tetrahedral. The trimetallic and dimeric complexes also show another similar feature in their magnetic properties. The unpaired electron resides in a molecular

orbital, which is primarily d_{z2} in character in both the dimer complexes and the zinc bridged trimetallic complexes.

The majority of dimeric compounds are diamagnetic. When the two metals possess unpaired electrons, they are able to exhibit magnetic properties and give information about the metal-metal distance and about the exchange interaction between the two metal centers by EPR studies. However, since the dimerization often gives rise to antiferromagnetic coupling, the dimeric systems are more difficult to study by EPR spectroscopy.

Another example of a dimeric compound is a complex in which the two metallic centers are held together carbonyl ligands. Its ferromagnetic behavior was deduced from magnetic susceptibility measurements that showed a populated triplet state.[129]

Titanocene derivatives do not only form monomers or dimers. In addition to these structures, it is possible to obtain trimers. An example for this form is the class of pseudo-halogen derivatives of bis(cyclopentadienyl) titanium compounds such as the cyanide or isothiocyanate compounds.[130] Both of them must be bridging through the cyanide ligands.The magnetic properties of both of cyanide complexes (**I** and **II** in Figure 1.12) are very similar, indicating the presence of a cyclic trinuclear unit and a titanium (III) cation. Interestingly, unlike the isothiocyanate and cyanide complexes, the isocyanate complex is formed as a monomer. (**III** in Figure 1.12)

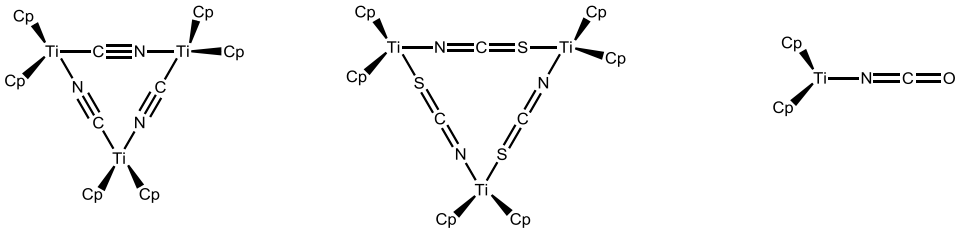

I II III

Figure 1.12. Trimeric or momomeric structure of pseudo-halogen derivatives of bis(cyclopentadienyl) titanium compounds.

1.4.3 Reactions Catalyzed by Titanocene Derivatives

Until this point, the structures of the titanocene-derivatives and their physical and chemical properties have been described. This section focusses on the various reactions that can be performed within radical chemistry using these titanocene derivative complexes.

As already described in the chapter (1.3), in addition to samarium(II) iodide as a SET reagent, the low-valent titanocene complexes can be used to generate reduced radicals. This SET method is realized by transfer of an electron from a low-valent metal to a suitable substrate. The absence of a radical initiator has some advantages, e.g., the variability of the reduction potential of the different metals and no loss of functionality of the generated a radical.

At the beginning of the 1970s, the McMurry reaction has been developed in organic chemistry, which is based on reductive coupling of carbonyl compounds to produce alkenes by low-valent titanium.[131] Ever since its discovery, low-valent titanium has become increasingly important in organic synthesis. Low-valent titanium has even become irreplaceable in many organic reactions, in particular, in

numerous syntheses of natural products. In addition, recent developments also showed that intermolecular couplings of esters and amides are possible with this type of reaction. Hence, the production of some aromatic heterocycles is realized by reductive carbonyl reactions, which have opened a new area for alkaloid syntheses and pharmaceutical research. Annelations, macrocyclizations, pinacol couplings and heterocycle syntheses are all carried out by using the low-valent Titanium.[132] We start by giving examples with pinacol coupling.

1.4.3.1 Pinacol Coupling

The first report of pinacol coupling in 1858 by *Fittig*[133] concerned the reaction of acetone with sodium, which is achieved by reductive coupling of two carbonyl compounds (Figure 1.13a). The stoichiometric reagents are titanium(III) complexes such as titanium trichloride or titanocene chloride. They can be successfully used for pinacol coupling of aromatic and α,β-unsaturated aldehydes. In this context, *Seebach*[134] reported that diastereoselective couplings of aromatic aldehydes to racemic 1,2-diols are carried out by using titanium trichloride and butyllithium. Because of the high chemeoselectivity of this reagent, neither aliphatic aldehydes nor ketones were effective. In 1987, *Inanaga* and *Handa*[135] found that aromatic and α,β-unsaturated aldehydes can be given to racemic 1,2-diols in high yield and in high diastereoselectives. In this context, titanocene dichloride is reduced by Grignard reagents, which produced a trinuclear titanium(III) complex. In another example for pinacol coupling, *Schwartz*[136] stated that aldehydes activated the highly diastereoselective coupling by using aluminum powder-reduced titanocene dichloride dimer compounds. However, these titanium(III) reagents react with a high chemoselectivity, which causes lack of activity with some of carbonyl compounds. *Mukaiyama*[137] has developed titanium(II) reagents, which in the absence of formation of deoxygenation products ketones can be coupled to 1,2-diols. Subsequently, in order to promote the performance of the titanium(II) reagents, *Matsubara*[138] improvemed the procedure to include the addition of chelating diamines and aminoalcohols to the reaction mixture.

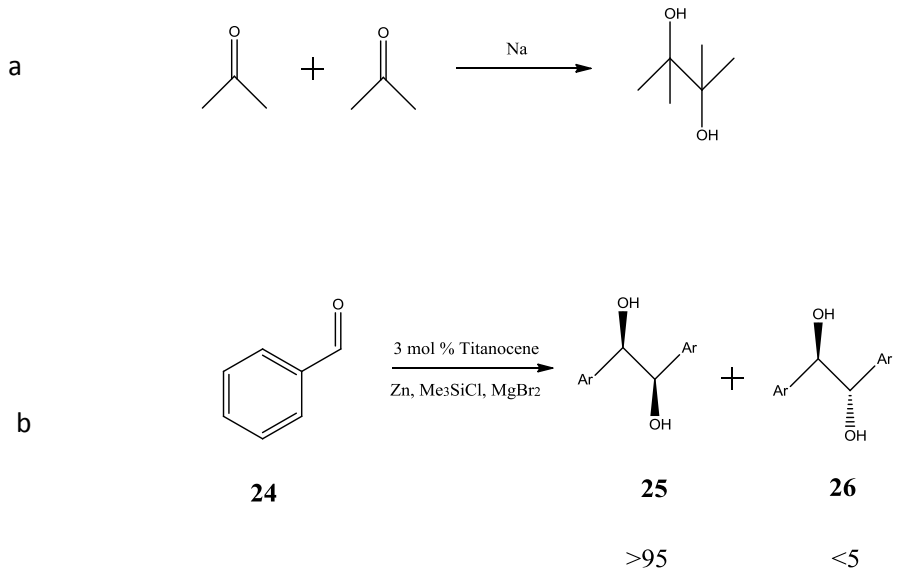

Figure 1.13. The first pinacol coupling by Fittig (a) Titanocene-catalyzed pinocol coupling (b).

The pinacol coupling can also be performed catalytically; this procedure requires harsh reaction conditions, low selectivities and low functional group tolerance. Based on the ability of the titanocene chloride reagent, the reaction conditions can be controlled. In this case, *Gansäuer et al.* developed a catalytic method for the titanocene-mediated pinacol coupling, in which titanium compound was used 3-5%[139-141] (Figure 1.13b).

In general, this reaction proceeds through the metal oxides or alkoxides. A low-valent redox-active metal compound is used as a catalyst. The low-valent metal compound is generated by silylation of the metal-oxygen bond with Me_3SiCl, which is used as a stoichiometric reagent to replace the catalyst. Thus, the metal oxides or alkoxides are converted to metal chlorides. However, the silylation process can cause problems. Firstly, the silylation step in catalytic cycle is the slowest step. Secondly, Me_3SiCl supports the electron transfer from metal to aldehydes and at this point, the undesired catalytic reaction takes place. Finally, after hydrolysis hexamethyldisiloxane is generated in stoichiometric amounts that cannot be recycled and therefore must be disposed of as waste. In this context, the first successful example was the McMurry catalytic reaction in Titanium. The samarium diiodide was also used by Nozaki-Hiyama coupling in catalytic reaction.[142] When comparing titanocene dichloride and samarium diiodide, samarium diiodide can be seen as more expensive and less selective than non-toxic titanocene dichloride.[135,136,143]

1.4.3.2 Reductive Ring Opening without Deoxygenation

The reduction of ketone to secondary alcohols via ketyl radicals is carried out by using titanocene in aqueous solution. This reductive process takes place under mild conditions, which means that safe, cheap reagents can be used. Mechanistically, the reaction proceeds by an organometallic complex as a catalyst and water as a proton donor. Along these lines, an oxygen-free THF-water mixture as the reaction medium is sufficient. The nature of the catalyst is suitable for the asymmetric synthesis.

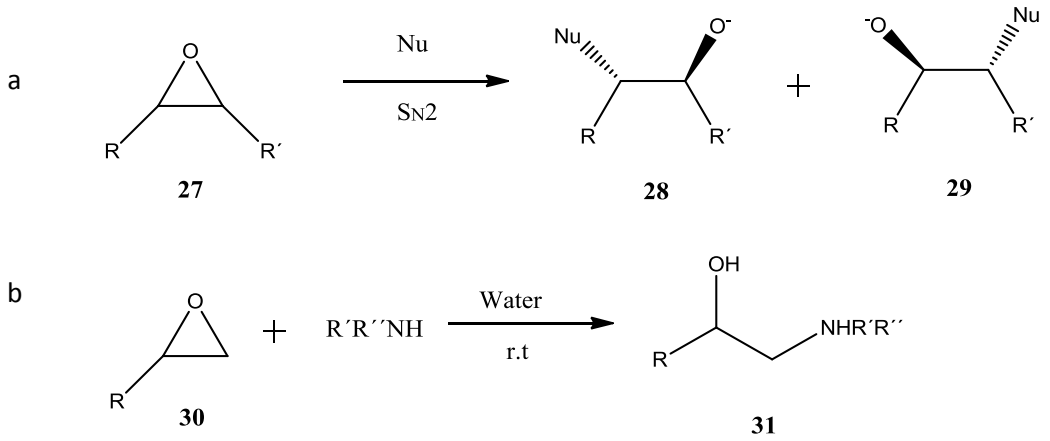

Figure 1.14. The nucleophile epoxide ring opening: (a) General nucleophilic mechanism for epoxide ring opening; (b) Epoxide ring reaction via S_N2 mechanism in the presence of amines.

The titanium complex is a reducing agent and simultaneously activates the epoxy function, in which epoxides open homolytically and an intermediate carbon-centered β-titanoxy is generated.[72] In order to understand the reaction mechanically, the behavior of the epoxide must be considered in the reaction. The epoxide can be also opened heterolytically by a nucleophile via an S_N2 mechanism. The nucleophile attacks to the electropositive carbon atom and displaces the oxygen atom; thus, a new bond is formed (Figure 1.14a). In the organic chemical context, *Azizi's* works can be given as an example. He has reported that a nitrogen atom can be used as a nucleophile and that the epoxide is opened in water at room temperature without a catalyst. This reaction results the β-amino alcohols (**31**) under mild conditions with high selectivity and in higher yield[144] (Figure 1.14b).

Additionally, the using of the titanocene(III) chloride as a SET reagent for the opening of the epoxide has some advantages. This process can be achieved through using the non-nucleophilic ligands, which reduce the strength of the Lewis-acidic metal center by σ- and π-donor interaction. Hence, the reaction does not proceed by S_N1 or S_N2 mechanism, so the convenient nucleophilic reagents must not be used. In this manner, Lewis acid catalysis and radical chemistry can be uniquely combined. Consequently, titanocene(III) chloride can be ideally applied for this procedure (Figure 1.15).

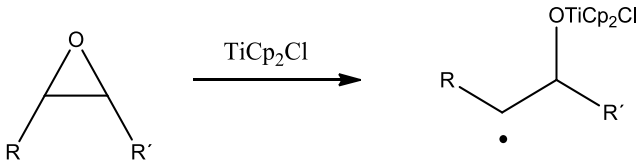

32 **33**

Figure 1.15. Reductive epoxide opening with titanocene(III) chloride.

The reductive epoxide opening is based on the reduction of ring strain and the formation of titanium-oxygen bond. Unlike the other reagent, e.g., the abstraction of the chloride by tributylstannane, the formation of metal-free radical is not formed by using titanocene(III) chloride. The oxygen atom is bound to the radical center in the β-position; thus, the titanocene complex can be influenced in principle in the reactivity of the radical.

The cyclopentadienyl ligand determines the chemoselectivity of the reaction, which relies on the regulation of the redox properties and the steric demand of the metal complex. Interestingly, the steric interaction between the cyclopentadienyl and the epoxide dominate the regioselectivity of epoxide opening. This is confirmed by computational investigations.[145] The steric interaction plays a crucial role in the intermediate step, in which the reduction of the carbon-centered radical is prevented by using a further equivalent of titanocene(III) chloride. The higher-substituted β-titanoxy radical is generated, and thus the radical is durable enough to take part in radical reactions. Consequently, no metal-free radical is formed via the reactivity of a Titanium complex.

1.4.3.3 Reductive Ring Opening with Deoxygenation

If the reaction medium contains additional stoichiometric amounts of titanocene(III) chloride, deoxygenation of epoxide is achieved. The first attempts were reported by *Kochi et al*.[146] in the area of β-metaloxy radical. The deoxygenation of styrene and cyclohexene oxide by using chromium (II)

reagents takes place by discrete one electron steps via the carbon-centered radical (**35**). However, stereoselectivity was not observed in this reaction (Figure 1.16).

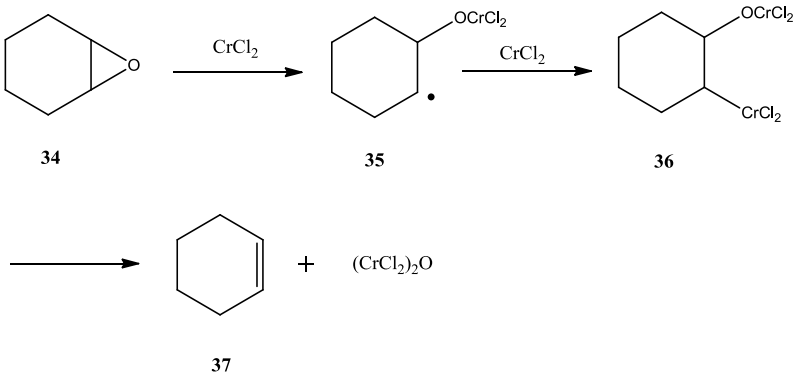

Figure 1.16. The first use of β-metaloxy radical in the deoxygenation reaction.

The deoxygenation step can be used for the synthesis of valuable natural products with an oxirane moiety. *Doris*[147,148] and coworkers have found that the deoxygenation of Leurosine (**38**) resulted in anhydrovinblastine (**39**) in higher yield (See Figure 1.17). Anhydrovinblastine is an important intermediate for the antitumor agent Navelbine, which is a member of crytophycin family of natural products. The reaction is based on a single-electron transfer from titanocene(III) chloride to the oxirane, in which the carbon-centered radical intermediate is generated through a β-alkoxy radical. Subsequently, titanium-oxo byproducts, which are reduced by a further equivalent of titanocene(III) chloride, are eliminated, which results in the deoxygenated anhydrovinblastine (**39**).

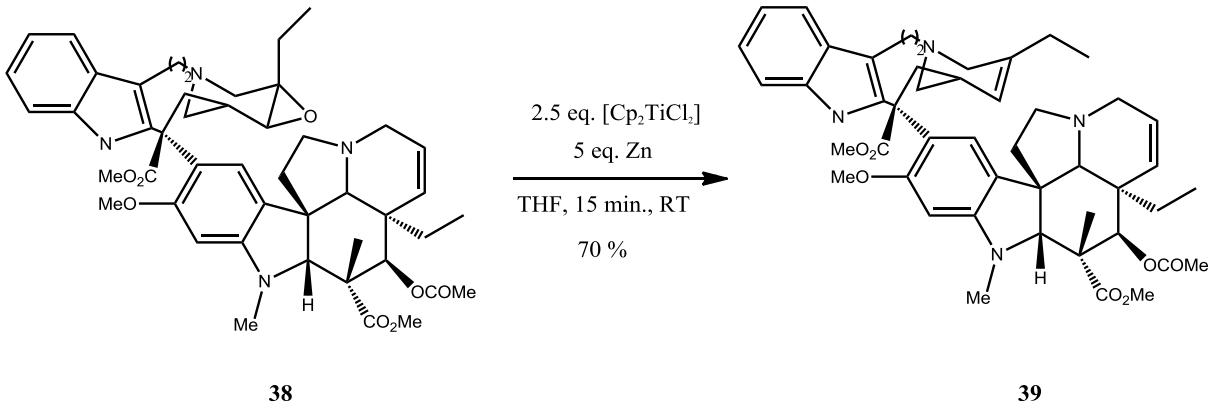

Figure 1.17. Synthesis of anhydrovinblastine by *Doris et al*.

The intermediate β-titanoxy radical (**41**) can subsequently be reduced by a hydrogen atom donor such as tert-butyl thiol, H_2O or 1,4-cylohexadiene to convenient alcohol (**42**)[149,150] (Figure 1.18).

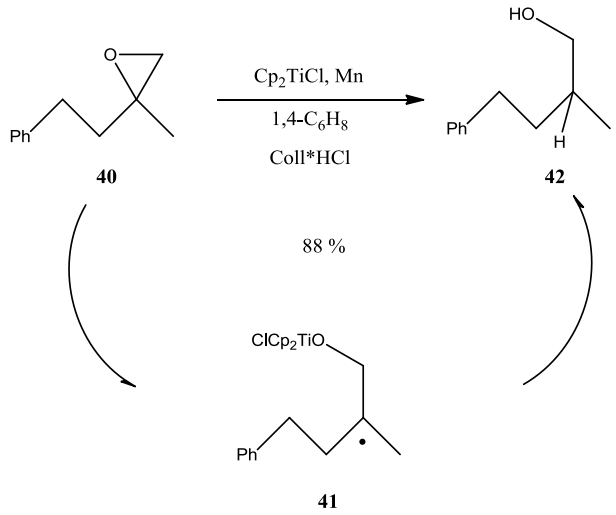

Figure 1.18. Mechanism of titanocene(III) chloride-mediated reductive opening epoxide.

This epoxide opening reaction can be also carried out by using stoichiometric amounts of titanocene(IV) chloride.[149,150] Also, collidine hydrochloride was added in stoichiometric amounts. In this method, the titanocene(III) chloride must be regenerated because during the reaction titanocene(III) chloride is consumed. The opening of the titanium-oxygen or titanium-carbon bond can proceed after any intermolecular or intramolecular addition. Therefore, the titanocene alkoxide should not be released. Titanium-oxygen bond is only *in situ* cleaved to regenerate titanium(IV) chloride. Thus, titanocene(III) chloride is formed again for the further epoxide.

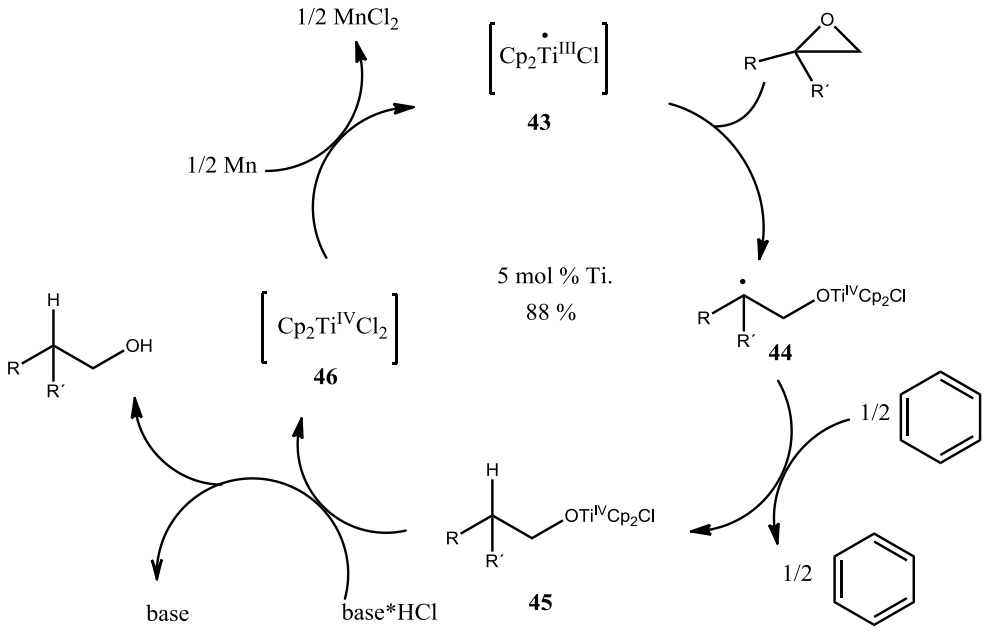

Figure 1.19. Titanocene-catalyzed reductive epoxide opening.

An alternative way for the formation of the alcohol through cleavage of titanium-oxygen bond is hydrolysis. This process is achieved under the stoichiometric amounts of titanocene(II) chloride. An *in situ* protonation of the titanium-oxygen bond step is important. To achieve this process, a suitable acid can be used. Thus, the titanocene alkoxide must be converted into alcohol and titanocene(IV) chloride. As described previously, the acidity of the used acid must be strong enough to protonate the titanium-oxygen bond. However, it should not promote the opening of the epoxide. Additionally, the conjugate base of the used acid must not be not nucleophilic in order to prevent nucleophilic opening of the epoxide and it should not be too basic. Pyridine hydrochloride seems to be appropriate for these conditions.[73]

A catalytic cycle is achieved with titanocene(IV) chloride, which is reduced with a metal dust (Zn or Mn) to titanocene(III) chloride, collidine hydrochloride and a suitable hydrogen-atom donor, which 1,4-cyclohexadiene is usually used as a hydrogen-atom donor. All of them form the backbone of this method. The planned catalytic cycle for the reductive opening is outlined in Figure 1.19.

After the opening of epoxide, the β-titanoxy radical (**44**) is generated that becomes β-titanoxy by the abstraction of a hydrogen atom from a hydrogen atom donor. 1,4-cyclohexadiene is usually used as a reducing reagent. However, γ-terpinene can be an alternative as a hydrogen atom donor, which is provided economically and in an ecologically benign condition in contrast to the more expensive and carcinogenic 1,4-cyclohexadiene. This reagent is also used for the highly selective opening of Sharpless epoxides and their derivatives, which are easily prepared in high enantiomeric purity.[151] As the next step, the resulting titanocene alkoxide (**46**) has to be cleaved to liberate the final products. This procedure is achieved by protonation by a suitable acid. As in the catalytic pinacol coupling, the acid should not deactivate any titanium species and should be weak enough not to open the epoxide. For these purposes, the Bronsted acids involving pK_a values between 5.25 and 12.5 should be suitable. Although pyridine hydrochloride and 2,6-lutidine is able to to protonate alkoxides, 2,4,6-collidine hydrochloride acid (pK_a = 7.43) gave the best results and can be combined with manganese as a reductant for protonation of titanocene alkoxide. After protonation, the metal powder reduces *in situ* titanocene(IV) chloride (**46**) again to active titanocene(III) chloride (**43**). When choosing metal powder as a stoichiometric reductant, an important point to consider is the redox potential of the metal. Undesired reduction to titanocene(III) chloride should not occur by a further redox reaction. The Lewis acid metal halide arises from the redox reaction and should not affect the catalytic cycle. Zinc and manganese meet these conditions. Moreover, zinc is a stronger reducing agent than manganese. This catalytic system showed the same regioselectivity as the stoichiometric system. In the stoichiometric reductive system, the electron transfer process from the metal powder was ensured so that the titanocene(IV) chloride is reduced. The highly active functional group of the stoichiometric reaction was protected under catalytic conditions. Nevertheless, in the catalytic cycle system, the mild acid is not able to promote the electron transfer from metal powder to variety functional groups such as ester, nitriles, ketones or aldehydes. This system is also useful for other radical reactions, for example, cyclization or additions.

A natural example is eudesmanolides that are synthesized by the *Oltra* and *Cuerva*[150] groups. These natural compounds are classified into two categories: 12,6-eudesmanolides and 12,8-eudesmanolides, which have pharmacological properties such as anti-inflammatory and anti-tumoral activities. Their proposed catalytic cycle was based on the single electron between titanocene(III) chloride and available epoxygermacrolide (Figure 1.20). The difference in the catalytic cyclic between

Gansäuer and Oltra groups is the use of the base. Collidine hydrochloride acid, the reagent 2,4,6-trimethylsilylpyridinium chloride, is used as a base in this cycle, which can be regenerated from titanocene(III) chloride and plays an important role for production of the exocyclic alkene. Because of the high Lewis acidity of silicon, the titanium-oxygen bond can only be cleaved. However, the authors have further developed this synthesis method, which is called biomimetic synthesis. In addition to the catalytic cyclic, before the reaction of the catalysis with suitable germacrolide, the alkaline isomerization is formed for providing accessible germacrolide. The selective epoxidation is followed by titanocene-mediated cyclization. Subsequently, the product can be achieved in four steps.

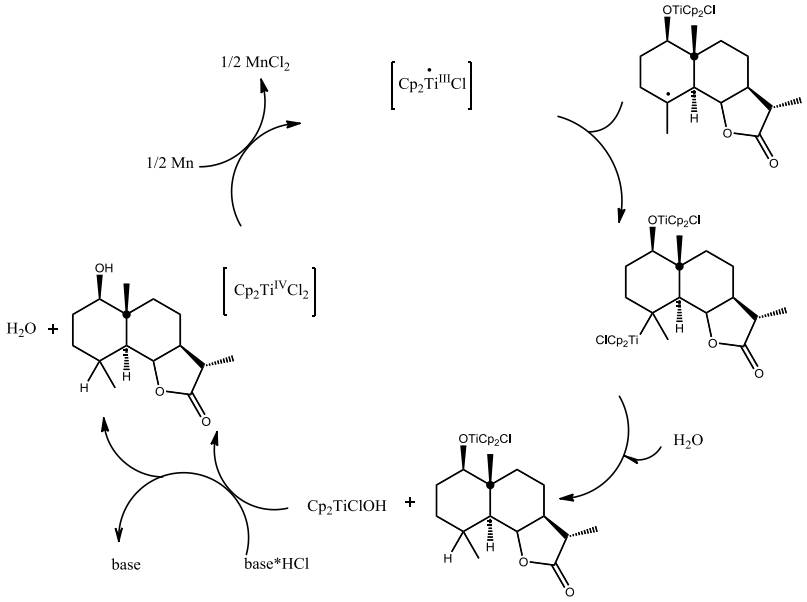

Figure 1.20. Hypothetical catalytic cycle for the synthesis of eudesmanolides by *Oltra and Cuerva*.

However, the tri-substituted epoxide can be reductively opened using titanocene(III), which results in regioisomeric products. The steric and electronic factors of the epoxide can influence which bond is going to be opened. In this manner, the researchers have demonstrated that the 2,3-epoxy alcohols yielded the asymmetric 1,3-diols by titanocene(III) chloride.[152] The substituents on the titanocene catalyst or substituents of the epoxide in the adjacent position to each other cause the steric and electronic factors. For example, in the presence of carbonyl or phenyl groups in the neighbor position on the epoxide, the generation of the radical and thus the regiochemistry of the opening of epoxide can be affected. *Doris et al.*[153] have shown that α,β-epoxy ketones can be selectively reduced to β-hydroxy ketones by titanocene(III) chloride (Figure 1.21). The reaction is successfully performed from a di- and tri-substituted epoxy ketone system to primary, benzylic and tertiary alcohols. The reaction mechanism proceeds via single electron transfer. Firstly, the single electron from titanocene(III) chloride is transferred to oxirane (**47**). After a further equivalent of the titanocene(III) chloride, enolate β-alcoholate is generated (**48**). Finally, the enolate β-alcoholate can be protonated by using of methanol and as a result the β-hydroxy ketone (**49**) is yielded. Additionally, this procedure can also be achieved for the aliphatic or cyclic ketone systems in a high yield.

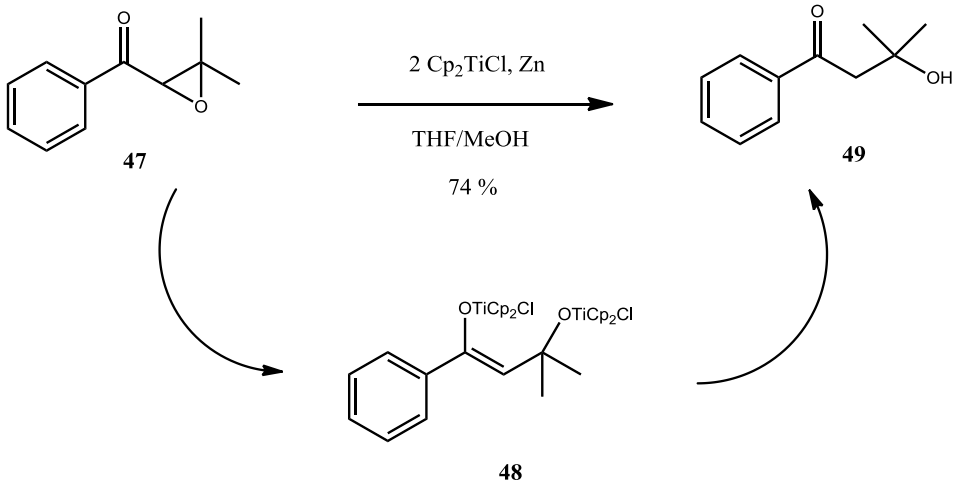

Figure 1.21. Reductive opening of the α-β-epoxy ketones by *Doris et al.*

As described in Section 1.4.1, the variation of ligands of the titanocene catalyst can control the regioselectivity of the epoxide and the steric interactions between the substituent of epoxide and the ligand of the catalyst influence on the regioselective opening of the epoxide. In this context, Gansäuer *et al.*[109,154] have disclosed that the catalytic opening of *meso*-epoxide can be carried out by using catalysis with the chirality contained in the ligand via electron transfer in high enantioselectivity and in high diastereoselectivity. They have used the designed catalysis with menthyl-substituents, which are synthesized from available menthol or *neo*-menthol from nature, because the methyl groups of menthyl can be shielded from the chloride atom bound to the titanium. The usage of these catalysts increases the enantioselectivity of the product (**51**) with the convenient *meso*-epoxide (**50**) (Figure 1.22). The coplanarity of the benzene rings and cyclopentadienyl rings of the catalyst causes the highly selective binding of the substrate due to π stacking.[113,155,156] The rationally designed catalyst is obtained with a yield of 71 % and is highly enantioselective (93 % when substituted with phenylmenthyl ligands (**52**)). However, the methyl-titanocene catalyst (**53**) results in a 76 % and 94 %, yield and enantioselectivity, respectively, under the same reaction conditions.

In the opening of epoxide, the β-titanoxyradical is generated as an intermediate step. Intermolecular addition of carbon-carbon multiple bonds can occur by adding a suitable free radical acceptor. In this way, new carbon-carbon and carbon-oxygen bonds can be generated. As an example for including the chemoselectivity of this method, *Dötz et al.*[157] have used alkenyl and alkynyl carbene complexes of chromium and tungsten. They have reported that bicyclic *trans*-fused tetrahydropyranosylidene and dihydropyranosylidene complexes are obtained by diastereoselective cyclization reaction with a suitable epoxide in the presence of titanocene(III) chloride. The products are characteristic building blocks in biologically active compounds in biomedical research. Under mild conditions, 1,2-dihydroglucose (**55**) can be opened via two alternatives of homolytic-cleavage: one possibility concerns a carbon-centered secondary radical and finally the bicyclic acetal pyranosylidene (**C**) is produced (path a). Another alternative for homolytic cleavage of the epoxide provided a secondary anomeric carbon radical, which finally yields the pyranosylidene complex (**D**) (path b). The reactions take place under stoichiometric addition of titanocene(III) chloride (Figure 1.23).

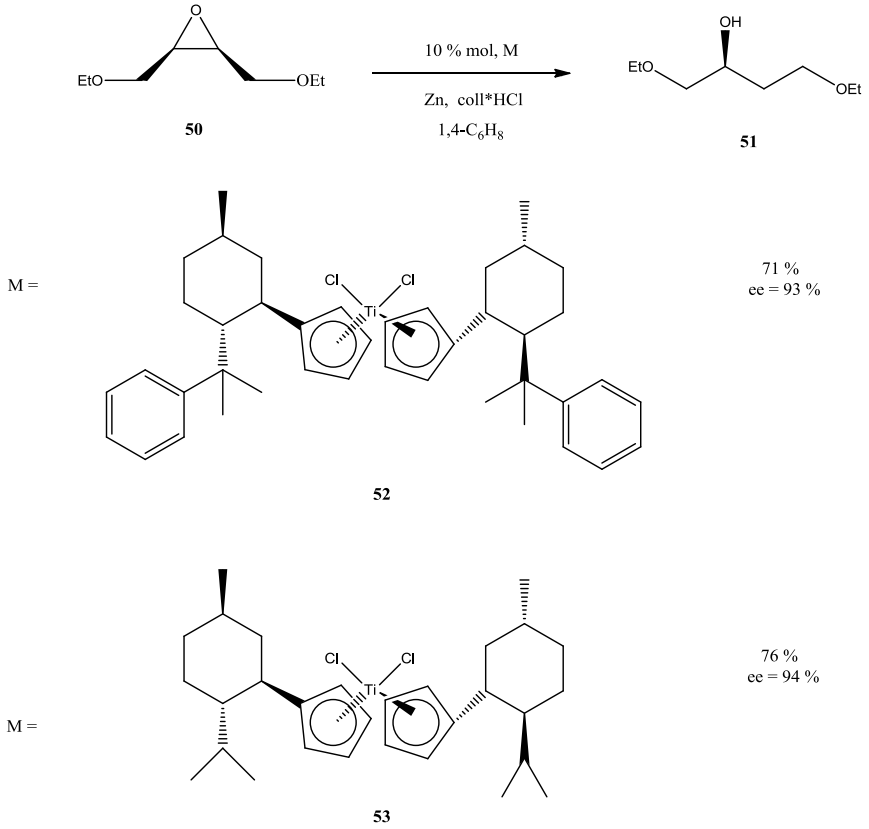

Figure 1.22. Enantioselective reductive opening by chiral titanocenes.

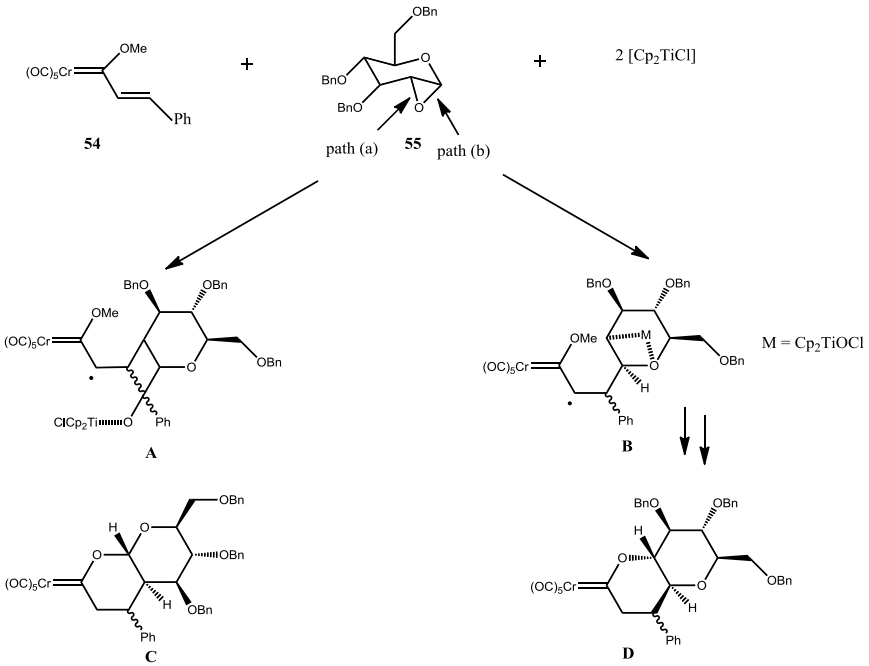

Figure 1.23. Synthesis of dihydropyranosylidene by Dötz.

Acrylic acid ester derivatives are particularly well-suited for the titanocene-mediated intermolecular addition of opened epoxides at carbon-carbon multiple bonds. In this case, δ-hydroxylesters, δ-lactones, δ-hydroxyamides or δ-hydroxynitriles are created by using titanocene dichloride containing sterically demanding alkyl substitutions[151,158] (Figure 1.24). After the reductive opening of the suitable epoxide (**56**) with an enantiopure catalyst, intermolecular addition can be achieved with the bond acceptor. The resulted products (**58**) prefer the formation of the trans-isomers. The reason of this unprecedented result can be explained by the fact that the cis-face of the radical is determined by shielding through the cyclopentadienyl groups and its substituted alkyl groups (anti-rule by Giese).[159] Interestingly, the titanocene(III) chloride without substituent (**61**) can give diastereoselectivite amounts of 77:23. Despite this issue, the catalyst with tert-butyl substituent (**59**) resulted in the highest diastereoselectivity (>97: < 3) and the small methyl substituent (**60**) containing catalyst yields the diastereoselectivite amounts of 94:6.

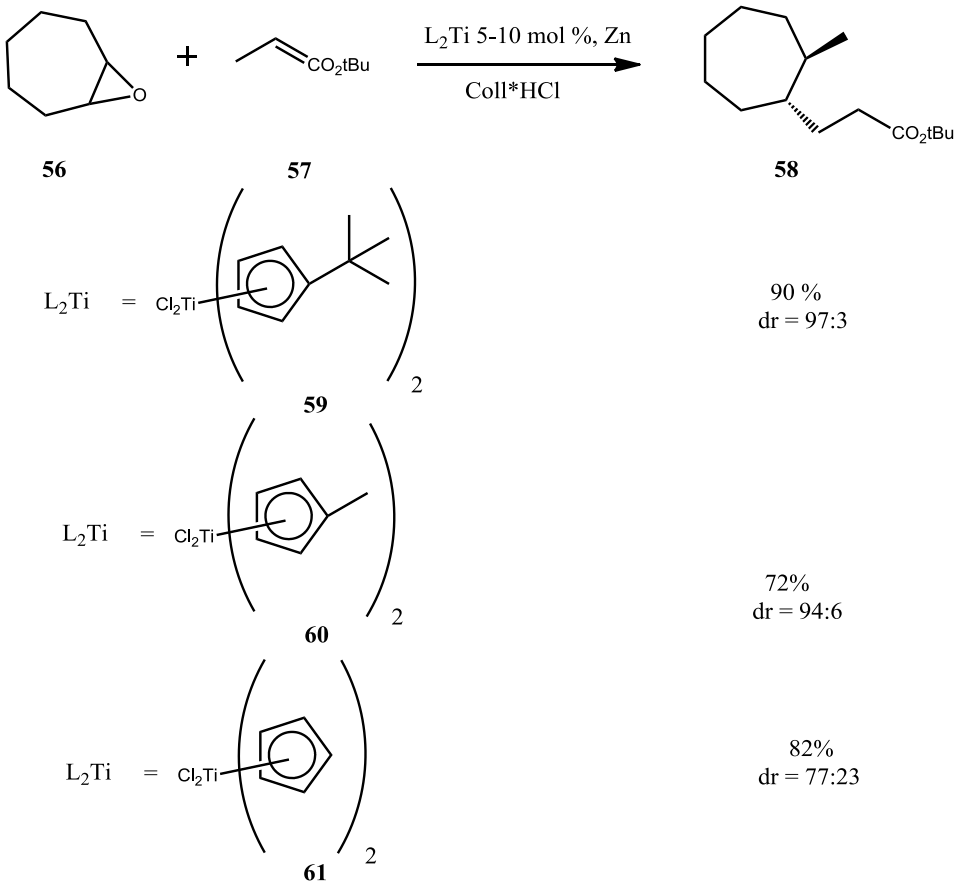

Figure 1.24. Titanocene-mediated intermolecular addition of α-β-unsaturated carbonyl compounds.

1.4.3.4 Cyclization Reactions

Many natural products can be synthesized by intermolecular cyclization. Unlike in the intermolecular addition, one or more multiple bonds are cyclizised in the intermolecular cyclization. Because of high speed of the 5-exo cyclization, this reaction is an ideal way for a radical cyclization. Additionally, the 6-endo cyclization and slower 6-exo cyclization have attracted less attention due to their kinetic results.[160] A significant advantage of 5-exo cyclization is that a substitution of radical acceptors by electron-withdrawing groups is not required, which is necessary in the previously discussed

intermolecular reaction. In this context, *Clive* and his group[161,162] have reported the synthesis of propellanes and triquinanes, e.g., ceratopicanol. Another study was done by *Roy et. al.*[163,164], who established the synthesis of a number of tetrahydrofuran-derivatives ring of natural products, for example methylenolactocin and protolichesterinic acid.

In general, the 5-exo cyclization is achieved by a spiro-cyclic epoxide as a starting reagent. In a further step, the epoxide is opened and carbon-centered radical is generated. In this manner, intermolecular 5-exo cyclization can be given as the first example, which has a terminal double bond in the α-positions (**62**) (Figure 1.25). The catalytic system can be started by the reductive opening of the epoxide using titanocene(III) chloride and yields the alcohol (**66**). The protonation of titanium-carbon and titanium-oxygen bonds is a key-step for this methodology, which is generally split by collidine hydrochloride acids. The cyclization products can be varied by using substituted cyclopentadienyl ligands, which are realized by an enantioselective opening of *meso*-epoxides.[165,166]

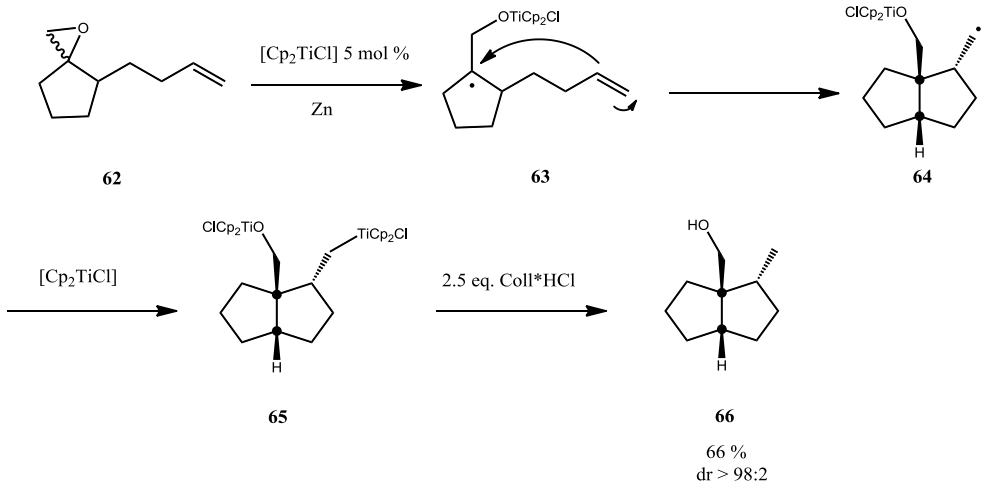

Figure 1.25. Titanocene-catalyzed intermolecular 5-exo cyclization.

1.4.3.5 Tandem Cyclization Reactions

A tetra-substituted alkene can be given as an example for carbocyclic and heterocyclic products by 5-exo cyclization[167] (Figure 1.26). In these types of reactions, the entire reaction sequence can be described as a domino cyclization addition reaction. If the cyclization is carried out with the terminal alkene (**67**) residues in α-position to the spiro-cyclic epoxide, then a tetra-substituted alkene with excellent diastereoselectivity, usually >97:3, can be obtained. No products have been observed from undesired reactions (< 3%).

In this respect, titanocene(III) chloride can catalyze the cyclization of suitable unsaturated epoxides, which proceed by intermolecular additions to α-β-unsaturated carbonyl compounds. In this case, *Gansäuer* and coworkers have devised an intermolecular synthesis of tri- and tetra-substituted olefins, which result in the formation of the polycyclic tetrahydrofuran (THF) derivatives in highly stereoselective yield. They have used tributlystannyl- and phenlyselenyl-substituted vinyl radicals for this purpose. The reductive opening of epoxide is formed by intermolecular cyclization of the

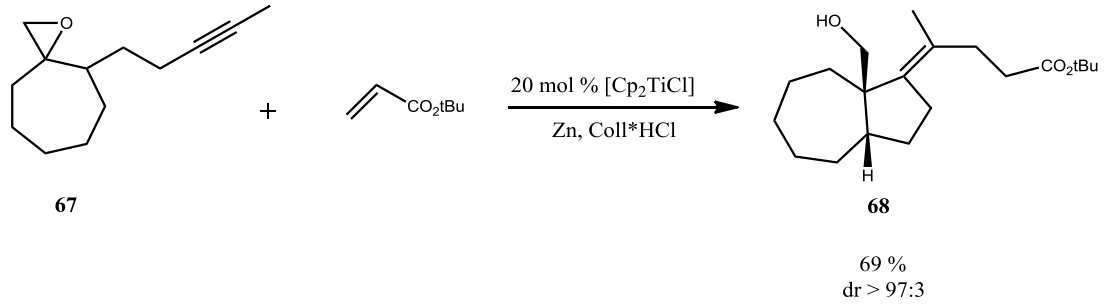

Figure 1.26. Titanocene-mediated tandem reaction with alkene.

intermediate. The key point of this reaction is the choice of the solvent. The solvent must feature a lower hydrogen atom donor propensity than THF in order to avoid reduction of vinyl and aryl radicals by abstraction of a hydrogen atom from the solvent. Under these conditions products of simple cyclization can be obtained. The domino cyclization-addition reaction results in the desired products in high yields. However, the undesired product can occur from intermolecular addition without cyclization or from simple cyclization in very small amounts.[167] The scope of this domino cyclization-addition reaction can be also extended to the heterocyclic products (**72**). In this example, N,N-dimethylacrylamide (**70**) is a radical acceptor in the solution (Figure 1.27).

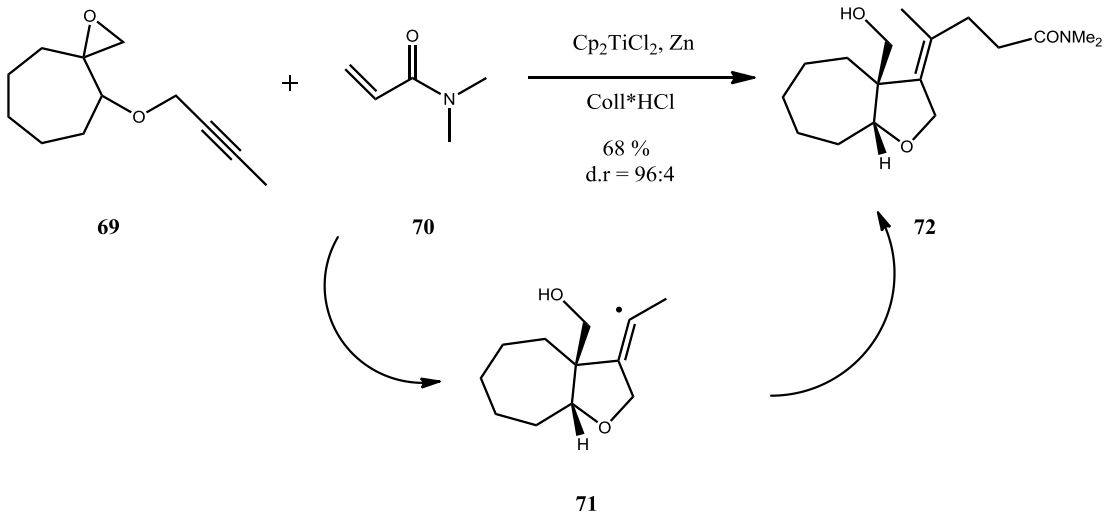

Figure 1.27. Radical domino cyclization-addition reaction involving vinyl radicals.

At the end of this section, a natural product synthesis is given as a last example, which is a γ-steroid from the plant Nolana rostrota. *Oltra et al*. have represented the tandem-cyclization successfully in the synthesis of Labdane diterpenoids that show interesting pharmacological properties such as antibacterial, antifungal, antiprotozoal or anti-inflammatory properties (Figure 1.28). Their strategy consists of three stages: (a) the selective epoxidation of the commercial available polyenes (**73**), (b) titanocene(III)-catalyzed cyclization of epoxypolyprenes (**74**), in which the double bond initially cycles in the ε-position (c) palladium-mediated remote functionalization of the equatorial methyl group. The 6-endo cyclization is followed by a further 6-endo cyclization, which results in bicyclic diterpenoids (**75**).[168]

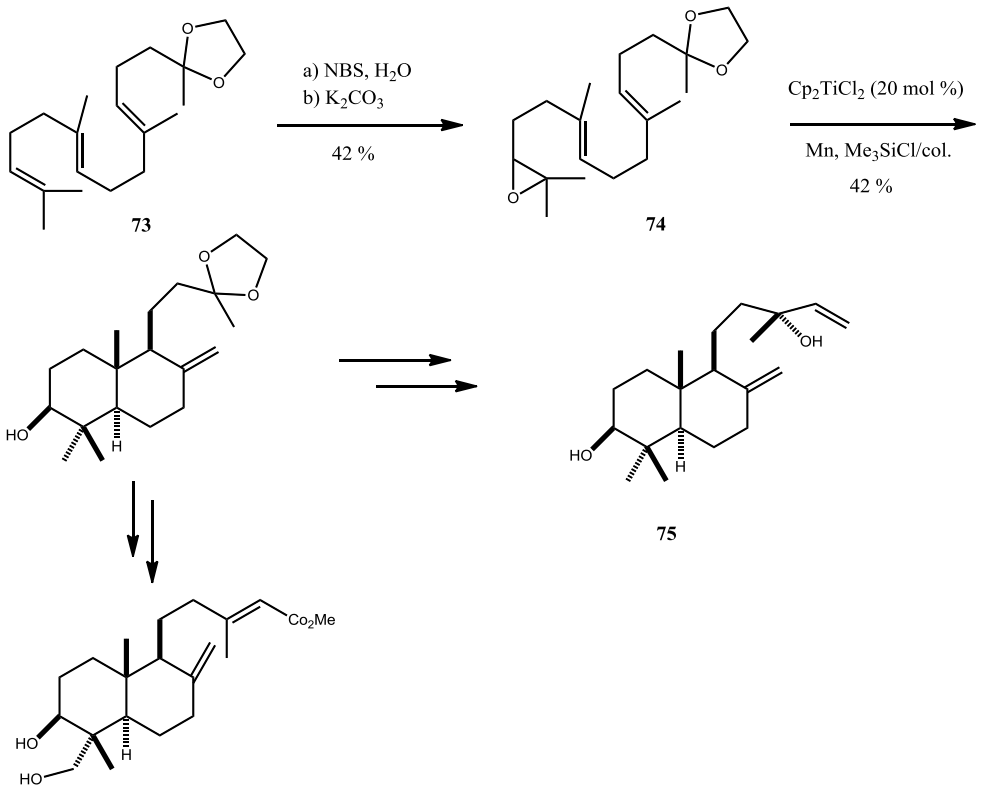

Figure 1.28. Titanocene-catalyzed synthesis of the diterpenoids.

1.5 4-*exo* Cyclization Reactions

As is outlined in chapter 1.4.3, unlike the cyclization of 3-member rings, 4-member rings, 7-member rings and 8-member rings, the cyclization of 5-member rings and 6-member rings is a common reaction catalyzed by titanocene(III) chloride in the presence of epoxides.[169] However, the synthesis of small rings, such as cyclobutanes and their derivatives or cyclopropanes, is usually difficult with respect to the kinetics.[170] The rate constant for the 3-member ring opening is 10^8-10^9 s^{-1} at 25 °C. It is clear from this value that the ring opening of the intermediate cyclopropylcarbinyl radicals is amongst the fastest radical reactions (Figure 1.29a). The rate constant of the 4-exo cyclization is 10^1 s^{-1}, so the ring closure of pentenylcarbinyl radicals is the slowest radical reaction due to its low rate. However, the ring opening of the cyclobutylcarbinyl radical is fast, based on the rate constant amount of 10^3-10^4 s^{-1} (Figure 1.29b).[171-174]

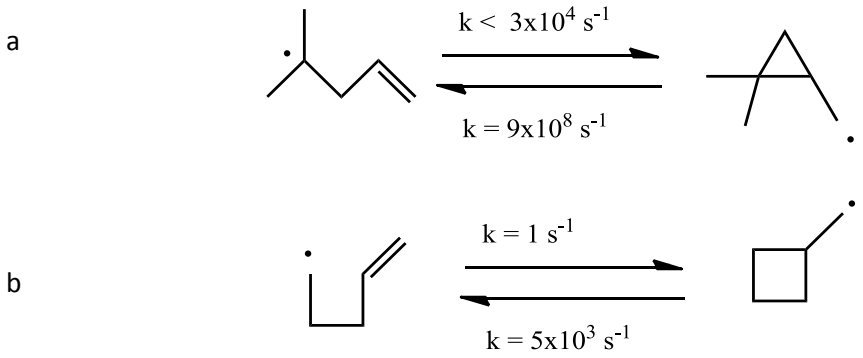

Figure 1.29. Kinetics of the 3-*exo* (a) and 4-*exo* cyclization (b).

1.5.1 The *gem*-dialkyl Effect

Interestingly, the addition of *gem*-dialkyl groups onto the pentenyl chain causes the fast cyclization of the pentenylcarbinyl radicals, which are substituted in the α-position to the carbon-centered carbon atom (k = 10^6 s^{-1}). The reason for the acceleration arises from the replacement of the hydrogen atoms with alkyl groups on the carbon atom including the two reacting centers. This effect was first explained by *Ingold* and *Thorpe* in 1915.[175,176] The repulsion of the opposing methyl groups to each other on the carbon atom give rises to an increase of the bond angle in β-position and simultaneously a decrease of the bond angle in the α-position. As a result, the carbon-carbon-carbon angle of propane is 112.2°; this angle is reduced to 111.1° and 109.5° in isobutene and in neopentane, respectively (Figure 1.30). The first example of this effect is observed in the cyclization of chlorohydrins to epoxide, where the rate of the ring closure is accelerated 200-fold due to the replacement of the methylene hydrogens with a *gem*-dialkyl group. *Allinger* and *Zalkow* have demonstrated the *gem*-dialkyl effect in the formation in the cyclohexenes from hexanes in 1960.[177] They reported that the enthalpy favors the cyclization of substituted hexanes. There are two reasons for this result. Firstly, the number of *gauche* interactions of the open chain substrate is increased. Secondly, entropy is increased because the branching is reduced in the rotation in the open chain more than in the ring.

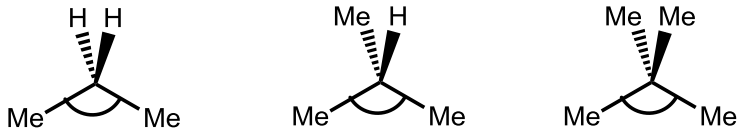

112,2° 111,1° 109.5 °

Figure 1.30. Thorpe-Ingold effect.

Although the radical cyclization of the 4-member ring is unusual, cyclobutanes and their derivates have generated increasing interest in synthetic organic chemistry, because the small ring cyclizations are important building blocks in organic synthesis and constitute a structural motif in natural products, such as in marine materials or terpenes. In 1973, the first study of radical 4-exo cyclization was presented. *Picardi et al.*[178] described the free radical reaction of carbon tetrachloride with 3,3,4,4-tetrafluoro-1,5-hexadiene, which was resulted tetrafluorocyclobutane. The calculation by *Newcomb* has shown that the carbon atom must be as a C2-quarternary and the functional of alkene on terminal must be possessed an electron withdrawing group for a successful radical cyclization.[173] Nevertheless, Cyclobutanes are most often prepared using photochemical [2+2] cycloaddition processes.

Cyclopropane does not as frequently occur in the synthesis of natural products as cylclobutane, which can be prepared by the addition of carbenes to alkenes. For example, the addition of a divalent carbon to unsaturated carbon-carbon compound would be a direct method for the formation of the 3-member rings, which is known as the Simmons-Smith-Reaction.[179] Cyclopropane can be also formed when the transition metal-catalyzed decomposition of diazo compounds with substitutuents is added to the double bond of the carbene.[180] Otherwise, the formation of cyclobutane is carried out via pericyclic reactions, nucleophilic substitutions or addition reactions. Among them, the intramolecular addition on the acceptor systems and the nucleophilic homolytic substitution are known such as intramolecular dimerization of a diradical.[181,182] However, the intermolecular nucleophilic substitution or addition reaction is commonly used in modern synthetic chemistry. The success of this methodology depends on the understanding of the rate constants of the various competing radical processes.

1.5.2 Examples of 4-*exo* Cyclization

The formation of cyclobutane can be accomplished by using γ-formyl-epoxide and stoichiometric amounts of titanocene chloride. After reductive opening, the radical center is converted to corresponding cyclobutane products (**77**) with an aldehyde function (Figure 1.31).

In addition to this example, radical cyclizations can be also started by other metals, for example samarium. As *Kagan* and coworkers found, samarium diiodide has been used for many applications in synthetic and radical chemistry.

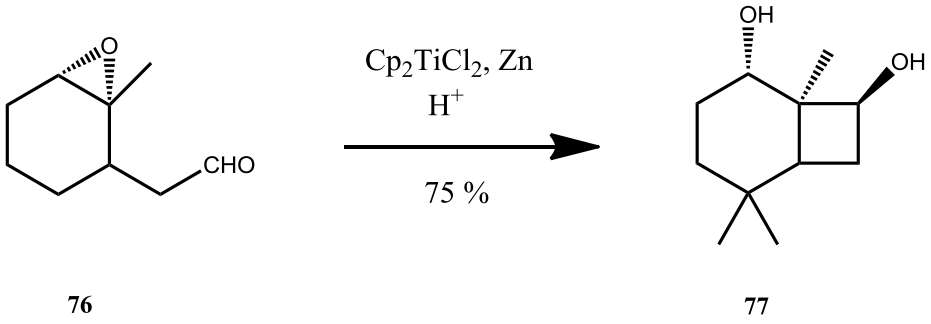

76 **77**

Figure 1.31. Titanocene-mediated 4-*exo*-cyclization of the γ-carbonyl epoxide.

Samarium diiodide is an incredibly versatile reagent, which can not only be used for 3-*exo* cyclization but also for 4-exo cyclization. *Procter* has proven that the cyclobutanols can be produced using radical ketyl-olefin cyclization by samarium diiodide. The samarium-mediated 4-exo-trig of α,β-unsaturated aldehydes (**78**) can produce anti-cyclobutanol products (**79**) in a stereoselective manner (Figure 1.32). Interestingly, the ester substrate gives the *anti*, *anti*-diastereoisomer as the only product in good yield. However, the sulfone substrate gives the corresponding *anti*, *anti*-cyclobutanol product by uncyclized aldehyde, which does not have the α-benzyloxy group. Also, the yield by using the ester was higher than the yield by using the sulfones.[183-186]

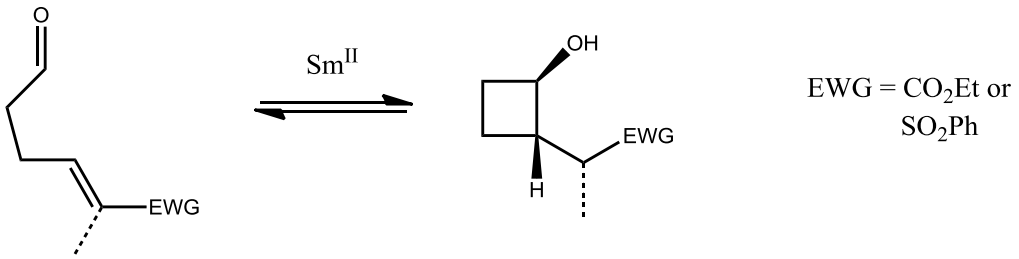

78 **79**

Figure 1.32. SmI_2-mediated 4-*exo* cyclization.

Another example for the cyclization of the 4-*exo*-trig comes from Nature. Pestalotiopsin A has been investigated by *Procter*[187] in 2001; it can be isolated from the endophytic fungus of Taxus brevifolia, the Pacific yew. The terpene derivative possesses an oxatricyclic structure in Nature products and has shown immunosuppressive properties and cytotoxicity activity. He has described the approach to prepare the functionalized 2-oxabicyclo[3.2.0]-heptane core of the Pestalotiopsin. This synthesis consists of five stereocontrolled steps, which are based on a samarium diiodide-mediated 4-*exo*-trig cyclization and trans-lactonization process trigged by the addition of the alkylterbium reagents to a cyclobutane intermediate. The corresponding γ,δ-unsaturated aldehyde (**80**) is converted into the *anti*-cyclobutane product (**81**) by using samarium(II) diiodide as a catalyst in a mixture of THF/MeOH (Figure 1.33).

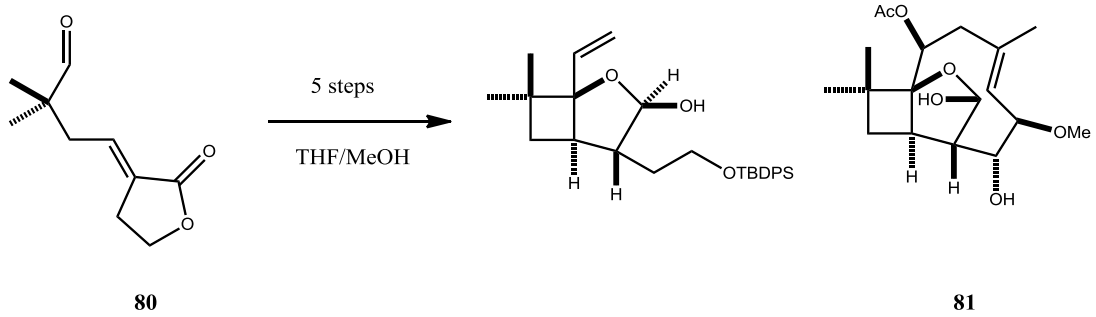

80 **81**

Figure 1.33. Synthesis of Pestalotiopsin A by samarium-mediated 4-*exo* cyclization.

In the early 1990s, *Jung* reported an efficient preparation of four-membered rings by radical cyclization.[188,189] The 4-*exo* cyclization by using tributlystannane is accompanied with an unusual oxidation of a dialkoxyalkyl radical and produces a vinyl transfer to give an ester in good yield (Figure 1.34a). Another four-membered ring formation using of tributlystannane has been demonstrated by *Ogura*.[190] In this context, the substitution of the methylthio and *p*-tolylsulfonyl groups stabilize the resulting radical (**82**), where the corresponding radical undergoes additional stabilization by electrostatic interaction between the methyl hydrogen and sulfonyl oxygen (Figure 1.34b). [191-194]

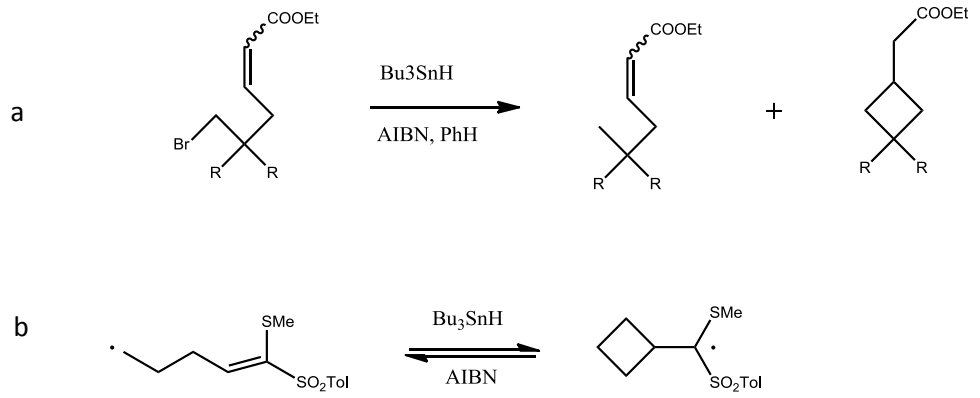

82 **83**

Figure 1.34. 4-*exo* cyclization by Jung *et al*. and by Ogura *et al.*

As described in the previous section, the cyclization of cyclobutane can also take place using titanocene(III) chloride. In this context, *Gansäuer* and coworkers have described a catalytic cycle of 4-*exo* cyclization (Figure 1.35).

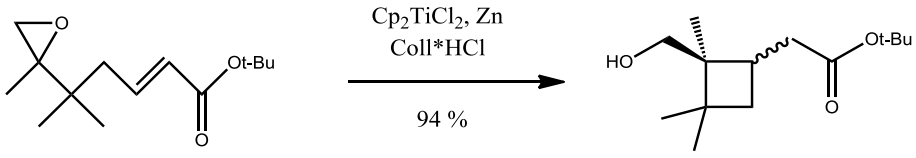

84 **89**

Figure 1.35. Titanocene-mediated 4-*exo* cyclization by Gansäuer.

The catalytic cycle is summarized in Figure 1.35's and outlined exhaustively in Figure 1.36. The catalytic cycle starts with the reduction of titanocene(IV) chloride to titanocene(III) chloride by Zinc. In the first SET step, epoxide (**84**) is reductively opened using titanocene(III) chloride and a quaternary carbon-centered radical (**85**) is generated, which is durable enough for the cyclization of the cyclobutylcarbinly radical (**86**). In the second SET step, titanoncene(III) chloride is reduced again. This step is irreversible and thus the equilibrium moves to the product side. In the final step, the hydrolysis of the titanium-oxygen bond occurs by using collidine hydrochloride. Subsequently, the cyclobutane (**89**) results and the released titanocene(IV) chloride is reduced to titanocene(III) chloride again in the catalytic cycle.

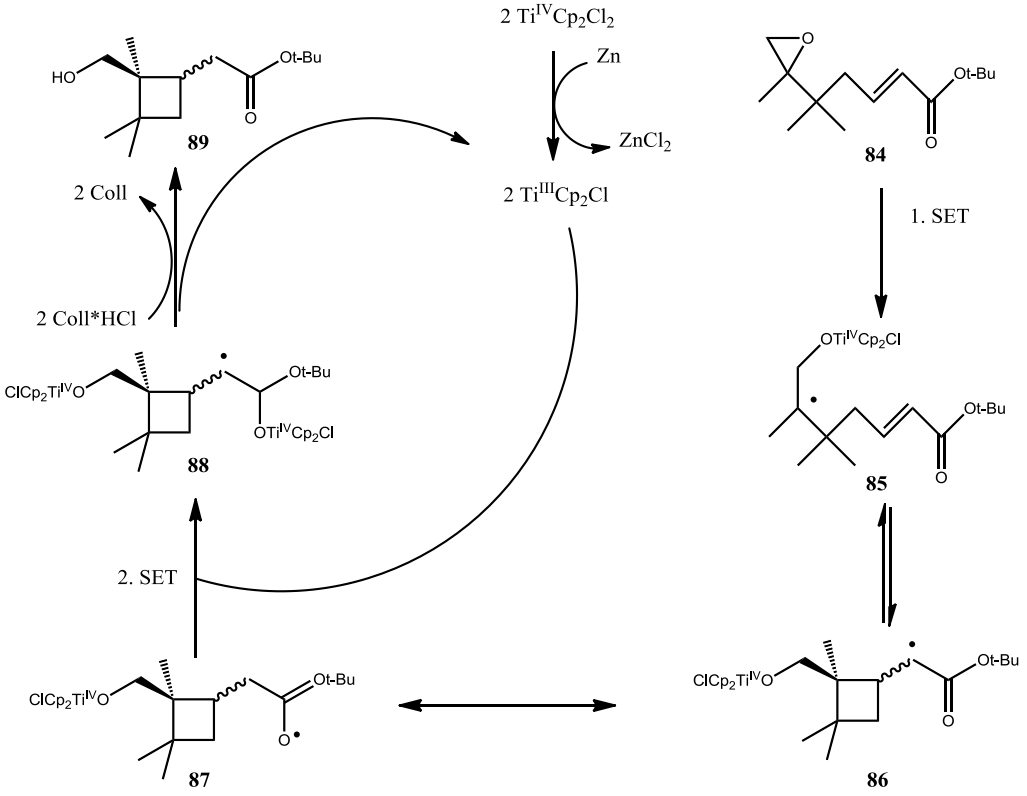

Figure 1.36. Titanocene-mediated catalytic cycle of the 4-*exo* cyclization.

As can be seen from all of the examples, the formation of cyclobutanes by radical cyclization results in good yields, provided suitable molecular structures and reaction pathways are used. Despite the 4-*exo* cyclization being the slowest free-radical reaction and the corresponding ring opened reaction being much faster, a considerable number of examples are present in the literature, which includes a successful 4-*exo* cyclization.

1.6 Hydrogen Atom Transfer (HAT)

Hydrogen atom transfer is a key step in many chemical and biological reactions and involves two elementary particles, a proton and an electron. Traditional HAT reactions have an abstracting group, which is a p-block radical such as t-butoxyl from organic molecules. In contrast, the transition metal complexes that abstract $H^{\bullet}$ typically have an oxidizing metal center to accept the electron and a basic ligand to accept the proton.

The HAT process from accessible hydrogen atom donors can be also used as a step in the reduction of carbon-based radicals. In this context, water would be used as the hydrogen atom source, which serves as a remarkable, safe and cheap HAT reagent. Nevertheless, it is generally believed that this potential HAT reaction is avoided by the carbon-centered radical due to the high dissociation energy (BDE) of the H-OH bond (around 118 kcal/mol). However, some years ago, *Cuerva J.* and coworkers demonstrated that water acts as an excellent hydrogen atom donor in the presence of [Cp_2TiCl] towards to carbon radicals.[195] To explain their proposition, they proposed that water is coordinated to titanocene(III) as a ligand; the H-OH bond is weakened and the corresponding aqua-complex (**90**) acts as an efficient hydrogen atom donor (Figure 1.37).

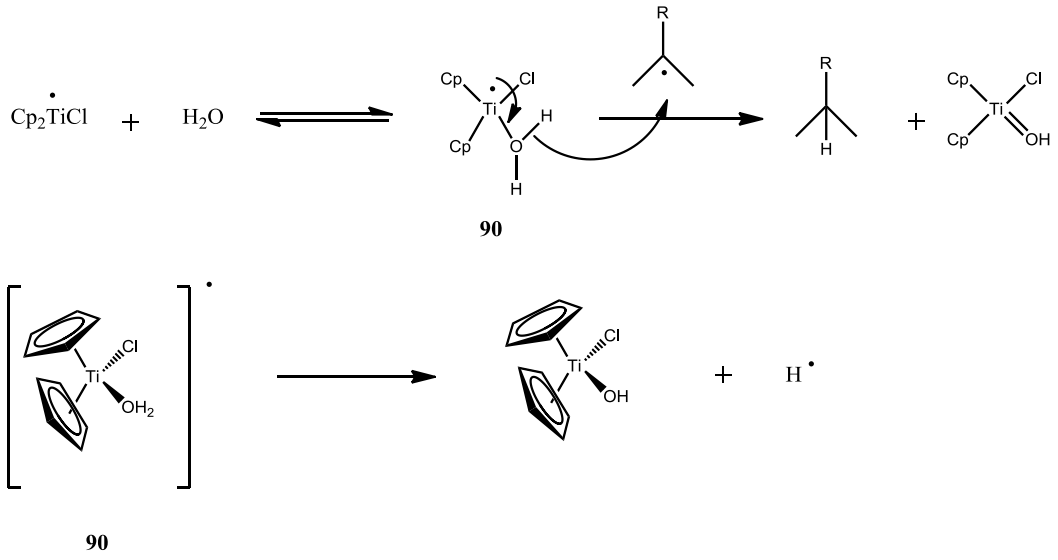

Figure 1.37. Mechanism of carbon-centered radical reduction through an aqua complex.

The unprecedented HAT reaction from water facilitate the efficient synthesis of alcohols from epoxides with anti-Markovnikov regiochemistry[196], the control of the final step in titanocene-catalyzed radical cyclization, which is useful for the synthesis of the polycyclic terpenoids[5,6,150,168,197], and the new hydrogenation reaction of alkenes and alkynes.[198] The [Cp_2TiCl]/H_2O-mediated asymmetric epoxidation the reductive epoxide opening can especially be an alternative with complementary stereoselectivity of hydroboration-epoxidation for the enantioselective synthesis of anti-Markovnikov alcohols from alkenes.[199] In all of these applications, water can be used as a safe and cheaper HAT reagent.

In addition, hydrogen transfer from water, mediated by samarium(II) diiodo or titanocene(III) chloride, can generate transient ketyl radicals from aromatic ketones, yielding either pinacol-coupling products or reduction products (alcohols), which are based on a conventional House's reduction

mechanism.[200] In this context, the carbonyl compounds mediated by $[Cp_2TiCl]/H_2O$ can be better described as unique HAT processes. The metal-mediated carbonyl reductions in protic media are often preceded by the HAT mechanism.

Consequently, the success of the titanocene(III) chloride aqua complexes are based on two features, which can serve as an excellent class of HAT reagent: firstly, excellent binding capabilities between water and titanocene(III) complexes and secondly, a low activation energy for the HAT step.

However, the transfer of hydrogen atoms of water onto free radicals can be mediated by complexes of the trialkyl boranes. Organoboranes can be easily prepared via hydroboration of alkenes.[201] This reaction is based on an anti-Markovnikov addition of water to alkenes. Under initiation of peroxide or other oxidizing reagents, alcohols are generated. Although the procedure for the reduction of the double bonds is more attractive, the reduction of alkylboranes is less common to alkanes. In this manner, *Renaud P.*[202] has reported a method for the reduction of organoboranes with alcohols under mild conditions, where his strategy consists of complexation of the O-H bond of alcohol with a Lewis acid and thus the release of hydrogen atoms.

1.7 Oxaphosphirane

The epoxide SET ring-opening mediated by titanium(III) species can be applied to oxaphosphirane. Unlike epoxide, the evolution of the oxaphisphirane is relatively new. The oxaphosphirane ring is of considerable interest due to its analogy to the oxirane rings, which are important building blocks for oxaphosphirane chemistry.

In 1978, $\sigma^4\lambda^5$-oxaphoshiranes (**93**) were first synthesized by *Röschenthaler* and *Schmutzler*[203] via a [2+1] cycloaddition reaction of iminophosphine derivative (**91**) and hexafluoroacetone (**92**), which has been characterized through spectroscopy (Figure 1.38).

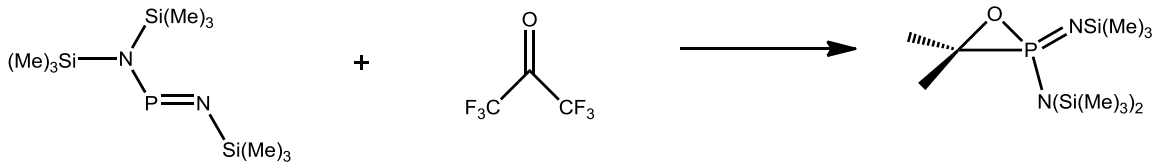

91 **92** **93**

Figure 1.38. The first synthesis of oxaphosphirane.

Four years later, *Bartlett*[204] found a $\sigma^4\lambda^5$-oxaphoshiranes phosphorus-oxide derivate in the ring expansion reaction. In 1988, the monomer-dimer equilibrium of a $\sigma^4\lambda^5$-oxaphoshiranes was investigated by *Boisdan* and *Barrans.*[205] In 1990, *Mathey* and coworkers have described oxaphosphirane transition-metal complexes, which were prepared by epoxidation of phosphaalkene complexes with meta-chloroperbenzoic acid[206] (**94** in Figure 1.39). This procedure is based on the oxidation of a series of phosphaalkene phosphorous-complexes, which often appears for free phosphaalkenes and was avoided by blocking the lone pair in the phosphorous by a metal carbonyl fragment ($W(CO)_5$).

In 1994, *Streubel* and coworkers discovered a new route in order to synthesize the oxaphosphirane complexes. They gained novel access to oxaphosphirane tungsten complexes using a transient Li/Cl phosphinidenoid tungsten complex, which reacted *in situ* with benz- or isobutyaldehyde[207,208] (**95** in Figure 1.39). However, the Streubel group also presented another method, which generates transition-phoshinidenoids under mild conditions and uses them selectively for substitution reaction and responses of end stage phosphinidenoid complexes[209] (**96** in Figure 1.39).

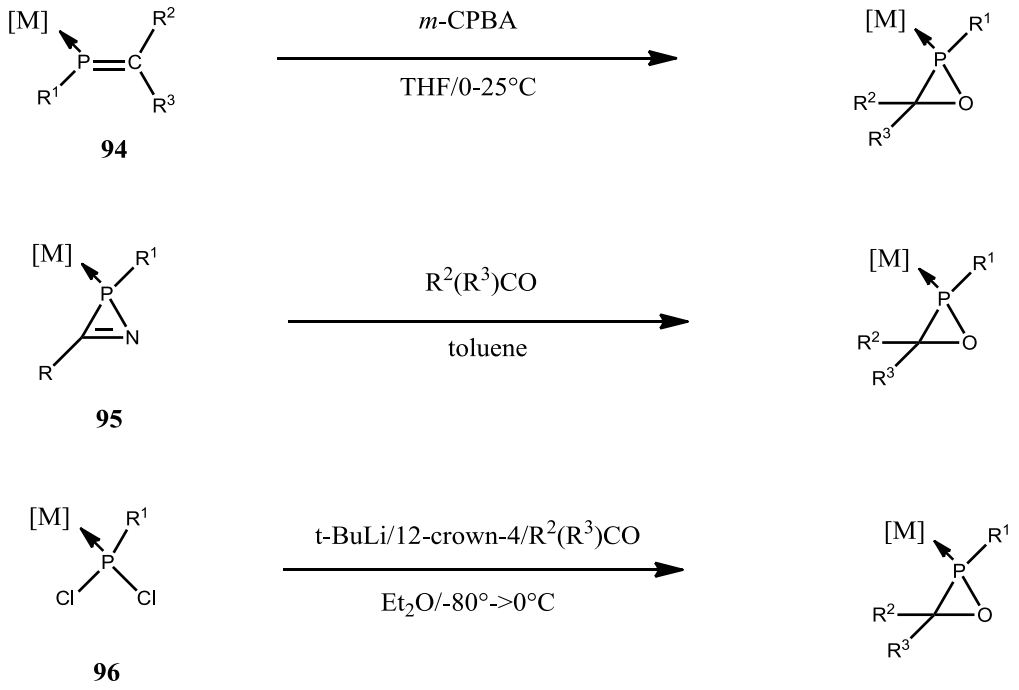

Figure 1.39. Established synthetic route to oxaphosphirane complexes.

The deprotonation of chlor-phosphane complex (**97**) with Lithiumdiisopropylamid (LDA) in the presence of [12] crown-4 selectively leads to compound (**98**) (Figure 1.40). In order to prove the existence of phoshinidenoid-complex, they showed that in the presence of the methyliodide, the obtained p-methyl-substituted chlorphosphane is the only phosphorus-containing product, and thus an intermediate incidence of complex (**98**) is proven beyond a reasonable doubt.

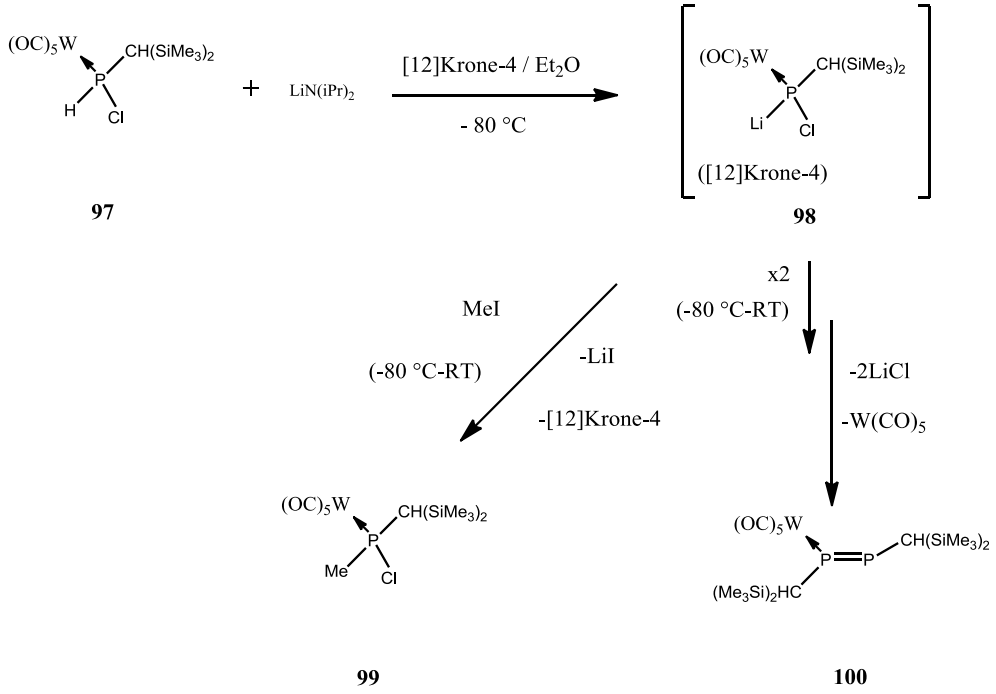

Figure 1.40. Synthesis of phosphanylidenoid complex **99**.

In summary, Streubel's group demonstrated two ways in which transient phoshinidenoid complexes are produced selectively under mild conditions by deprotonation or by an exchange of the chloride/lithium. In addition, based on DFT calculations, a mechanism was proposed starting with a P-O bond cleavage in the parent oxaphosphirane.[210,211]

1.8 The Aim of the Work

Despite the described advantages of the titanocene-catalyst, curiously enough, no mention is made in the literature about their physical molecular properties and their exact electronic structure.

The aim of this work is to elucidate the electronic structure of the paramagnetic titanocene(III) complex and the exact reaction mechanism of the epoxide ring opening reaction, which is achieved by titanocene(III) chloride as the catalyst. This allows for an unambiguous identification of the reactive intermediates.

Electron Paramagnetic Resonance (EPR) is a spectroscopic method that is used to investigate paramagnetic electronic states. The sample is placed in a magnetic field and exposed to microwaves of the appropriate frequency, which generates resonant transitions in the electronic spin system. The information of the electronic and geometric structure and the bonding of ligands, dynamics and concentration dependence can be investigated by using EPR methods. Most importantly, the paramagnetic species can be identified. Consequently, EPR spectroscopy is widely used.[212-216]

In addition, EPR spectroscopy is one of the most sensitive techniques for the detection of free radicals. These are paramagnetic owing to the unpaired electrons, which have a magnetic moment.

In many chemical reactions and in a number of biochemical processes, intermediate free radicals are formed. These radicals are highly reactive, but in general their quasi-stationary concentration and their life time are very small. These are not often sufficient for direct detection by EPR spectroscopy to demonstrate the formation of such radicals. However, they can still detected by using spin traps. Such spin trap molecules are diamagnetic and react with reactive free radicals to form stable nitroxide radicals.

In this work, the EPR studies are used to obtain information about g-values, the hyperfine coupling and the quadrupole interaction, which is obtained from cw-EPR and pulse EPR techniques. In order to characterize titanocene(III) chloride complexes with bound small molecules such as water or methanol, epoxide or oxirane or phosphanylidenoid complexes, the interactions between the electron spin S of the unpaired electron and nuclear spin I of the direct (strongly coupled) or indirectly (weakly coupled) neighboring atoms are measured. These interactions provide important information about the structure of the investigated complexes.

Hyperfine couplings of the hydrogen atoms of the same titanocene(III) chloride complexes have been determined by the pulsed ENDOR method. The pulsed ENDOR method, provides a.o. information about the relative orientation of the g-tensor and hyperfine and quadrupole interaction tensors.

In EPR spectra, the hyperfine couplings, which derive from the more distant nuclei from unpaired electron, cannot be resolved. The information about this coupling can be obtained by ESEEM and HYSCORE spectroscopy. We used the ESEEM method for the determination of chloride or deuterium hyperfine couplings. The 2D HYSCORE method provides better resolution in case of overlapping signals in the 1D ESEEM spectra.

This thesis is divided into eight chapters. After the introduction, in the second chapter, the theoretical foundations of EPR spectroscopy are introduced. In third chapter, the employed modern EPR- and electrochemistry-techniques are described in more detail, including a technical perspective. Also in this part, Density Functianal Theory is explained. Chapters four to seven describe the obtained results and a discussion, which have been communicated in three peer-reviewed papers. In chapter 4, experiments of the titanocene(III) chloride in the presence of water molecules are described. The resulting hydrogen atom transfer is corroborated with theoretical results. Chapter 5 describes the binding of titanocene(III) chloride and epoxide and the reaction mechanism of the epoxide ring opening reaction, which is achieved by using titanocene(III) chloride. To determine the reaction mechanism, spin trap techniques are used. Chapter 6 describes the 4-exo cyclization with theoretical, spectroscopic and synthetic perspectives. In chapter 7, information about the geometry and the electronic structure of phosphanyl radicals is reported. The bonding and reactivity of phosphanyl radicals are investigated by spectroscopic and theoretic methods. In the chapter 8, the results of this work will be briefly summarized.

2 Theoretical Fundamentals of Electron Paramagnetic Resonance Spectroscopy

2.1 History of Electron Paramagnetic Resonance (EPR) Spectroscopy

Electron paramagnetic resonance (EPR) is a spectroscopic method for studies of paramagnetic species. The theoretical description of electron paramagnetic resonance (EPR) spectroscopy is very similar in concept to the more familiar nuclear magnetic resonance spectroscopy (NMR). Although they have the same basic principles, in the case of EPR, the magnetic moments arise from electrons, whereas they are derived from nuclei in NMR. Since the discovery of this method by E. K. Zavoisky, who used samples of $CuCl_2.2H_2O$, this method has evolved to an important tool in chemistry, physics, biology and materials science.

This chapter explains the theoretical basis of EPR spectroscopy, which is necessary for understanding the measurements performed here.

2.1.1 Electron Spin

The EPR spectroscopy is based on measurements of the interaction between electromagnetic radiation and the magnetic moment of an electron, the electron spin. In 1920, an experiment in basic quantum mechanics by Otto Stern and Walther Gerlach showed that the magnetic moment of the electron in a magnetic field can take only discrete orientations. The Stern-Gerlach experiment involves a beam of particles through an inhomogeneous magnetic field and observing their deflection. Five years later, Goudsmit and Uhlenbeck demonstrated that there are previously unknown quantum numbers of the electron, the spin quantum number needed. It characterizes the “angular momentum” of the electron, its so-called spin.

Each angular momentum with a magnetic moment associated, which can be written:

$$\vec{\mu}_{spin} = \gamma \vec{s} \tag{2.1}$$

The proportionality factor is known as the magnetogyric ratio γ. Equation (2.1) describes only a portion of the total magnetic moment of an electron, because in addition to the spin the orbital angular momentum still exists. The eigenvalues of the spin operators are half-integer multiples of Planck’s constant, so that operates as a convenience to the product. This is given by:

$$\gamma\hbar = g \cdot \mu_B \tag{2.2}$$

where μ_B is the Bohr magneton. The so-called g-factor of the free electron can be determined as 2.00232; in organic radicals, the g-factor differs only slightly from this value.

If one applies a homogeneous magnetic field B_0, the electron spins in the sample take a parallel (M_s = + 1/2) or anti parallel (M_s = - 1/2) towards the outer magnetic field. There is therefore to a Zeeman splitting of energies with

$$\Delta E = g \cdot \beta \cdot B_0 \tag{2.3}$$

and the formation of the Zeeman levels:

$$W_\alpha = \frac{1}{2} g \cdot \beta \cdot B_0 \tag{2.4}$$

$$W_\beta = -\frac{1}{2} g \cdot \beta \cdot B_0 \tag{2.5}$$

The Zeeman splitting is proportional to the external magnetic field B_0.

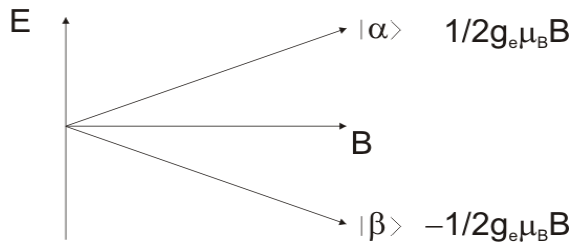

Figure 2.1. Zeeman splitting of the energy of an unpaired electron in a magnetic field B_0.

The energy difference between W_α and W_β results in a thermodynamic equilibrium in the sample to a population difference, according to the Boltzmann distribution:

$$\frac{N_\alpha}{N_\beta} = exp\left[-\frac{\Delta E}{k_B T}\right] = exp\left[-\frac{g \cdot \beta \cdot Bo}{k_B T}\right] \tag{2.6}$$

k_B is the Boltzmann constant ($1.38066 \cdot 10^{-23}$ J·K^{-1}) and T the absolute temperature in Kelvin. It is clear that the population difference increases with the magnetic field strength. The transition between two levels can be achieved by irradiating electromagnetic waves reaching the microwave range. After irradiation at the resonance frequency ν_{EPR} on the sample absorption is observed, which is proportional to the population difference.

2.2 The Spin Hamilton Operator

The Hamilton operator $\hat{H}$ describes the properties of a quantum mechanical system, which includes all energy contributions of the spin system. To describe the EPR spectra certain contributions are neglected in the Hamilton-operator. In this way, the analysis of the EPR spectra is facilitated.[227]

The description of the interaction energy of a paramagnetic atom in a constant external magnetic field B_0 is given by the following spin Hamilton operator $\widehat{H}$:

$$\widehat{H} = \widehat{H_{EZ}} + \widehat{H_{NZ}} + \widehat{H_{HF}} + \widehat{H_{NQ}} \quad (2.7)$$

$\widehat{H_{EZ}}$ = Zeeman-interaction of the electron with an external magnetic field

$\widehat{H_{NZ}}$ = Zeeman interaction of the nuclei with an external magnetic field

$\widehat{H_{HF}}$ = Hyperfine interaction between the electron and the nuclei

$\widehat{H_{NQ}}$ = Nuclear-quadrupole interaction between the quadrupole moment of the nucleus and the gradient of the electronic field

In the high-field approximation with $\widehat{H_{EZ}} \gg \widehat{H_{NZ}}, \widehat{H_{HFS}}$, the electron Zeeman term represents the strongest interaction. In this approximation, the quantization axis of the electron spin is mainly determined by the electron Zeeman interaction. The influence of nuclear spins on this axis is negligibly small. Nuclear Zeeman and hyperfine interactions are often of similar magnitude. Thus, the nuclear spin quantization direction aligns along a direction of the resultant from nuclear Zeeman term and local filed. In EPR spectroscopy, a lot of information about the electronic and geometric structure of a paramagnetic compound can be obtained from the listed interactions from eq. (2.7). They provide information about the electronic ground state, the "site" symmetry, the spin density distribution, the type of atom, the distance, the type of binding and electronic field gradients, and the distribution of charge.

In the followingthe different interactions are explained briefly.

2.2.1 The Electron Zeeman Interaction

The interaction energy is indicated between the spin of a free electron and the magnetic field. The g-value generally depends on the bonding situation of the electron. Then the nucleus framework and the orbitals preferred directions in a molecule-related coordinate system are defined, and the g-value is also dependent on the direction. Therefore, the electron-Zeeman interaction can be written:

$$H_{EZ} = \frac{\mu_B}{\hbar} \cdot B \cdot g \cdot S \quad (2.8)$$

where g is the g-tensor, $\hbar$ is Plank's constant, B is the external magnetic field and S denotes the spin operator.

In general, many interactions are dependent on the direction of magnetic resonance in particular (anisotropic). According to the directions we formulate eq. (2.8):

$$H_{EZ} = \frac{\mu_B}{\hbar} B \cdot (g_{zz}S_z + g_{zx}S_x + g_{zy}S_y) \quad (2.9)$$

The effective field for the spin is not along the z-direction. To consider this effect, a symmetric g-tensor can be taken. Some tensor can be diagonalized; i.e., there is a coordinate system in which all the off-diagonal elements are zero. This coordinate system is called the principal axis system (PAS), the values on the diagonal are the main values and they can be called g_{11}, g_{22} and g_{33}. For the

description of symmetric tensors we also like to use the isotropic mean value (g_{iso}), the anisotropic (Δg) and the asymmetry η. They are given by the following equation:

$$g_{iso} = \frac{1}{3}(g_{11} + g_{22} + g_{33}) \tag{2.10}$$

$$\Delta g = g_{33} - g_{iso} \tag{2.11}$$

$$\eta = \frac{g_{22} - g_{11}}{\Delta g} \tag{2.12}$$

where the values are arranged such that η is the smallest positive number. (0≤η≤1) analogous definitions apply for other tensors.

The magnetic field vector can be expressed by the polar angle θ and ϕ in the principal axis system:

$$B = B_0 \cdot [\sin(\theta)\cos(\phi), \sin(\theta)\sin(\phi), \cos(\theta)] \tag{2.13}$$

Then we can write eq. (2.9):

$$\widehat{H_{EZ}} = \frac{\mu_B}{\hbar} B_0 \cdot [\sin(\theta)\cos(\phi) g_{11} S_x + \sin(\theta)\sin(\phi) g_{22} S_y + \cos(\theta) g_{33} S_z] \tag{2.14}$$

The quantization direction with the magnetic field direction is consistent under these conditions; exactly for $g_{11} = g_{22} = g_{33}$ (anisotropic g-tensor). In the case for for $|g_{ii} - g_{iso}| \ll g_{iso}$, a good approximation is valid, which is fulfilled almost always with organic radicals. From eq. (2.14) an effective g value can be obtained for an orthorhombic symmetry ($g_{11} \neq g_{22} \neq g_{33}$):

$$g_{eff} = [\sin^2(\theta)\cos^2(\phi) g_{11}^2 + \sin^2(\theta)\sin^2(\phi) g_{22}^2 + \cos^2(\theta) g_{33}^2]^{1/2} \tag{2.15}$$

This equation allows a geometric interpretation of the tensor by an ellipsoid, which presents three axes g_{11}, g_{22} and g_{33} in X, Y and Z directions. Then, g_{eff} is precisely the length of a vector from the origin to the surface with the polar angles θ and ϕ (Figure 2.2).

In transition metal complexes, the g-value is largely determined by the nature of the directly coordinated ligands to the central ion, which includes information about the symmetry and electronic structure of the paramagnetic metal ion. In disordered powder systems or frozen solutions, the molecules have a statistical distribution of the directions of their g-tensor axis with respect to external magnetic field B_0. Due to the rapid movement of molecules in the liquid, only an isotropic average g_{iso} is observed. However, this average differs from the general g-value of the free electron, because the spin-orbit coupling (SOC) is a small admixture of orbital angular moment. Such mixtures of various interactions are generally relevant when interactions are similar in magnitude or if there are nearly degenerate states. SOC effects are large when two orbitals have an energy difference, which is not much larger than the electron Zeeman energy.

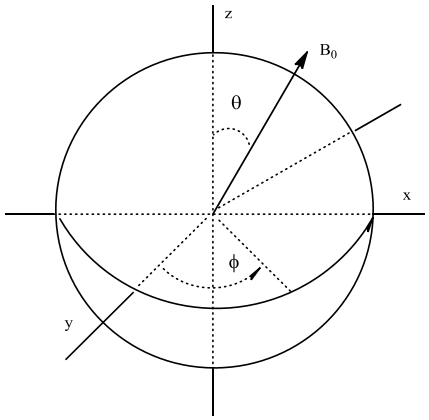

Figure 2.2. Schematic representation of an axial ellipsoid with the principal axes of the g-tensor and its dependence on the angle θ.

2.2.2 Nuclear-Zeeman Interaction

The electron spin is coupled to the nuclear spins by the hyperfine interaction. There are commonly three interactions in the used magnetic field of a similar magnitude: the hyperfine interaction, the nuclear-Zeeman interaction and the nuclear quadrupole interaction. In solution they are not generally more relevant. Because the anisotropic parts of all the interactions average out, the quantization direction of the nuclear spins are determined only by the nuclear-Zeeman interaction and is parallel to the magnetic field axis. With this information, the behavior of the electron spins can be described precisely without knowing the nuclear spin. The situation is different in the solid state, where the quantization direction of the nuclear spins can be determined through a combination of all three interactions. Because the quantization affects the observed hyperfine splitting and the transition probabilities, then the nuclear-Zeeman interaction and nuclear quadrupole interaction must be included in the spin-Hamilton. Even interactions that do not influence the quantization direction must be considered when the spectra of the nuclear spins over the electron spins are detected by double resonance methods.
The nuclear-Zeeman interaction can be described as follows:

$$H_{NZ} = -\frac{g_n \beta_n \widetilde{B_0}}{\hbar} I \qquad (2.16)$$

where g_n and I are the designated nuclear g-factor and the nuclear spin operator, which are inherent properties of a nucleus, respectively.

The nuclear-Zeeman interaction usually has little influence on the EPR spectrum, which can be neglected in the analysis of EPR spectra, unless it is of the same order of magnitude as a resolved hyperfine coupling of the same nucleus. In the case of ESEEM or ENDOR spectroscopy, the nuclear-Zeeman interaction becomes important and can be used to assign the hyperfine couplings to elements.

2.2.3 Hyperfine Interaction

The interaction of the magnetic moment of the electron spin S with the local magnetic field, which is generated by the neighboring nuclear spin I, causes the hyperfine splitting. The hyperfine interaction, which is between an electron and a nuclear spin, term of the Hamiltonian is given by

$$H_{HF} = \tilde{S}AI \tag{2.17}$$

where A is the sum of the isotropic part (the Fermi contact interaction) and the anisotropic dipole-dipole coupling term (electron-nuclear).

The Fermi-contact interaction can be written:

$$H_{hfi,iso} = \sum_k a_{iso,k} S I_k \tag{2.18}$$

If both spins are quantized along the magnetic field, the individual summands are simplified to $a_{iso,k} S_z I_{kz}$. The Fermi-contact interaction is due to the non-zero probability to find the electron at the nucleus. This happens only when an unpaired electron is in an s orbitals, which are both spherically symmetric and the Fermi contact term is necessary isotropic. The isotropic coupling a_{iso} is calculated by:

$$a_{iso} = \frac{2}{3}\frac{\mu_0}{\hbar} g_e \beta_e g_n \beta_n |\Psi_0(0)|^2 \tag{2.19}$$

The isotropic hyperfine coupling a_{iso} is caused by the electron spin density in the s orbitals and thus provides information about the spin density distribution in paramagnetic compounds. The factor $|\Psi_0(0)|^2$ is the probability to find the electron at the nucleus in the ground state with wave function Ψ_0. The hyperfine coupling of the different isotopes of the same element is proportional to corresponding g_n values. When the unpaired electron resides in p, d or f orbitals such as transition metal complexes, they do not contribute to Fermi contact interaction; spin density at the nucleus is induced by configuration integrals or the spin polarization mechanism.

The isotropic hyperfine interaction plays a major role for determining the electronic structure of organic radicals. This means that in π-radicals (the unpaired electron in a π-orbital) the isotropic hyperfine coupling is proportional to non-zero probability of electrons at the neighboring carbon atom.

The anisotropic part of the hyperfine interaction results from the interaction between the magnetic moments of the electron and the magnetic moments of the nuclei. This electron-nuclear dipolar-dipolar interaction is analogous such that there is a dipole-dipole interaction between electrons spins. The Hamiltonian for the anisotropic dipolar-dipolar interaction is given by:

$$H_{hfi,DD} = \sum_k S T_k I_k \tag{2.20}$$

with the dipolar coupling tensor T. In general, the matrix element T_{ij} of the total anisotropic hyperfine coupling tensor T is given with the ground state wave function:

$$T_{ij} = \frac{\mu_0}{4\pi\hbar} g_e \beta_e g_n \beta_n \left\langle \Psi_0 \left| \frac{3 r_i r_j - \delta_{ij} r^2}{r^5} \right| \Psi_0 \right\rangle \tag{2.21}$$

The anisotropic hyperfine interaction provides information about the distance and the orientation of the nuclear spins to the electron spin. The dipole-dipole interaction depends on the relative orientation of the magnetic moments and its anisotropy. When the unpaired electron is localized in a p, d or f orbital, the anisotropic contribution can only arise from through-space dipole-dipole coupling to other centers of spin density. The hyperfine coupling tensor can be approximated by the point-dipole formula:

$$T = \frac{\mu_0}{4\pi\hbar} g_e \beta_e g_n \beta_n \sum_{k \neq N} \rho_k \frac{(3n_k \widetilde{n_k} - 1)}{R_k^3} \tag{2.22}$$

ρ_k is the spin density which is summed over all orbitals at the center, R_k is the distance between the nucleus and the centers of spin density and n_k is the unit vector denoting the direction cosines of R_k in the molecular frame. In ENDOR spectroscopy of the transition metal complexes, the point-dipole approximation is often used to determine the position of the protons from their hyperfine interactions.

Consequently, the hyperfine interaction contains information about the spin density distribution, the type of the coupled nucleus, the type of chemical bond between the atoms in the considered molecules and the distance between the unpaired electrons and neighboring nucleus. All this information can be used to elucidate the electronic structure and geometry of the molecule.

The hyperfine interaction can be summarized as follows:

$$H_{hfi} = H_{iso} + H_{DD} = \sum_k S A_k I \tag{2.23}$$

The symbols A_k are total hyperfine coupling tensors and I are nuclear spin vector operators.

2.2.4 Nuclear-Quadrupole Interaction

Nuclear spins with $I_k > 1/2$ have an electronic quadrupole moment that can interact with the electric field gradient at the nucleus. This interaction can also be written in tensor form:

$$H_{NQ} = \sum_{I_k > 1/2} I_k P I_k \tag{2.24}$$

where P is the nuclear quadrupole tensor, which is traceless in its principal axis. The nuclear quadrupole Hamiltonian can be written as:

$$H_{NQ} = P_x I_x^2 + P_y I_y^2 + P_z I_z^2 = \frac{e^2 qQ}{4I(2I-1)\hbar} \left[(3I_z^2 - I(I+1)^2) + \eta \left(I_x^2 - I_y^2 \right) \right] \tag{2.25}$$

where eq is the electric field gradient and η is the asymmetry parameter given by:

$$\eta = \frac{(P_x - P_y)}{P_z} \quad \text{with} \quad |P_z| \geq |P_y| \geq |P_x| \quad \text{and} \quad 0 \leq \eta \leq 1 \tag{2.26}$$

The electric field gradient characterizes the symmetry of the charge distribution in the vicinity of the considered nucleus. The charge distribution is dependent on the bonds, which enter the atom and its neighbors. Thus, the knowledge of the experimentally quantity η provides detailed information about the charge distribution and the bonding properties of the atom.

A determination of P from EPR spectra is only very rarely possible, because this interaction leads to only small second-order contributions. However, in ENDOR or ESEEM spectra, the nuclear quadrupole interaction is observed as first-order contributions.

2.2.5 The Entire Spin Hamilton Operator

The entire Hamiltonian for an electron spin S, which is coupled to n nuclear spins I_k, can be summarized as follows:

$$H = H_{EZ} + H_{NZ} + H_{HF} + H_{NQ}$$

$$H = \frac{\beta_e B_0}{\hbar} gS - \beta_n \sum_{k=1}^{m} \frac{g_{n,k} \widetilde{B_0} I_k}{\hbar} + \sum_{k=1}^{m} \tilde{S} A_k I_k + \sum_{I_k > 1/2} \widetilde{I_k} P_k I_k \qquad (2.27)$$

This spin Hamiltonian was first derived by Abraham and Pryce[228] from Hamiltonian governing the wavefunction of bound electrons using perturbation approach.

2.3 Multi-Frequency EPR Spectroscopy

For a successful structural characterization of a paramagnetic compound using the EPR method, it is often necessary to consider at which frequencies different interactions can be best detected. The optimal EPR frequency strongly depends on the studied system. Much of the information, which the EPR spectroscopy provides through the structure and binding of paramagnetic metal centers, can be obtained by an analysis of g-tensor, hyperfine and nuclear quadrupole couplings. The change of the magnetic field B_0 frequently alters the appearance of a spectrum and additional information may become observable to facilitate the interpretation.

The commonly used microwave frequencies associated with magnetic fields are listed in Table 2.1. In this work only the X- and Q-bands are used. The electron and nuclear Zeeman interactions linearly depend on the applied field B_0; the stronger the magnetic field the higher the microwave frequency. Thus, the spectra are wider at higher frequencies, in which a strong increase of the microwave frequency can lead to the complete loss of resolution of the hyperfine structure. This often happens in frozen solutions because they have a distribution of g-tensors. However, at the higher frequencies and the higher magnetic fields the anisotropy of the g-tensor can be resolved because the line width of the EPR spectrum is dominated by the g-anisotropy. As compared to X-band (9.75 GHz), the high-field G-band (180 GHz) is stretched by about a factor of 20. Thus, high-field EPR allows effective analysis of the g-tensor anisotropy due to the increasing in resolution and absolute sensitivity, which is achieved by the use of superconducting magnets and quasi-optical methods.

Table 2.1. Microwave frequency bands used in EPR spectroscopy with corresponding external magnetic field B_0 for $g_e = 2$

MW-Band	MW-Frequency range	Typical EPR Frequency n [GHz]	Typical wavelength [mm]	Typical EPR Field B_0 [mT]
L	1-2	1.5	200	54
S	2-4	3.0	100	110
X	8-12	9.5	30	340
K_u	12-18	17	17	600
Q	30-50	36	8	1280
V	50-75	70	4	2500
W	75-110	95	3	3390
D	110-170	140	2	5000

3 Methods

Below, a short summary of all methods employed in the work described in this thesis is given. In the subsequent sections, each method is described in more detail.

EPR Spectroscopy: EPR spectroscopy is used to elucidate the electronic and geometric structures of paramagnetic compounds. Information is obtained through the analysis of the hyperfine- and quadrupole-coupling constants. An electron is mostly surrounded by many nuclei with magnetic moments. From the specific interaction between the electron and the nuclear spin, information about the structure and binding of the paramagnetic metal-center is achieved. These couplings can sometimes be derived from a characteristic splitting in an EPR spectrum. However, this information can not always be obtained directly. The information is then accessible by modern EPR methods such as ENDOR, ESEEM and HYSCORE spectroscopy.

For strong coupling, the ENDOR method is best suited. In contrast, the ESEEM and HYSCORE methods are more effective for the weak hyperfine interaction. EPR, ESEEM, HYSCORE and ENDOR spectra were recorded for frozen solutions using a Bruker ELEXSYS E580 FT-EPR spectrometer. The EPR, ESEEM, HYSCORE and Davies-ENDOR experiments were performed with a Bruker MD4 (ENDOR) or MD5 (EPR, ESEEM, HYSCORE) resonator. All methodologies and their backrounds are described in section 3.1.

Electrochemistry: Cyclic voltammetry is an established electrochemical method, which gives information about the reduction potentials of the compounds studied, but also on the kinetics of electron transfer. The cyclic voltammograms were recorded on a 600D Electrochemical Analyzer/Workstation (CH-Instruments). The working electrode was a glassy carbon disk of diameter 1 mm. The electrode surface was polished using 0.25 µm diamond paste (Struers A/S), followed by cleaning in an ethanol bath. The counter electrode consisted of a platinum coil melted into glass, while a Ag/AgI electrode (silver wire immersed in a Pyrex tube containing 0.2 M Bu_4NPF_6 + 0.02 M Bu_4NI in THF) separated from the main solution by a ceramic frit served as the reference electrode. All potentials were reported against the Fc^+/Fc redox couple, the potential of which is equal to 0.52 V vs. SCE in 0.2 M Bu_4NPF_6/THF.

DFT Calculations: Finally, in Section 3.3, the density functional theory is given. Density Functional Theory is a method to calculate the properties of quantum mechanical many-electron systems in the ground state in the Born-Oppenheimer approximation. The existing geometry optimization methods in the quantum chemistry program package ORCA were extended. The geometry optimization was carried out with the BP functional and a split-valence basis set with additional polarization functions (SVP). After geometry optimization, the B3LYP functional and a triple-zeta basis set with polarization functions (TZVP) was employed to calculate g values and hyperfine coupling constants. Results obtained with the DFT theoretical treatment are compared to those results obtained with the experimental treatment in Chapters 4 to 7.

3.1 EPR Spectroscopy

The basic methods in EPR spectroscopy used in this thesis are summarized in Table 3.1; these methods are applied to elucidate the electronic and geometric structure of paramagnetic compounds.[216,229]

Table 3.1. EPR spectroscopic methods used in this work.

cw-Method	Pulse-Method
cw-EPR	FT-EPR
	Pulsed-ENDOR (Mims-ENDOR, Davies-ENDOR)
	ESEEM
	HYSCORE

The cw-EPR (continuous wave) and pulse EPR techniques provide information about the electron Zeeman interaction, which is characteristic for the electronic state of the investigated complex. In addition to this, strong hyperfine interactions are observed, which provide information about the couplings between the unpaired electron and the directly neighboring nuclei. Pulse ENDOR spectroscopy provides information about strongly coupled nuclei. Using ESEEM and HYSCORE spectroscopy, the interactions with more distant nuclei can be investigated. The 1D-ESEEM and -ENDOR experiments are the equivalent of 1D-NMR spectra. HYSCORE is the equivalent of 2D NMR spectroscopy.

3.1.1 cw-EPR

The cw-EPR spectrometer and the cw-EPR spectrum are described in this section. A cw-EPR spectrometer basically consists of a microwave bridge, a resonator, a magnet system and control electronics, which are depicted in Figure 3.1. The microwave bridge houses the oscillator, attenuator, circulator, detector, phase shifter and bias. Their properties can be described as follows: the oscillator generates microwave power, and ideally the microwave power is absorbed by the sample in the resonator. The attenuator is used for attenuating microwave power. The detector converts microwave power into a zero frequency voltage. The phase shifter changes the travelling path length of the microwave radiation. The microwave resonator has two important purposes. Firstly, they collimate a sufficient microwave magnetic field at the sample for driving the EPR transition; secondly, they convert the sample response into a detectable microwave signal. To fulfill both these requirements, specialized resonators have been designed such as the dual mode resonator for the investigation of forbidden transitions and the double resonator for quantitative EPR.

A magnet system comprises the magnet, the power supply, a field sensor and a field regulator. If the magnetic field fulfills the resonator condition of the sample, a spin transition is induced and registered by the data system. Information about the components of the cw-spectrometer is shown below; the experimental cw-EPR spectrum is then explained.

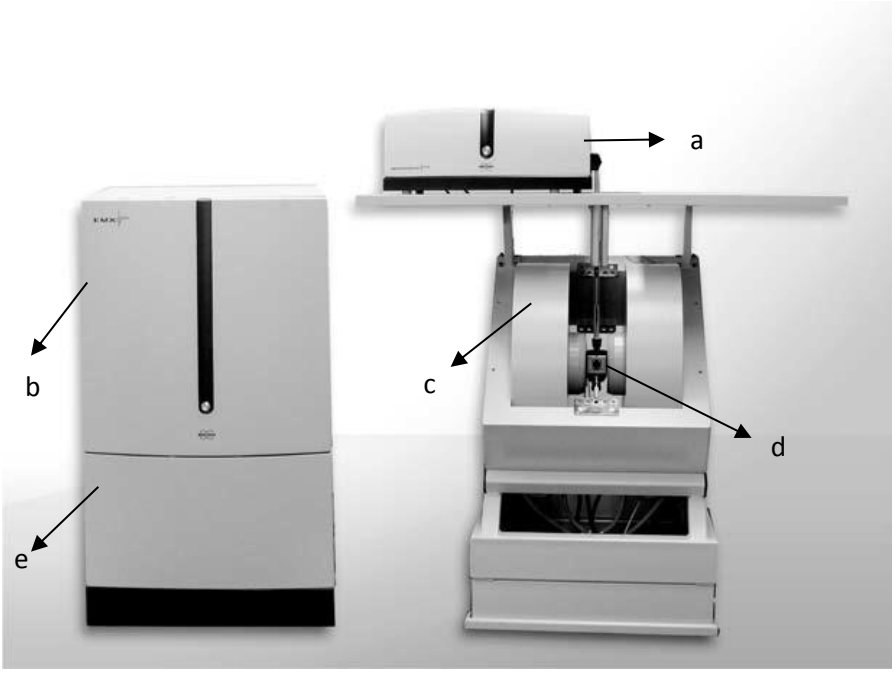

Figure 3.1. The hardware components of a cw-EPR spectrometer: a) microwave bridge; b) spectrometer electronics; c) electromagnet; d) resonator and e) magnet power supply.

The EPR spectrum records the response of the sample as a synchronous detection. In the cw-EPR the microwave frequency is kept constant and the external magnetic field varies continuously. Due to a phase sensitive measurement method, the first derivative of the spectra is recorded. The magnetic field is modulated with additional coils. With the setting of a particular magnetic field value, a certain g-value is also set in which the microwave absorption takes place. The g-value provides direct information about the electronic structure of the system. The stronger the magnetic field, the better the resolution of the g-value due to the electron Zeeman Effect.

In most of the paramagnetic compounds, the unpaired electron is surrounded by many neighboring magnetic nuclei. If the hyperfine coupling A is greater than the natural ERR line width, the EPR lines are dependent on the nuclear spin I and the number of equivalent nuclei N into $\prod(2N_k I_k + 1)$ single lines are split. Thus, the number of EPR lines is multiplicatively increased with the number of coupling nuclei. The distance between the EPR lines corresponds to the hyperfine coupling. If the electron spin S interacts with several groups of non-equivalent nuclei, a very complicated pattern of lines in the EPR spectrum can be obtained. Moreover, the anisotropic components of the hyperfine coupling cause an inhomogeneous broadening of the observed EPR line. Because of that, many hyperfine interactions are not resolved.

In general, in a cw-EPR spectrum the couplings to directly neighboring nuclei are only spectrally resolved. In contrast, the interactions with more distance nuclei are not detected. In order to resolve the smaller hyperfine coupling, different strategies are needed for increasing the spectral resolution, which are described in the following sections.

3.1.2 Pulse EPR

An important area in the modern EPR methods includes pulsed EPR, in which the electron spins are excited by a series of pulses. In typical pulsed EPR experiments, the signal is emitted by the spin system following a series of one or more pulses and contains spectral information and spin relaxation information.

The pulse EPR has no microwave applied during signal acquisition, but the pulse timing and resonator bandwidth are critical. These differences require a different structure compared to a cw-EPR spectrometer. Much larger B_1 fields are required for pulse EPR than cw-EPR. To magnify the microwave field at the sample location, the output power of the microwave source must be amplified by a travelling wave tube (TWT) amplifier. An essential requirement of this amplifier is its phase stability. To exploit the fixed phase relationship between the pulses and the signal, the signal must be referenced in the detection on the phase of the microwave source. This step is performed in a mixer and ensures simultaneously that only the modulation of the microwave carrier frequency is measured. Before the mixer, the original signal must be increased for obtaining a good signal-to-noise ratio.

3.1.2.1 Vector Model for Pulse EPR

An ensemble of non-interacting spins can be described by the sum average of the electronic spin moments, often called as magnetization, which follows the laws of classical mechanics and behaves as a classical vector. Magnetization is an exact description of the quantum mechanical density matrix describing a single unpaired electron.

As it is outlined in chapter 2.1.1, the population of the energy levels follows the Boltzmann law (eq. (2.6)). In thermal equilibrium, the individual unpaired electron spins in the external magnetic field are oriented along B_0 (B_0 = (0, 0, B_0)). Under the influence of an external magnetic field, on the hand, the difference in the occupation of spin states leads to a macroscopic total magnetization **M**. For an ensemble of unpaired electron spins, the macroscopic magnetization **M** from the vector sum results over all magnetic moments μ_i in volume V:

$$M = \frac{1}{V}\sum_i \mu_i \tag{3.1}$$

The magnetization $\mathbf{M_0}$ in thermal equilibrium is referred to as longitudinal magnetization $\mathbf{M_z}$ because it is oriented parallel to the magnetic field B_0 ($\mathbf{M}_0$ = (0, 0, M_z)). The population difference is called as polarization. The macroscopic magnetization constitutes a macroscopic magnetic moment of the sample. This macroscopic size allows for a classical consideration of the phenomena of magnetic resonance.

In the thermal equilibrium, the magnetization vector is aligned along the external magnetic field. The individual electron spins precess in thermal equilibrium in the laboratory coordinate system with Larmor frequency ν_L at an external magnetic field B_0:

$$\nu_L = \frac{g_e \beta_e}{h} B_0 = \frac{\gamma_e B_0}{2\pi} \tag{3.2}$$

where γ_e is the gyromagnetic ratio of an electron.

For the description of the pulse EPR method, a coordinate system is introduced where the laboratory coordinate system (x, y, z) is replaced by a rotating coordinate system (x´, y´, z´). This offers the advantage that the associated spin Hamilton operators are no longer explicitly time-dependent. The Hamiltonian is transformed into a system that rotates with the irradiated microwave frequency about the z axis of the laboratory coordinate system. In a pulse experiment, the microwave pulses are applied perpendicular to B_0 in the x direction in the rotating coordinate system. These pulses lead to a strong time- dependency to the spin system. . The linearly polarized magnetic field $B_1 = \cos(2\pi\nu_{MW}t)$ is formally divided into two circularly polarized components with equal amplitudes ($B_{1,right} = \cos(2\pi\nu_{MW}t) + i\sin(2\pi\nu_{MW}t)$ and $B_{1,left} = \cos(2\pi\nu_{MW}t) - i\sin(2\pi\nu_{MW}t)$). A component in the same direction rotates as the rotating coordinate system; it is independent of time through this transformation. It is arranged parallel to the x-axis of the rotating coordinate system. The other component is non-resonant and can be neglected, because it leads to very small, usually not experimentally detectable shift in the transition. The macroscopic magnetization **M** in the absence of a microwave excitation precesses the z´-axis of the rotating coordinate system with the offset frequency $\Omega_S = \nu_L - \nu_{MW}$.

The linearly polarized magnetic field can cause a rotation of the macroscopic magnetization **M**. During the period of a pulse, t_p, an additional precession of the macroscopic magnetization **M** about B_1 with the frequency $\nu_1 = \frac{\gamma_e B_1}{2\pi}$ occurs. The flip angle Φ of the magnetization, $\mathbf{M_z}$, about the x-axis is proportional to the effective magnetic field strength, B_1, and the period of the pulse t_p

$$\Phi = \nu_1 t_p. \tag{3.3}$$

The macroscopic magnetization in the thermal equilibrium $\mathbf{M}_0$ is thus rotated by the flip angle of Φ = 90° in a magnetization along the y´-direction of the rotating coordinate system (See the right side of Figure 3.2).

Upon application of a microwave pulse with a period of $t_p = {}^{\pi}/_{2}$, ${}^{\pi}/_{2}$-MW-pulse, is applied to an "on-resonance"-magnetization, once the resonance condition $\nu_{MW} = \frac{\gamma_e B_0}{2\pi} = \nu_L$, is exactly fulfilled, the initial longitudinal magnetization $\mathbf{M_z}$ is transferred into transverse magnetization in y´-direction of the rotating coordinate system. In the laboratory coordinate system, macroscopic magnetization exhibits a helical motion, which is composed of a precession with the Larmor frequency ν_L about the z-axis and a precession with frequency ν_1 about the x-axis of the rotating coordinate system (See the left side of Figure 3.2).

In a non-resonance microwave pulse or at "off-resonance", magnetization is presessing with Larmor-frequency ν_L. In this case, the external magnetic field B_0 is not completely transformed, but only the magnitude ($B_0 > B_{0,eff}$) becomes smaller. Therefore, the magnetization precesses about an effective magnetic field B_{eff}, which consists of B_1 and $B_{0,eff}$. The macroscopic magnetization vector precesses with the effective frequency ν_{eff} around this effective magnetic field B_{eff}, which forms an angle $\theta = arc\tan(\frac{\nu_1}{\Omega_S})$ between the z-axis of the external magnetic field B_0 and the linearly polarized magnetic field $\mathbf{B_1}$. This precession has the frequency $\nu_{eff} = \sqrt{\Omega_S^2 + \nu_1^2}$.

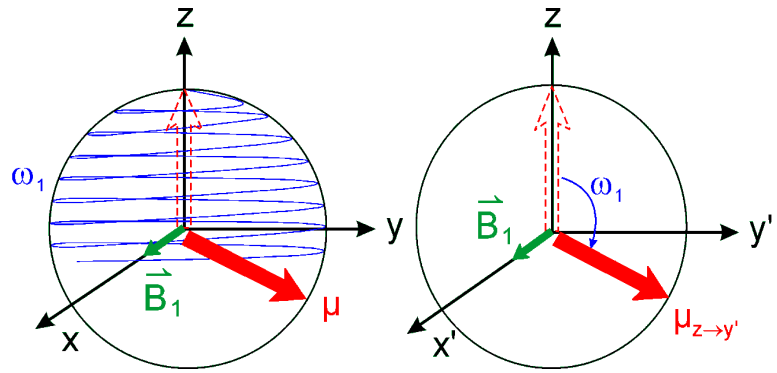

Figure 3.2. Left: Movement of the macroscopic magnetization in a static field in the z direction and a microwave field in the laboratory axis system. Right: Movement of the macroscopic magnetization in a static field in the z direction and a microwave field in the rotating system.

For example, in the two-pulse echo sequence, a transverse y-magnetization (perpendicular to $\mathbf{B_0}$) is generated by the first $\frac{\pi}{2}$ pulse ($\phi = 90°$), which is illustrated in Figure 3.3. At thermal equilibrium, the magnetization vector is oriented along the z-axis. The $\frac{\pi}{2}$ pulse along the x-axis rotates the magnetization to the y-axis. After the pulse, different spin packets begin to precess with their individual Larmor frequencies $\Omega_S = \nu_S - \nu_{MW}$ around the z-axis, resulting in a defocusing of the transverse magnetization. After time τ, a π pulse again along the x-axis turns all the magnetization vectors through 180° about this axis. Since the directions of rotation of the individual spin packets are not changed by the refocusing pulse, after another time τ, all the vectors are aligned along the y-axis. The resulting net y magnetization is called an *electron spin echo*.

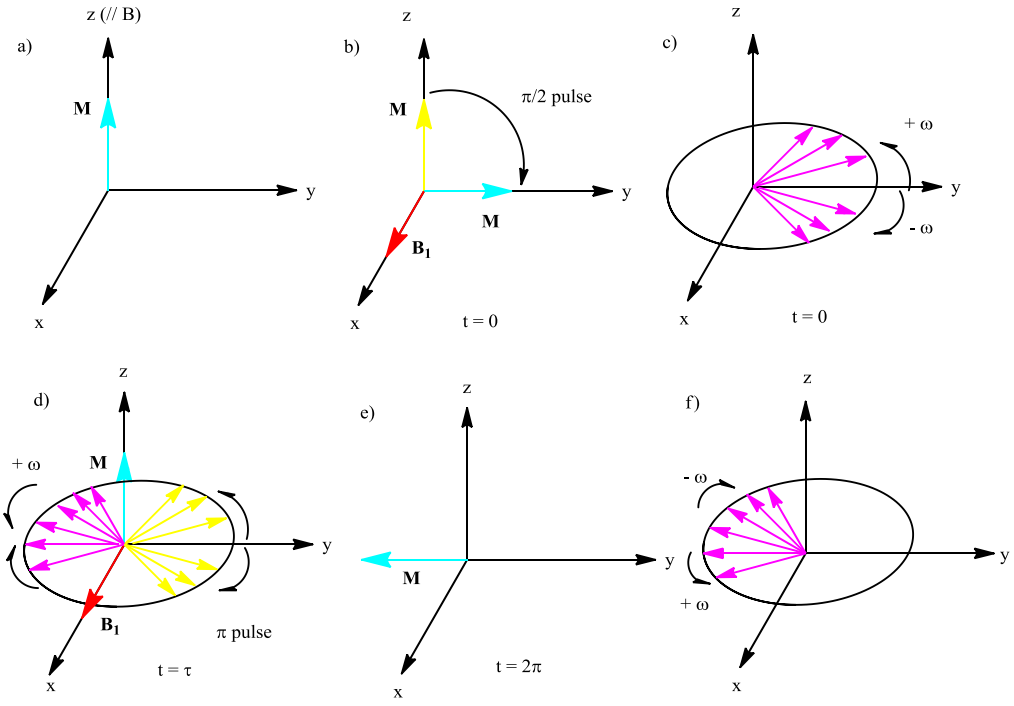

Figure 3.3. Vector model for the reorientation of the spins by the microwave pulses.

3.1.3 Electron Spin Echo Spectroscopy

In 1950, Erwin Hahn invented the spin echo, which is based on the non-linear behavior of an ensemble of spins with different Larmor frequencies.[230] After eight years, Blume[231] reported the first observation of an electron spin echo. In this section, the electron spin echo of non-interacting electron spins in an inhomogeneous internal or external magnetic field is described. The procedure of an electron-spin-echo experiment requires either the presence of an inhomogeneous broadened ERP-line or an inhomogeneity of the external magnetic field, which is caused by static interactions. The spins of a homogeneous line have the same Larmor frequency, so that they cannot be refocused. Thus, they do not contribute to the echo. The inhomogeneous line broadening is represented as a superposition of the homogeneous line width of individual spin packets that different frequencies (different electron-Zeeman-interaction) possess. In addition, unresolved hyperfine splitting and inhomogeneity of the external magnetic field lead to an inhomogeneous line broadening.

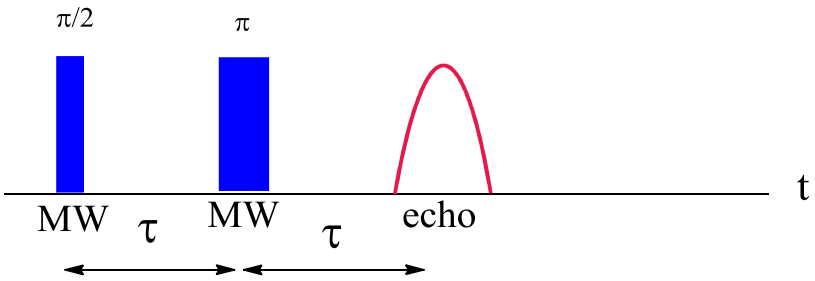

Figure 3.4. Two-pulse sequence for the generation of electron spin echoes.

In his original paper, Hahn described nuclear spin echoes created by the pulse sequence ($\pi/2$-τ-π-τ-echo), which is called the primary echo. However, most EPR pulse sequences are based either on the one or two pulse sequence. The one pulse sequence strategy is the measurement, the relaxation times from the free evolution of the spin system between or following microwave pulses. The second pulse sequence shows that the relaxation times can be measured from the recovery of the spin system following perturbation.

The field-swept electron spin echo (FS-ESE) method is especially suitable for studies of systems with large EPR-line broadening and short-lived paramagnetic species. In the FS-ESE spectroscopy (field swept electron spin echo) the echo intensity for the two-pulse echo sequence ($\pi/2$-τ-π-τ-echo) is measured as a function of the magnetic field B_0. In this connection, integration over the spin-echo signal as a function of the external magnetic field B_0 is performed. In this way, an electron-spin-echo (ESE) detected spectrum is obtained. The advantage of the pulse EPR is that very broad EPR lines can often be resolved, which are not observable by the application of the conventional cw-EPR method.

3.1.4 Pulse ENDOR Spectroscopy

ENDOR is a member of a family of EPR methods that measures the magnetic resonance frequencies of nuclei interacting with an electron spin by exiting the electron spins with a microwave field and the nuclei with an RF field. G. Feher[232] developed the cw-ENDOR technique in 1956, in which the intensity depends on a balance between the relaxation times of the electron and the nuclei. The analog pulse ENDOR technique was introduced by Mims and Davies.[233] There are two basic

approaches to pulsed ENDOR: the Mims-ENDOR, which based on the simulated echo and the Davies-ENDOR based on the inversion recovery measurement.

As already mentioned, the number of the transitions with the number of coupled nuclei N multiplicative (Π) increases in EPR spectroscopy:

$$N_{EPR} = \prod_{k=1}^{N}(2I_k + 1) \tag{3.4}$$

In the ENDOR spectroscopy, the additive attitude ($\sum$) is observed.

$$N_{ENDOR} = 4 \cdot \sum_{k=1}^{N} I_k \tag{3.5}$$

In addition to the smaller number of lines, an ENDOR spectrum has also a simpler splitting pattern (multiple structures). The lines in the ENDOR spectrum are usually narrower, so that this causes a better resolved spectrum. This is because the transverse relaxation time of nuclear spins is in general longer than the transverse relaxation time of electron spins.

In the ENDOR experiment, nuclear spin transitions are detected via electron spins transitions. This is advantageous because the electron spins exhibit a much larger magnetic moment. The polarization of electron spins transitions is larger than the polarization of nuclear spin transitions, so that this results a larger population difference or a larger polarization in thermal equilibrium.

In this work, the investigations are performed with the pulse EPR, ENDOR, ESEEM, and HYSCORE techniques in disordered system or frozen solution. In the following sections ENDOR, ESEEM, and HYSCORE methods are described in detail.

3.1.4.1 Model System for Pulse ENDOR Experiments for the Spin Systems of S = ½, I = ½

The spin Hamilton operator of the spin system S = ½, I = ½ is defined for an isotropic g-value and an anisotropic hyperfine coupling in the laboratory coordinate system, which the external magnetic field B_0 is orientated along z-axis, by:

$$\widehat{H_0} = \nu_S S_z + \nu_L I_z + A\left(S_z I_z + S_x I_x + S_y I_y\right) \tag{3.6}$$

where $\nu_S = \frac{g_e \beta_e B_0}{h}$ is the electron Zeeman frequency and $\nu_L = -\frac{g_N \beta_N B_0}{h}$ is the nuclear Zeeman frequency. The hyperfine coupling tensor contains secular ($S_z I_z$), pseudo-secular $\left(S_z I_x, S_z I_y\right)$ and non-secular $\left(S_x I_x, S_x I_y, S_y I_x, S_y I_y\right)$ terms. The non-secular terms combine the energy levels with different spin quantum numbers m_s. The pseudo-secular terms couple different nuclear spin quantum numbers m_I (shift of the EPR-lines) within a m_s-substate. The non-secular term $A\left(S_x I_x + S_y I_y\right)$ causes an effect of the second-order and this term can be neglected in the high-field approximation ($\nu_S \gg A$). In the rotating coordinate system, the Hamilton-operator can be written as:

$$\widehat{H_0} = \Omega_S S_z + \nu_L I_z + A S_z I_z + B S_z I_x \tag{3.7}$$

where $A = A_{zz}$ and $B = \left(A_{zx}^2 + A_{zy}^2\right)^{1/2}$ are defined as secular and pseudo-secular parts of the hyperfine coupling, respectively. The axially symmetric **A**-tensor is applied for the coefficients A and B from eq. (3.7):

$$A = A_{\perp} \sin^2\theta + A_{\parallel} \cos^2\theta = a_{iso} + (3\cos^2\theta - 1)A_{dip}$$

$$B = (A_{\parallel} - A_{\perp}) \sin\theta \cos\theta = 3A_{dip} \sin\theta \cos\theta \quad (3.8)$$

The diagonalization of the spin Hamiltonian of eq. (3.7) gives the nuclear transition frequencies ν_α and ν_β, which are described in eqs. (3.9) and (3.10).

$$\nu_\alpha = |\nu_{12}| = \left[\left(\nu_L + \frac{A}{2}\right)^2 + \left(\frac{B}{2}\right)^2\right]^{\frac{1}{2}} \quad (3.9)$$

$$\nu_\beta = |\nu_{34}| = \left[\left(\nu_L - \frac{A}{2}\right)^2 + \left(\frac{B}{2}\right)^2\right]^{\frac{1}{2}} \quad (3.10)$$

For an isotropic hyperfine interaction, eqs. (3.9) and (3.10) can be written as:

$$\nu_\alpha = |\nu_{12}| = \left|\nu_L + \frac{A}{2}\right|$$

$$\nu_\beta = |\nu_{34}| = \left|\nu_L - \frac{A}{2}\right| \quad (3.11)$$

The ENDOR transition frequencies for spin systems for S = ½, I = ½ (a) and the weak coupling and strong coupling (b) are illustrated in Figure (3.5). In the weak-coupling case the ENDOR frequency is centered at $|\nu_L|$ and split by $\frac{|A|}{2\pi}$. In the strong-coupling case, the ENDOR frequency is centered at $\frac{|A|}{4\pi}$ and split by $2|\nu_L|$.

In the "*exact cancelation*" condition ($|A| = 2|\nu_L|$), the magnetic field B_0 cancels the hyperfine field. For quadrupolar nuclei (I > ½) with small hyperfine anisotropy the nucleus experiences a near zero-field situation. The three characteristic nuclear quadrupole frequencies (NQR) are given by:

$$\nu_0 = \frac{e^2qQ}{2h}\eta = 2\kappa\eta \quad (3.12)$$

$$\nu_- = \frac{3e^2qQ}{4h}\left(1 - \frac{\eta}{3}\right) = \kappa(3 - \eta) \quad (3.13)$$

$$\nu_+ = \frac{3e^2qQ}{4h}\left(1 + \frac{\eta}{3}\right) = \kappa(3 + \eta) \quad (3.14)$$

These nuclear quadrupole frequencies can be calculated by eq. (3.12) with the nuclear quadrupole coupling constant κ and the asymmetry parameter η. If the anisotropic hyperfine coupling is small compared to the isotropic hyperfine and nuclear quadrupole interaction, a double-quantum transition with $\Delta m_I = \pm 2$ is represented. This double-quantum transition frequency of a nucleus with spin I = 1 can be expressed by:

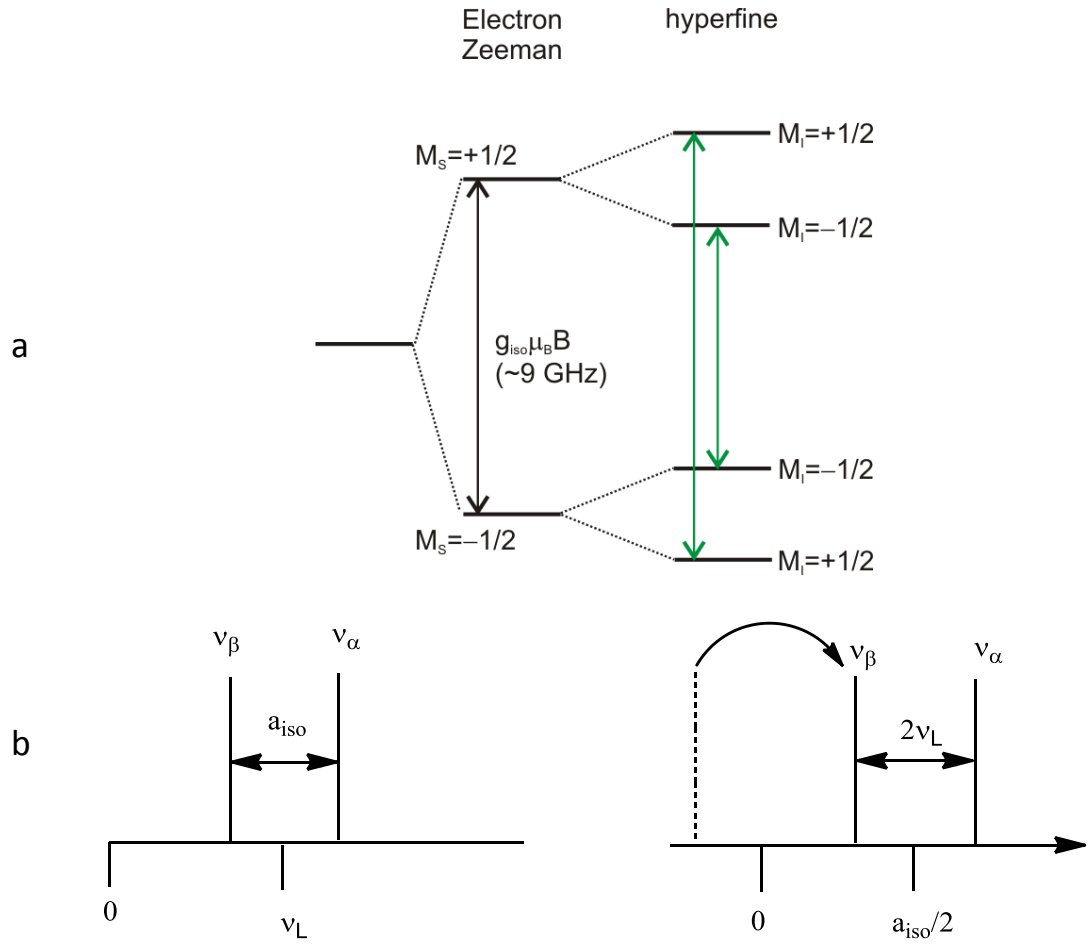

Figure 3.5. Schematic representation of a) the energy levels diagram for a spin system of S = ½, I = ½ and b) ENDOR frequencies for a weak-(left) and strong-coupling (right) case.

$$\nu_{dq} \approx 2\left[\left(|\nu_L| + \left|\frac{a_{iso}}{2}\right|\right)^2 + \kappa^2(3+\eta^2)\right]^{1/2} \tag{3.15}$$

In addition, in the ESEEM spectra of disordered systems, the nuclear quadrupole frequencies $(\nu_0, \nu_- \; and \; \nu_+)$ are observed as narrow lines because they have no dependence of orientation on the external magnetic field. In contrast, the double-quantum transition frequency ν_{dq} is observed as a broad line

3.1.4.2 Davies ENDOR

The Davies ENDOR method is based on the transfer of spin polarization.[234] In this experiment the much larger polarization of the electron spin transitions are used for the sensitive detection of nuclear spin transition. The pulse sequence of Davies ENDOR is sketched schematically in Figure 3.6A.

In the thermal equilibrium, the spin system in the state of a spin-polarization is represented (Figure 3.6B). An EPR transition can take place only under this condition, which a population difference in

the energy levels exists the electron spins. The state of a spin system is defined by $|m_s m_I\rangle$ or for example by $|++\rangle$ or $|1\rangle$. Based on a selective excitation of the EPR transition from $|1\rangle$ to $|3\rangle$, the ENDOR experiment begins with a selective π-microwave pulse. As in Figure (3.6B, bottom b) shown, this pulse is inverted the electron spin population or occupation of the levels of a single EPR-transition between levels $|1\rangle$ and $|3\rangle$. The Figure (3.6, bottom c) shows that the nuclear spin populations in the states $|1\rangle$ and $|2\rangle$ are inverted by a selective π-RF pulse. The resonant π-RF pulse (see Figure 3.6, bottom c) leads to the disappearance of the population difference of the excited EPR transition ($|1\rangle \leftrightarrow |3\rangle$) and thus also of the echo intensity. However an echo is measured at a non-resonant π-RF pulse (see Figure 3.6, bottom d). A similar description can be applied for other nuclear spin transition or other observed EPR transitions.

A superposition of homogeneous lines with different resonant frequencies causes an inhomogeneous line broadening. In the microwave excitation, an inhomogeneous line can be only a part of the spins "*on-resonance*." The resonant part of contributing spins can be saturated the complete inhomogeneous line. Through this process, which is called the "hole burning," a hole is burned into the line. This inversion pulse causes a "spectral hole" in the inhomogeneous line of the EPR spectrum. Under certain conditions, a homogeneous line can disappear by microwave irradiation. This effect, which makes the disappearance of line, is known as "saturation." The hole-width corresponds to the width of the homogeneous lines. The nuclear spin transitions are polarized by this π-microwave pulse in both m_S states. Because the electron-spin-lattice relaxation time T_1 in frozen solutions amount to a dependence on temperature, this time is usually extended in order to invert the nuclear spin polarization in one of the both m_s-states by a selective RF pulse.

In the case of the exact inversion of the populations there is no population difference between levels of $|1\rangle$ and $|3\rangle$ (see Figure 3.6, bottom c) or between $|2\rangle$ and $|4\rangle$, which leads to the disappearance of the echo. The intensity of the ENDOR signal with optimal experimental parameters amounts to only a few percent of the intensity of the EPR signal. The nuclear spin transition can be detected indirectly via a $(\frac{\pi}{2} - \tau - \pi - Echo)$ pulse sequence. This detector-pulse sequence (Hahn echo) generates an echo-signal, which detects real electron spin polarization at the magnetization hole by the electron coherence. In the Davies ENDOR experiment, the echo amplitude of the inverted echo at a fixed position of the external magnetic field B_0 is observed in dependence on the radio frequency that is varied. The ENDOR intensity does not correspond to the exact multiplicity of nucleuses because the RF pulses strongly encourage the different NMR- or ENDOR-transitions due to the hyperfine coupling.

The sensitivity of the Davies ENDOR experiments depends on the hyperfine interaction. For small couplings, which are located within the burned hole, the Davies ENDOR method is insensitive. Therefore, this method is better qualified for the detection of large hyperfine couplings, whereas the Mims-ENDOR method (described below) is better suited for the detection of small couplings.

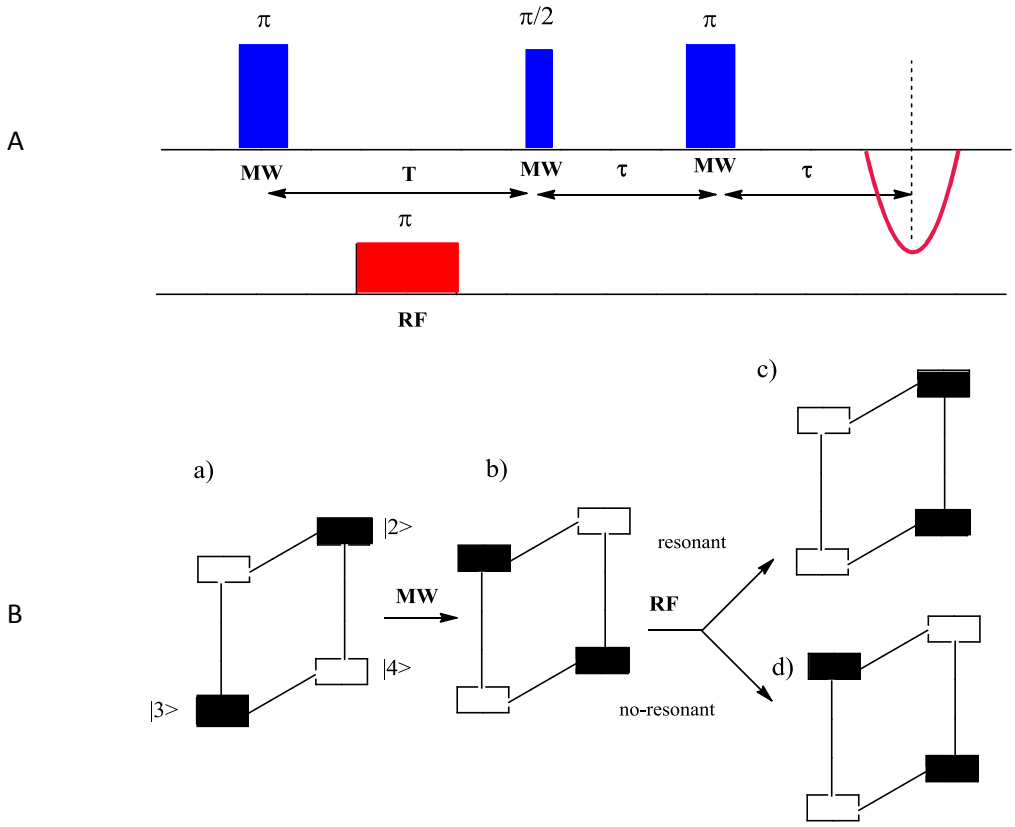

Figure 3.6. Schematic representation of A) Pulse sequence for a Davies ENDOR experiment, consisting of a microwave and radio pulse and B) Polarization transfer in the Davies-ENDOR experiment for a spin system with S = ½, I = ½. Black (high population) and white (low occupancy) boxes describe the population differences of the energy levels of a spin system with S = ½, I = ½ according to Boltzmann.

3.1.4.3 Mims ENDOR

The first pulsed ENDOR was performed by Mims in 1965, in which a stimulated echo is measured as a function of the variable frequency of the RF pulses. The selective RF pulse is used in the time T between the second and third microwave pulse.

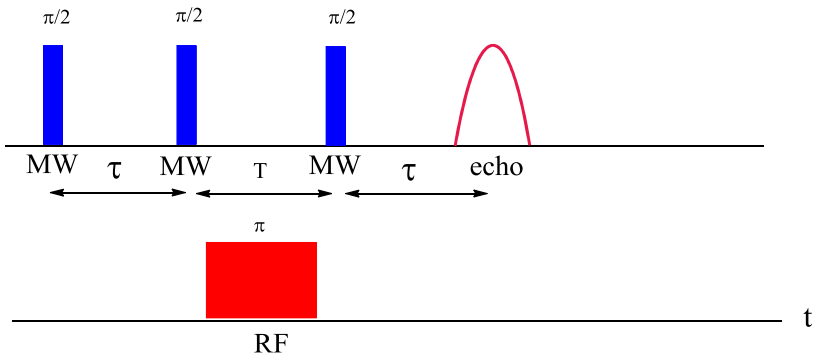

Figure 3.7. Pulse sequence for the Mims ENDOR experiment, consisting of a microwave and RF pulse.

In general, the microwave pulses in the Mims ENDOR experiment are chosen as very short, and non-selective so that a large spectral excitation bandwidth is achieved, which is sketched in Figure 3.7. The first $\frac{\pi}{2}$ microwave pulse is transferred into a transverse magnetization in the x, y-plane. Thereby, electron coherence is generated. By the following $\frac{\pi}{2}$ microwave pulse, the magnetization in nuclear coherence is rotated back into the z-direction so that the initial electron spins polarization is transferred though the second $\frac{\pi}{2}$ microwave pulse. This pulse sequence ($\frac{\pi}{2} - \tau - \frac{\pi}{2}$) produces a magnetization pattern (polarization pattern) in the inhomogeneous EPR-line with a frequency $\nu_p = \frac{2\pi}{\tau}$. The generated nuclear coherence can be influenced by a selective π-RF-pulse between the nuclear spin states. When the following RF pulse is resonant, the populations are modified at this nuclear spin transition. Consequently, the polarization pattern is changed so that a transfer of spin packets is generated within this polarization pattern.

The excitation of a nuclear spin transition shifts the Larmor frequencies of the electrons, which causes a shift of the frequency scale of the z-magnetization. Hence, this results in a changing of the rephasing of the pattern that forms the echo. Through the RF pulse (selective) changed nuclear spin polarization is transformed by the non-selective microwave pulse in electron spin coherence, which is detected as the *stimulated* echo. The simulated echo is measured as a function of the variable radio frequency, in which is kept constant. Due to the complicated τ-dependent magnetization patterns on the EPR-line, blind spots are observed in the Mims-ENDOR spectrum. These blind spots occur in Mims-ENDOR spectra for values of:

$$\tau = \frac{2\pi n}{a} \qquad n = 1, 2, 3, \ldots. \tag{3.16}$$

where a is characterized as the hyperfine coupling. By a longer τ-value, the magnetization pattern is fine. This gives rise to the fact that small hyperfine coupling constants can be detected. Because of the "blind spots," the Mims-ENDOR experiment at several τ-values should be performed. Thus, a complete overview of the ENDOR spectrum and the correct line shape are obtained. Davies ENDOR has no "blind spots" but exhibits small echo amplitude. However Mims-ENDOR methods are carried out with non-selective microwave pulses. Therefore a comparison of the relative echo intensities of these two ENDOR-methods is not possible.
The pulse sequence ($\frac{\pi}{2} - \tau - \frac{\pi}{2}$) is used in the Mims-ENDOR experiment but it is also used in the ESEEM and HYSCORE experiment.

3.1.5 ESEEM Spectroscopy

After the observation of the primary electron spin echoes, the nuclear modulation effect was developed by Mims in 1972, which is the so-called electron spin echo envelope modulation (ESEEM). ESEEM spectroscopy has been become very popular for studying hyperfine and nuclear quadrupole coupling.

In ENDOR spectroscopy, the nucleus transitions are directly encouraged with RF pulses, where the sensitivity of the electron spins is exploited in ESEEM spectroscopy. For both methods, the nuclear frequencies are indirectly detected by microwave pulses.[235] The ESEEM method has the advantage

that there is no complex apparatus structure such as the ENDOR resonator and RF amplifier, which is necessary for an ENDOR experiment. In general, the hyperfine couplings of nuclei with small magnetic moments (due to the low probabilities of transition) are detected difficult using the ENDOR technique. ESEEM spectroscopy is commonly used to detect the hyperfine interactions of the paramagnetic metal center with a weakly coupled nucleus. This method allows to resolve the hyperfine couplings of nuclei with small gyromagnetic ratios such as ^{14}N and ^{2}D. In addition, it also allows the observation of nuclear quadrupole coupling.

In general, in comparison to ENDOR spectroscopy the advantage of ESEEM spectroscopy is the possibility of determining of small couplings. The large couplings are not detectable due to technical limitations such as spectrometer-dead time. With modern 2D methods such as HYSCORE this is partly circumvented.

3.1.5.1 Three-Pulse ESEEM Experiment

The hyperfine interaction leads to modulation of the echo intensity, which occurs by the simultaneous excitation of allowed ($\Delta m_I = 0$) and forbidden ($m_I = \pm 1$) EPR-transitions. These nuclear modulation effects can occur only in systems that have an anisotropic hyperfine interaction.

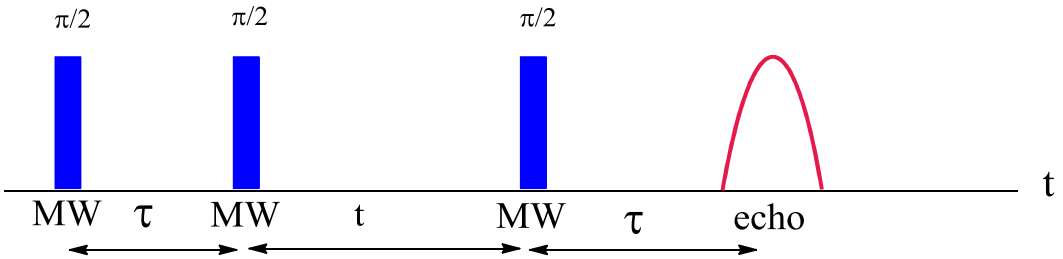

Figure 3.8. Pulse sequence for the three-pulse ESEEM experiment.

A three-pulse ESEEM experiment consists of the pulse sequence ($\frac{\pi}{2} - \tau - \frac{\pi}{2} - t - \frac{\pi}{2} - \tau - Echo$), which is shown in Figure (3.8).[236] Based on the in-thermal-equilibrium existed electron-spin-polarization (longitudinal magnetization), nuclear-coherence is generated by the pulse sequence $\left(\frac{\pi}{2} - \tau - \frac{\pi}{2}\right)$. During the time t, the nuclear coherence develops. The third $\frac{\pi}{2}$-pulse converts these nuclear coherences back into an observable electron coherence that can be observed as a “stimulated” echo. When the time t is incremented between the second and third pulse, then a modulation of the echo intensity can be measured. This modulation of the echo intensity is described by the term “echo envelope.” The echo-envelope modulation is caused by the nuclear-Zeeman and hyperfine-interaction. The nuclear transition frequencies of the interacting nuclei correspond to the modulation frequencies. During the experiment the time τ persists constant between the first and second pulse. The echo envelope is recorded as a function of the variable time interval t in the time domain. A Fourier transform provides a spectrum in the frequency domain, in which can be given the information about the type and size of the hyperfine interaction. The modulated echo amplitude decays in the time t with the relaxation time T_1. Thereby, the modulation can be observed longer, so that the Fourier transform of the experimental recorded time domain spectrum obtains a good

resolution of the frequency domain spectrum. This is characterized by narrow ESEEM-lines in the frequency domain spectrum. For the S = ½, I = ½ spin system the three-pulse ESEEM modulation formula is given by:

$$V(\tau,t) = V_\alpha(\tau,t) + V_\beta(\tau,t)$$

$$= 1 - \frac{k}{4}[(1-\cos(\omega_\alpha\tau))]\left[1-\cos\left(\omega_\beta(\tau+t)\right)\right] + \left[1-\cos(\omega_\beta\tau)\right]\left[1-\cos\left(\omega_\alpha(\tau+t)\right)\right] \qquad (3.17)$$

where k is the modulation depth parameter. An observation of the echo modulation requires the presence of a pseudo-secular coupling (B) between electrons and nuclei. If the spin-Hamilton operator contains pseudo-secular terms of the form BS_zI_x and BS_zI_y, forbidden transitions appear in the corresponding spin systems. The intensity of modulation depends on the strength of the nuclear-Zeeman and hyperfine-interaction. By using a low external magnetic field B_0 an enhancement of the intensity is allowed the modulation amplitude.

For the case of an isotropic hyperfine coupling or an orientation of the external magnetic field along a direction of the principal axes of the **A**-tensor, the condition is considered B = 0. This causes the disappearance of the ESEEM modulation. In the ESEEM spectrum, ENDOR or NMR transitions under the condition that the terms $\left[1-\cos\left(\omega_{\alpha,\beta}\tau\right)\right] \neq 0$ are observed. In the three-pulse ESEEM experiment as well as in the Mims ENDOR experiment "blind spots" make an appearance.[237] By a suitable choice of the value, for example signals from ^{1}H, can be completely suppressed. Thereby, the τ-value corresponds to the integer periodicity of the Larmor frequency of the suppressed nuclei.

$$\tau_{blind\ spots} = \frac{n}{\nu_L} \qquad with\ n = 1,2,3,\ldots. \qquad (3.18)$$

Because of these effects, a repeated measurement of the three-pulse ESEEM spectra for various τ-values is required to detect these "blind spots" and to detect all nuclei frequencies. Another disadvantage of the three-pulse ESEEM experiment represent the spectrometer-dead time because no signals can be recorded at this time. This dead time is important for a disordered system, because the anisotropy of the hyperfine and nuclear quadrupole interaction leads to a rapid decay of the ESEEM signals.

Under that condition, the interactions between individual nuclei spins can be neglected; the echo modulation is expressed for multiple nucleus by the following product rule:

$$V_{Mod}(n) = \frac{1}{2}\left[\prod_i^n V_i^\alpha(\tau,T) + \prod_i^n V_i{}^\beta(\tau,T)\right] \qquad (3.19)$$

V_{Mod} describes the dependence of the echo intensity on τ and t and V_i that is, according to eq. (3.17), the calculated the modulation intensity or the amplitude of modulation of the individual nuclei. This rule also simplifies the treatment of a larger spin system. In the ESEEM spectrum, combination of frequencies is formed according to eq. (3.19) within the same m_s-state, in which exhibit usually a low intensity.

The nuclear transition in ESEEM spectra is analogous to the situation of the nuclear transition in the ENDOR spectra, in which the shape of the line is different. The ESEEM and ENDOR spectroscopy represent complementary methods. However, the ESEEM method assumes an anisotropic hyperfine coupling, in which the ENDOR method allows to determine the hyperfine coupling.

3.1.6 HYSCORE Spectroscopy

Hyperfine sublevel correlation (HYSCORE) spectra represent the four-pulse 2D measurement, which was developed in 1986.[238] Hyperfine couplings provide information about structure. The isotropic part is a function of the spin density in the s-orbital at the nucleus, which is defined by the Fermi-contact term. The anisotropic part describes the dipole-dipole interaction between the electron and nuclear spin. The determination of these quantities can be difficult for the single crystals due to the overlaps of signals. Moreover, for the disordered system, the experimental determination is often not possible for insufficient resolution because of the overlap of the signals and strongly anisotropic hyperfine coupling constants, the interpretation of the spectra can be complicated. The 2D hyperfine correlation spectroscopy allows a better spectral resolution and separation of different hyperfine couplings. In this section, the 2D-HYSCORE method is described.

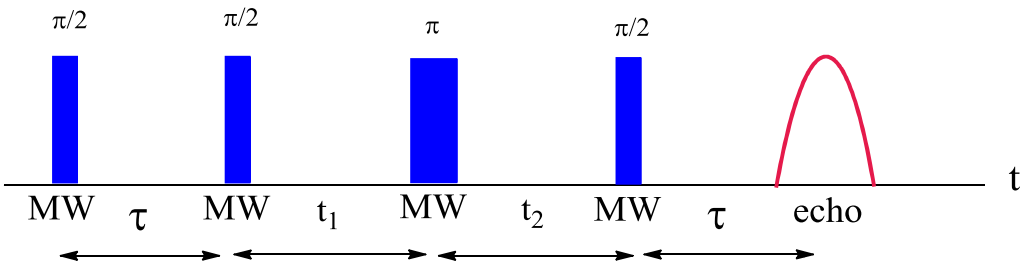

Figure 3.9. Pulse sequence for the HYSCORE experiment.

The HYSCORE pulse sequence is shown schematically in Figure 3.9. The HYSCORE spectrum is experimentally measured at a fixed value of the external magnetic field and at a fixed τ–value. In HYSCORE experiment, nuclear coherences are generated by the pulse sequence $\left(\frac{\pi}{2} - \tau - \frac{\pi}{2}\right)$. This nuclear coherence can evolve during the time t_1. Through the subsequent inversion pulse π the nuclear coherence is mixed. A coherence of the nucleus in an exact m_s-state is transferred into coherence of the same nucleus of another m_s-state. During the time t_2 the coherence is developed again after π-pulse. By a $\frac{\pi}{2}$ pulse this nuclear spin coherence in the observable electron spin coherence is converted, whereby the amplitude of the echo is influenced. The times t_1 and t_2 are independently incremented. The inverted echo is measured as a function of the times t_1 and t_2 so that the recording of the spectra is carried out in the two time domains. The first time domain is detected for a fixed value t_2, while the echo modulation is measured as a function of the increment of t_1. The signal of the second time domain is recorded as a function of the variable time t_2 at constant t_1. Subsequently by 2D fourier transformed of the measured modulated time signal, a 2D frequency spectrum with the frequency axes ν_1 and ν_2 is obtained. The echo in the HYSCORE experiment decays with the longitudinal spin-lattice-relaxation time T_1. Thus, a good resolution of the frequency is achieved in both two dimensions.

For the S = ½ and I = ½ spin system, the correlation between the ENDOR frequencies ν_α and ν_β or ν_β and ν_α occurs, which is referred to as the cross-correlation peak. The frequencies ν_α and ν_β are characterized by the nuclear transitions $|3\rangle \leftrightarrow |4\rangle$ or $|1\rangle \leftrightarrow |2\rangle$. The excitation band width of the inversion pulse represents an important factor for the resolution of the spectra. For a non-selective π-pulse, the mixture of the nuclear spin state is to be complete in the various m_s-states. In the case

of a selective pulse, the π-pulse is not completely transferred to the coherence and they are developed on the same transitions. Therefore, the diagonal of a HYSCORE spectrum is experimentally observed such as (ν_α, ν_α) or (ν_β, ν_β), which is called autocorrelation peaks. However, this is not for an ideal π-pulse. The cross-peaks only appear that are observed between the same nuclear frequencies. In an analogy to the three-pulse ESEEM experiment (eq. 3.17), the combination peaks also occur in HYSCORE experiment also occur (eq. 3.20). The combinations of peaks considerably exhibit weaker intensity than the desired cross-peaks, so they do not occur frequently in the HYSCORE spectrum[239], which contain information about the relative sign of the coupling. The observed combination frequencies are defined as sums and difference of the nuclear frequencies from the same m_s-state. The correlations peaks couple the nuclear transition from different m_s-state with each other.

3.1.6.1 Quantitative Description for Ideal Pulses in HYSCORE Experiment

3.1.6.1.1 The Case of the S = ½, I = ½ Spin System

For S = ½ and I = ½ spin system, the HYSCORE modulation formula is defined as the analogy to the three-pulse ESEEM modulation formula (eq. 3.17):

$$V(\tau, t_1, t_2) = \frac{1}{2}\left[V_\alpha(\tau, t_1, t_2) + V_\beta(\tau, t_1, t_2)\right] \tag{3.20}$$

$$V_\alpha(\tau, t_1, t_2) = 1 - k\left[\frac{C_0}{4} + \frac{C_\alpha}{2}\cos\left(\omega_\alpha t_1 + \frac{\omega_\alpha \tau}{2}\right) + \frac{C_\beta}{2}\cos\left(\omega_\beta t_2 + \frac{\omega_\beta \tau}{2}\right) + \frac{C_c}{2}\left[c^2\cos\left(\omega_\alpha t_1 + \omega_\beta t_2 + \frac{\omega_+ \tau}{2}\right) - s^2\cos\left(\omega_\alpha t_1 - \omega_\beta t_2 + \frac{\omega_- \tau}{2}\right)\right]\right]$$

$$V_\beta(\tau, t_1, t_2) = 1 - k\left[\frac{C_0}{4} + \frac{C_\alpha}{2}\cos\left(\omega_\alpha t_2 + \frac{\omega_\alpha \tau}{2}\right) + \frac{C_\beta}{2}\cos\left(\omega_\beta t_1 + \frac{\omega_\beta \tau}{2}\right) + \frac{C_c}{2}\left[c^2\cos\left(\omega_\alpha t_2 + \omega_\beta t_1 + \frac{\omega_+ \tau}{2}\right) - s^2\cos\left(\omega_\beta t_1 - \omega_\alpha t_2 - \frac{\omega_- \tau}{2}\right)\right]\right] \tag{3.21}$$

$$C_0 = 3 - \cos(\omega_\beta \tau) - \cos(\omega_\alpha \tau) - s^2\cos(\omega_+ \tau) - c^2\cos(\omega_- \tau)$$

$$C_\alpha = c^2\cos\left(\omega_\beta \tau - \frac{\omega_\alpha \tau}{2}\right) + s^2\cos\left(\omega_\beta \tau + \frac{\omega_\alpha \tau}{2}\right) - \cos\left(\frac{\omega_\beta \tau}{2}\right)$$

$$C_\beta = c^2\cos\left(\omega_\alpha \tau - \frac{\omega_\beta \tau}{2}\right) + s^2\cos\left(\omega_\alpha \tau + \frac{\omega_\beta \tau}{2}\right) - \cos\left(\frac{\omega_\beta \tau}{2}\right)$$

$$C_c = -2\sin\left(\frac{\omega_\alpha \tau}{2}\right)\sin\left(\frac{\omega_\beta \tau}{2}\right) \text{ and } \omega_+ = \omega_\alpha + \omega_\beta, \omega_- = \omega_\alpha - \omega_\beta \text{ and } k = s^2 \cdot c^2 \tag{3.22}$$

V_{Mod} describes the dependence of the echo intensity on τ, t_1 and t_2. V_α and V_β are represented as the calculated modulation. The transition probabilities of the allowed and forbidden nuclear-transitions are described by $s^2 = \sin^2\left(\frac{\eta}{2}\right)$ and $c^2 = \cos^2\left(\frac{\eta}{2}\right)$, respectively. η symbolizes the angle between two effective fields at the nucleus of the two m_s-states. The correlation of the two NMR frequencies is described by the term C_c, in which the intensity of the correlation peaks is a function of the τ-values. This term also causes the blind spots in the HYSCORE spectrum.[240]

3.1.6.1.2 The Case of the S = ½, I = 1 Spin System

The experimental HYSCORE spectrum is more complicated for the nuclear I = 1, such as ^{14}N, because the number of the nuclear spin states m_I is increased and the nuclear quadrupole interactions must be considered. In this case, the frequencies of the nuclear transition in two quadrants are observed simultaneously in the HYSCORE spectrum. The three characteristic nuclear quadrupole frequencies (zero-field transition) are given by:

$$\nu_o = 2\kappa\eta \tag{3.23}$$

$$\nu_- = \kappa(3-\eta) \tag{3.24}$$

$$\nu_+ = \kappa(3+\eta) \tag{3.25}$$

A single-quantum marked transitions $\nu_{0,-}$ with $\Delta m_I = \pm 1$ and a double-quantum transition $\nu_{+,dq}$ with $\Delta m_I = \pm 2$ are represented. The location of the double-quantum transitions ν_{dq} can be described by eq. (3.26).

$$\nu^{dq} \approx 2\left[\left(|\nu_L| + \left|\frac{a_{iso}}{2}\right|\right)^2 + \kappa^2(3+\eta^2)\right]^{1/2} \tag{3.26}$$

The 2D HYSCORE spectroscopy has several advantages compared to 1D ESEEM and ENDOR spectroscopy. In these 1D spectra the signals from different magnetic nuclei often overlap. Due to overlap of the signals, the interpretation and analysis of the spectra can be difficult. In addition, an ENDOR measurement is often not possible for low-frequency signal components (< 5 MHz) because of the technical problems. The HYSCORE method makes possible interpretation of complex spectra by the second dimension. In HYSCORE spectra, the unordered systems appear anisotropically broadened ESEEM lines as “ridge-correlations”, so that the HYSCORE method allows an improved resolution of the broad signals in comparison with the three-pulse ESEEM experiments. Also in contrast to the ENDOR method, the HYSCORE method offers the possibility of detection for low frequency signals (< 5 MHz). To avoid the “blind spot,” the SMART (single pulse matched resonance transfer) HYSCORE is described.[241] In addition the application of the “matched” pulses can be also called HTA (high tuning angle), and the intensity of the cross-correlation peaks of the translations increase with small modulation depth parameters.[242] Thus, measured signals are amplified and peaks are clearly visible.[243,244]

3.2 Electrochemistry

The electrochemistry method is based on the fact that, between two electrodes, a voltage is applied and the current, which is generated by a voltage caused by the chemical reaction, is measured. The applied voltage is generated by a potentiostat, and such a potentiostat can be switched in a two or three electrode system. The two or three electrode system differs in the control of the working electrode applied potential. The circuit design of a potentiostat is illustrated in the Figure 3.10.

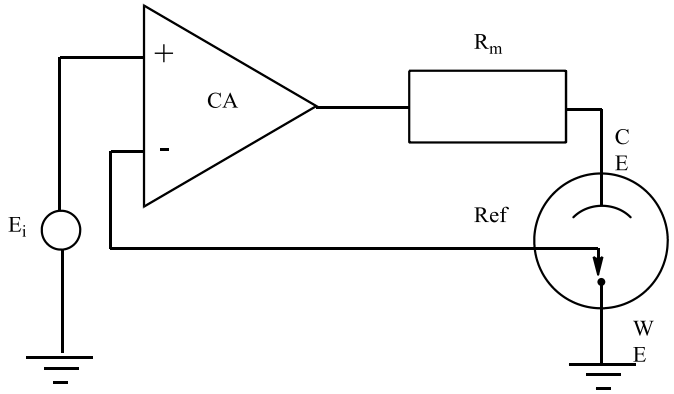

Figure 3.10. Schematic of the potentiostat.

A potenstiotat regulates the output voltage so that in the (+) and (–) from the input of the potenstiostat the fitting voltages have same value. In the two-electrode system, the (-) from input of the potenstiostat is connected directly to the counter electrode and the output of the potenstiostat. In this case, the difference of the voltage between the counter electrode and the working electrode is controlled. However, the difference in the voltage between the solution and the working electrode cannot be controlled. The created voltage between the counter electrode and the working electrode differs because the other transitions from the counter electrode in the solution and the solution resistor themselves represent the current.

In a three-electrode system a reference electrode, which is usually arranged to be the working electrode, is used to control the voltage. Thus, the potenstiostat is controlled by the voltage between the working electrode and the solution itself. The voltage drop that occurs between the working electrodes and the solution in the transition will be compensated for. The reference electrode is an electrochemically active electrode having a well-defined potential. In this case, they are applied by the potentiostat on the measuring cell, which creates potentials related to the known substance or the voltage. The voltage drop, which occurs in the transition between the counter electrode and the solution, will be compensated from the potentiostat by a higher voltage between the electrodes themselves.

Consequently, in the two-electrode system, the effective voltage generated by an electrochemical reaction at the working electrode is always smaller than in a three-electrode system. In the two-electrode system electrochemical reactions appear slower than in a three-electrode system.

3.2.1 Chronoamperometry

Chronoamperometry is the simplest electrochemical measurement method. Between the counter electrode and the working electrode, a voltage is applied and the resulting current is measured as a function of the time. The equilibrium composition of the electrochemically active substance on the working electrode can be calculated by using the *Nernst-equation*.

$$E = E^0 + \frac{R*T}{n*F} * In\left[\frac{C_{ox}}{C_{red}}\right] \tag{3.27}$$

The composition in the solution differs from those calculated according to the *Nernst-equation*, due to an electron transfer. This diffusion is a result of concentration gradient. The oxidized or reduced form of the electrochemically active substance deposits on the electrode. The measured current is dependent on the quantity of the material that arrives on the surface of the electrode. A diffusion layer is formed in the course of time, in which the converted substance is depleted. At the diffusion layer, the dependence of the current on the time is influenced; it depends on whether the diffusion is carried out planar or spherical. The corresponding current-time curves can be calculated using the *Cottrell equation* for the planar diffusion (3.28) and for the spherical diffusion (3.29).

$$i(t) = \frac{nFA\sqrt{D}C_0}{\sqrt{\pi t}} \tag{3.28}$$

$$i(t) = nFADC_0\left[\frac{1}{\sqrt{\pi Dt}} + \frac{1}{r_0}\right] \tag{3.29}$$

For the case of planar diffusion, a permanent chronological reduction of the current occurs, for the case of spherical diffusion, the current is assumed to be at the constant value. The radial diffusion occurs not only to spherical electrodes, but after a certain period also in square or circular microelectrodes. The date in which a radial diffusion is observed at microelectrodes, is dependent on the magnitude of the microelectrode. For example, in the small electrodes a mixed behavior of planar and radial diffusion can be expected.

Another deviation from the denoted current-time curves can be observed in measurements in a thin film system. When the diffusion layer is in contact with the wall of the capillary, the diffusion layer depletes faster than the electrochemically convertible substance.

3.2.2 Cyclic Voltammetry

In cyclic voltammetry (CV) a triangular voltage is applied in the working electrode. The ratio of the oxidized and reduced substance on the surface of the electrode arises according to the Nernst equation. The amount of substance that deposits on the electrode increases at once, so that a rise of the current is observed. The diffusion layers are formed as in with the chronoamperometric measurements. If it is a planar diffusion, in principle the drop of the current intensity occurs. In a radial diffusion a constant current arises in the course of time. With increasingly larger and smaller potentials, a further shift of the redox equilibrium is carried out in the direction of the oxidized and reduced species. Although the concentration difference between the electrode surface and the electrolyte solution is increased, the decisive diffusion gradient for the diffusion cannot be increased because of the spread of the diffusion layer. According to the Nernst equation, the change in the composition of the electrochemically active substance is progressively cancelled.

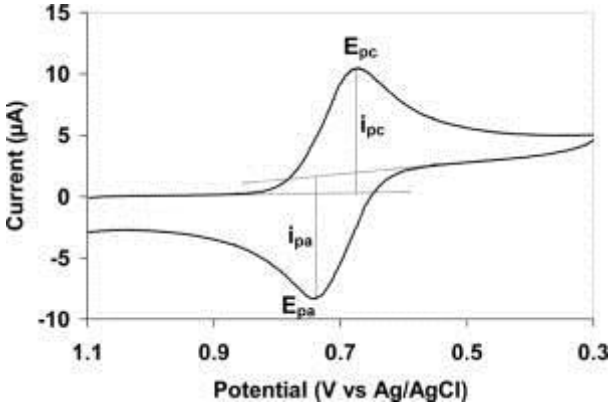

Figure 3.11. Typical cyclic voltammogram, whereas i_{pc} and i_{pa} show the peak cathodic and anodic current respectively, for a reversible reaction.

The presence of a one-dimensional diffusion perpendicular to the surface of the electrode results in a CV that has oxidation and reduction peaks (Figure 3.11). The electrochemically active substance is arranged in the free electrolyte solution, so the difference between the oxidation and the reduction peak is of 59 mV, if it is a reversible system. The electrochemical substance is directly bound to the surface of the electrode, and the oxidation and the reduction peaks are arranged at the same potential. With an increasingly slower running electrochemical reaction, while the composition is lagged to the electrode surface, the distance between the peaks is increasingly larger. The same effect is observed if a high ohmic resistance lies between the electrode surface and the potentiostat; this resistance from the potentiostat cannot be compensated for in a two-electrode system, and the counter electrode limits the current flow.

By the alternative oxidation and the reduction at the working electrode, the initial conditions at the electrode are installed after the cycle of the back scans again. The following scans are repeated in the same manner. However, an electrochemical reaction at the electrode can be coupled to a chemical reaction. It is possible, for example, that the oxidized substance is immediately reduced by using a catalyst, which is located on the surface of the electrode. In this case, with the CVs, only a reduced reduction peak is visible and the oxidation peak is increased.

3.3 Density Functional Theory (DFT)

Density Functional Theory is a way to calculate the properties of quantum mechanical many-electron systems in the ground state usually in the Born-Oppenheimer approximation. All properties are considered and not as a functional of the wave function or the density matrix, as the electron density distribution.

In 1998, Walter Kohn was awarded the Nobel Prize in chemistry for the development of density functional theory.

3.3.1 Kohn-Sham Equations

The first Hohenberg-Kohn theorem[245] proved that the three space coordinate-dependent electron density $\rho^0(r)$ is a sufficient basic parameter for the description of the ground state of a molecule. One does not need to consider the complicated multi electron wave function $\Psi^\tau = (X; R)$, which depends on the location- and spin-coordinates of all electrons in the molecule. In particular, Hohenberg and Kohn showed that the total energy of a molecule in the ground state can be calculated from the functional of the electron density ρ:

$$E[\rho] = F_{HK}[\rho] + \int \rho(r) v(r; R) dr \tag{3.30}$$

where the number of electrons in the molecule is defined by $\int \rho(r) dr = n$. In the equation (3.30) $F_{HK}[\rho]$ is a universal functional of the electron density ρ and it is often referred to as the *Hohenberg-Kohn functional.* The molecule specific contribution, that is the potential $v(r; R)$, is a part of the integral term. The Hohenberg-Kohn functional includes the kinetic energy $T[\rho]$ and the electron-electron interaction energy $V_{ee}[\rho]$, both of which are dependent on the electron density ρ.

$$F_{HK}[\rho] = T[\rho] + V_{ee}[\rho] \tag{3.31}$$

Further, the Hohenberg-Kohn second theorem[245] says that for any test electron density $\tilde{\rho}(r)$ with the condition $\int \tilde{\rho}(r) dr = n$, the variation principle

$$E^0 = E[\rho^0] \leq E[\tilde{\rho}] \tag{3.32}$$

applies. It means that the exact ground state electron density ρ^0 minimizes the energy functional $E[\rho]$ and therefore the minimum E^0 is the ground state energy of the molecule.

However, neither $T[\rho]$ nor $V_{ee}[\rho]$ for the relevant molecular case is explicitly known, and hence we have to use the best possible approximations for $F_{HK}[\rho]$. A good approach for this approximation of $F_{HK}[\rho]$ is found in the work of Kohn and Sham[246], which introduces molecular spin orbitals Ψ_i. Instead of the existing interacting electron gas, a non-interactive electron gas is considered with an effective potential $v_{eff}(r; R)$, in which the lowest energy orbitals are occupied. As in other molecular orbital methods, the wave function Ψ_S is obtained as antisymmetric product in the form of a Slater determinant:

$$\Psi_S = \frac{1}{\sqrt{n!}} det[\Psi_1, \Psi_2, \ldots., \Psi_n]. \tag{3.33}$$

The electron density $\rho(r)$ and the kinetic energy $T_S[\rho]$ are given by:

$\rho(r) = \sum_{i=1\ldots n}|\Psi_i(r)|^2$ and

$$T_S[\rho] = \sum_{i=1\ldots n}\left\langle \Psi_i \middle| \frac{1}{2}\nabla^2 \middle| \Psi_i \right\rangle. \quad (3.34)$$

From this approach follows that n one-electron Schrödinger equations of the form:

$$\left[-\frac{1}{2}\nabla^2 + v_{eff}(r;R)\right]\Psi_i = \varepsilon_i \Psi_i \quad \text{with } i = 1, \ldots\ldots, n \quad (3.35)$$

to be solved. The effective electron potential $v_{eff}(r;R)$ is constructed as equation (3.43) A convenient representation of the Hohenberg-Kohn functional is given by:

$$F_{HK}[\rho] = T_S[\rho] + J[\rho] + Ecx[\rho] \quad (3.36)$$

where $T_S[\rho]$ represents the kinetic energy of the non-interacting electron gas, which is given by equation (3.33), $J[\rho]$ is the classical Coulomb electronic repulsion ρ,

$$J[\rho] = \iint \frac{\rho(r)\rho(r')}{|r-r'|}dxdx' \quad (3.37)$$

and $Exc[\rho]$ is so-called Exchange-Correlation-Functional. In $Exc[\rho]$ should be defined as the difference between $T_S[\rho]$ and $T[\rho]$ and it should also include the non-classical part of the electron-electron interaction $V_{ee}[\rho]$:

$$Ecx[\rho] \equiv T[\rho] - T_S[\rho] + V_{ee}[\rho] - J[\rho] \quad (3.38)$$

The functional form of $F_{HK}[\rho]$ and the functional from of $Exc[\rho]$ are not exactly known. However, approximations for $Exc[\rho]$ have been developed, which allow the calculation of molecular force fields with high accuracy.

If we assume an explicit form for $Exc[\rho]$, then the effective potential energy term in equation (3.34) can be given by:

$$v_{eff}(r;R) = v(r;R) + \frac{\delta J[\rho]}{\delta\rho(r)} + \frac{\delta Exc[\rho]}{\delta\rho(r)} = v(r;R) + \int \frac{\rho(r')}{|r-r'|}dx' + v_{xc}(r). \quad (3.39)$$

The equations (3.32)-(3.34) represent the so-called *Kohn-Sham equations* where the effective potential energy $v_{eff}(r;R)$ is given as in equation (3.38). Since $v_{eff}(r;R)$ depends on the electron density ρ, which in turn depends on the functions (orbitals) Ψ_i, the n one-electron Schrödinger equations are coupled, and their relation must be iterative.

3.3.2 The Exchange-Correlations-Functional

To complete the Kohn-Sham equations in the previous section, an appropriate approximation for $Exc[\rho]$ is still missing. The simplest approach is already found in the Thomas-Fermi model, in which an electron gas of homogeneous density with $Exc[\rho] = 0$ is considered.[247] From this model, the famous Thomas-Fermi functional $T_{TF}[\rho]$ for the kinetic energy of a homogeneous electron gas is derived. In the cited work, the foundations of the modern DFT were laid. The kinetic energy functional $T_{TF}[\rho]$ of a homogeneous electron gas is applied as an approximation of the kinetic energy of an inhomogeneous electron gas. It is assumed here that the kinetic energy of an inhomogeneous electron gas can be obtained approximately by summation over $T_{TF}[\rho]$ in infinitesimally small volume areas with locally homogeneous electron density. However, as demonstrated, this simple approach is not sufficient to describe chemical bonds in molecules.[247]

A further development of the Thomas-Fermi model was undertaken by Dirac, who also considered the Exchange-Energy $Ex[\rho] = V_{ee}[\rho] - J[\rho]$ of a homogeneous electron gas. But only through the inclusion of the electron correlation energy $E_C[\rho] = T[\rho] - T_S[\rho]$ of a homogeneous electron gas[246] could molecular properties be reproduced with sufficient accuracy . This Exchange-Correlation-Functional ($Exc[\rho] = E_x[\rho] + E_C[\rho]$) is derived from the assumption of a locally homogeneous electron gas. Approximations of this kind are defined as local-density approximation (LDA). The applicability of the LDA-approximation for the description of an inhomogeneous electron system in atoms and molecules cannot be justified in a purely formal way, but arises solely from the success of numerous calculations. [247]

The LDA-approximation has still some serious weaknesses. For example, atomization energies and energy differences of molecular configurations will be incorrectly predicted by up to a factor two. In addition, the strength of hydrogen bonds in the LDA-approximation is generally overestimated by about 15 kJ/mol, or more than half of the actual binding energy (20-25 kJ/mol)[248]. The cause of the misbehaviour of the LDA-approximation is based on an underestimation of the exchange energy E_x by about 10% and an overestimation of the correlation energy E_C by about a factor of two. Therefore, many improved exchange-correlation functionals E_{xc} have been developed. A first successful step was made by Perdew who corrected for the self repultion energy of an electron gas in the LDA- approximation.[249] Also the so-called gradient-corrected Exchange-Correlation-Functionals have been developed, in which the gradient of an inhomogeneous electron gas is taken into account. [250-252]

A widely used gradient corrected functional $E_{xc}[\rho]$ arises from the combination of the Exchange-Functional by Becke[251] and the correlation functional by Lee, Yang and Parr[253]. This functional is labeled as BLYP functional (the initials of the given authors) and it managed to fix many weaknesses of the LDA- approximation. The very popular B3LYP functional consist of the B88 exchange part by Becke, and the correlation part LYP by Lee, Yang and Parr as well as the exchange from Hartree-Fock theory:

$$E_{XC}^{B3LYP} = aE_X^{HF} + (1-a)E_x^{LSD} + bE_x^{B88} + E_C^{LSD} + c\left(E_c^{LYP} - E_C^{LSD}\right) \tag{3.40}$$

where a, b and c are empirical constants, obtained by fitting to experimental data. Because of the inclusion of the Hartree-Fock exchange, these functionals are called hybrid functionals.

In this thesis, the functionals used for the calculations are the BP86 and B3LYP functionals, which were built from different terms for the exchange and correlation parts. The BP86 functional consists of an exchange part by Becke and a correlation part by Perdew.

4 H_2O-Activation for HAT: Correct Structures and Revised Mechanism

This Chapter has been published in: A. Gansäuer, A. Cangönül, M. Behlendorf, C. Kube, J. M. Cuerva, J. Friedrich, and M. van Gastel *Angew. Chem. Int. Ed.* **2012**, 51, 3266-3270.

4.1 Introduction

The reduction of radicals to hydrocarbons through hydrogen atom transfer (HAT) is a fundamental radical reaction.[4.1] Recent developments in the field concentrate on alcohols and H_2O as HAT reagents in the presence of boranes[4.2] and Cp_2TiCl,[4.3] the use of H_2O as final reductant,[4.4] and on BH_3-NHC-complexes (NHC = N-heterocyclic carbene).[4.5] All cases feature a weakening of otherwise strong H-X bonds.

The propensity of H_2O to act as a HAT-reagent has been explained by a reduction of the bond dissociation energy (BDE) of the O–H by about 60 kcal mol-1 in the presence of Cp_2TiCl.[4.3] Here, we demonstrate by EPR spectroscopy and cyclic voltammetry (CV) that the proposed HAT-reagent **1** is not present in THF solutions of Znreduced Cp_2TiCl_2 containing H_2O. Instead, our results hint at **2** and **3** as the active HAT-reagents (Figure 4.1). Moreover, we show that previous data in support of **1**[4.3c] are in agreement with **2**, **3a**, and **3b** and that an older computational study [4.3c] needs extension and refinement.

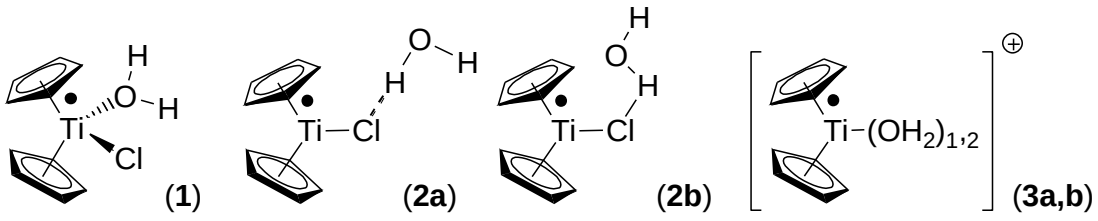

Figure 4.1. Proposed modes of complexation of $[Cp_2TiCl]$ by H_2O.

Electron paramagnetic resonance (EPR) spectroscopy and the hyperfine resolving techniques Electron Spin Echo Envelope Modulation (ESEEM)[4.6] and Hyperfine Sublevel Correlation (HYSCORE) spectroscopy[4.6d,4.7] are excellent methods for studying interactions between H_2O and Cp_2TiCl. The g values provide direct information about unpaired electron's orbital. The ESEEM and HYSCORE methods are well suited for examining the coordination sphere of the $[Cp_2TiCl]$-H_2O system by the detection of magnetic hyperfine couplings with surrounding nuclear spins. Here, this allows studying the binding of chloride (I = 3/2) and the coordination of H_2O or D_2O through the coupling to protons (I = ½) or deuterons (I =1).

4.2 Results and Discussion

Pulsed EPR spectra of Zn-reduced [Cp_2TiCl_2] in THF were recorded. Without H_2O, they are in agreement with a previous study[4.8] on Cp_2TiCl and show that the unpaired electron resides in a $3d^1_{z^2}$ orbital at Ti^{III}. This is also the case upon addition of H_2O. However, the shape of the spectrum and especially the g_x value change significantly upon addition of various molar equivalents of H_2O (See Supporting Information for the Spectra).

In order to understand these effects, ESEEM spectra of Zn-reduced [Cp_2TiCl_2] in THF with different amounts of added H_2O (Figure 4.2, left panel) and D_2O (Figure 4.2, right panel) were recorded. Under the experimental conditions (microwave frequency of 34 GHz) they contain nuclear modulations derived from chloride (I = 3/2) and from deuterons (I = 1). Protons (I = 1/2) do not contribute, because their Zeeman frequency amounts to 50 MHz and their modulations have zero amplitude.[4.9]

The frequency of the nuclear modulations changes noticeably upon addition of 10 or 20 equivalents of H_2O (left panel) indicating an interaction of the halide with H_2O. The modulations become weaker for 40 and more equivalents of H_2O. This suggests that the Ti-Cl is eventually cleaved through the generation of hydrated chloride and a titanocene cation. However, from this particular ESEEM spectrum it is not clear if the titanocene cation is hydrated or not.

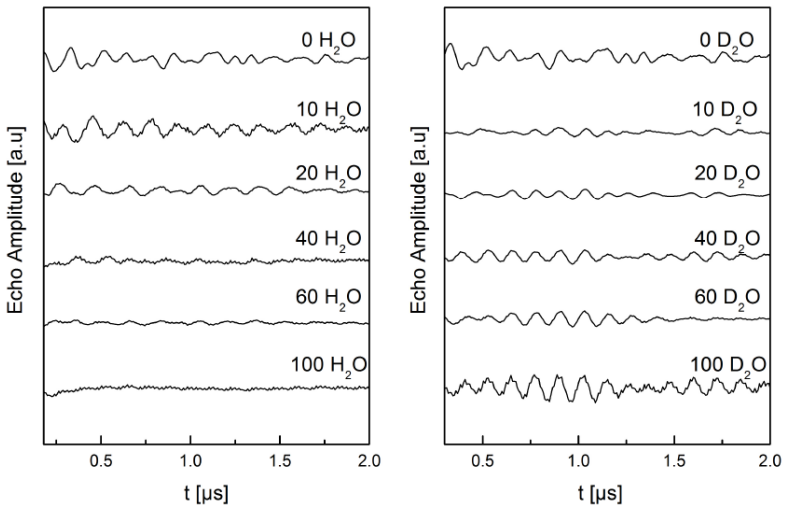

Figure 4.2. Normalized Q-Band 3-pulse modulation patterns (T = 30 K) of Zn-reduced Cp_2TiCl_2 in THF with different added molar equivalents of H_2O and D_2O. For the same spectra in the frequency domain see supporting Information.

Therefore, to directly study the interaction of water with the titanocene moiety, ESEEM spectra of Zn-reduced [Cp_2TiCl_2] in THF with different equivalents of added D_2O were recorded (Figure 4.2, right panel). Addition of 10 equivalents D_2O resulted in similar, albeit not identical, initial changes of the chloride modulations. This is related to the different hydrogen bonding propensities of H and D and to a beginning superposition of the modulations caused by D and Cl. Starting from 20 molar equivalents D_2O, the modulations with a frequency of 8 MHz became clearly observable In presenceof more than 40 equivalents these signals dominate the appearance of the ESEEM

spectrum. This coupling constitutes the direct experimental proof for the coordination of D_2O to titanium that occurs via a Ti-O bond. Moreover, the combination of the ESEEM experiments highlights that coordination of water is especially favourable after dissociation of the halide ligand. Thus, H_2O is coordinated in a dissociative mechanism that is caused by the low Lewis-acidity of $[Cp_2TiCl]$.

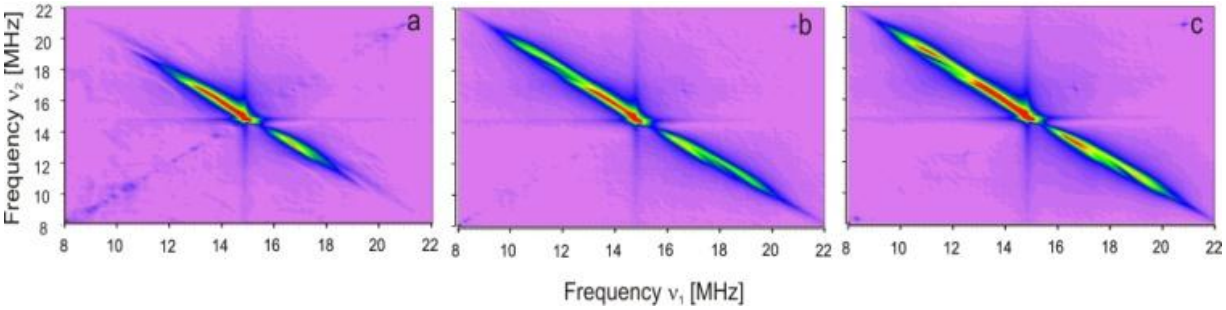

Figure 4.3. X-band (9.68 GHz) HYSCORE spectra recorded at 30 K of Zn-reduced Cp_2TiCl_2 in THF (a) without H_2O (b) with 10 eq. of H_2O, (c) with 100 eq. of H_2O, recorded at the g_y canonical orientations.

These conclusions were further verified by HYSCORE experiments. At the employed microwave frequency (X-band, 9.7 GHz) all proton signals appear in the spectral region around 14 MHz Off-diagonal signals (cross-peaks) appear between nuclear transition frequencies that belong to the same proton, similar to 2D-NMR experiments. Striking differences are observed between the spectra of Zn-reduced $[Cp_2TiCl_2]$ without added H_2O and those with 10 and 100 molar equivalents H_2O (Figure 4.3). This is especially apparent at the frequency coordinates (11, 19) MHz and (19, 11) MHz Cross peaks are absent for Zn-reduced $[Cp_2TiCl_2]$ but weak signals appear with 10 eq. of H_2O. With 100 eq. H_2O this cross-peaks become very intense. Interestingly, the line shape of the signals observed with 10 eq. and 100 eq. of water is essentially identical. This once again supports our notion of a cationic titanocene coordinated to H_2O in the presence of a hydrated chloride counter-ion. Neither the ESEEM nor the HYSCORE experiments thus provide any evidence for the presence of **1** in Zn-reduced $[Cp_2TiCl_2]$ in THF upon addition of H_2O.

Moreover, the HYSCORE allows an estimation of the distance between the protons of the bound H_2O and Ti. The ridges of these cross-peaks do not form straight lines, but are rather bent, indicative of the presence of anisotropic hyperfine interaction.[4.10] Careful analysis allows a determination of the dipolar hyperfine coupling constant $T_\perp$ of 5.7 MHz This value is comparable to that found for the equatorial protons of $[Cu(H_2O)_6]^{2+}$ and indicates that the effective distance between the protons of H_2O and the unpaired electron is smaller than 3.3 Å.[4.10]

To verity these conclusions, the Zn-reduced THF solutions of $[Cp_2TiCl_2]$ with added H_2O were investigated by cyclic voltammetry (CV) with concentrations of all regents being identical to those of the EPR samples. The voltammograms recorded at sweep rates of 0.1 and 1 V s^{-1} are shown in Figure 4.4 (For CVs with higher sweep rates see Supporting Information). For both sweep rates two oxidation waves were observed for all cases investigated. Zn reduced $[Cp_2TiCl_2]$ these are assigned to the oxidation of $[(Cp_2TiCl)_2]$ and $[Cp_2TiCl]$ (first wave) and $[Cp_2Ti^+]$ (second wave) in analogy toprevious studies.[4.11] Several features of the CVs obtained upon addition of H_2O deserve closer attention:

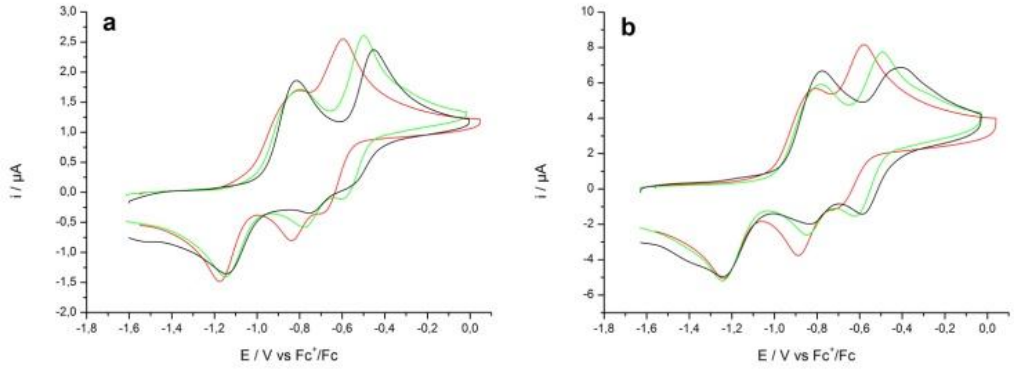

Figure 4.4. CV of Zn-reduced Cp_2TiCl_2 (a 0.1 V s^{-1}, b 1 V s^{-1}) in THF with 0 (black), 10 (green), and 100 (red) equivalents of added H_2O in 0.2 M $TBAPF_6$/THF.

First, in the presence of H_2O the peak current ratio of the two oxidation waves remains essentially constant as a function of sweep rate. This suggests that in agreement with the heterolytic breaking of the Ti-Cl bond observed in the ESEEM experiment the [Cp_2Ti^+] derived species are present in Zn-reduced solutions in THF with added H_2O. This is not the case without H_2O. It should be noted that not even the addition of the strongly coordinating HMPA to Zn-reduced solutions of [Cp_2TiCl_2] results in the generation of solvated [Cp_2Ti^+] [4.12] Thus, the solvation of chloride through hydrogen bonding by H_2O is essential for generation of the titanocene cation.

Second, the first oxidation wave of Zn-reduced [Cp_2TiCl_2] in the presence of H_2O does not consist of two individual processes (oxidation of [Cp_2TiCl] and [Cp_2TiCl_2])) because no second oxidation peak appears at higher sweep rates.[4.11a] This results indicate that [$(Cp_2TiCl)_2$] dissociates into monomeric species upon addition of H_2O.

Third, the oxidation wave of the [Cp_2Ti^+] derived species is shifted to more negative values upon addition of H_2O. For 10 equivalent of H_2O this shift is 50 and 80 mV suggesting the formation of [$Cp_2Ti(OH_2)^+$]. In the presence of 100 equivalents of H_2O shits of 130 and 180 mV were observed. This change suggests the coordination of a further molecule of water and hence at the presence of [$Cp_2Ti(OH_2)^+$].

Finally, the peak potential of the first oxidation wave does not change upon addition of H_2O. This implies that H_2O does not bind to the Ti nucleus of [Cp_2TiCl] because in that case a noticeably more negative peak potential shifted by 50-80 mV in analogy to [$Cp_2Ti(OH_2)^+$] should have been observed.

The interaction of H_2O with [Cp_2TiCl] was studied by computational means next. The geometries were optimized at the BP86/TZVP[4.13,4.14] level of theory using density fitting. Stationary points were characterized by analyzing the hessian matrix.[4.15] The energies were obtained by B3LYP-d/def2-TZVPP[4.16] single-point calculations using COSMO[4.17] with $\varepsilon = 7.6$ including the zero-point energy correction of the BP86 level.

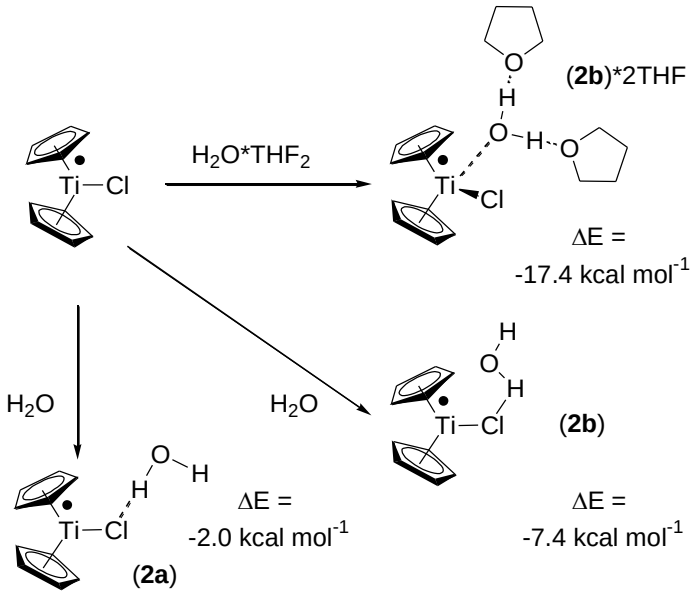

Scheme 4.1. Computational results on the complexation of Cp_2TiCl by H_2O with and without THF (B3LYP-d/def2-TZVPP). COSMO[4.17] with ($\varepsilon = 7.6$)

In Scheme 4.1 the behavior of [Cp_2TiCl] in the presence of H_2O and in the presence of H_2O and THF is summarized. If specific interactions of H_2O with THF are excluded, the two structures **2a** and **2b** with hydrogen bonding of H_2O to the Ti-Cl bond are identified as minima. **2b** is more favorable than **2a** because of a dipole-dipole interaction between O and Ti. However, the complexation energy is far too weak for a covalent Ti-O bond present in the postulated **1**. With the inclusion of specific interactions of H_2O and THF, the situation becomes slightly more complex. H_2O and 2 equivalents of THF form a hydrogen bonded complex with a ΔE of -7.8 kcal mol^{-1}. Both hydrogen bonds are of equal strength (-3.9 kcal mol^{-1}). Based on these values it is clear that hydrogen bonding in **2a** is too weak to persist when specific THF interactions are included. For **2b**, the inclusion of H_2O*2THF leads to a noticeably more favorable binding (-7.4 kcal mol^{-1} vs. -17.4 kcal mol^{-1}). This is mainly because of the increase of negative charge on the O of H_2O due to hydrogen bonding that leads to a stronger interaction with Ti. It should be noted that an interaction between an α–H of THF and Cl also contributes to the stability of **2b***2THF (See the Supporting Information for the structure). However, even the binding of **2b***2THF is characteristic of a dipole-dipole interaction and not of a Ti-O bond.

The computational investigation of the formation of cationic titanocenes in the presence of H_2O is summarized in Scheme 4.2. For our study it is important to recall that Zn-reduced solutions of [Cp_2TiCl_2] contain $ZnCl_2$. This strong Lewis-acid is rendering the heterolytic cleavage of the T-Cl bond more favourable through the formation of $ZnCl_4^{2-}$. Even so, the cleavage of the Ti-Cl bonds is highly endothermic because of charge separation.

For the solvation of the titanocene cations, the inclusion of THF in the mechanistic analysis must not be neglected. Whereas, the complexation of a single H_2O is exothermic (-25.0 kcal mol^{-1} per Ti), the complexation of the first H_2O*2THF is much more favorable (-41.4 kcal mol^{-1} per Ti). Binding of the second equivalent of H_2O*2THF is less exothermic (-19.7 kcal mol^{-1} per Ti) but more advantageous than THF alone (-16.4 kcal mol^{-1} per Ti).

Therefore, the reaction of $4H_2O$*2THF with $2[Cp_2TiCl]$ and $ZnCl_2$ results in an exothermic formation of solvated titanocene cations (-19.1 kcal mol^{-1} per Ti). This value is 2.7 kcal mol^{-1} more favourable than the energy of generation of **3b***4THF (-17.4 kcal mol^{-1}) from Cp_2TiCl and H_2O*2THF. The preference of **3b***2THF over **2b***2THF should become even more pronounced if solvation of $ZnCl_4^{2-}$ is included in the analysis. While, the calculation of the complete solvation sphere of $ZnCl_4^{2-}$ is beyond the scope of this study, the correctness of our assumption is highlighted by that fact that the interaction of $ZnCl_4^{2-}$ with 6 eq. of H_2O is exothermic by -30.9 kcal mol^{-1}

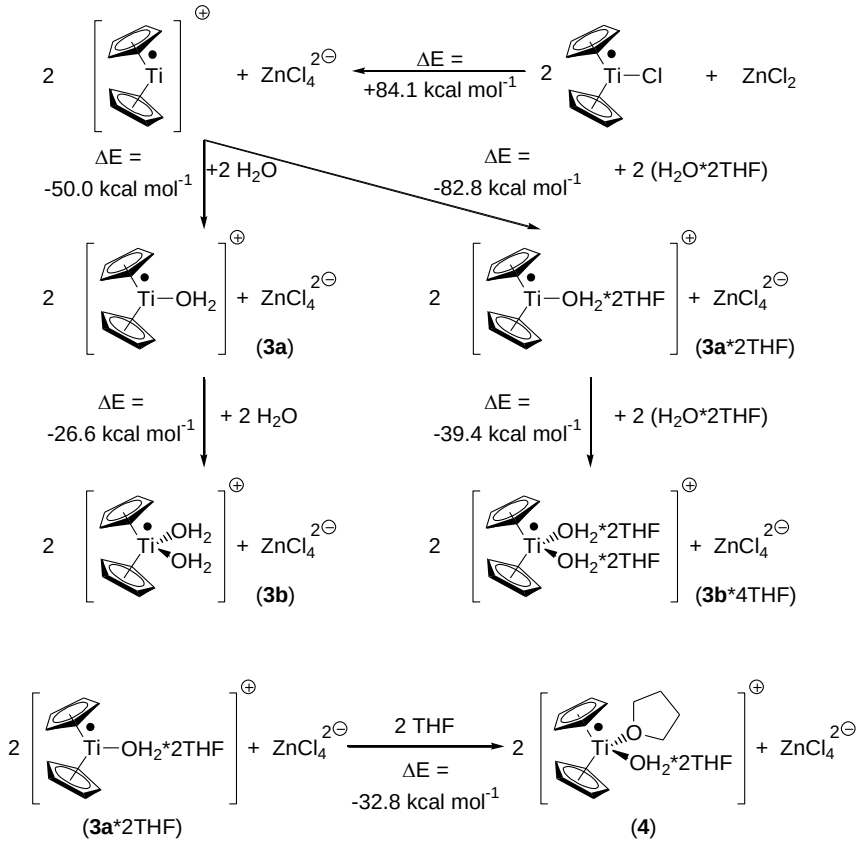

Scheme 4.2. Computational results on the formation of cationic titanocene(III) complexes in the presence of $ZnCl_2$ (B3LYP-d/def2-TZVPP). COSMO[4.17] with (ε = 7.6).

The computed bond dissociation energies (BDEs) of **2b***THF, **3a***THF, and **3b***3THF (52.3, 64.7, and 53.5 kcal mol^{-1}) are summarized in Scheme 3. We propose that a dissociation of one THF from the more stable fully hydrogen bonded species is necessary for an unhindered backside attack of a radical on H. As expected this dissociation of THF is especially difficult for the most Lewis-acidic **3a***2THF. The difference in BDE between **3a***THF and **3b***3THF is most likely due to the better stabilization of the Ti^{IV} in **7** through complexation. All species investigated constitute more efficient HAT reagents than traditionally employed cyclohexadienes, stannanes, silanes, and germanes.[4.1]

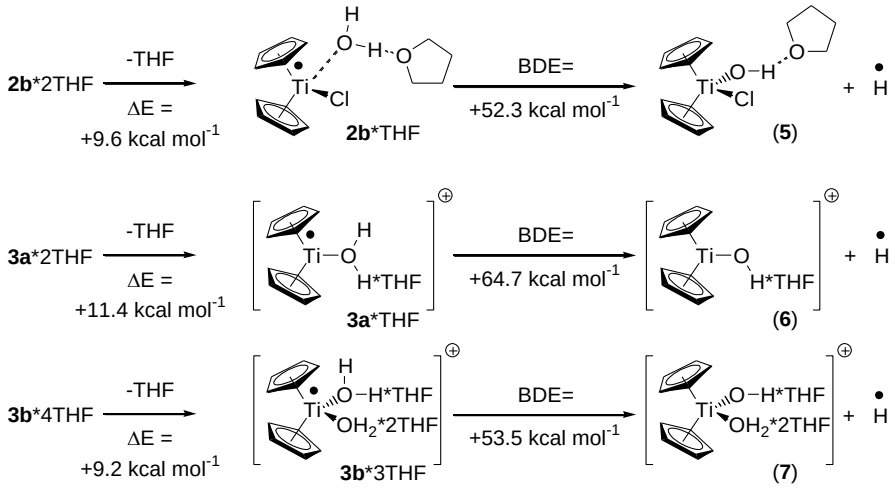

Scheme 4.3. Bond dissociation energies (BDE) of 2b*THF, 3a*THF, and 3b*3THF by DFT calculations (B3LYP-d/def2-TZVPP) with COSMO[4.17] (ε = 7.6).

4.3 Conclusion

Taking all of our experimental and computational results into account, it seems clear that addition of H_2O to Zn reduced [Cp_2TiCl_2] does not lead to the formation of **1**. The ESEEM spectra show that at a high concentration of H_2O, the chloride ligand is removed from the Ti^{III} center. The HYSCORE spectra demonstrate that with 10 and 100 equivalents of H_2O identical species are obtained. Both findings imply that even at low concentrations of H_2O no **1** is formed. This conclusion is supported by the CV measurements that also preclude a coordination of H_2O to a TiIII center with a chloride ligand. Instead, the shifts of the oxidation waves of the titanocene cations demonstrate the presence of waterligated $[Cp_2Ti]^+$ as in **3a** and **3b**. These experimental results are supported by the calculations that suggest that the formation of hydrated titanocene cations is more favorable than the formation of **1** even in the presence of a low number of equivalents of H_2O. Moreover, it has been demonstrated that the inclusion of THF is essential for the understanding of the structures and relative stabilities of the complexes involved.

It should be noted that the previous computational study[4.3c] did not consider the possibility of cationic structures. Moreover, the effects of specific interactions of H_2O with THF were neglected. None of the earlier experimental data provided direct structural data for the existence of **1**. A UV/ Vis study on the interaction of H_2O with $[(Cp_2TiCl)_2]$[4.3c] has demonstrated that the addition of more than 10 equivalents of H_2O results in dissociation of $[(Cp_2TiCl)_2]$. The resulting Ti species were not characterized further, though. While the observation of the dissociation is in agreement with our data, our EPR and CV measurements provide evidence for the cationic species **3**.

In a kinetic study, the rate constants for HAT from "[Cp_2TiCl]-complexed H_2O" to alkyl radicals were reported.[4.18] However, rate constants do not provide any structural information. Moreover, the measured rate constants are lower than those of stannanes even though the BDEs of the titanocene-derived species are substantially lower. This discrepancy can be readily explained with our results because an unfavorable loss of THF from **3a**·2THF and **3b**·4THF is required for HAT (Scheme 4.3). This

leads to a low concentration of the active HAT reagent and hence a reduction of the observed rate constant for HAT.

The mechanism of H_2O activation by Zn-reduced [Cp_2TiCl_2] is fundamentally different from that of MeOH activation by boranes.[4.2] This is due to the inability of boranes to form cationic species. Thus, boranes react with alcohols by associative processes to form classical Lewis base adducts. For these species the loss of alkyl radicals during HAT is essential.[4.2]

Our mechanistic proposal for the generation of Ti(III)-based HAT-reagents and the HAT itself should be valid for the activation of other molecules and electron transfer reagents,[4.19] also. This opens fascinating perspectives for the development of even more efficient and sustainable reagents. Cationic low-valent metal complexes, not necessarily derived from titanium,[4.20] with donor ligands containing O-H or N-H bonds should give such HAT-reagents. Amides and especially peptides or even proteins are prime candidates for such activation towards HAT.

4.4 References

[4.1] G. J. Rowlands, *Tetrahedron* **2009**, *65*, 8603–8655.

[4.2] a) D. A. Spiegel, K. B. Wiberg, L. N. Schacherer, M. R. Medeiros, J. L. Wood, *J. Am. Chem. Soc*. **2005**, *127*, 12513–12515; b) D. Pozzi, E. M. Scanlan, P. Renaud, *J. Am. Chem. Soc*. **2005**, *127*, 14204–14205.

[4.3] a) J. M. Cuerva, A. G. Campaña, J. Justicia, A. Rosales, J. L. Oller-López, R. Robles, D. J. Cárdenas, E. Buñuel, J. E. Oltra, *Angew.Chem.* **2006**, *118*, 5648–5652; *Angew. Chem. Int. Ed.* **2006**, *45*, 5522–5526; b) A. G. Campaña, R. E. Estévez, N. Fuentes, R. Robles, J. M.Cuerva, E. Buñuel, D. Cárdenas, J. E. Oltra, *Org. Lett.* **2007**, *9*, 2195–2198; c) M. Paradas, A. G. Campaña, T. Jiménez, R. Robles, J. E. Oltra, E. Buñuel, J. Justicia, D. J. Cárdenas, J, M. Cuerva, *J. Am.Chem. Soc.* **2010**, *132*, 12748–12756; d) M. Paradas, A. G. Campaña, M. L. Marcos, J. Justicia, A. Haidour, R. Robles, D. J. Cárdenas, J. E. Oltra, J. M. Cuerva, *Dalton Trans.* **2010**, *39*, 8796-8800.

[4.4] a) D. M. Smith, M. E. Pulling, J. R. Norton, *J. Am. Chem. Soc.* **2007**, *129*, 770–771; b) A. Gansäuer, C.-A. Fan, F. Piestert, *J. Am. Chem. Soc.* **2008**, *130*, 6916–6917; c) A. Gansäuer, M. Otte, L. Shi, *J. Am. Chem. Soc.* **2011**, *133*, 416–417.

[4.5] a) S.-H. Ueng, M. M. Brahmi, E. Derat, L. Fensterbank, E. Lacôte, M. Malacria, D. P. Curran, *J. Am. Chem. Soc.* **2008**, *130*, 10082–10083; b) S.-H. Ueng, A. Solovyev, X. Yuan, S. J. Geib, L. Fensterbank, E. Lacôte, M. Malacria, M. Newcomb, J. C. Walton, D. P. Curran, *J. Am. Chem. Soc.* **2009**, *131*, 11256–11262; c) J. C. Walton, M. M. Brahmi, L. Fensterbank, E. Lacôte, M. Malacria, Q. Chu, S.-H. Ueng, A. Solovyev, D. P. Curran, *J. Am. Chem. Soc.* **2010**, *132*, 2350–2358.

[4.6] a) W. B. Mims, J. Peisach, *Biochemistry* **1976**, *15*, 3863-3869; b) W. B. Mims, *Phys. Rev. B* **1972**, *5*, 2409-2419; c) W. B. Mims, *Phys. Rev. B* **1972**, *6*, 3543-3545; d) A. Schweiger, G. Jeschke, *Principles of Pulse Electron Paramagnetic Resonance;* Oxford University Press, Oxford, 2001.

[4.7] P. Höfer, A. Grupp, H. Nebenführ, M. Mehring, *Chem. Phys. Lett.* **1986**, *132*, 279-282.

[4.8] M. C. R. Symons, S. P. Mishra, *J. Chem. Soc. Dalton Trans.* **1981**, 2258-2262.

[4.9] H. L. Flanagan, D. J. Singel, *J. Chem. Phys.* **1987**, *87*, 5606-5616.

[4.10] A. Pöppl, L. Kevan, *J. Phys. Chem.* **1996**, *100*, 3387-3394.

[4.11] a) R. J. Enemærke, J. Larsen, T. Skrydstrup, K. Daasbjerg, *J. Am. Chem. Soc.* **2004**, *126*, 7853–7864; b) A. Gansäuer, A. Barchuk, F. Keller, M. Schmitt, S. Grimme, M. Gerenkamp, C. Mück-Lichtenfeld, K. Daasbjerg, H. Svith, *J. Am. Chem. Soc.* **2007**, *129*, 1359–1371.

[4.12] J. Larsen, R. J. Enemærke, T. Skrydstrup, K. Daasbjerg, *Organometallics* **2006**, *25*, 2031–2036.

[4.13] a) A. D. Becke, *Phys. Rev. A* **1988**, *38*, 3098-3100; b) J. P. Perdew. *Phys. Rev. B* **1986**, *33*, 8822-8824.

[4.14] A. Schäfer, C. Huber, R. Ahlrichs, *J. Chem. Phys*. **1994**, *100*, 5829-5835.

[4.15] a) R. Ahlrichs, M. Bär, H.-P. Baron, R. Bauernschmitt, S. Böcker, M. Ehrig, K. Eichkorn, S. Elliott, F. Furche, F. Haase, M. Häser, H. Horn, C. Huber, U. Huniar, C. Kölmel, M. Kollwitz, C. Ochsenfeld, H. Öhm, A. Schäfer, U. Schneider, O. Treutler, M. von Arnim, F. Weigand, P. Weis, H. Weiss, *Turbomole 5*, Institut für Physikal. Chemie, Universität Karlsruhe, **2002**; b) M. Häser, R. Ahlrichs, *J. Comput. Chem.* **1989**, *10*, 104-111; c) O. Treutler, R. Ahlrichs, *J. Chem. Phys.* **1995**, *102*, 346-354; d) P. Deglmann, F. Furche. Ahlrichs, R. *Chem. Phys. Lett*. **2002**, *362*, 511-518.

[4.16] a) C. Lee, W. Yang, R. G. Parr, *Phys. Rev. B*. **1988**, *37*, 785-789; b) A. D. Becke, *J. Chem. Phys.* **1993,** *98*, 5648-5652; c) F. Weigend, R. Ahlrichs, *Phys. Chem. Chem. Phys.* **2002**, *7*, 3297-3305; d) S. Grimme, *J. Comput. Chem.* **2004,** *25*, 1463-1473; e) S. Grimme, *J. Comput. Chem.* **2006**, *27*, 1787-1799.

[4.17] A. Klamt, G. Schüürmann, *J. Chem. Soc., Perkin Trans. 2* **1993**, 799-805.

[4.18] J. Jin, M. Newcomb, *J. Org. Chem.* **2008**, *73*, 7901-7905.

[4.19] a) E. Prasad, R. A. Flowers II, *J. Am. Chem. Soc*. **2005**, *127*, 18093–18099; b) D. Parmar, L. A. Duffy, D. Sadasivam, H. Matsubara, P. A. Bradley, R. A. Flowers II, D. J. Procter, *J. Am. Chem. Soc.* **2009**, *131*,15467–15473; c) D. V. Sadasivam, J. A. Teprovich, Jr., D. J. Procter, R. A. Flowers II, *Org. Lett.* **2010**, *12*, 4140–4143; d) D. Parmar, K.Price, M. Spain, H. Matsubara, P. A. Bradley, D. J. Procter, *J. Am. Chem. Soc.* **2011**, *133*, 2418–2420; e) D. J. Cárdenas, J. M. Cuerva, M. Alías, E. Buñuel, A. G. Campaña *Chem. Eur. J.* **2011**, *17*, 8318-8323.

[4.20] a) A. Gansäuer, D. Franke, T. Lauterbach, M. Nieger, *J. Am. Chem. Soc*. **2005**, *127*, 11622-11623; b) A. Gansäuer, I. Winkler, D. Worgull, D. Franke, T. Lauterbach, A. Okkel, M. Nieger, *Organometallics* **2008**, *27*, 5699-5707.

5 Trapping Radicals in Reductive Epoxide Opening

5.1 Introduction

Free radicals are reactive intermediates of considerable importance in the organic chemistry.[5.1,5.2] Especially, radical chain reactions are useful in synthesis such as in the formation of C-C bonds. Compared to the ionic counterparts the advantages of these reactions are the mildness of radical generation, the wide applicability to many functional groups and the high predictability of C-C bond-forming reactions. Also they are usually stable under protic conditions. All of these advantages, the use of chain reactions has increased the number in total syntheses of natural product.

However, the stereoselectivity and the chemoselectivity of the radical reaction cannot be controlled by using these transformations. An alternative approach to control radical selectivity is represented by reagent controlled transformations.[5.3,5.4] This reagent control is achieved by the use of transition metals, in which an electron transfer from low-valent metal complexes occurs . In this field, titanocene-mediated and titanocene-catalyzed radical reactions are attractive for the generation of the organic radicals.

Epoxides are one of the intriguing classes of radical sources in metal-initiated reactions due to their high reactivity and the ease of preparation from alkenes or carbonyl compounds.[5.5-5.7] The strain inherent (approximately 27 kcal/mol) in the three member ring causes the high reactivity during the ring opening event.

Additionally, an interesting alternative to chain radical reactions is the reductive ring opening reaction via single electron transfer from titanocene complexes. In this manner, Nugent and Rajanbabu[5.8-5.11] have demonstrated a novel method, which includes β-titanoxy radical from titanocene chloride. The cleavage of the titanium-oxygen bond features prevention of the ring opening reaction by S_N2 due to the low Lewis acidity of titanocene chloride reagent. Examples for titanocene-catalyzed epoxide opening reactions are the radical cyclizations such as 3-exo or 4-exo-cyclization, which have been employed in synthesis of natural products or biological active substances. Moreover, the titanocene-mediated epoxide ring opening reaction has been successfully used for radical-induced polymerization.[5.12-5.14]

An attractive feature of titanocene catalysis is the variety of titanocene complexes, which can influence the stereoselectivity by the chirality in the ligand. In particularly, the enantioselective opening of meso–epoxides has successfully been performed by using a chiral catalyst.[5.15] The chirality of the titanocene catalyst derives from either the ligand such as cyclopentadienyl

or from the titanium center. For example, the chiral menthyl-derived cyclopentadienyl[5.16] is prepared from the nature product pure menthol or ansa-metallocenes.[5.17,5.18]

Despite the advantage of the titanocene-mediated reductive ring opening reaction of epoxide, the reaction mechanism has only been studied computationally, hence the knowledge of the

determination of the structure and the electronic properties of intermediates of epoxide opening are not exactly understood.

In this contribution we investigate the reaction mechanism of the epoxide ring opening reaction by using the electron paramagnetic resonance (EPR) spectroscopy. Additionally, we used the hyperfine resolving techniques Electron Spin Echo Modulation (ESEEM)[5.20-5.22] and Hyperfine Sublevel Correlation (HYSCORE)[5.23,5.24] to obtain the detailed information of the electronic and geometric structure. In order to determine the hyperfine coupling of the hydrogen atoms and the magnetic hyperfine interaction between the unpaired electron and nearby nuclear spins, the pulsed electron nuclear double resonance (ENDOR)[5.25-5.27] technique is used. The magnitude of the hyperfine interaction reveals information about the effective distance between the unpaired electron and the nuclear spin. By using the EPR techniques, carbon radicals have not been directly observed. Therefore we used spin traps, which react with reactive free radicals to form stable nitroxide radicals.

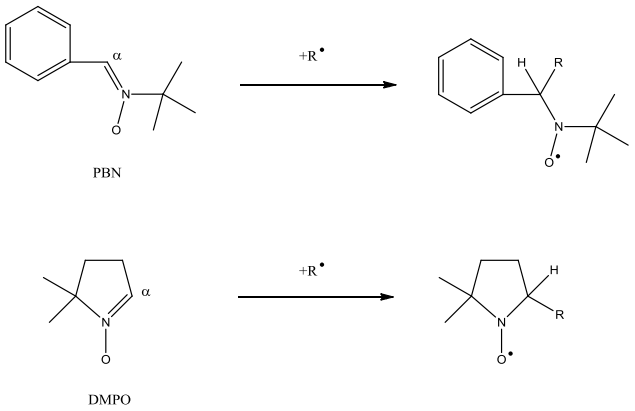

Scheme 5.1. Reaction of the spin traps N-*tert*-butyl-α-phenylnitrone (PBN) or 5,5-dimethyl-1-pyrroline N-oxide (DMPO) with free radicals $R^{\bullet}$.

The EPR spin trapping technique[5.28-5.31] is based on the indirect detection of the short-lived radicals by trapping with a diamagnetic compound. The most important class of diamagnetic spin traps are nitrones such as 5,5-dimethyl-1-pyrroline N-oxide (DMPO), α-(4-Pyridyl-1-oxide)-N-*tert*-butylnitrone (POBN) or N-*tert*-butyl-α-phenylnitrone (PBN), which DMPO is used as spin trap in this work. A characterization is possible on the dominant hyperfine coupling of the product, which derives from the nitrogen and the proton in the vicinity of reactive carbon atom. (See in Scheme 5.1)

In this paper, our results are summarized in two parts. The first part contains the results of the epoxide binding, which occurs in the reaction between epoxide and titanocene monochloride in the absence of the spin trap molecules. The results of the spin trap process are examined in the second part of our results. However, in general we report that DMPO binds directly to titanocene(III) molecules and the radical intermediates are observed during epoxide opening by titanocene monochloride. Also, the DFT calculations of the epoxide ring opening reaction evidence the spectral observations. Moreover, our results are the first proof for epoxide-titanocene complexes in reductive ring opening by electron transfer, in which the reaction proceeds via a radical reaction.

5.2 Experimental Section

Sample Preparation: All samples were prepared under an atmosphere of dry N_2 or Ar using standard Schlenk techniques. The solvent THF was distilled prior to use from sodium and benzophenone under N_2 or Ar. Cp_2TiCl_2 (Aldrich) and 1,1-diphenyl epoxide (Acros) were purchased and used as received.

A stock solution of Cp_2TiCl in THF was prepared by dissolving Cp_2TiCl_2 in THF to an end concentration of 10 mM and addition one or a varied equivalent of Zn powder.[5.11] Five molar equivalent 1,1-diphenyl epoxide was added to the green solution of Cp_2TiCl in THF at the room temperature or at -80° C. For the spin process, firstly one molar equivalent DMPO in THF was added into Cp_2TiCl in THF solution and after a few seconds. Ten or varied molar equivalents of 1,1-diphenyl epoxide were added to solution of Cp_2TiCl, DMPO in THF at room temperature.

The following samples have been prepared: (**1**) Cp_2TiCl in THF; (**2**) Cp_2TiCl in THF and 1,1-diphenyl epoxide; (**3**) Cp_2TiCl in THF with 1,1-diphenly epoxide and DMPO; (**4**) Cp_2TiCl in THF and DMPO. The solutions were transferred from a Schlenk tube into the EPR tube.

Measurements: EPR, ESEEM, HYSCORE and ENDOR spectra were recorded for frozen solutions (T = 30 K) of 10 mM concentration using a Bruker ELEXSYS E580 FT-EPR spectrometer. The EPR, ESEEM, HYSCORE and Davies-ENDOR experiments were performed with a Bruker MD4 (ENDOR) or MD5 (EPR, ESEEM, HYSCORE) resonator. For the Electron Spin Echo (ESE) detected EPR experiments, a Hahn echo pulse sequence with pulses of 24 ns and 48 ns and a pulse separation of 300 ns was employed. The three-pulse ESEEM[5.32] and HYSCORE experiments were carried out with pulses of 16 ns length. The time between the first two pulses was fixed at 200 ns. A mono-exponential background was subtracted from the modulation pattern. The resulting modulations were multiplied with a Hamming window function, zero-filled to 2048 points and Fourier transformed into frequency domain. The spectra were displayed as magnitude ESEEM spectra. Davies ENDOR spectra were recorded with a pulse sequence, which features an RF pulse of 10 µs, an inversion pulse of 200 ns, and a Hahn echo detection sequence with pulses of 100 ns and 200 ns. In the ENDOR experiment, the magnetic field and all microwave pulses are fixed and the frequency of the RF pulse is swept while monitoring the ESE detected EPR signal. The exact RF frequency, at which the echo-signal changes, provides information about the magnitude of the hyperfine interaction.

DFT calculations and geometry optimization of models for Cp_2TiCl and 1,1-diphenyl epoxide, Cp_2TiCl and DMPO and Cp_2TiCl with 1,1-diphenly epoxide and DMPO were performed with the ORCA program package.[5.33] The geometry optimization was carried out with the BP functional and a split-valence basis set with additional polarization functions (SVP).[5.34,5.35] After geometry optimization, the B3LYP functional and a triple-zeta basis set with polarization functions (TZVP)[5.36] was employed to calculate g values and hyperfine coupling constants.

5.3 Results and Discussion

Epoxide binding:

Q-band ESE detected EPR spectra (left), three-pulse time-domain ESEEM spectra (middle) and ENDOR spectra (right) of frozen solution of (**1**) and (**2**) are shown in Figure 5.1. The canonical g values read from the spectra are representative for a monomeric, species, which is in agreement with previous observations.[5.37] Interestingly, upon addition of 1,1-diphenyl epoxide, an EPR signal is still observable at 30 K, even though the color of the solution changes to red. The spectrum is characterized by essentially the same g values as those for Cp_2TiCl, though the intensity of (**2**) has redistributed such that the amplitude at g_x has increased.

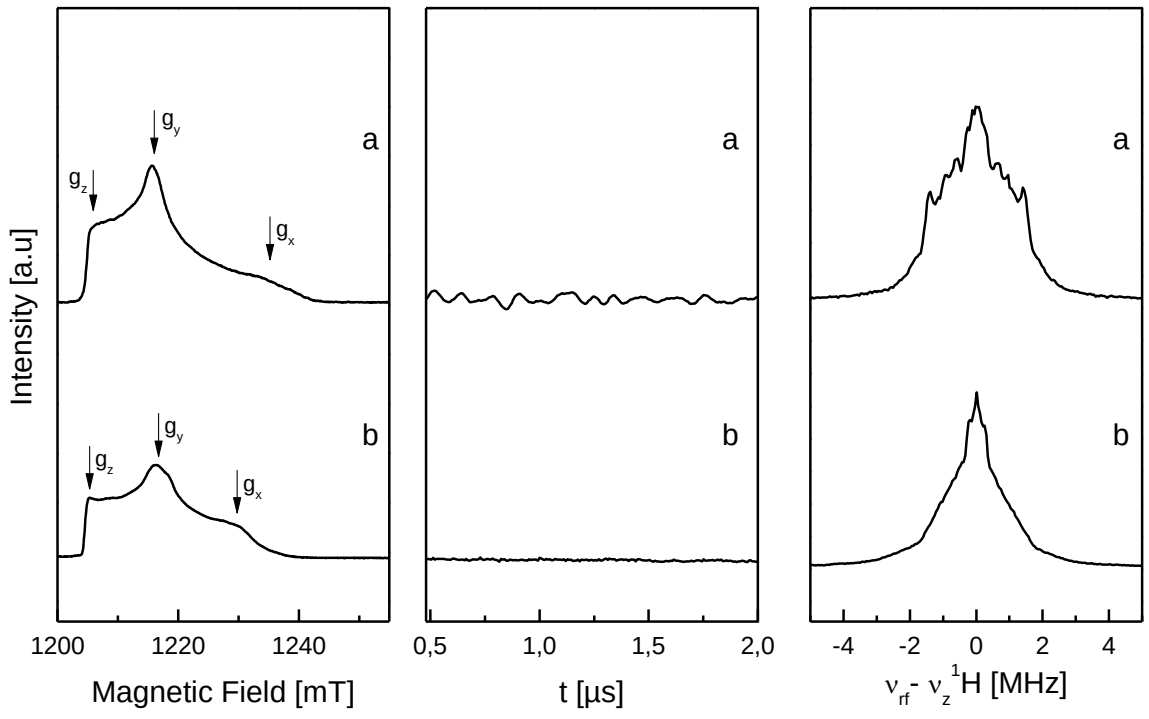

Figure 5.1. Q-band ESE detected EPR spectrum (left) (T = 30 K) of (a) Cp_2TiCl in THF, ν_{mw} = 33.117 GHz; (b) Cp_2TiCl in THF and 1,1-diphenyl epoxide, ν_{mw} = 33.914 GHz; Q-band three-pulse modulation patterns (middle) and ENDOR spectra (right) of (a) Cp_2TiCl in THF; (b) Cp_2TiCl in THF and 1,1-diphenyl epoxide, recorded at the g_y canonical orientations. Experimental conditions: Pulse sequence 90° - τ - 90° - T - 90° - T - echo. Length of 90° pulses 36 ns, τ = 300 ns. For ENDOR, RF Pulse length 10 µs, length of inversion pulse 200 ns.

The EPR experiments selectively investigate the paramagnetic monomeric species. The ESE detected EPR spectra indicate that the unpaired electron resides in essentially the same molecular orbital. Although the observed small changes in the canonical g values of (**1**) and (**2**), the g values, which are shifted away from g_z implies that the unpaired electron occupies orbital. This result can be corroborated by DFT calculations.

Table 5.1. Canonical and average g values for Cp_2TiCl, Cp_2TiCl and 1,1-diphenyl and g values derived from a DFT calculation for a Cp_2TiCl model.

Complex	g values			
	x	y	z	av.
Cp_2TiCl	1.955	1.983	2.001	1.979
Cp_2TiCl with 1,1-diphenyl epoxide	1.959	1.980	1.998	1.979
DFT	1.954	1.985	1.999	1.979

The hyperfine resolving ESEEM and ENDOR methods examine the chemical environment of spins and thus information about the binding of 1,1-diphenyl epoxide to Cp_2TiCl is obtained. The ESEEM method is suitable for detection of signals from nearby nuclear spins such that the frequency of the nuclear spin transition is close to 0 MHz. At Q-band, the nuclei of chloride can contribute to the ESEEM spectrum, but hydrogen does not contribute.

Q-band three-pulse time-domain ESEEM spectra (middle) and ENDOR spectra (right) of (**1**) and (**2**) have been recorded at the g_y canonical orientation. In Figure 5.1a (middle) displays a rich structure completely derived from coupling of the unpaired electron to the nuclear spin of Cl^- (I = 3/2). For Cp_2TiCl and 1,1-diphenyl epoxide, the echo invariably lacked significant modulations. As compared to the time-domain ESEEM spectrum of Cp_2TiCl to which only Cl^- contributes, the absence of echo modulation thus implies a removal of the chloride anion from the titanocene upon addition of epoxide.

The most striking observation is completely the disappearance of the signal upon addition of 1,1-diphenyl epoxide. Given that, the overall electronic structure has remained the same according to the EPR measurements, the changes observed in the ESEEM spectra upon addition of 1,1-diphenyl epoxide must be related to dissociate of chloride. The echo amplitude is not modulated for (**2**) as compared (**1**). Moreover, an intensity redistribution observed in the ESE detected the EPR spectrum of (**2**) corroborates dissociation of chloride.

In order to investigate the interaction of unpaired electron with nearby protons, Q-band Davies-ENDOR spectra were recorded, which are ideally suited for detection of nuclei with large gyromagnetic ratios for which the transition frequencies are far away from 0 MHz. The ENDOR spectra of complex (**1**) and (**2**) are given in Figure 5.1 (right panel). For free protons, the nuclear spin transitions are expected near the protons Zeeman frequency. The ENDOR spectrum of complex (**1**) spans the frequency region from -2.64 MHz to 2.96 MHz, indicating the presence of a proton with an effective hyperfine coupling constant of 5.6 MHz and the Zeeman frequency ν_z = 53.1 MHz. The ENDOR spectrum of (**1**) markedly differs from that of (**2**). In respect of Cp_2TiCl and 1,1-diphenyl epoxide, the signals span almost same range from -2.96 MHz and 2.98 MHz. With added 1,1-diphenyl epoxide, the decreased span of the ENDOR spectrum of (**2**), the binding of 1,1-diphenyl epoxide does not give rise to a proton, which is close to the unpaired electron of the titanium(III) center.

The observed nuclear hyperfine couplings between the unpaired electron and the protons visible in the ENDOR spectra corroborate the observations of the ESEEM spectra. Particularly, the ENDOR spectra of (**1**) and (**2**) are completely different, indicating that a strong interaction between the unpaired electron and proton from 1,1-diphenyl epoxide is absent.

Upon addition of 1,1-diphenyl epoxide, the intensity distribution in the ENDOR spectrum of the differs from of that Cp_2TiCl in THF. This observation may be related to the fact that the epoxide is bulkier than chloride. Because in the presence of the bulkier epoxide, the angle of the two cyclopentadienyl becomes larger, thus the hyperfine coupling constants of the cyclopentadienyl protons are affected thought this effect, which are observed in the ENDOR spectrum. The experimental and calculatedhyperfine coupling constants are summarized in the Table 5.2.

Table 5.2. Average isotropic hyperfine coupling constants (a_{epx}) [MHz] for Cp_2TiCl derived from ENDOR spectra and calculated values a_{DFT} from DFT calculations.

	a_{exp}	a_{DFT}		
Cyclopentadienyl Protons				
8	1.86	-2.02	-2.98	5.01
9	5.91	-3.32	-2.11	5.43
19	2.93	-2.62	-2.32	4.95
20	3.85	-2.78	-2.39	5.18

In summary, the experimentally found hyperfine coupling constants for Cp_2TiCl are agreement with the hyperfine constants derived from DFT calculations on Cp_2TiCl.

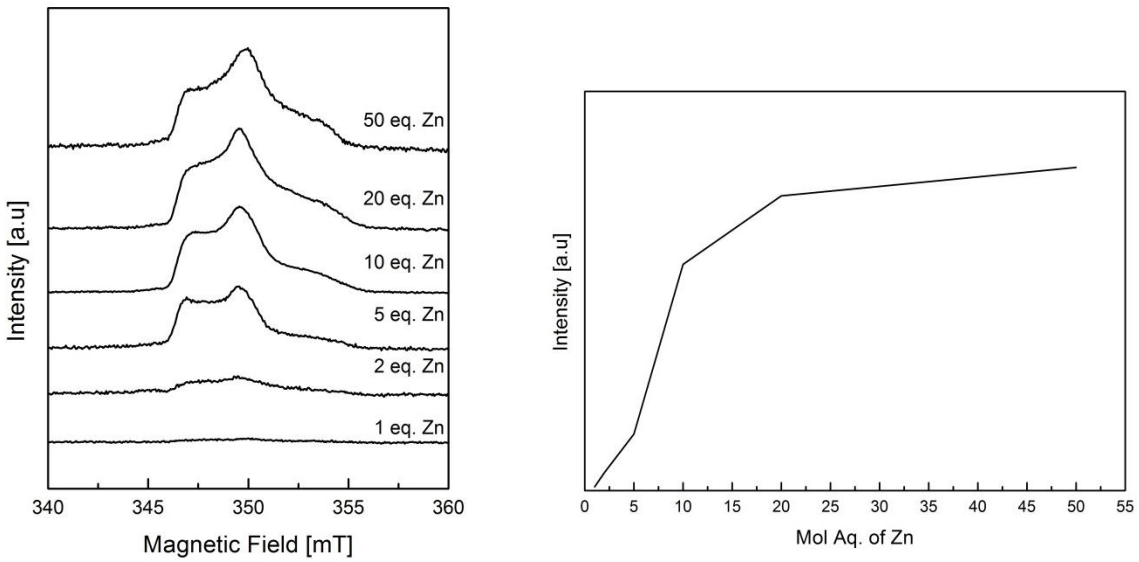

Figure 5.2. Left: X-band EPR spectra (T = 30 K) of 1 equivalent Cp_2TiCl_2 and 5 equivalent 1,1-diphenyl epoxide in THF with different added molar equivalents of Zn. Right: Amplitude of EPR signal at g_y as a function of the added molar equivalents Zn.

ESE detected EPR spectra of (**2**) with varied added molar equivalent of Zinc are given in the Figure 5.2. The spectra are characterized rhombic g values and completely identical of the spectrum of (**1**). Addition of one molar equivalent of Zinc, Cp_2TiCl fully reacts with epoxide, thus no signal can be

observed, because of the completely oxidation of $Ti^{(III)}$ to $Ti^{(IV)}$. With addition of increased molar equivalent of Zinc, an EPR signal is observed again. $Ti^{(IV)}$ can be reduced back to $Ti^{(III)}$ by added molar equivalents of Zinc. The $Ti^{(III)}$ signal can be saturated at 15 molar equivalent of Zinc (Figure 5.2, right panel).

Spin trapping:

The X-band ESE detected EPR spectra of frozen solution of (**1**) (left), (**4**) (middle) and (**3**) (right) are shown in Figure 5.3. The X-band EPR spectrum of (**1**) confirms once again that unpaired electron resides in molecular orbital at titanium. With respect to Cp_2TiCl in THF and DMPO, the spectrum is characterized by basically the same g values as those of Cp_2TiCl (See Table 5.3). The distance between the three most intense bands amounts to 2.9 mT. In contrast, in the spectrum of (**4**), the signal changed and the intensity distribution in the EPR spectrum differs from that of Cp_2TiCl in THF. The EPR spectrum of Cp_2TiCl in THF with 1,1-diphenyl epoxide and DMPO spans from g = 2.025 to g = 2.002, typical for a DMPO radical signal.

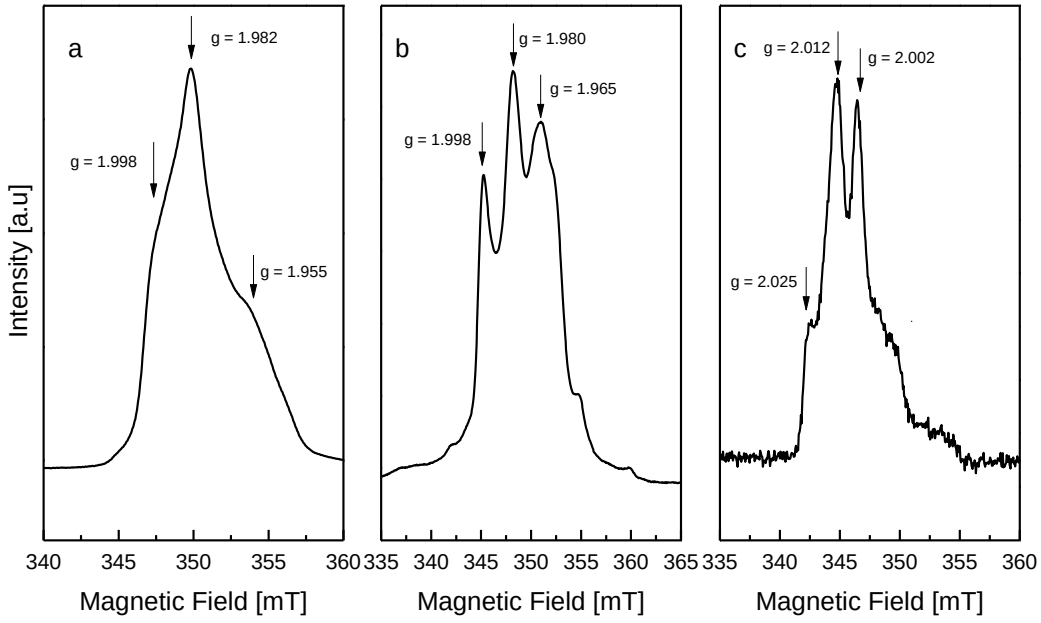

Figure 5.3. X-Band ESE detected EPR spectra (T = 30 K) of (a) Cp_2TiCl in THF, ν_{mw} = 9.7118 GHz; (b) $[TiCp_2]^+$ with DMPO in THF, ν_{mw} = 9.6617 GHz; (c) $[TiCp_2]^+$ with 1,1-diphenyl epoxide and DMPO in THF, ν_{mw} = 9.7188 GHz.

For a nitroxide radical, the unpaired electron in nitroxides is mainly distributed in a π orbital along the N-O bond. (See in Figure 5.7) Typical g values and typical hyperfine couplings are g_{xx} = 2.0090, g_{yy} = 2.0060, g_{zz} = 2.024 and $A_{xx} = A_{yy}$ = 18 MHz, A_{zz} = 96 MHz are found.[5.38-5.40]

Table 5.3. Canonical and average g values for Cp_2TiCl, Cp_2TiCl and 1,1-diphenyl epoxide, $[Cp_2Ti]^+$ with DMPO and $[Cp_2Ti]^+$ with DMPO and 1,1-diphenyl epoxide and g values derived from a DFT calculation for each model.

Complex	g values			
	x	y	z	av.
$TiCp_2Cl$	1.953	1.982	1.993	1.976
$[Cp_2Ti]^+$ with 1,1-diphenyl epoxide	1.959	1.979	1.997	1.978
$[Cp_2Ti]^+$ with DMPO	1.967	1.983	1.999	1.983
$[Cp_2Ti]^+$ with DMPO and 1,1-diphenyl epoxide	2.025	2.012	2.002	2.013
DFT ($[Cp_2Ti]^+$ with DMPO)	1.965	1.982	2.001	1.982
DFT ($[Cp_2Ti]^+$ with 1,1-diphenyl epoxide)	1.954	1.985	1.999	1.979
DFT ($TiCp_2Cl$ with 1,1-diphenyl epoxide and DMPO)	2.002	2.006	2.009	2.005

Epoxide binding has been investigated with DMPO as a spin trapping agent. As a control experiment, we measured no signals for DMPO in THF. Upon mixing of Cp_2TiCl with DMPO and with 1,1-diphenyl epoxide, an NO radical has been observed, which is characterized with typical g value for a nitroxide radical. When DMPO was added to Cp_2TiCl, a broader spectrum is obtained, in which titanium and nitrogen structure dominates, thus contributions of Ti are present. This indicates that DMPO most likely binds to Cp_2TiCl, but the unpaired electron is located still at titanium, so the electron transfer to form $Cp_2Ti^{(IV)}Cl$-epoxide radical has not occurred.

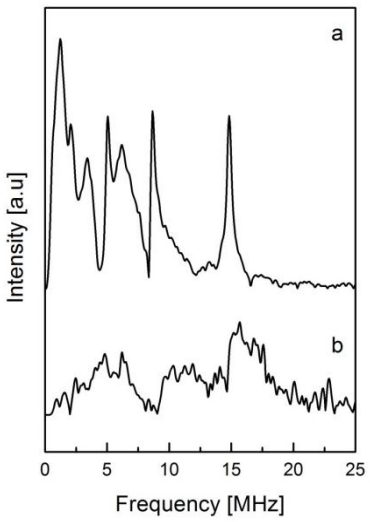

Figure 5.4. X-band frequency-domain ESEEM spectra (T=30 K) of (a) $[TiCp_2]^+$ with DMPO in THF, ν_{mw} = 9.6603 GHz; and (b) $[TiCp_2]^+$ with 1,1-diphenyl epoxide and DMPO, ν_{mw} = 9.7209 GHz.

In order to further investigate the electronic structure of the complexes, three-pulse ESEEM experiments have been performed at the low temperature. The X-band frequency-domain ESEEM spectra of frozen solutions of (**3**) and (**4**) are shown in Figure 5.4. The distance between the three most intense bands amounts to 2.9 mT. The three-pulse X-band ESEEM spectra of (**3**) and (**4**) have been recorded at the g_y canonical orientation. All signals are located between 0 MHz and 20 MHz. The two spectra look very different. The bands in the spectrum of complex (**4**) are significantly

broader than those of complex (**3**). The bands below 10 MHz in Figure 5.4a occur at 1.22, 2.08, 3.42, 5.07, 6.16, 8.67 MHz.

The ESEEM spectrum of Cp_2TiCl in THF and DMPO displays a rich structure completely derived from coupling of the unpaired electron to $^{14}N/^{15}N$ (Zeeman frequency ν_Z = 1.077 MHz). Thus, the coordination of the DMPO to the metal center is directly demonstrated through spectroscopic evidence.

These estimations were further confirmed by HYSCORE experiments. The HYSCORE spectrum of (**4**) recorded at the g_y canonical orientation is shown in Figure 5.5. The spectrum displays two sets of signals. One set stems from ^1H and is centered around the ^1H Zeeman frequency at coordinates (14.9, 14.9) MHz. The second set concerns signals with frequency below 10 MHz, for which cross peaks occur at the same frequencies as those observed in the ESEEM spectrum (Figure 5.4a).

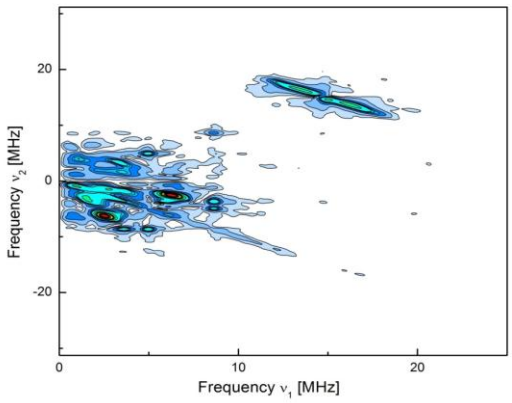

Figure 5.5. X-band HYSCORE spectra (T = 30) of $[Cp_2Ti]^+$ with DMPO in THF, recorded at the g_y canonical orientations. Experimental conditions: Pulse sequence 90° - τ - 90° - T - 90° - T - echo. Length of 90° pulses 16 ns, τ = 200 ns.

Signals of $^{35}Cl/^{37}Cl$ (ν_z = 1.467 MHz) cannot be distinguished from signals of the nitrogen atom. The Zeeman frequencies of these two atoms are close to each either, thus the signal of chloride and the signals of nitrogen overlap. Neither the ESEEM nor the HYSCORE experiments provide any evidence for dissociate of chloride. But DFT calculations support the motion of DMPO coordinated to the cationic Cp_2Ti containing without chloride ligand. However, the second set of signals derives from the $^{14}N/^{15}N$ (Zeeman frequency ν_Z = 1.077 MHz). In additional to the ESSEM spectrum of Cp_2TiCl in THF and DMPO, given these observed conclusions of the HYSCORE spectrum of the complex of Cp_2TiCl in THF and DMPO, the N does directly bind to titanium.

DFT calculations:

The singly occupied molecular orbitals (SOMOs) obtained for models of (**2**), (**3**) and (**4**) are shown in Figure 5.6. The singly occupied orbital at Ti is clearly recognizable for (**2**) and (**4**) complexes. Upon introduction of 1,1-diphenyl epoxide to the model geometry of (**2**), it turns out that epoxide bonding cannot be realized due to steric interactions of the phenyl groups with either the Cp ligands or Cl^-. Geometry optimization of this structure indeed leads to dissociation of the epoxide. Upon removal of Cl^- from the model structure and geometry optimization, the epoxide does bind and the optimized Ti-O distance amounts to 2.065 Å, indicating that a weak bond between Ti and the epoxide oxygen has been formed. For this optimized geometry, a SOMO is found as well. The epoxide does not open upon binding to titanium (III) complex. The two C-O distances amount to 1.60 Å and 1.44 Å and are slightly longer than the optimized distances of 1.45 Å and 1.43 Å for isolated 1,1-diphenyl epoxide. Although the epoxide does not open in the complex (**2**), for complex (**3**) the epoxide open upon binding to titanium (II), which the Ti-O distance amounts to 1.785 Å and indicating that Ti has not unpaired electron anymore. However, for complex (**4**), the singly occupied orbital at Ti is clearly visible. The optimized geometry of the complex (**4**) appears that the DMPO is hanging on Ti and Ti-O distance amount to 1.980 Å.

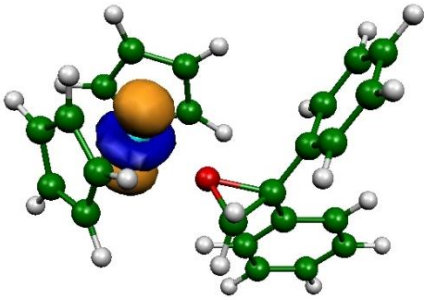

$[Cp_2Ti]^+$ ∗ 1,1-diphenyl epoxide

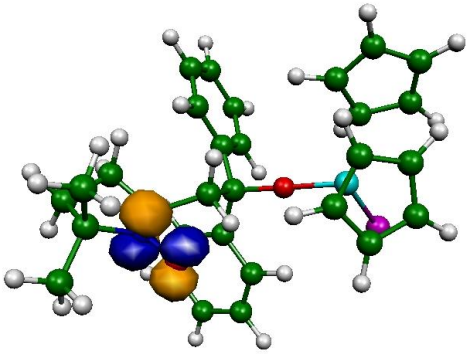

$[Cp_2TiCl]$ ∗ 1,1-diphenyl epoxide with DMPO

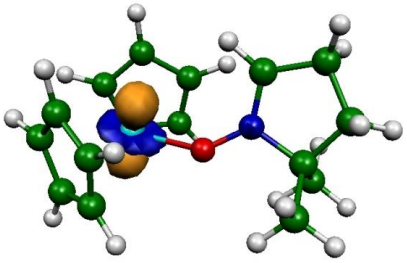

$[Cp_2Ti]^+ * DMPO$

Figure 5.6: Singly occupied orbitals for geometry-optimized models (B3LYP functional, SVP basis set)[34,35] of $[Cp_2Ti]^+$ with 1,1-diphenyl epoxide, $[Cp_2Ti]^+$ with DMPO and Cp_2TiCl with 1,1-diphenyl epoxide and DMPO.

The DFT calculations of (**2**) corroborate the dissociation of chloride, which is evident from the disappeared nuclear modulations of chloride upon addition of 1,1-diphenyl epoxide in the ESEEM spectra. (See in Figure 5.2b, middle) As understood from DFT calculations, in the presence of chloride, epoxide does not coordinate to $Ti^{(III)}$. Interestingly, after epoxide binding to titanium, DFT calculation shows that chloride can bind again to titanium.

Mechanistic Aspect:

Epoxide Binding:

The mechanistic pictures of reductive ring opening reaction of epoxide are shown in Scheme 5.2. We propose that the reaction proceeds in two steps. In the first step, epoxide reacts with Cp_2TiCl, which acts as a catalyst for this reaction. As an intermediate step, chloride is cleaved, $Ti^{(III)}$ binds to oxygen, thus β-titanoxy (**A**) radical is formed. For the next step, epoxide is opened and a carbon radical (**B** or **C**) is generated. In this step, there are two possibilities for generation of these carbon radicals.

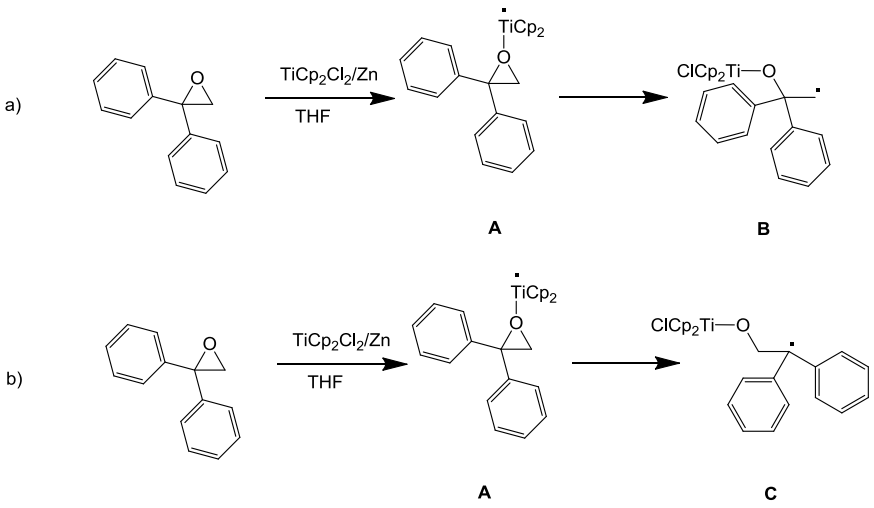

Scheme 5.2. Mechanistic picture for epoxide opening.

The singly occupied molecular orbitals (SOMOs) pictures of the two possible for the carbon radical (**B**, **C**) are given in the Figure 5.7. From the DFT calculations, the second radical (**C**) is more energetically more favorable amount to ΔE = - 22.703 kcal/mol. This result can be expected because the primary radical is more stable than according to the secondary radical.

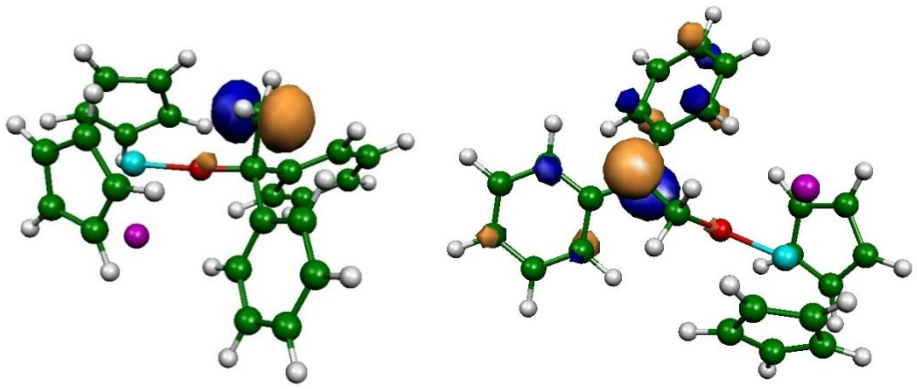

Figure 5.7: SOMO picture of for two possible carbons radicals for **3**.

In this manner, the second step is critical step for this reaction. The generation of the high energy species can be most likely avoided through electron transfer from titanium(III) to oxygen.

5.4 Conclusion

In this work, an EPR study of the reductive ring opening reaction of epoxide by titanocene(III) chloride has been performed. The generated carbon radical has been trapped by using of spin trap molecule and was investigated further by ESE detected EPR, ^{1}H ENDOR spectroscopy and ESEEM spectroscopy and HYSCORE spectroscopy at 9.7 GHz and at 34 GHz (X-band and Q-band, respectively). The interpretation of the spectra was supported by spin-unrestricted DFT calculations.

The addition of 1,1diphenyl epoxide to the green solution of Cp_2TiCl in THF results in a red solution. The change of color highlights that a large change in the first coordination sphere of titanium occurs upon addition of 1,1diphenyl epoxide that can be probed an ideal manner by the advanced EPR methods. The electronic ground state of all monomeric species is characterized by a $d_{z^2}^1$ singly occupied molecular orbital (SOMO) at $Ti^{(III)}$.

According to the ESEEM spectra, epoxide binding results in dissociation of the chloride ligand. To verify our results we plan to measure ESEEM and ENDOR spectra of deuterated 1,1-diphenyl epoxide under the same experimental conditions.

For the reduction of Cp_2TiCl_2 with different molar equivalents of Zinc, we demonstrated that epoxide does not polymerize due to saturation of the titanium(III).

A radical signal has been observed in the ESE detected EPR spectra using DMPO as a spin trap molecule. This suggests that DMPO molecule binds to epoxide. However, from this particular EPR spectrum it is unfortunately not clear if the epoxide is opened or not. Moreover, the ESEEM and HYSCORE spectra at X-band of Cp_2TiCl with DMPO have indicated that DMPO binds directly to titanium. The DFT calculation of the according to complex supports the experimental observations and also indicates that upon addition of DMPO to Cp_2TiCl, chloride dissociates.

5.5 References

[5.1] In *Radicals in Organic Synthesis*; P. Renaud, M. S., Ed.; Wiley-VCH: Weinheim, 2001.

[5.2] McCarroll, A. J.; Walton, J. C. *Angew. Chem.-Int. Edit.* **2001**, *40*, 2225.

[5.3] Gansäuer, A.; Bluhm, H. *Chem. Rev.* **2000**, 100, 2771.

[5.4] Gansäuer, A.; Pierobon, M.; Bluhm, H. *Angew. Chem.-Int. Edit.* **1998**, *37*, 101.

[5.5] Gansäuer, A.; Rink, B. *Tetrahedron*, **2002**, 58, 7017.

[5.6] Gansäuer, A. *Angew. Chem.* **1997**, 109, 2701. *Angew. Chem. Int. Ed.,* **1997**, 36, 2591.

[5.7] Meunier, B. *Chem. Rev.* **1992**, 92, 1411.

[5.8] Nugent, W. A.; RajanBabu, T. V. *J. Am. Chem. Soc*. **1988,** 110, 8561.

[5.9] RajanBabu, T. V.; Nugent, W. A. *J. Am. Chem. Soc.* **1989**, 111, 4525.

[5.10] RajanBabu, T. V.; Nugent, W. A.; Beattie, M. S. *J. Am. Chem. Soc.* **1990**, 112, 6408.

[5.11] RajanBabu, T. V.; Nugent, W. A. *J. Am. Chem. Soc.* **1994**, 116, 986.

[5.12] Asandei, A. D.; Moran, I. W. *J. Am. Chem. Soc.* **2004**, *126*, 15932.

[5.13] Mahanthappa, M. K.; Waymouth, R. M. *J. Am. Chem. Soc.* **2001**, *123*, 12093.

[5.14] Bohm, L. L. *Angew. Chem.-Int. Edit.* **2003**, *42*, 5010.

[5.15] Gansäuer, A.; Lauterbach, T.; Bluhm, H.; Noltemeyer, M. *Angew. Chem.-Int. Edit.* **1999**, *38*, 2909.

[5.16] Cesarotti, E.; Kagan, H. B.; Goddard, R.; Kruger, C. *J. Organomet. Chem.* **1978**, *162*, 297.

[5.17] Wild, F.; Zsolnai, L.; Huttner, G.; Brintzinger, H. H. *J. Organomet. Chem.* **1982**, *232*, 233.

[5.18] Collins, S.; Kuntz, B. A.; Taylor, N. J.; Ward, D. G. *J. Organomet. Chem.* **1988**, *342*, 21.

[5.19] Halterman, R. L. *Chem. Rev.* **1992**, *92*, 965.

[5.20] W. B. Mims, J. Peisach, *Biochemistry* **1976**, *15*, 3863.

[5.21] W. B. Mims, *Phys. Rev. B* **1972**, *5*, 2409.

[5.22] W. B. Mims, *Phys. Rev. B* **1972**, *6*, 3543.

[5.23] A. Schweiger, G. Jeschke, *Principles of Pulse Electron Paramagnetic Resonance;* Oxford University Press Oxford, 2001

[5.24] P. Höfer, A. Grupp, H. Nebenführ, M. Mehring, *Chem. Phys. Lett.* **1986**, *132*, 279.

[5.25] Mims, W. B. *Proc. Roy. Soc. London A* **1965,** *283*, 452.

[5.26] Davies, E. R. *Phys. Lett. A* **1974,** *A 47*, 1.

[5.27] Gemperle, C.; Sorensen, O. W.; Schweiger, A.; Ernst, R. R. *J. Magn. Reson.* **1990,** *87*, 502.

[5.28] Arroyo, C. M.; Kramer, J. H.; Leiboff, R. H.; Mergner, G. W.; Dickens, B. F.; Weglicki, W. B. *Free Radic. Biol. Med.* **1987**, *3*, 313.

[5.29] Tsai, P.; Elas, M.; Parasca, A. D.; Barth, E. D.; Mailer, C.; Halpern, H. J.; Rosen, G. M. *J. Chem. Soc.-Perkin Trans. 2* **2001**, 875

[5.30] Reszka, K. J.; McCormick, M. L.; Buettner, G. R.; Hart, C. M.; Britigan, B. E. *Nitric Oxide-Biol. Chem.* **2006**, *15*, 133

[5.31] Alvarez, M. N.; Peluffo, G.; Folkes, L.; Wardman, P.; Radi, R. *Free Radic. Biol. Med.* **2007**, *43*, 1523.

[5.32] Mims, W. B.; Peisach, J. *J. Chem. Phys.* **1978,** *69*, 4921.

[5.33] Neese, F. *ORCA - An ab initio, DFT and semiempirical SCF-MO package,* version 2.8r2556; University of Bonn: Bonn, Germany, 2010

[5.34] Eichkorn, K.; Treutler, O.; Ohm, H.; Haser, M.; Ahlrichs, R. *Chem. Phys. Lett.* **1995,** *240*, 283.

[5.35] Eichkorn, K.; Weigend, F.; Treutler, O.; Ahlrichs, R. *Theor. Chem. Acc.* **1997,** *97*, 119.

[5.36] Schäfer, A.; Horn, H.; Ahlrichs, R. *J. Chem. Phys.* **1992,** *97*, 2571.

[5.37] Symons, M. C. R.; Mishra, S. P. *J. Chem. Soc. Dalton Trans.* **1981,** 2258.

[5.38] Samuni, A.; Krishna, C. M.; Riesz, P.; Finkelstein, E.; Russo, A. *Free Radic. Biol. Med.* **1989**, *6*, 141.

[5.39] Migita, C. T.; Migita, K. *Chem. Lett.* **2003**, *32*, 466.

[5.40] Zhao, H. T.; Joseph, J.; Zhang, H.; Karoui, H.; Kalyanaraman, B. *Free Radic. Biol. Med.* **2001**, *31*, 599.

6 Radical 4-exo Cyclizations via Template Catalysis

This Chapter has been published in: A. Gansäuer, K. Knebel, C. Kube, A. Cangönül, M. van Gastel, K. Daasbjerg, T. Hangele, M. Hülsen, M. Dolg, and J. Friedrich *Chem. Eur. J.* **2012**, 18, 2591-2599.

6.1 Introduction

Radical cyclizations are amongst the most powerful methods for the construction of C-C bonds and have thus been extensively employed as key steps in the synthesis of natural products and biologically active substances.[6.1] However, serious limitations exist in the access to small rings, especially four-membered carbocyclic and heterocyclic compounds. This is due to the high strain of the cyclobutylcarbinyl radicals formed and the low rate constants of 4-*exo* cyclizations.[6.2]

In order to enforce an efficient propagation in classical radical chain reactions, either the use of substrates with *gem*-dialkyl or *gem*-dialkoxyl substitution and with activated radical acceptors, such as α-β-unsaturated carbonyl compounds,[6.3] or the incorporation of the 4-*exo* cyclization into transannular sequences is mandatory.[6.4]

Transition metal mediated and catalyzed processes offer a more general approach to slow cyclizations because chain propagation is not an issue. However, even the use of the most popular electron transfer reagents, SmI_2[6.5] and Cp_2TiCl derived complexes,[6.6] has only resulted in a limited number of 4-*exo* cyclizations that moreover rely on the aid of the *gem*-dialkyl effect.[6.7]

Recently, we described the first examples of such 4-*exo* cyclizations without assistance by the *gem*-dialkyl effect.[6.8] The use of our novel cationic catalyst **2**[6.9] was essential as shown for substrate **1** in Scheme 6.1. The opening of a coordination site for a two-point radical binding was postulated to be essential. In this manner, the radical and the radical acceptor are forced into spatial proximity at the titanocene template and the overall process should be rendered thermodynamically more favorable.

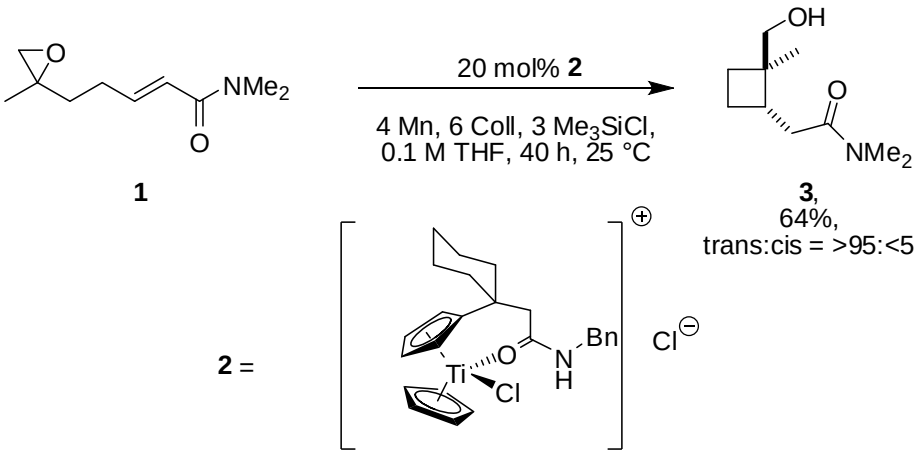

Scheme 6.1. 4-*exo* Cyclization of **1** catalyzed by Mn-reduced **2**.

Here, a combined synthetic, electrochemical, spectroscopic and computational study is presented that provides evidence for the postulated two-point binding mode at the catalyst and against a single-point radical binding. The surprisingly complex structures of our novel catalysts in solution could be determined and the origins of the diastereoselectivity of the 4-*exo* cyclizations are outlined. The mechanism is far more intricate than initially anticipated. Moreover, our results are of importance for the development of other unusual radical cyclizations.

6.2 Results and Discussion

Structure of Mn-reduced 2 in Solution: In order to study the mechanism of the 4-*exo* cyclization it is essential to establish the structure of Mn- or Zn-reduced **2**, the species responsible for radical generation through epoxide opening, in solution. This issue was addressed by using cyclic voltammetry (CV) and EPR spectroscopy. The combination of these methods is ideally suited for studying the coordination sphere of Mn-reduced **2** with its unpaired spin and its redox behavior. Potential structures for Mn-reduced **2** that contain $MnCl_2$ are shown in Figure 6.1.

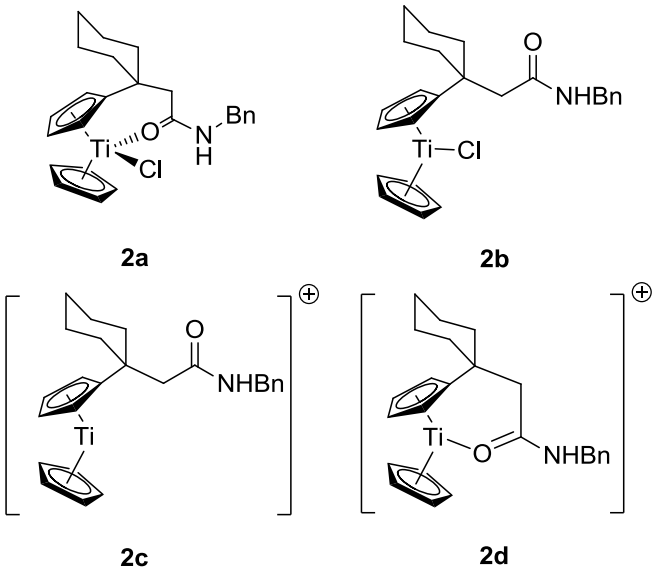

Figure 6.1. Potential structures of the titanocene components of **2** reduced by either Mn or Zn.

In **2a** the coordinated pending amide results in a neutral 17-electron complex.[6.10] **2b** is a 15-electron complex similar to simple alkyl substituted titanocenes such as (tBuC$_5$H$_4$)CpTiCl. The super-unsaturated 13-electron complex **2c** would be formed from **2b** by abstraction of chloride. The formation of a hydrogen bond to amide N-H by chloride and complexation of $MnCl_2$ or $ZnCl_2$ by the amide could provide the driving force for ionization. Finally, the seemingly more stabilized 15-electron complex **2d** can either be formed through chloride abstraction from **2a** or by complexation of the amide from **2c**.

CV of Mn- and Zn-reduced 2: To establish the composition of THF solutions of Mn-reduced **2**, cyclic voltammograms of **2** and (tBuC$_5$H$_4$)CpTiCl$_2$ (**4**) were recorded at a sweep rate, ν, of 50 or 500 mV s^{-1} (Figures 6.2A and B, respectively) along with corresponding voltammograms of Mn-reduced **2** and **4** (Figures 6.3A-C). In the discussion of the redox features it is important to recall that CV is a dynamic technique, in which the species generated and detected at the electrode are not necessarily the same as those actually present in the bulk solution.

The voltammograms of **4** are similar to those of other alkyl substituted titanocene complexes.[6.11] Thus, the redox wave appearing with a characteristic potential of -1.33 V vs. Fc$^+$/Fc for ν = 500 mV s^{-1} (taking as the average of the two peak potentials) is assigned to **4/4$^-$**, where **4$^-$** is the anionic species [(tBuC$_5$H$_4$)CpTiCl$_2$]$^-$. In comparison, the voltammograms of **2** also show a distinct redox wave shifted in a positive direction by ~300 mV relative to that of **4/4$^-$**. This large potential shift cannot be attributed to a difference in the inductive effect of the alkyl substituents, since in both cases a tertiary carbon atom is attached directly to the cyclopentadienyl ring. Rather this is a reflection of the ionic structure of **2** caused by the ability of the pending alkyl amide to displace chloride from the titanium atom. Formally, the reduction of **2** should afford **2a** which is substantiated through an analysis of the constitution of the Mn-reduced solutions (vide infra). On the basis of the oxidation potentials recorded for **4$^-$** and **2a** it may be concluded that the former with its negative charge is a more potent reductant than the latter. Importantly, this does not imply that it also the most reactive titanium(III) species.[6.11]

For a Mn-reduced solution of **4** the neutral (tBuC$_5$H$_4$)CpTiCl would be the main constituent according to earlier studies.[6.11] Indeed the same characteristic voltammetric features are observed with the peak at -0.78 V vs. Fc$^+$/Fc for ν = 500 mV s^{-1} assigned to the oxidation of (tBuC$_5$H$_4$)CpTiCl (Figures 3A and C). The second oxidation wave at -0.47 V vs. Fc$^+$/Fc for ν = 500 mV s^{-1} pertains to the cation (tBuC$_5$H$_4$)CpTi$^+$ that is generated along with (tBuC$_5$H$_4$)CpTiCl$_2$ at the electrode in a so-called parent-child reaction. (tBuC$_5$H$_4$)CpTi$^+$ is not present in the bulk solution but only formed at the electrode surface during the sweep. This is because the relative intensity of the second oxidation wave decreases with respect to the first wave on increasing ν (see Supporting Info).[6.11a-c] Finally, on the reverse sweep a reduction peak appears at -1.26 V vs. Fc$^+$/Fc for ν = 500 mV s^{-1} due to the reduction of the (tBuC$_5$H$_4$)CpTiCl$_2$ formed in the electrode processes.

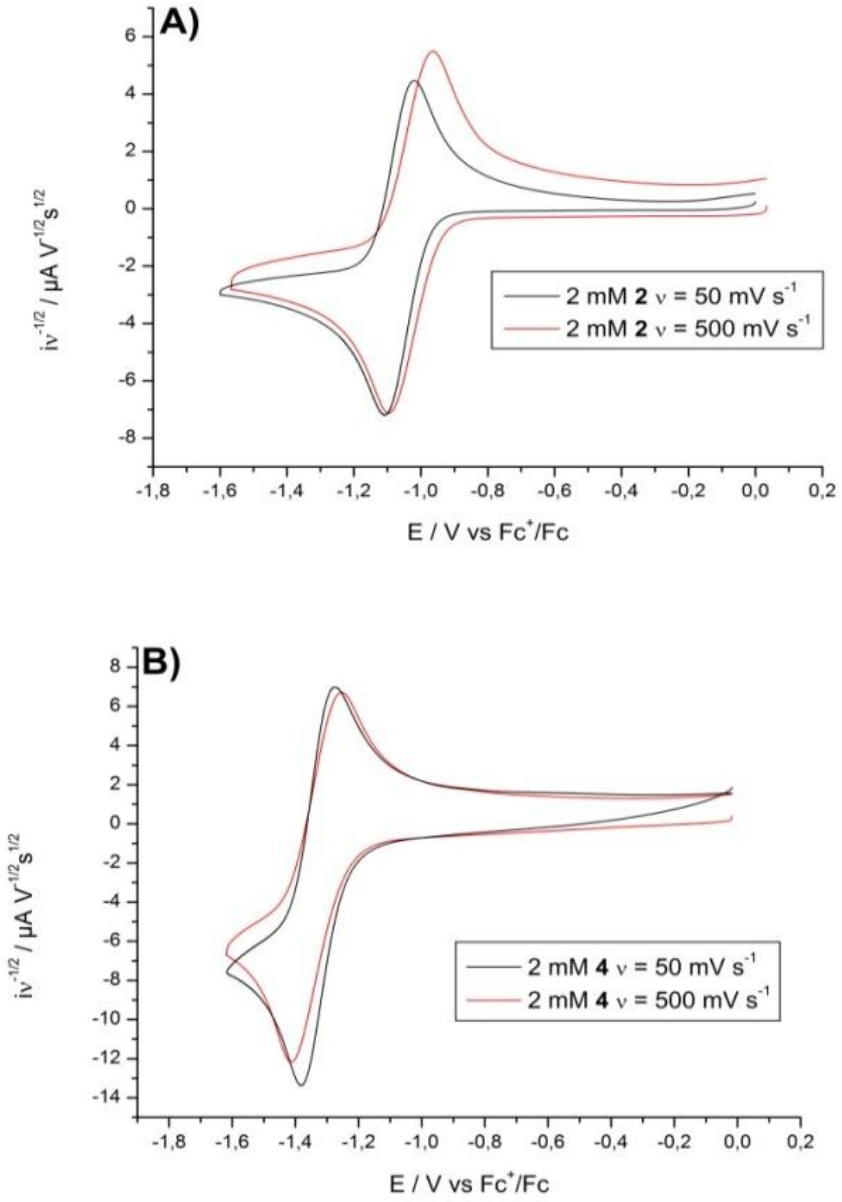

Figure 6.2. CV of **2** and **4** recorded at ν = 50 and 500 mV s^{-1} in 0.2 M $TBAPF_6$/THF.

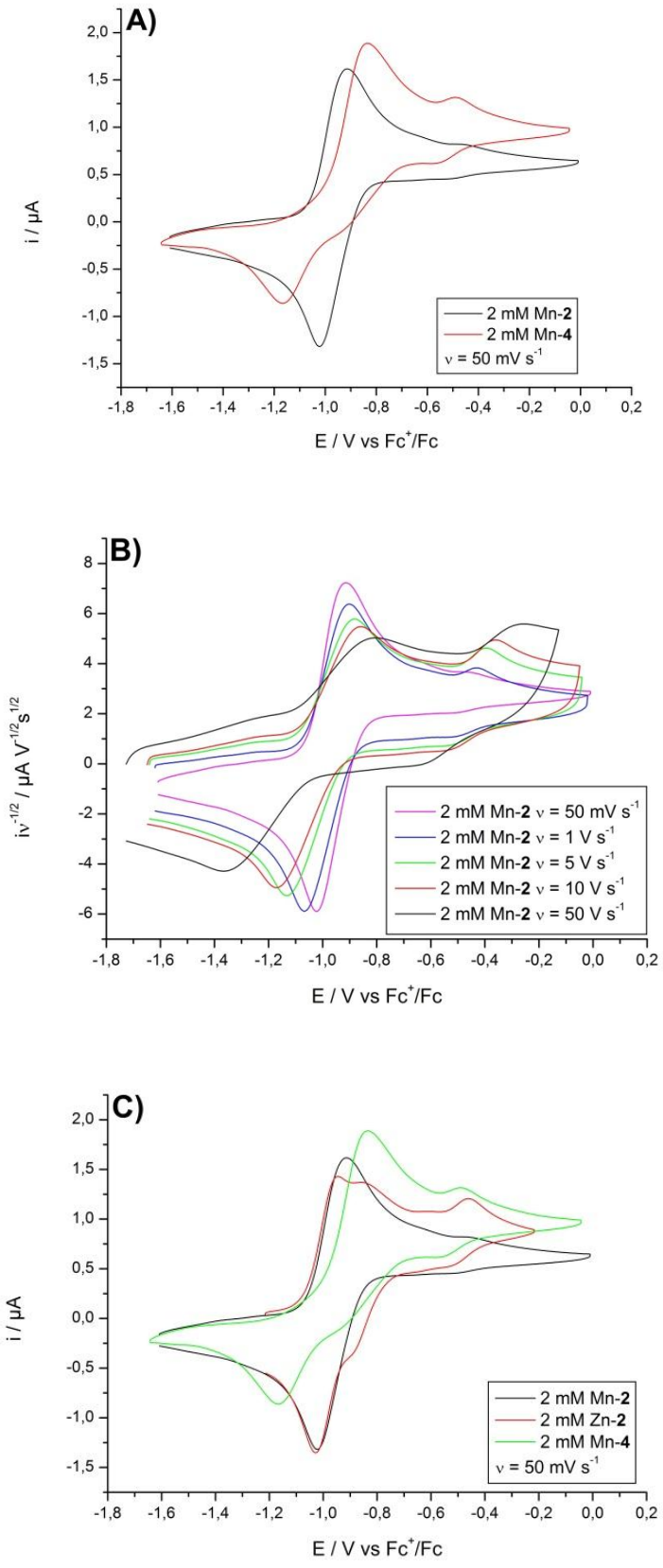

Figure 6.3. CV of Mn- and Zn-reduced **2** and **4** in 0.2 M $TBAPF_6$/THF.

For Mn-reduced **2** the oxidative features on the forward sweep are independent on the time scale of the experiment. Two peaks are observable at -0.91 and -0.48 V vs. Fc^+/Fc for ν = 50 mV s^{-1}. A comparison of this voltammogram with those of the Mn-reduced **2** and **4** demonstrate that the first peak of Mn-reduced **2** is not due to **2b** that should have a peak at about -0.83 V vs. Fc^+/Fc (Figure 6.3A and 6.3C) exactly as the first peak observed in the CV of Mn-reduced-**4** that corresponds to (tBuC$_5$H$_4$)CpTiCl.[6.11]

Further, this implies that the first peak at -0.91 V vs. Fc^+/Fc most likely originates from the oxidation of the amide-coordinated **2a** species, which exactly is the one detected on the backward oxidative sweep in the voltammogram of **2** (vide supra; Figure 6.2A). This interpretation is supported by the fact that for the unsubstituted Cp_2TiCl prepared in a Mn-reduced solution of Cp_2TiCl_2 the oxidation wave shifts by ~200 mV in negative direction upon addition of the oxygen-containing coordinating agent .[6.10]

Also, an oxidation wave at -0.48 V vs. Fc^+/Fc was observed for Mn-reduced **2** that is, by analogy to Mn-reduced **4** (exhibiting a wave at -0.48 V vs. Fc^+/Fc), attributed to the oxidation of the uncoordinated cationic **2c**. However, in sharp contrast to the voltammetric behavior seen for Mn-reduced **4** the relative intensity of this wave increases with increasing ν (Figure 6.3B) which would suggest that **2c** might be genuinely generated in the Mn-induced reduction of **2** rather than just temporarily through secondary reactions at the electrodes.

In principle, if sufficiently high sweep rates are employed in CV to decrease the time scale of the experiment and hence outrun follow-up reactions a true picture of the solution content would be obtainable. Unfortunately, with the ordinary microelectrodes used here it is not possible to attain such a situation, meaning that even when employing ν = 50 V s^{-1} the precise equilibrium ratio of **2a** and **2c** is not revealed. Still, it may be stated that to the best of our knowledge this is the first instance that a cationic species has been observed for titanocene(III) chlorides. Since there are no further unassigned oxidation waves it may be concluded on the basis of the CV investigations that a solution of Mn-reduced **2** consists of **2a** and the unusual **2c**, although in an unknown equilibrium proportion.

The situation is somewhat more complicated for Zn-reduced **2**. Besides the two peaks observable for all sweep rates (-0.94 and -0.43 V vs. Fc^+/Fc at ν = 500 mV s^{-1}, see Supporting Information for further details) a third peak appears at -0.85 V vs. Fc^+/Fc for ν = 50 mV s^{-1} (Figure 6.3C, red CV). A comparison of the voltammograms of Zn-reduced **2** and **4** (see Supporting Information) reveals coincidence of the peaks at -0.85 V vs. Fc^+/Fc. This suggests that the non-amide coordinated **2b** species is the one giving rise to this small oxidation wave. Since **2b** is only observed at rather low sweep rates it must be formed in a slow equilibrium process, involving another species such as the cationic **2c** or **2d** being more difficult to oxidize.

It is surprising that the 13-electron complex **2c** should be favored over the 15-electron amide-coordinated **2d**, in particular, when taking into account that of the two neutral titanocene(III) chlorides, **2a** and **2b**, the former amide-coordinated was the favored one as deduced from the cyclic voltammograms. Thus, one might consider the option, that the peak at -0.48 V vs. Fc^+/Fc originates from the oxidation of **2d** rather than **2c**, assuming that the ligand stabilization of **2d** and its oxidized form would be the same. However, this suggestion seems highly unlikely since coordination of an

amide to titanium(IV) is stronger than to the corresponding titanium(III) core. Moreover, we have previously found that the wave pertaining to the unsubstituted Cp_2Ti^+ cation was shifted by ~400 mV in a negative direction upon addition of HMPA.[6.10] Thus, a significantly lower potential for the oxidation peak of **2d** than -0.48 V vs. Fc^+/Fc is expected.

A mechanism for generation of **2c** from **2a** must account for the abstraction of chloride and the removal of the amide ligand from the titanium center. This can be accomplished by a hydrogen bond between the chloride ion and the N-H bond of the pending amide and a complexation of the amide carbonyl group by the MCl_2 (M = Mn, Zn) salts generated during the reduction of **2**.

EPR–Measurements of Zn-reduced 2: In order to provide further experimental support for a coordination of the pending amide to titanium, Electron Spin Echo Envelope Modulation (ESEEM) spectra were recorded. The ESEEM method is especially well suited for studying the coordination sphere of metal center by detecting magnetic couplings of the electron to atoms with nuclear spin greater than zero.[6.12] In our case this could allow the recognition of amide complexation [I(^{14}N = 1)], since a magnetic coupling is only present if the amide ligand is directly bound to Ti. The ESEEM spectrum of Zn-reduced **2** in THF at 30 K is shown in Figure 6.4.

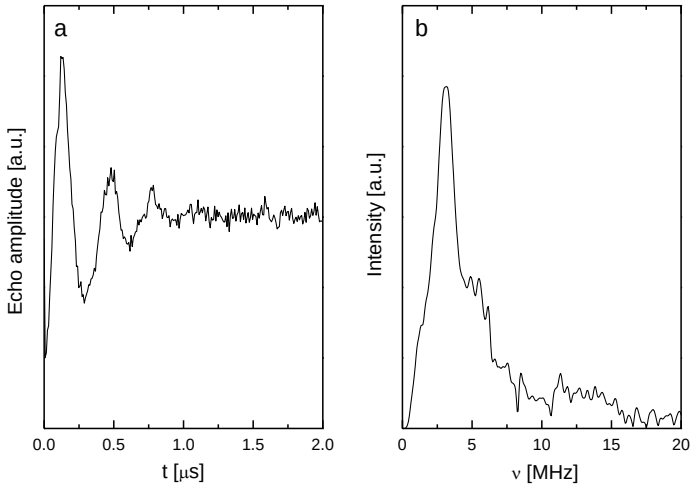

Figure 6.4. a) Modulation pattern and b) 3-pulse ESEEM spectrum of Zn-reduced **2**. Experimental conditions: T = 30 K, microwave frequency = 33.1962 GHz, B = 1.1942 T, length of $\pi/2$ pulse = 40 ns, pulse sequence = $\pi/2$ – 200 ns – $\pi/2$ – t – $\pi/2$ – echo.

The modulation pattern in the time domain and the corresponding signal at 3.23 MHz in the frequency domain are indeed indicative of a coupling between the electron located on titanium and ^{14}N. Thus, unambiguous direct spectroscopic evidence for the coordination of the amide ligand to the metal center and hence for the presence of **2a** is provided by EPR spectroscopy.

Epoxide Opening by Mn- or Zn-reduced 2: Knowledge of the active species of epoxide opening,[6.13] the radical generating step of the 4-*exo* cyclization, and of the binding of the radical to titanium is essential for the understanding of the 4-*exo* cyclization.

Of the complexes present in THF solutions of Mn-reduced **2**, **2a** is unlikely to be responsible for epoxide opening because it has no free coordination site. The super-unsaturated 13-electron complex **2c** is cationic and hence a strong Lewis acid with vacant coordination sites and should bind the epoxide easily. Ensuing electron transfer results in the formation of radical **6** containing a cationic 14-electron titanium(IV) center that will either coordinate the pending amide or the α,β–unsaturated amide of the substrate.[6.9] In this manner **7** and **8** are formed from **6** (Scheme 6.2).

It should be noted, that the minor neutral and hence less reactive minor 15-electron complex **2b** that is only present in Zn-reduced **2** can also be an active species for epoxide opening. After electron transfer, radical **9** containing a 16-electron titanium(IV) center is formed. Substitution of the chloride ligand by the amides results in the generation of **7** or **8**.

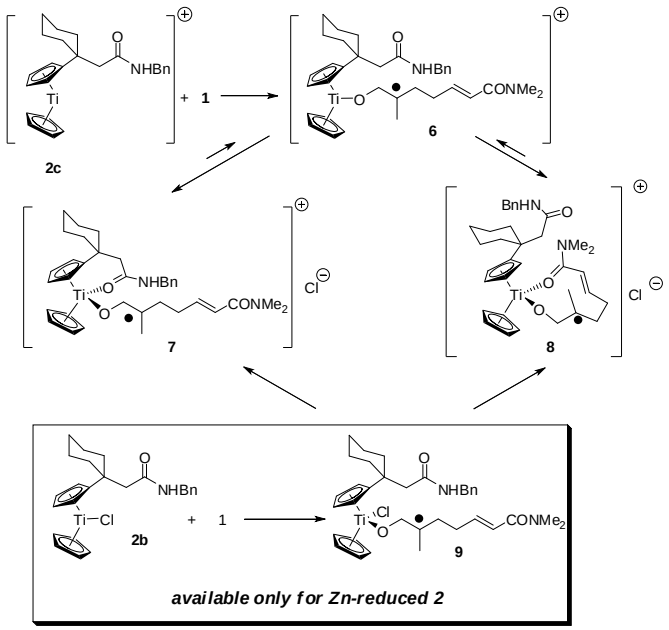

Scheme 6.2. Proposed mechanism of the ring-opening of **1** with Mn- or Zn-reduced solutions of **2** and possible structure of radical intermediates. For reasons of clarity **8** is only shown with the *trans*-orientation of the α,β–unsaturated amide and alkoxide groups.

The formation of **7** should be more favorable in analogy to **2** because the titanium containing ring is not strained. This should result in a cyclization similar to those of any unsaturated epoxide catalyzed by alkyl substituted titanocene complexes.[6.7f,i] Complexation by the unsaturated amide, on the other hand, leads to a strained ten-membered ring with a two point-binding of the radical to titanium. In this less favorable binding mode, the amide is additionally activated towards radical addition by complexation to the metal center and the 4-*exo* cyclization should be promoted.

One other aspect is important for the understanding of the 4-*exo* cyclization. In titanocene(IV) complexes with pending amides it has been demonstrated that amide coordination is reversible.[6.9] This implies that **7** and **8** equilibrate via **6**. A complete conversion is impossible if **7** and **8** cannot interconvert and only one leads to the desired product.

The mechanism of these cyclizations was investigated by a combined analysis of synthetic and computational studies next. The computational results, if in agreement with the outcome of the experiments, are especially revealing because they provide not only reaction and activation energies of the processes involved but also structures of pertinent intermediates, transition structures, and products that can be employed for the design of more efficient catalysts.

Experimental and Computational Analysis of the Mechanism of the 4-*exo* Cyclization, Origin of Diastereoselectivity:

Experimental Results of the 4-*exo* Cyclization:

Critical experimental results for a mechanistic analysis of the template catalyzed 4-*exo* cyclization are summarized in Scheme 6.3.[6.8] Only the use of the template catalyst **2** and closely related titanocenes resulted in conversion to **3**. Complete *trans*-diastereoselectivity of the cyclization at 0 °C, room temperature, and 68 °C (refluxing THF) was observed. This is quite unusual as the diastereoselectivity of most radical cyclizations normally strongly decreases with increasing reaction temperature. With larger primary substituents than CH_3 as in **10** at the tetrasubstituted epoxide carbon, the diastereoselectivity of the formation of **11** is slightly reduced but also constant over the same temperature range. With Zn as reductant the same diastereoselectivity was observed. The isolated yield of **3** was lower, however, when Zn was used as reductant. This is due to competing decomposition of the substrate in the presence of $ZnCl_2$ during the extended reaction time.

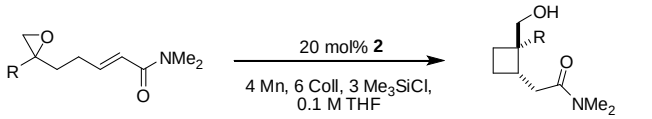

1: R = CH_3
40 h, 25 °C
24 h, 68 °C
72 h, 0 °C

3: R = CH_3
64%, trans:cis = >95:<5
64%, trans:cis = >95:<5
41%, trans:cis = >95:<5

10: R = CH_2CH_3
40 h, 25 °C

11: R = CH_2CH_3
63%, trans:cis = 90:10

1: R = CH_3, Zn as reductant
40 h, 25 °C

3: R = CH_3
48%, trans:cis = >95:<5

Scheme 6.3. Experimental results of the template catalyzed cyclization of **1** and **10**.

Any proposed mechanism of the 4-*exo* cyclization must account for this behavior. Possible courses of the cyclobutane formation were investigated next with the aid of computational chemistry.

Computational Details: The geometry optimizations were carried out within the framework of DFT with the BP86/TZVP method (Becke-Perdew gradient corrected exchange and correlation density functional[6.14] combined with a polarized split-valence basis set of triple-zeta quality[6.15]) using the RI-approximation (resolution of identity) within the TURBOMOLE program package.[6.16] The stationary points on the potential energy surface were characterized by analyzing the Hessian matrix.[6.17] The energies were corrected for the zero point vibrational energy (ZPVE).[6.17] In our earlier work on radical cyclizations it was found that BP86/TZVP calculations yield satisfactory results for these types of reactions.[6.7i] Solvation effects were estimated by single point calculations at the gas phase structure using the COSMO model.[6.18]

Computational Study of the Reaction Mechanism: In this computational study, the cyclohexylidene group in **7** and **8** was replaced by a *gem*-dimethyl group and the NHBn group by an NHMe group to reduce the complexity of the system. This is justified because the experimental results are essentially identical for titanocenes containing such changes.[6.8]

Single Point Binding of the Radicals:

The simplest starting point of the study of the 4-*exo* cyclization is radical **12** featuring a single-point binding of the radical to the titanocene. It should be noted that this single-point binding results in a reaction similar to that of free-radical reactions where the titanocene acts as a radical generating agent and bulky group as potential passive control element of diastereoselectivity. No further activation of the radical or the radical acceptor towards the 4-*exo* cyclization is operative in this scenario.

The coordination of the pending amide to the a cationic Ti(IV) center is analogous to **2**. As yet, there are no examples of such compounds without this particular complexation.[6.9a,c] In all structures similar to **2**, the chloride ligand is found close to the coordinated pending amide, presumably for electrostatic reasons. If, as in **2**, the amide possesses an N-H bond, the chloride is additionally stabilized by a hydrogen bond to the N-H proton. Thus, in the starting geometry of **12**, chloride was hydrogen bonded to the proton of the NHMe group in close vicinity of the pending amide. The results of the calculations of the cyclizations of **12** are summarized in Table 6.1. Since charged species are involved, solvents effects were simulated by using the COSMO model with a dielectric constant of $\varepsilon = 10$.

Table 6.1. Relative energies of substrates, products, and transition states of the 4-*exo* cyclization of **12**. The ZPVE is included from the BP86/TZVP calculation.

Method	**12**	**TS12cis**	**TS12trans**	**12Pcis**	**12Ptrans**
BP86/TZVP	0.0	+10.2	+10.6	+2.8	+2.0
BP86/TZVP/COSMO	0.0	+12.9	+12.9	+5.4	+4.7

Using the COSMO model the relative energies of the transition states and products are increased by about 2.5 kcal mol^{-1}. Thus, the trends predicted by the BP86/TZVP remain unaffected by the COSMO model for the cyclization of **12**. Even a value of $\varepsilon = \infty$ did not change the qualitative trends.

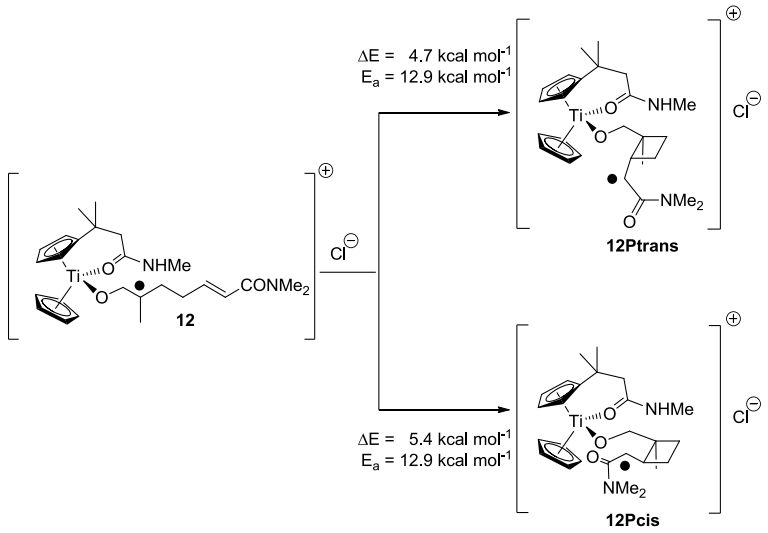

Scheme 6.4. Computational study of the cyclization of **12** with single-point radical binding (For the computational structures see Supporting Information).

Thermodynamically, the cyclizations are highly unfavorable (ΔE = +4.7 kcal mol^{-1} and 5.4 kcal mol^{-1}, respectively) with only a slight preference for **12P*trans*** (76:24 at 25 °C). The differences in activation energies (ΔE_a= 0.4 kcal mol^{-1}) predict an unselective reaction. These results are in contradiction with the experimental results obtained with **2** as catalyst but in line with the inability of simple alkyl substituted titanocenes to induce reactions of **1**.[6.7i] In both product radicals, the radical center can be readily approached by a second equivalent of the titanocene. Therefore, a selective reductive trapping of either **12P*cis*** or **12P*trans*** that renders the cyclization irreversible is improbable. Thus, the formation of both isomers of **3** is highly unlikely to occur via a single-point binding of the radical to a cationic titanocene complex as in **12** and a more elaborate mechanism must be operating for the 4-*exo* cyclization.

Two Point Binding of the Radicals: To this end, two-point binding of the radical by a cationic titanocene(IV) complex as in **8** (Figure 6.5) was investigated. In this manner, the radical center and the radical acceptor are forced into close proximity and the α,β-unsaturated amide is activated for radical addition through complexation by the Lewis acid titanocene cation.

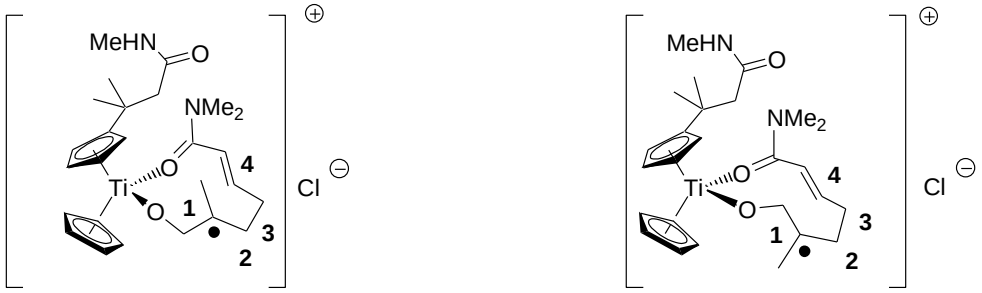

A
two point binding leading to
the formation of trans-**3**

B
two point binding leading to
the formation of cis-**3**

Figure 6.5. Schematic two point binding of the radicals with *trans*- and *cis*-orientation of the unsaturated amide and the alkoxide substituents with numbering of the future cyclobutane C-atoms.

The generation of these ten-membered rings containing a titanium and two oxygen atoms as well as the radical center raises fascinating issues. First, it is not clear if *trans*-(**A**) or *cis*-(**B**) is more favorable and how many minima of **A** and **B** exist. Second, it is interesting to understand the influence of stereochemical control elements, such as the eclipsing substituents, on the relative stabilities of the medium sized rings, the corresponding transition states, and products of the cyclization.

Comparison of the BP86/TZVP with COSMO and Potential Energy Surfaces: After two-point binding by the radicals the cationic titanium(IV) center is tetrahedrally coordinated and no covalent bonds to chloride can be formed as in **2** and **12**. Chloride was therefore placed close to the coordinated amide in strict analogy to the experimentally observed positioning of the halide in **2** and the 'computational radical' **12**.

Table 6.2. Relative energies of substrates, products, and transition states of the 4-*exo* cyclization after two-point binding to titanium in kcal mol^{-1} (BP86/TZVP with COSMO). The ZPVE is included from the BP86/TZVP calculation.

Radical	Substrate	Transition State	Product	ΔE	E_a
13	0.0	+14.6	+11.1	+11.1	+14.6
14	+2.5	+12.9	+2.5	-0.0	+10.4
15	+4.1	+17.1	+11.0	+6.9	+13.0

Geometry optimization (BP86/TZVP) resulted in three structures **13**, **14**, and **15** of the templated radical **8**. Of these, **13** and **15** lead to the formation of a *cis*- and **14** to a *trans*-cyclobutylcarbinyl radical. The relative energies (BP86/TZVP with COSMO) of these species, the transition states, and products of the cyclization are summarized in Table 6.2. The potential energy surface is depicted in Figure 6.6.

Since all structures contain chloride anions and cationic titanocenes, the COSMO model was applied to account for solvent effects.

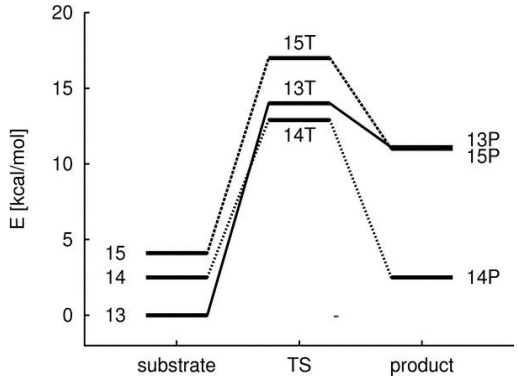

Figure 6.6. Relative energies of species relevant for the formation of **13P**, **14P**, and **15P** BP86/TZVP with COSMO bottom.

Cleary, the presence of three substrate radicals complicates matters and it has to be established if they can interconvert. Amide complexation at titanocene(IV) complexes is usually fast and reversible.[6.9] Because the energy differences between the substrate radicals are additionally relatively low, it can be assumed that **13**, **14**, and **15** are in a fast equilibrium. From the equilibrating radicals the formation of **13P** and **15P** is kinetically possible (E_a = +14.6 kcal mol^{-1} and +13.0 kcal mol^{-1}) but thermodynamically unfavorable (ΔE = +11.1 kcal mol^{-1} and +6.9 kcal mol^{-1}). This implies that ring opening of the cyclobutylcarbinyl radicals **13P** and **15P** (E_a = +3.5 kcal mol^{-1} and +6.1 kcal mol^{-1}) will be very fast. Due to their short lifetimes the bimolecular trapping of **13P** and **15P** by a second equivalent of the titanocene that is present in concentrations of less than 0.02 M under the experimental conditions will be kinetically disfavored and is therefore highly unlikely, exactly as for **12P**.

The situation is markedly different for radical **14**. First, the cyclization is thermoneutral (ΔE = -0.0 kcal mol^{-1}) and thus the two-point binding in **14** leads to the only case where the inherent thermodynamic disadvantages of the 4-*exo* cyclization studied here can at least be compensated. Second and equally important, the activation energy of the cyclization is lower (E_a = +10.4 kcal mol^{-1}) than for **13** and **15**. Both points imply that **14P** has a longer life-time than **13P** and **15P** because opening of **14P** (E_a = +10.4 kcal mol^{-1}) is less favored than for **13P** and **15P**. As a consequence, of all product radicals **14P** is formed most readily thermodynamically and kinetically and, as a consequence, will have the longest life-time. Its reduction by a second equivalent of the titanocene will therefore also be accomplished most readily.

Thus, the two-point binding in radicals **13**, **14**, and **15** to the titanocene results in a peculiar situation. Only the 4-*exo* cyclization leading to the *trans*-cyclobutane is possible, exactly as observed experimentally. An activation of the cyclization by the *gem*-dialkyl effect that is essential for the 4-*exo* cyclization catalyzed by simple alkyl substituted titanocenes is therefore not necessary. The structural reasons for this reactivity pattern will be discussed next.

Structures of the Substrate Radicals: There are two interesting issues concerning the structure of the substrate radicals. First, formation of a *cis*-**3** can be accomplished from two species, **13** and **15**, that differ in relative stability by +4.1 kcal mol^{-1}. Second, only **14** that is intermediate in stability leads to the formation of *trans*-**3**.

The main reason for the highest stability of **13** (Fig. 6.7) is the presence of a hydrogen bond between chloride and the N-H bond of the amide that is absent in **14** and **15**. The CH_3 substituent of the radical center is pointing towards the ‘upper’ substituted cyclopentadienyl ligand. This arrangement results in a distance of 2.98 Å between C1 (radical center) and C4 (β–C of the olefin). Moreover, close contacts between the β–hydrogen of the olefin and the *tert*-alkyl group of the pending amide (2.00 Å) and the α–hydrogen of the olefin and one of the CH_3 groups of the amide are present.

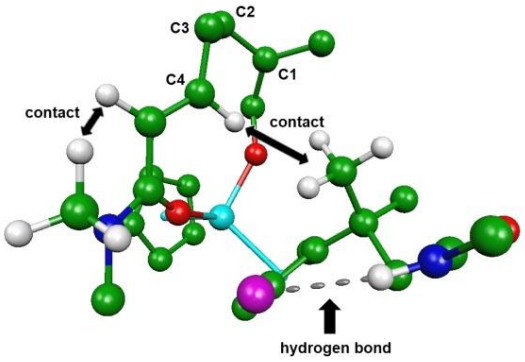

Figure 6.7. BP86/TZVP structure of **13**. The structure is depicted as viewed along the C3-C2 bond (see Figure 6.5 for numbering).

In **15** the CH_3 substituent of the radical center is pointing towards the 'lower' unsubstituted cyclopentadienyl ligand. This binding mode prevents the formation of the hydrogen bond but avoids steric interactions between the titanocene and the radical. The conformation of the ten-membered ring is otherwise very similar to that of **13**.

In **14** the hydrogen bonding observed for **13** is also not possible. However, the binding of the radical that leads to *trans*-**3** results in a looser structure as indicated by the distance between C1 and C4 (3.21 Å). Therefore, a less strained ten-membered ring can be formed with close contacts to the titanocene moiety being absent. This effect is clearly significant in comparison to **15** but it cannot compensate the hydrogen bond in **13**.

Structures of the Transition States: The relative energies of the transition states do not reflect the relative stabilities of the substrate radicals.

The compression of the structures due to the presence of the forming C1-C4 bond (2.08 Å) prevents the hydrogen bonding present in **13** for **13T**. The more compact structure also results in a relatively small dihedral angle C1,C2,C3,C4 (17.7°, numbering see Fig.6.5) and pronounced eclipsing interactions in the forming cyclobutane. Moreover, the amide is significantly rotated out of conjugation (120°) and thus orbital overlap between the SOMO of the radical and the LUMO of the olefin is not ideal.[6.19] Close contacts between the substituents of the ten-membered radical and the catalyst are absent, however.

The forming bond between C1 and C4 also results in a more compact structure for **14T** (Figure 6.8). However, the dihedral angle C1,C2,C3,C4 (24.0°) is larger than in **13T** and thus eclipsing interactions are weaker. Moreover, the amide is rotated out of conjugation by only 18.8° and therefore, the cyclization is electronically more favorable than in **13T**. The presence of one close contact between the CH_2O-group and the lower Cp-ring must destabilize **14T** somewhat. However, the above mentioned contributions seem more relevant as **14T** is more stable than **13T** by 1.5 kcal mol^{-1}.

Of the transition states **15T** is the least stable. This is due to a strong contact between the CH_3 substituent of the radical and the lower Cp-ring and the amide being rotated out of conjugation by 117.5°.

These data suggest that a favorable overlap between the SOMO of the radical and the HOMO of the radical acceptor through binding of the α,β–unsaturated amide without of a significant weakening of conjugation constitutes the single most important factor for the lowest energy of **14T**.[6.19]

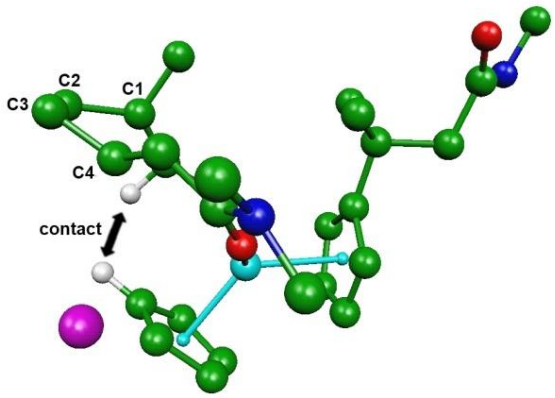

Figure 6.8. BP86/TZVP structure of **14T**. The structure is depicted as viewed along the C3-C2 bond (see Figure 6.5 for numbering).

Structures of the Product Radicals: The cyclization of the most stable substrate radical **13** is highly endothermic (ΔE = +11.1 kcal mol^{-1}). This is for two three reasons. First, the stabilization by hydrogen bonding in **13** is not possible in **13P**. Second, the cyclobutane in **13P** is generated in a strained puckered form. This is indicated by the dihedral angle C1, C2, C3, C4 of 21.6° that is larger than in *cis*-**3** (16.4°). Finally, there are close contacts between the protons of the CH_2O-group and the 'lower' Cp-ligand (2.13 Å) and the protons of the CH_3-group of the cyclobutane and both CH_3-groups of the *tert*-alkyl group of the pending amide (2.09 Å and 2.11 Å). Thus, the favorable features of **13** do not translate into **13P**.

The generation of **14P** (Figure 6.9) is thermoneutral (ΔE = 0.0 kcal mol^{-1}). The increased stability of **14P** compared to **13P** is due to two factors. First, the dihedral angle C1, C2, C3, C4 of 15.9° is significantly smaller. Indeed, this value is close to the one observed in *trans*-**3** (17.6°) and indicates that the binding of the product radical to the template does not result in a significant puckering of the cyclobutane. Second, compared to **13P** there is only one close contact that occurs between the CH_2O-group and the 'lower' Cp ligand (2.03 Å).

Finally, cyclization leading to **15P** is endothermic (ΔE = +6.9 kcal mol^{-1}), also. The cyclobutane ring is noticeably more puckered (dihedral angle C1, C2, C3, C4 of 19.5°) than in **14P** but less so than in **13P**. A rather close contact (1.95 Å) is observed between the protons of the CH_2O-group and one of the CH_3 groups of the *tert*-alkyl group of the pending amide that seems to be significantly more unfavorable than the interactions in **13P** and **14P**.

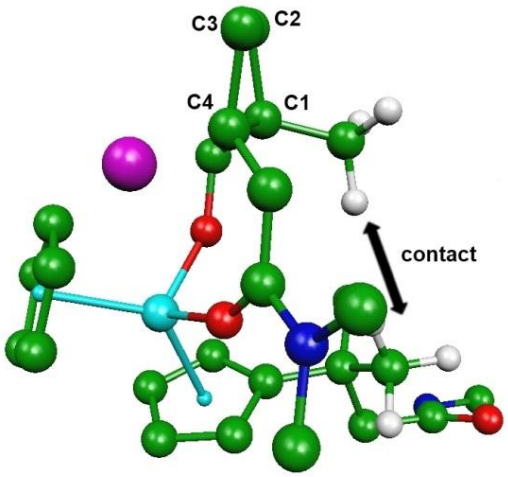

Figure 6.9. BP86/TZVP structure of **14P**. The structures are depicted as viewed along the C3-C2 bond (see Figure 6.5 for numbering).

Thus, the contraction of the two-point bound substrate radicals through cyclization is highly unfavorable kinetically and thermodynamically for the formation of *cis*-cyclobutanes but does allow the formation of the *trans*-cyclobutane.

Finally, the computational results can also rationalize the experimentally observed lower diastereoselectivity in the cyclization of **9** (*trans*:*cis* = 90:10; R = Et). In both **14T** and **14P** larger groups than CH_3 at C1 of the (forming) cyclobutane will strongly interact with the *tert*-alkyl group of the pending amide. This contact was not observed in **13T** and **13P**. Thus, the thermodynamic and kinetic preference for the products such as *trans*-**11** will decrease compared to *trans*-**3**. According to the analysis above, this leads to a reduction in diastereoselectivity of the 4-*exo* cyclization.

6.3 Conclusion

In summary, we have demonstrated a novel concept for catalytic radical 4-*exo* cyclizations that does not require the assistance of the *gem*-dialkyl effect. It relies on a two-point binding of radicals to titanocene complex that is able to compensate the intrinsically unfavorable reaction and activation energy of the 4-*exo* cyclization occurring without templating of the radical intermediates. Our method features a novel class of titanocene(III) catalysts that are activated through hydrogen bonding of the pending amide ligand to yield a coordinatively super-unsaturated 13-electron complex as corroborated by cyclic voltammetry. The computational study of the effect of the two-point binding on the structures and relative energies of the substrate radicals, transition states, and product radicals revealed a peculiar mechanistic situation related to but more complicated than a classic Curtin-Hammett-scenario. The equilibrating substrate radicals can all react to yield the corresponding cyclobutyl carbinyl radicals. However, only the formation of the *trans*-substituted product **14P** results in a sufficient life-time of the cyclization product for reductive trapping by a second equivalent of the titanocene(III) reagent. The formation of the corresponding *cis*-products is

thermodynamically unfavorable and hence their ring opening is too fast to allow the pivotal radical reduction.

Our approach of rendering the kinetically and thermodynamically disfavored 4-*exo* cyclization feasible by a two-point binding through the action of a catalyst will be of interest for the realization of other intrinsically unfavorable radical reactions also.

6.4 References

[6.1] a) G. J. Rowlands, *Tetrohedron* **2009**, 65, 8603-8655; b) G. J. Rowlands, *Tetrohedron* **2010**, 66, 1593-1636.

[6.2] a) A. L. J. Beckwith, G. Moad, *J. Chem. Soc., Perkin Trans. 2* **1980**, 1083-1092; b) K. U. Ingold, B. Maillard, J. C. Walton, *J. Chem. Soc., Perkin Trans. 2* **1981**, 970-974; c) S. U. Park, T. R. Varick, M. Newcomb, *Tetrahedron Lett.* **1990**, *31*, 2975-2978.

[6.3] a) M. E. Jung, I. D. Trifunovich, N. Lensen, *Tetrahedron Lett*. **1992**, *33*, 6719-6722; b) M. E. Jung, R. Marquez, K. N. Houk, *Tetrahedron Lett.* **1999**, 40, 2661-2664; c) M. E. Jung, *Synlett* **1999**, 843-846; d) M. E. Jung, G. Piizzi, *Chem. Rev.* **2005**, *105*, 1735-1766.

[6.4] a) M. R. Elliot, A.-L. Dhimane, M. Malacria, *J. Am. Chem. Soc.* **1997**, *119*, 3427-3428; b) A.-L.Dhimane, C. Aïssa, M. Malacria, *Angew. Chem.* **2002**, *41*, 3418-3421; *Angew. Chem. Int. Ed.* **2002**, *41*, 3284-3286.

[6.5] a) G. A. Molander, C. R. Harris, *Chem. Rev*. **1996**, *96*, 307-338; b) A. Krief, A.-M. Laval, *Chem. Rev.* **1999**, *99*, 745-778; c) D. J. Edmonds, D. Johnston, D. J. Procter, *Chem. Rev.* **2004**, *104*, 3371-3404; d) K. Gopalaiah, H. B. Kagan, *New. J. Chem.* **2008**, *32*, 607-637; e) D. J. Procter, R. A. II Flowers, T. Skrydstrup, *Organic Synthesis Using Samarium Diiodide: A Practical Guide*; Royal Society of Chemistry Publishing, London, **2010**.

[6.6] a) T. V. RajanBabu, W. A. Nugent, *J. Am. Chem. Soc*. **1994**, *116*, 986-997; b) A. Gansäuer, H. Bluhm, M. Pierobon, *J. Am. Chem. Soc.* **1998**, *120*, 12849-12859; c) A. Gansäuer, T. Lauterbach, S. Narayan, *Angew. Chem.* **2003**, *115*, 5714-5731; *Angew. Chem. Int. Ed.* **2003**, *42*, 5556-5573; d) J. M. Cuerva, J. Justicia, J. L. Oller-López, J. E. Oltra, *Top. Curr. Chem.* **2006**, *264*, 63-92; e) A. Gansäuer, J. Justicia, C.-A.Fan, D. Worgull, F. Piestert, *Top.Curr.Chem.* **2007**, *279*, 25-52.

[6.7] a) K. Weinges, S. B. Schmidbauer, H. Schick, *Chem. Ber*. **1994**, 1305-1309; b) M. R. Elliot, A.-L. Dhimane, M. Malacria, *J. Am. Chem. Soc.* **1997**, *119*, 3427-3428; c) A. Fernández-Mateos, E. Martin de la Nava, G. Pascual Coca, A. Ramos Silva, R. Rubio González, *Org. Lett.* **1999**, *1*, 607-609; d) D. Johnston, C.M. McCusker, D. J. Procter, *Tetrahedron Lett.* **1999**, *40*, 4913-4916; e) A.-L. Dhimane, C. Aïssa, M. Malacria, *Angew. Chem*. **2002**, *114*, 3418-3421; *Angew. Chem. Int. Ed*. **2002**, *41*, 3284-3286; f) T. K. Hutton, K. Muir, D. J. Procter, *Org. Lett.* **2002**, *4*, 2345-2347; g) D. J. Edmonds, K. Muir, D. J. Procter, *J. Org. Chem.* **2004**, *69*, 790-801; h) A. Gansäuer, T. Lauterbach, D. Geich-Gimbel, *Chem. Eur. J.* **2004**, *10*, 4983-4990; i) D. B. G. William, K. Blann, *Eur. J. Org. Chem.* **2004**, 3286-3291; j) J. Friedrich, M. Dolg, A. Gansäuer, D. Geich-Gimbel, T.

Lauterbach, *J. Am. Chem. Soc.* **2005**, *127*, 7071-7077; k) J. Friedrich, K. Walczak, M. Dolg, F. Piestert, T. Lauterbach, D. Worgull, A. Gansäuer, *J. Am. Chem. Soc.* **2008**, *130*, 1788-1796.

[6.8] A. Gansäuer, D. Worgull, K. Knebel, I. Huth, G. Schnakenburg, *Angew. Chem.* **2009**, *121*, 9044-9047; *Angew. Chem. Int. Ed.* **2009**, *48*, 8882-8885.

[6.9] a) A. Gansäuer, D. Franke, T. Lauterbach, M. Nieger, *J. Am. Chem. Soc*. **2005**, *127*, 11622-11623; b) T. Klawonn, A. Gansäuer, I Winkler, T. Lauterbach, D. Franke, R. J. M. Nolte, M. C. Feiters, H. Börner, J. Hentschel, K. H. Dötz, *Chem. Commun*. **2007**, 1894; c) A. Gansäuer, I Winkler, D. Worgull, D. Franke, T. Lauterbach, A. Okkel, M. Nieger, *Organometallics* **2008**, *27*, 5699-5707.

[6.10] J. Larsen, R. J. Enemærke, T. Skrydstrup, K. Daasbjerg, *Organometallics* **2006**, *25*, 2031-2036.

[6,11] a) R. J. Enemærke, G. H. Hjøllund, K. Daasbjerg, T. Skrydstrup, *C. R. Acad. Sci.* **2001**, *4*, 435-438; b) R. J. Enemærke, J. Larsen, T. Skrydstrup, K. Daasbjerg, *Organometallics* **2004**, *23*, 1866-1874; c) R. J. Enemærke, J. Larsen, T. Skrydstrup, K. Daasbjerg, *J. Am. Chem. Soc.* **2004**, *126*, 7853-7864; d) R. J. Enemærke, J. Larsen, G. H. Hjøllund, T. Skrydstrup, K. Daasbjerg, *Organometallics* **2005**, *24*, 1252-1262; e) A. Gansäuer, A. Barchuk, F. Keller, M. Schmitt, S. Grimme, M. Gerenkamp, C. Mück-Lichtenfeld, K. Daasbjerg, H. Svith, *J. Am. Chem. Soc.* **2007**, *129*, 1359-1371.

[6.12] a) W. B. Mims, J. Peisach, *Biochemistry* **1976**, *15*, 3863-3869; b) W. B. Mims, *Phys. Rev. B* **1972**, *5*, 2409-2419; c) W. B. Mims, *Phys. Rev. B* **1972**, *6*, 3543-3545; d) A. Schweiger, G. Jeschke, *Principles of Pulse Electron Paramagnetic Resonance*, Oxford University Press, Oxford, **2001**.

[6.13] a) A. Gansäuer, C.-A. Fan, F. Keller, J. Keil, *J. Am. Chem. Soc.* **2007**, *129*, 3484-3485; b) A. Gansäuer, C.-A. Fan, F. Piestert, *J. Am. Chem. Soc*. **2008**, *130*, 6916; c) A. Gansäuer, S. Lei, M. Otte, *J. Am. Chem. Soc.* **2010**, *132*, 11858-11859.

[6.14] a) A. D. Becke, *Phys. Rev. A* **1988**, *38*, 3098-3100; b) J. P. Perdew, *Phys. Rev. B,* **1986**, *33*, 8822-8824.

[6.15] a) K. Eichkorn, F. Weigend, O. Treutler, R. Ahlrichs, *Theor. Chem. Acc*. **1997**, 97, 119-124. b) A. Schäfer, C. Huber, R. Ahlrichs, *J. Chem. Phys.* **1994**, 100, 5829-5835.

[6.16] a) R. Ahlrichs, M. Bär, H.-P. Baron, R. Bauernschmitt, S. Böcker, M. Ehrig,K. Eichkorn, S. Elliott, F. Furche, F. Haase, M Häser, H. Horn, C. Huber, U. Huniar, C. Kölmel, M. Kollwitz, C. Ochsenfeld, H. Öhm, A. Schäfer, U. Schneider, O. Treutler, M. von Arnim, F. Weigand, P. Weis, H. Weiss, *Turbomole 5*, Institut für Physikal. Chemie, Universität Karlsruhe, **2002**; b) M. Häser, R. Ahlrichs, *J. Comput. Chem.* **1989**, *10*, 104-111; c) O. Treutler, R. Ahlrichs, *J. Chem. Phys.* **1995**, *102*, 346-354.

[6.17] P. Deglmann, F. Furche, R. Ahlrichs, *Chem. Phys. Lett*. **2002**, *362*, 511-518.

[6.18] A. Klamt, G. Schüürmann, *J. Chem. Soc., Perkin Trans. 2* **1993**, 799-805.

[6.19] a) B. Giese, *Angew. Chem.* **1983**, *95*, 771-782; *Angew. Chem. Int. Ed. Engl*. **1983**, *22*, 753-764; b) H. Fischer, L. Radom, *Angew. Chem.* **2001**, *113*, 1380-1414; *Angew. Chem. Int. Ed.* **2001**, *40*, 1340-1371.

7 An Unusual Case of Facile Non-Degenerate P-C Bond Making and Breaking

This Chapter has been published in: V. Nesterov, A. Özbolat-Schön, G. Schnakenburg, L. Shi, A. Cangönül, M. van Gastel, F. Neese, and R. Streubel *Chem. Asian J.* **2012**, 7, 1708-1712.

7.1 Introduction

Transient phosphorus radicals having different oxidation states and geometries are known to be involved in numerous chemical reactions and have been studied for more than fifty years.[7.1] To obtain insight into the bonding and reactivity of phosphorus radicals great efforts were undertaken to synthesize relatively stable and/or persistent radicals,[7.2] and important results were achieved especially in the area of phosphanyl radicals.[7.3] Fresh stimulus has been provided recently by the work of Studer and Grimme who elegantly demonstrated radical substitution reactions using silyl- and/or stannylphosphanes[7.4] and Cummins et al. who showed the feasability of direct functionalisation of white phos-phorus using his tris(amido)titanium(III) complex.[7.5] By contrast, information is still scarce about the bonding and reactivity of radicals containing a functional group at the phosphorus atom that could serve as a leaving group.[7.6] On the other hand, P−C bond making and breaking is of fundamental interest in synthesis and catalysis and the knowledge about facile processes that allow for both is extremely scarce. One special case is represented by so-called circumabulatory rearrangements, *e.g.*, the circumambulation of a phosphirane was described by Lammertsma.[7.7]

Recently, formation of the first transient *P*-chlorophosphanyl complexes were described,[7.8,7.9] using oxidation of Li/Cl phosphi-nidenoid tungsten complexes[7.10] by tritylium tetrafluoroborate. Although electron paramagnetic resonance (EPR) evidence for the open-shell derivatives was obtained, the actual reaction course of this single-electron oxidation remained largely speculative as only the final products, a *P*-chlorophosphane and a phosphaquinomethane complex, were characterized.

To obtain more insight into mechanistic aspects of this oxidation reaction, we have now investigated reactivity of a Li/F phos-phinidenoid complex towards two different tritylium salts $[Ph_3C]BF_4$ and $[(p\text{-}Tol)_3C]BF_4$. In the latter case, the results provide strong evidence for the existence of new intermediates and a facile conversion into a single final product, a P-F, P-trityl*-substituted organophosphane complex (trityl*=tris(*p* methylphenyl)methyl). State-of-the-art theoretical calculations reveal the structures of the in situ formed combined singlet diradical pairs formed in the first step and the nature of intermediates on the way to the final product.

7.2 Results and Discussion

Oxidation of complex **2**[7.11] with 1.2 equiv. of $[Ph_3C]BF_4$ (**3**), at low temperature (–78 °C), proceeded with immediate color change from yellow to deep red, to blue and, finally, to orange (0°C). Supported by EPR measurements (see below and Supporting Infomation) the formation of a radical pair containing the radicals **4** and **5** can be concluded, and as the radicals were not inert[7.12] a P-C coupling occurred to give selectively the *P*-fluoro organophosphanyl complex **7** as final product (Scheme 7.1); the formation of the kinetically favored intermediate complex **6** was not detected. Complex **7** was purified by column chromatography, obtained as a colorless solid (40% isolated yield) and its structure confirmed by single-crystal X-ray diffraction analysis [7.13] (Figure 7.1).

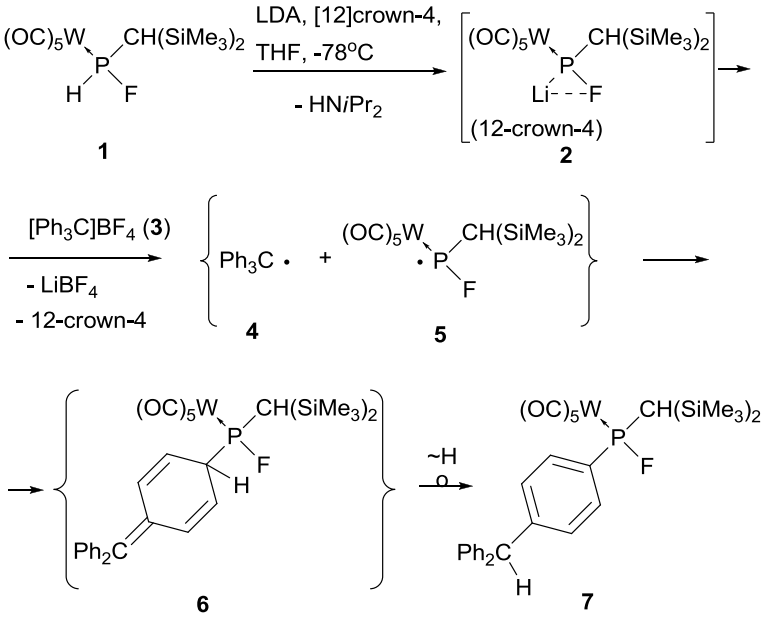

Scheme 7.1. Oxidation of Li/F phosphinidenoid complex **2** with $[Ph_3C]BF_4$.

Unexpectedly, complex **6** could be obtained as the major product if a larger excess (3.2 equiv.) of the tritylium salt **3** was used; phosphane complexes **1** and **7** were observed as minor products (total amount less than 5%) together with Ph_3CH. Product **6** was purified by column chromatography and obtained as a colorless solid that was stable in the solid state at low temperature but rearranged quantitatively in solution (*n*-pentane, 25°C) to give **7**. This was further supported by DFT calculations[7.14] at the B3LYP/def2-TZVPP//BP86/def2-TZVP level of theory (see also Supporting Information): isomer **7** is 24.6 kcal/mol lower in energy than isomer **6**. While the ^{31}P NMR data of complex **6** (δ_P = 193.2, $^1J_{W,P}$ = 288.6 Hz, $^1J_{P,F}$ = 845.6 Hz) are similar to **7** (δ_P = 187.3, $^1J_{P,W}$ = 292.7 Hz, $^1J_{P,F}$ = 811.6 Hz), the ^{19}F NMR resonances differ significantly (**6**: δ_F = –118.3, and **7**: δ_F = –108.9 ppm).

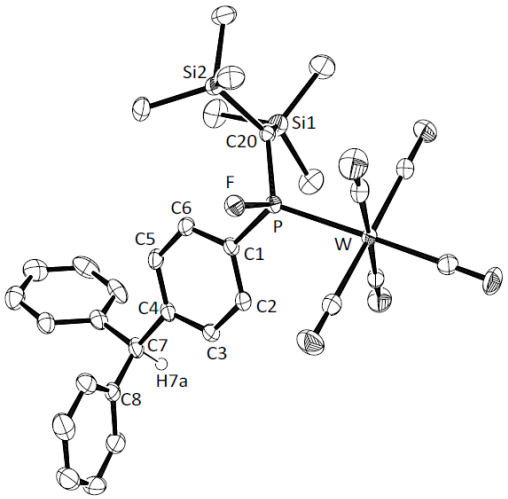

Figure 7.1. Molecular structure of complex **7** (50% probability level; except H7a hydrogen atoms are omitted for clarity). Selected bond lengths [Å] and angles [°]: W–P 2.4878(8), P–F 1.6127(19), P–C(20) 1.808(3), P–C(1) 1.818(3); C(1)–P–C(20) 108.96(14), C(1)–P–F 97.81(12), C(1)–P–W 119.50(10).

To investigate the reactivity of the transient radical **5** towards a trityl radical with a substituent in *para* position, Li/F phosphinidenoid complex **2** was reacted with $[(p\text{-Tol})_3C]BF_4$ (1.2 equiv.); this led to complex **11** (δ_P = 207.1, $^1J_{P,W}$ = 283.5, and $^1J_{P,F}$ = 821.4 Hz) as the final product, obtained in pure form (55% isolated yield) by column chromato-graphy (Scheme 7.2). Monitoring of the reaction by $^{31}P(^1H)$ NMR spectroscopy (–78 °C to 25 °C) revealed the formation of three major and one minor intermediates **10a,a´** and **10c,c`** (ratio: ~ 1:1:1:0.3) distinguished by their relative orientations of the $CH(SiMe_3)_2$ and W(CO)5 groups (see also the discussion of the theoretical results below). All intermediates have very similar chemical shifts and phosphorus-tungsten and phosphorus-fluorine couplings (δ_P = 216.1, $^1J_{P,W}$ = 284 Hz, $^1J_{P,F}$ = 843.0 Hz; δ_P = 211.0, $^1J_{P,W}$ = 284.8 Hz, $^1J_{P,F}$ = 878.7 Hz, δ_P = 203.4, $^1J_{P,W}$ = 281.2 Hz, $^1J_{P,F}$ = 836.7 Hz, and δ_P = 191.8, $^1J_{P,F}$ = 846.8 Hz[7.15]). At 0 °C, one of them (δ_P = 203.4 ppm) remained as major component but also disappeared in favor of **11**, which was the final product at ambient temperature. We failed to isolate the major component by crystallization at 0°. Further attemps to obtain this compound using 3.2 equivalents of **8** were also not successful.

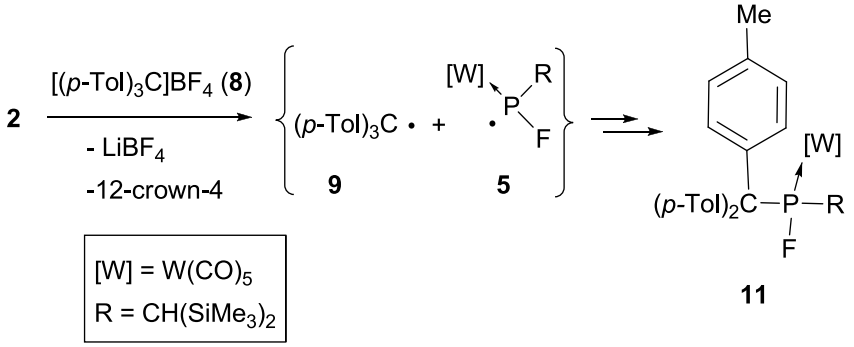

Scheme 7.2. Oxidation of complex **2** with $[(p\text{-Tol})_3C]BF_4$.

The structure of complex **11** was unambiguously confirmed (Fig. 7.2) and displayed a P–C1 bond of 1.954(3) Å, which is significantly longer than the average P–C single bond length of trivalent

phosphanes and/or their transition metal complexes (the sum of the covalent radii of P and C atoms is ~ 1.83 Å).

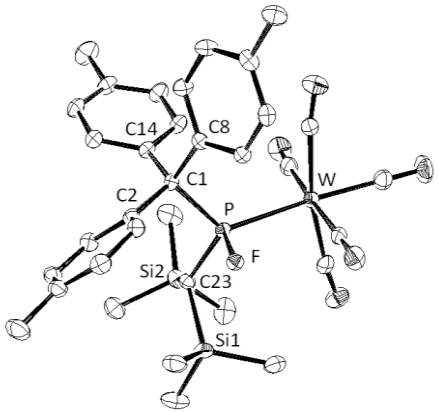

Figure 7.2. Molecular structure of complex **11** (50% probability level; hydrogen atoms are omitted for clarity). Selected bond lengths [Å] and angles [°]: W–P 2.5675(8), P–F 1.6184(19), P–C(1) 1.954(3), P–C(23) 1.826(3), C(1)–P–C(23) 107.17(14), C(1)–P–F 94.66(12), C(23)–P–F 97.73(12), C(1)–P–W 122.85(9), C(23)–P–W 122.42(10), F–P–W 104.23(7).

To achieve a better understanding of the observed intermediates and the formation of complex **11**, DFT calculations were carried out on various closed-shell, open-shell and zwitterionic isomers based on the assumption that complex **10a** is the kinetically favored product and the starting point (for **10b**,**d** see the Supporting Information). Of all calculated structures, the ones lowest in energy are shown in Figure 7.3 (**10b**,**d** are very high in energy and therefore not shown here). Compared to the energy of the combined singlet diradicals **5+9**, the ZPE-corrected energies (kcal/mol) of complexes **10a** and **10c** were found to be lower only by 12.7 kcal/mol and 12.8 kcal/mol, respectively.

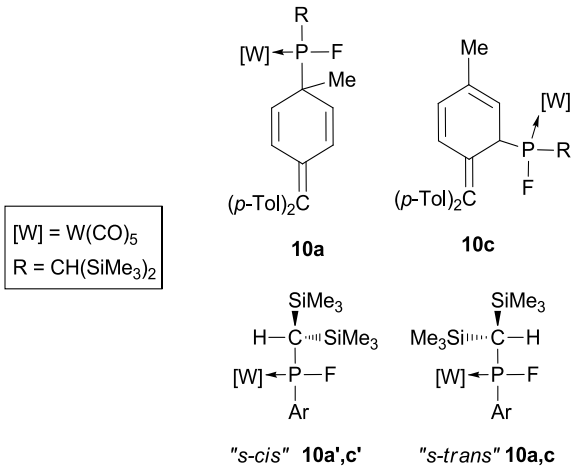

Figure 7.3: Calculated low-energy isomeric structures of complex **11**.

Further inspection revealed that **10a** and **10c** can appear as P−C atropisomers **10a'** (–9.2 kcal/mol) and **10c'** (–6.8 kcal/mol) being close in energy but differing in the relative orientation of their CH and

PW bonds (Figure 7.3), thus leading to *s-cis* and *s-trans* conformers,[7.16] the latter being favored in both cases. The final product, complex **11**, was more stable than **5+9** by 19.4 kcal/mol; **11** also adopts the *s-trans* con-formation. Stimulated by these theoretical results and especially by the prediction of a small energy difference between **5+9** and **11** a preliminary study on the thermal stability of complex **11** was performed. Heating a toluene solution at moderate temperatures (75°C, 4h) led to a selective cleavage of the (long) P–C bond and to the formation of the phosphane complex **1**.

EPR investigations of the reactions described in Schemes 1 and 2 confirmed the presence of long-lived carbon-centered radicals formed in the initial reaction steps, thus confirming their radical-based nature (see the Supporting Information for details on the EPR experiments). Typical EPR spectra of a liquid solution containing Li/F phosphinidenoid complex **2** and 1.2 equivalents $[(p\text{-Tol})_3C]BF_4$ (Figure 7.4a) and revealed that different reactions coexist. In the presence of $[(p\text{-Tol})_3C]BF_4$, the EPR spectrum consists of a narrow signal at 336 mT and a broad signal with a peak-to-peak width of 1.18 mT. In addition, an oscillatory structure is present with a low amplitude on top of the broad signal. In the presence of $[Ph_3C]BF_4$, the oscillatory structure dominates the EPR spectrum, which was assigned to **4** based on camparison with literature data.[7.17]

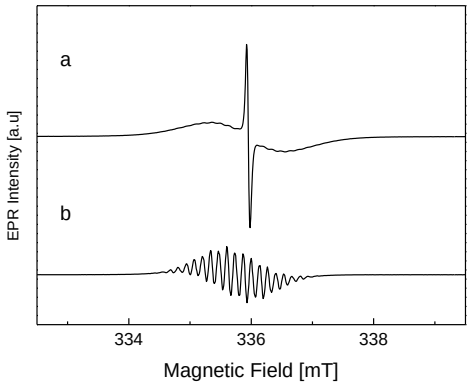

Figure 7.4. EPR spectra of (**2**) with 1.2 equiv. $[(p\text{-Tol})_3C]BF_4$ (a) and $[Ph_3C]BF_4$ (b). Experimental conditions: T = 150 K, ν_{mw} = 9.42 GHz, modulation amplitude 0.05 mT.

Given the observation that the widths of the EPR signals of the broad signal in Figure 7.4a and that of **9** are similar, the broad signal very likely also stems from a radical with a trityl-related core. The narrow signal disappears completely upon freezing to T = 100 K. As is the case for NMR spectroscopy, the anisotropic contributions do not average out in the solid state, and this species is thus subject to a very strong anisotropic coupling, for example with the nuclear spin of ^{31}P. Moreover, if the temperature is raised to 180 K, the narrow signal rapidly becomes smaller in intensity, indicating that a reaction is occuring inside the EPR tube. This signal is therefore tentatively assigned to **5**, in which the unpaired electron occupies a pure 3p orbital at ^{31}P without admixture of the 3s orbital. The spin density distribution in complex **5** obtained from a DFT calculation[7.14] is given in Figure 7.5. Geometry optimization of the complex resulted in a local geometry of phosphorus, which is almost planar ∠(W,P,F) = 115.6°; ∠(W,P,C) = 129.6°, P–W 2.484, P–F 1.669, P–C(23) 1.830. As shown in the figure, the majority of spin density is located at P (68%). Small amounts of spin density are found at the adjacent W (9%), C (-0.6%) and F (4%) atom and the remaining part distributed over the CO ligands.

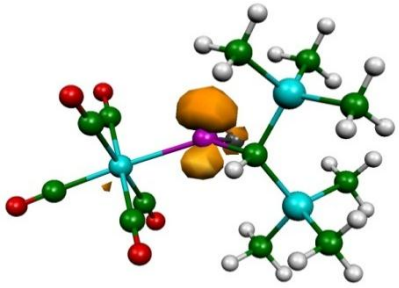

Figure 7.5. Calculated spin density distribution in complex **5**.

7.3 Conclusion

First insights into an unusual case of facile non-degenerate P–C bond making and breaking was obtained using a radical pair of a trityl derivative and a short-lived P−F organophosphanyl complex as starting point. State-of-the-art theoretical calculations on real molecular entities revealed the structures of the *in situ* formed combined singlet diradicals (**4+5** and **5+9**) and the nature of intermediates, presumably being two pairs of atropisomers **10a,a´** and **10c,c´,** on the way to the final product, the complex **11**. Two aspects deserve special attention: the narrow energy regime (~ 20 kcal/mol) of all isomers of **11** may constitute an ideal test bed for further studies on dispersion effects in low-symmetry radical pairs, and the sterically encumbered P–F diorganophosphane complex **11** may serve as blueprint for the exploitation of *P*-trityl derivatives as new entry into open-shell phosphorus chemistry.

7.4 Experimental Section

General Procedures. All manipulations involving air- and moisture-sensitive compounds were carried out under an atmosphere of purified argon by using standard Schlenk-line techniques or a glove-box. Solvents were dried with appropriate drying agents and degassed before use. The ^{1}H, $^{13}C(^{1}H)$, and $^{31}P(^{1}H)$ NMR spectroscopic data were recorded on a Bruker DMX 300 spectrometer. Mass spectra were recorded on a MAT 95 XL.

6: To a stirred solution of phosphane **1** (534.2 mg, 1 mmol) and 12-crown-4 (0.175 mL, 1.12 mmol) in 40 mL of THF at –78 °C was slowly added solution of *n*-BuLi (1.6 M, 0.7 mL, 1.12 mmol). After 15 min the mixture was cooled down up to –90 °C and triphenylcarbenium tetrafluoroborate (1.056 g, 3.2 mmol) was added under Ar atmosphere as a solid. Stirred reaction mixture was slowly warmed up to 0 °C in a cooling bath (ca. 4 h). Volatiles were removed under reduced pressure. Crude product was extracted with *n*-pentane (ca. –35 °C) and subjected to column chromatography (silica gel, –20 °C, petrol ether, petrol ether/diethyl ether = 10/0.5). Eluation of a second band and evaporation of volatiles gave brownish oil. Fractional crystallization from *n*-pentane at –35 °C gave triphenyl methane (total amount 225 mg, 0.68 mmol) as a white solid . Evaporation of the solvent from mother liquid gave complex **6** as a pale yellow solid containing triphenyl methane and complex **7** as impurities (total amount less than 5%). Yield: 340 mg, (0.44 mmol, 44%). ^{1}H NMR (300.13 MHz, $CDCl_3$,

25°C):δ = 0.28 (s, 9H, $Si(CH_3)_3$), 0.34 (s, 9H, $Si(CH_3)_3$), 2.29 (d, 1H, $^2J_{H,P}$ = 16.4 Hz, $PCH(Si(CH_3)_3)_2$), 4.21–4.29 (m, 1H, PCH), 5.97 (m, 2H, $CH(CH{=}CH)_2C$), 6.76 (m, 2H, $CH(CH{=}CH)_2C$), 7.10–7.31 (m, 10H, 2Ph). $^{13}C\{1H\}$ NMR (125.77 MHz, $CDCl_3$, 25°C):δ = 3.1 (pt, $^3J_{C,P}$ = 2.6 Hz, $^4J_{C,F}$ = 2.6 Hz, $Si(CH_3)_3$), 3.4 (dd, $^3J_{C,P}$ = 2.6 Hz, $^4J_{C,F}$ = 1.9 Hz, $Si(CH_3)_3$), 28.8 (dd, $^1J_{C,P}$ = 18.7 Hz, $^2J_{C,F}$ = 12.2 Hz, $P\underline{C}H(Si(CH_3)_3)_2$), 53.8 (pt, $^1J_{C,P}$ = 14.6 Hz, $^2J_{C,F}$ = 14.6 Hz, PCH), 123.40 (dd, $^2J_{C,P}$ = 5.5 Hz, $^3J_{C,F}$ = 2.7 Hz, CH), 124.43 (dd, $^2J_{C,P}$ = 5.5 Hz, $^3J_{C,F}$ = 1.8 Hz, C'H), 127.5 (s, Ph), 127.6 (s, Ph'), 127.8 (d, $^5J_{C,P}$ = 11.9 Hz, CPh_2), 128.20 (s, Ph), 128.26 (s, Ph'), 129.42 (s, Ph), 129.45 (s, Ph'), 130.60 (d, $^8J_{C,P}$ = 3.7 Hz, Ph), 130.67 (d, $^8J_{C,P}$ = 2.8 Hz, Ph'), 131.3 (d, $^3J_{C,P}$ = 10.1 Hz, CH), 131.4 (d, $^3J_{C,P}$ = 11.0 Hz, C'H),140.8 (d, $^4J_{C,P}$ = 12.8 Hz, $\underline{C}{=}CPh_2$), 141.4 (d, $^6J_{C,P}$ = 4.5 Hz, Ph), 196.7 (dd, $^2J_{C,P}$ = 7.3 Hz, $^3J_{C,F}$ = 3.7 Hz, *cis*-CO), 198.3 (d, $^2J_{P,C}$ = 29.3 Hz, *trans*-CO). $^{19}F\{^1H\}$ NMR (282.37 MHz, $CDCl_3$, 25°C): δ = –118.3 (d_{sat}, $^1J_{F,P}$ = 844.8 Hz). $^{31}P\{^1H\}$ NMR (121.51 MHz, $CDCl_3$; 25 °C): δ = 193.13 (d_{sat}, $^1J_{P,W}$ = 288.6, $^1J_{P,F}$ = 844.3). MS: *m/z* (%): 776 [M^+, 29]. IR (ν (CO), KBr pellet): tilde = 1930 (s), 2075 (s) cm^{-1}.

7: To a stirred solution of freshly prepared LDA (0.55 mmol) in 2.5 mL of THF at –78 °C was added cooled solution of phosphane complex **1** (267 mg, 0.5 mmol) and 12-crown-4 (85 µL, 0.55 mmol) in 5 mL of THF. After 15 min at –78 °C triphenylcarbenium tetrafluoroborate was added (250 mg, 0.76 mmol) as a solid. Immediate color change from yellow to deep violet was observed. The mixture was warmed up to 0 °C (ca. 2.5 h) to give yellow solution. Volatiles were removed under reduced pressure (ca. 0.01 mbar) and the residue was extracted with petroleum ether (3 x 0.5 mL). Combined extracts were used for the column chromatography (silica gel, –20 °C, petrol ether, petrol ether/diethyl ether 90:10). Elution of a second band and evaporation gave complex **7** as a colorless solid. Yield: 158 mg (0.20 mmol, 40%); m.p. 122 °C (dec.). ^{1}H-NMR (300.13 MHz, $CDCl_3$, 25°C):δ = 0.09 (s, 9H, $SiMe_3$), 0.26 (s, 9H, $SiMe_3$), 2.24 (dd, $^2J_{H,P}$ = 11.9 Hz, $^3J_{H,F}$ = 6.1 Hz, 1H, PCH), 5.62 (s, 1H, Ph_2CH), 7.77 (m, Ar). $^{13}C\{^1H\}$ NMR (75.5 MHz, $CDCl_3$; 25 °C):δ = 2.6 (dd, $^3J_{C,P}$ = 3.3 Hz, $^4J_{C,F}$ = 1.0 Hz, $Si(CH_3)_3$), 3.3 (pt, $^3J_{C,P}$ = 2.3, $Si(CH_3)_3$), 35.8 (dd, $^1J_{C,P}$ 17.1, $^2J_{C,F}$ 4.5, PCH), 56.6 (s, Ph_2CH), 138.2 (dd, $^1J_{C,P}$ = 37.8 Hz, $^2J_{C,F}$ = 18.0 Hz, P-Ph), 131.4 (dd, $^2J_{C,P}$ = 16.2 Hz, $^3J_{C,P}$ = 3.5 Hz, P-Ph), 129.4 (d, $^3J_{C,P}$ = 10.7, P-Ph), 148.8 (pt, $^4J_{C,P}$ = 1.4 Hz, P-Ph), 126.7 (s, Ph), 129.4 (s, Ph), 128.5 (s, Ph), 142.9 (s, Ph), 196.5 (d_{sat}, $^1J_{C,W}$ = 126.0 Hz, $^2J_{C,P}$ = 8.1 Hz, $^3J_{C,F}$ = 3.3 Hz, *cis*-CO), 198.6 (dd, $^2J_{C,P}$ = 28.2 Hz, $^3J_{C,F}$ = 1.1 Hz, *trans*-CO). $^{19}F\{^1H\}$ NMR (282.37 MHz, $CDCl_3$, 25°C): δ = –108.9 (d_{sat}, $^1J_{F,P}$ = 811.8 Hz, $^1J_{F,W}$ = 11.5 Hz). $^{31}P\{^1H\}$ NMR (121.51 MHz, $CDCl_3$, 25 °C): δ = 187.3 (d_{sat}, $^1J_{P,W}$ = 292.7 Hz, $^1J_{P,F}$ = 811.6 Hz). MS: *m/z* (%): 776 [M^+, 29]. IR (ν(CO, KBr pellet): tilde = 1910 (s), 1939 (s), 1992 (m), 2073 (m) cm^{-1}

11: Phosphinidenoid complex **2** was prepared as described above in 9 mL of THF, from phosphane **1** (265 mg, 0.5 mmol), 12-crown-4 (87.5 µL, 0.56 mmol) and *n*-BuLi (1.6 M, 0.35 mL, 0.56 mmol). After 15 min at –78 °C, the mixture was cooled up to –90 °C and *tris*(*p*-methylphenyl)carbenium tetrafluoroborate (210 mg, 0.56 mmol) was added as a solid. Stirred reaction mixture was slowly warmed up to room temperature (ca. 4 h) and stirred further 2 h. The solvent was evaporated and the residue was subjected to column chromatography (silica gel, –20 °C, petrol ether, petrol ether/diethyl ether = 10/0.5). Elution of a second band and evaporation of volatiles gave crude product, which was crystallized at –40 °C from *n*-pentane to give **11** as a white solid, m.p. 132 °C. Yield: 226 mg, (0.27 mmol, 55%). ^{1}H NMR (300.13 MHz, $CDCl_3$, 25°C):δ = 0.01 (s, 9H, $Si(CH_3)_3$) 0.19 (d, 9H, $^4J_{H,P}$ = 2.2 Hz, $Si(CH_3)_3$, 2.38 (s, 9H, $3CH_3$), 2.76 (dd, 1H, $^2J_{H,P}$ 18.1, $^2J_{H,F}$ 1.3, PCH) 7.15 (d, 6H, $^3J_{H,H}$ 8.3, Ar), 7.44 (d, 6H, $^3J_{H,H}$ 7.3, Ar). $^{13}C\{^1H\}$ NMR (75.5 MHz, $CDCl_3$; 25 °C):δ = 3.66 (d, $^3J_{C,P}$ = 2.9 Hz, $Si(CH_3)_3$), 4.48 (dd, $^3J_{C,P}$ = 4.2 Hz, $^4J_{C,F}$ = 1.2 Hz, $Si(CH_3)_3$), 21.05 (s, CH_3), 29.2 (dd, $^1J_{P,C}$ = 29.5 Hz, $^1J_{P,F}$ = 14.0 Hz, PCH), 70.67 (dd, $^1J_{C,P}$ = 13.7 Hz, $^2J_{C,F}$ = 1.8 Hz, CAr_3), 128.9 (s, Ar), 132.1 (dd, $^3J_{C,P}$ = 5.9 Hz, $^4J_{C,F}$ = 2.9 Hz,

Ar), 137.3 (d, $^{4}J_{C,P}$ = 2.4 Hz, Ar), 138.24 (br, Ar), 197.3 (dd, $^{2}J_{C,P}$ = 6.5 Hz, $^{3}J_{C,F}$ = 4.7 Hz, *cis*-CO), 198.2 (d, $^{2}J_{C,P}$ = 1.1 Hz, *trans*-CO). $^{19}F\{^{1}H\}$ NMR (282.37 MHz, $CDCl_3$, 25°C): δ = –109.4 (d_{sat}, $^{1}J_{F,P}$ = 821.4 Hz, $^{3}J_{F,W}$ = 10.1 Hz). $^{31}P\{^{1}H\}$ NMR (121.51 MHz, $CDCl_3$; 25 °C): δ = 207.1 (d_{sat}, $^{1}J_{P,W}$ = 283.5 Hz, $^{1}J_{P,F}$ = 821.4 Hz). MS: *m/z* (%): 818.1 [M^+, 17]. IR (ν(CO, KBr pellet): tilde = 1934 (s), 1984 (m), 2073 (s) cm^{-1}.

7.5 References

[7.1] a) S. Marque, P. Tordo, Top. Curr. Chem. 2005, 250, 43-76; b) D. Leca, L. Fensterbank, E. Lacôte, M. Malacria, *Chem. Soc. Rev.* **2005**, *34*, 858-865.

[7.2] Example for books: a) J. Conu, T. Chivers in Stable Radicals: Fundamentals and Applied AspectsofOdd-Electron Compounds, (Ed.:R. Hicks), Wiley, Chichester, 2010, pp. 381 –406; b) J. W. Grate, G. C. Frye, in Sensors Update, Vol. 2 (Eds: H. Baltes, W. Gçpel, J.Hesse), Wiley-VCH, Weinheim, 1996, pp. 10 –20.

[7.3] Selected examples: a) M. J. S. Gynane, A. Hudson**,** M. F. Lappert, P. P. Power, H. Goldwhite, *J. Chem. Soc., Chem. Commun.* **1976**, 623-624; b) M. J. S. Gynane, A. Hudson, M. F. Lappert, P. P. Power, H. Goldwhite, *J. Chem. Soc., Dalton Trans.* **1980**, 2428-2433; c) S. L. Hinchley, C. A. Morrison, D. W. H. Rankin, C. L. B. Macdonald, R. J. Wiacek, A. H. Cowley, M. F. Lappert, G. Gundersen, J. A. C. Clyburne, P. P. Power*, J. Chem. Soc., Chem. Commun.* **2000**, 2045-2046; d) J.-P. Bezombes, K. B. Borisenko, P. B. Hitchcock, M. F. Lappert, J. E. Nycz, D. W. H. Rankin, H. E. Robertson, *Dalton Trans.* **2004**, 1980-1988; e) O. Back, M. A. Celik, G. Frenking, M. Melaimi, B. Donadieu, G. Bertrand, *J. Am. Chem. Soc.* **2010**, 132, 10262-10263; f) O. Back, B. Donnadieu, M. von Hopffgarten, S. Klein, R. Tonner, G. Frenking, G. Bertrand, *Chem. Sci.* **2011**, *2*, 858-861; g) S. Ishida, F. Hirakawa, T. Iwamoto, *J. Am. Chem. Soc.* **2011**, 133, 12968-12971.

[7.4] a) S. E. Vaillard, C. Mück-Lichtenfeld, S. Grimme, A. Studer, Angew. Chem. **2007**, 119, 1-5; b) A. Bruch, A. Ambrosius, R. Fröhlich, A. Studer, D. B. Guthrie, H. Zhang, D. P. Curran, *J. Am. Chem. Soc.* **2010**, *132,* 11452-11454.

[7.5] B. M. Cossairt, C. Cummins, *New J. Chem.* **2010**, 34, 1533-1536.

[7.6] a) B. Cetinkaya, A. Hudson, M. F. Lappert, H. Goldwhite, *J. Chem. Soc., Chem. Commun.* **1982**, 609-610; b) J. Geier, H. Rüegger, M. Wörle, H. Grützmacher, *Angew. Chem.* **2003**, *115*, 4081-4085; *Angew. Chem. Int. Ed.* **2003**, *42*, 3951-3954.

[7.7] R. E. Bulo, H. Jansen, A. W. Ehlers, F.F. J. de Kanter, M. Schakel, M. Lutz, A. L. Spek, K. Lammertsma, *Angew. Chem.* **2004**, *116*, 732-735; *Angew. Chem. Int. Ed*. **2003**, 42, 3951-3954.

[7.8] For earlier studies on non-functional phosphanyl radicals as transition metal ligands, see: a) B. Ndiaye, S. Bhat, A. Jouaiti, T. Berclaz, G. Bernardinelli, M. Geoffroy, *J. Phys. Chem. A*. **2006**, *110*, 9736-9742; b) A. H. Cowley, R. A. Kemp, J. C. Wilburn, *J. Am. Chem. Soc.* **1982**, *104*, 332-334.

[7.9] A. Özbolat-Schön, M. Bode, G. Schnakenburg, A. Anoop, M. van Gastel, F. Neese, R. Streubel, *Angew. Chem.* **2010**, *122*, 7047-7051; *Angew. Chem. Int. Ed.* **2010**, *49*, 6894-6898.

[7.10] a) A. Özbolat, G. von Frantzius, J. Marinas Pérez, M. Nieger, R. Streubel, *Angew. Chem.* **2007**, *119*, 9488-9491; *Angew. Chem. Int. Ed.* **2007**, *46*, 9327-9330; b) M. Bode, J. Daniels, R. Streubel, *Organometallics* **2009**, *28*, 4636-4638.

[7.11] A. Özbolat, G. von Frantzius, W. Hoffbauer, R. Streubel, *Dalton Trans.* **2008**, 2674-2676.

[7.12] Tritylium salts can be used as an one electron oxidant for the generation of stable radicals which are quite inert to each other with the possibility of their separation, *e.g.*, see: a) N. G. Connelly, W. E. Geiger, *Chem. Rev.* **1996**, *96*, 877-910; b) ref. 3e.

[7.13] CCDC 848521 (**7**) and CCDC 848522 (**11**) contain the supplementary crystallographic data for t his paper. These data can be obtained free of charge from The Cambridge Crystallographic Data Centre via www.ccdc.cam.ac.uk/data request.cif.

[7.14] F. Neese, *ORCA* – An ab initio, DFT and semiempirical SCF-MO package, version 2.8r2556, Bonn, Germany, University of Bonn, **2010**.

[7.15] Due to the low intensity of this signal, the $^{1}J_{P,W}$ coupling constant magnitude was not determined.

[7.16] The importance of the P–C atropisomerism of this particular substituent R = $CH(SiMe_3)_2$ was observed before: a) in monomeri-sation/dimerisation processses of R_2P: S. L. Hinchley, C. A. Morrison, D. W. H. Rankin, C. L. B. Macdonald, R. J. Wiacek, A. Voigt, A. H. Cowley, M. F. Lappert, G. Gundersen, J. A. C. Clyburne, P. P. Power, *J. Am. Chem. Soc.* **2001**, *123*, 9045-9053; b) in oxaphosphirane complexes: J. M. Pérez, M. Klein, A. Kyri, G. Schnakenburg, R. Streubel, *Organometallics* **2011**, DOI: 10.1021/om200431f.

[7.17] H. Kurreck, B. Kirste, W. Lubitz, *Electron Nuclear Double Resonance Spectroscopy of Radicals in Solution*, VCH Pulblishers, Deerfield Beach, Florida,**1988**.

8 Summary

This work focusses on the spectroscopic investigation of reactions catalyzed by titanocene(III) chloride, in particular the reductive ring opening of epoxides. Both cw-EPR and modern pulse EPR methods have been employed for this purpose, in order to investigate the electronic structure of the catalyst and key reaction intermediates.

EPR spectroscopy has been a useful tool for elucidating the electronic and geometric structure of the paramagnetic reaction intermediates, since no NMR or X-ray data is available. The investigated reaction mechanism proceeds via a radical mechanism.

The obtained EPR parameters (g-tensor, hyperfine tensors) provide information about the structure of titanocene(III) chloride as well as titanocene(III) chloride complexed by small molecules such as water or methanol. Furthermore, titanocene(III) chloride with coordinated oxophosphirane was analyzed. The determination of the spin Hamiltonian parameters provided a detailed picture of the electronic structure and coordination environment of the spin-bearing titanium center.

In the first part of this work, the interaction between titanocene(III) chloride and H_2O or D_2O has been examined by Q-band EPR spectroscopy combined with electrochemistry. Compared to X-band (9.7 GHz), Q-band (34 GHz) features a four-times-larger Zeeman splitting. This allows for a better resolution of the g-tensor and the hyperfine and quadrupole couplings, in particular for the chloride atom. Based on these measurements, the existence of a cationic titanocene(III) species coordinated by water or D_2O has been unambiguously demonstrated. A detailed study of the interaction of the titanium(III) atom with the ligand environment was carried out with ESEEM and HYSCORE spectroscopy. The disappearance of the characteristic signal of chloride accompanied by the increase of the deuterium signal in the ESEEM spectra is clear evidence for the displacement of chloride by D_2O.

In the second part, the reaction mechanism of the epoxide opening catalyzed by titanocene(III) chloride has been investigated with pulse EPR experiments. The short lifetime of carbon radical species occurring in the catalytic cycle necessitates the use of spin trapping techniques. The EPR spectrum of the initial titanocene-epoxide-DMPO complex showed a radical signal. ESEEM and HYSCORE spectroscopy additionally allowed for the study of weakly coupled nuclei. These experiments have shown that epoxide is opened and a carbon radical is generated. To further prove this result, UV-vis measurements were carried out by using titanocene(III) chloride with the epoxide in the absence of DMPO.

This part describes pulsed EPR and ESEEM experiments of the titanocene(III)-DMPO complex, in which the complexation of the DMPO to the titanocene(III) was demonstrated. The obtained ESEEM spectra revealed important details about the nitrogen hyperfine coupling, which was used as additional information to elucidate the geometric structure of the investigated titanocene-DMPO complex.

The second section of this part of this work describes pulsed EPR and ESEEM experiments of the titanocene(III)-DMPO complex, in which the complexation of the DMPO to the titanocene(III) was demonstrated. The obtained ESEEM spectra revealed important details about the nitrogen hyperfine coupling, which was used as additional information to elucidate the geometric structure of the investigated titanocene-DMPO complex.

In the third part of this work, building on the pulsed EPR and ESEEM studies, the couplings of the nitrogen nucleus determines the coordination the amide ligand to the titanium center. The obtained ESEEM spectra showed unambiguous direct spectroscopic evidence for the coordination of the amide ligand to the metal center. Hence, the presence of amide complexation [I(^{14}N = 1)] is provided by EPR spectroscopy.

In the fourth part, the coordination of oxaphosphiranes to titanocene(III) was studied by means of cw EPR methods. Upon coordination the oxaphosphiranes undergo ring opening, forming transient phosphanyl radical intermediates. These radical have been detected by using either spin trapping agents or freeze quench techniques. The EPR investigations of this reaction have shown that the unpaired electron occupies a pure 3p orbital at ^{31}P without admixture of the 3s orbital. Small amounts of spin density were found at the adjacent W, C and F atom and the remaining part distributed over the CO ligands.

The experimentally determined EPR data of the various titanocene(III) complexes were complemented by density functional calculations. The computed EPR parameters of the structural models of titanocene(III) coordinated by water, epoxide, DMPO or oxaphosphirane showed good agreement with the experimental values. The calculations of the titanocene(III) chloride catalyst indicate that the unpaired electron resides in the titanium d_z2 orbital. It was shown that the titanocene(III) chloride complex is monomeric in THF. Interestingly, THF does not bind to the metal center, because of steric congestion around the central ion.

The use of EPR techniques such as ENDOR, ESEEM and HYSCORE spectroscopy in this study has been essential for the elucidation of both the electronic and geometric structure of the investigated titanocene(III) complexes, which represent key paramagnetic intermediates within the catalytic cycle of the epoxide ring opening reaction. Further insight into the details of the electronic structure of these compounds has been obtained from DFT calculations.

The results of this study shed light on an important reaction in organic radical chemistry. In particular, the observed dissociation of chloride indicates that the catalytically active species concerns a cationic titanocene(III) complex which has lost the chloride ligand. This provides strong experimental evidence for the postulated inner sphere electron transfer between epoxides and titanocenes that has been put forward to explain the high regioselectivity of ring opening. The structure of the complex provides an experimental basis for the design of novel reactions based on enantioselective interactions between epoxides and titanocenes.

The dissociation of chloride from monomeric titanocene upon binding of 1,1-diphenyl epoxide demonstrates that for the finding of catalysts for the kinetic resolution of 1,1-disubstituted and tri-substituted epoxides another ligand design has to be applied than for regioselective opening of *meso*-epoxides or *cis*-1,2-disubstituted epoxides. In contrast to the complex identified above the catalytically active species for these epoxides were postulated to retain their chloride ligands. These

different binding modes explain the poor performance of the catalysts successful in regioselective opening of the latter two classes of epoxides when applied for kinetic resolutions of 1,1-disubstituted and tri-substituted epoxides.

Appendices

A. Additional Results on H_2O-Activation for HAT Study (Chapter 4)

[1] (a) A. Schweiger, G. Jeschke. *Principles of Pulse Electron Paramagnetic Resonance,* Oxford, Oxford University Press, **2001**. (b) W. B. Mims, J. Peisach, *J. Chem. Phys.* **1978**, *69*, 4921-4930. (c) W. B. Mims, *Proc. Roy. Soc. London A* **1965**, *283*, 452-457.

[2] a) R. J. Enemærke, J. Larsen, T. Skrydstrup, K. Daasbjerg, *J. Am. Chem. Soc*. **2004**, *126*, 7853-7864; b) K. Daasbjerg, H. Svith, S. Grimme, M. Gerenkamp, C. Mück-Lichtenfeld, A. Gansäuer, A. Barchuk, F. Keller, *Angew. Chem.* **2006**, *118*, 2095-2098; *Angew. Chem. Int. Ed.* **2006**, *45*, 2041-2044.

Experimental details:

Sample preparation: All samples were prepared under an atmosphere of argon using standard Schlenk techniques. THF was freshly distilled over potassium under an atmosphere of argon. The distilled water or D_2O was degased and kept under an atmosphere of argon prior to use. Samples were prepared from 12.6 mg of Cp_2TiCl_2 (0.05 mmol, 1.0 eq.) and 3.3 mg of Zn (0.05 mmol, 1.0 eq.) in 5 mL of THF and stirring at room temperature until the solution was green. After addition of the appropriate amount of water or D_2O the solution was allowed to stir for 5 minutes. Samples were transferred under argon atmospere into the EPR-tubes and instantly frozen in liquid nitrogen.

Measurements: Q-band EPR, ESEEM and HYSCORE spectra were recorded for frozen solutions (T = 30 K) of 10 mM concentration using a Bruker ELEXSYS E580 FT-EPR spectrometer using a Bruker EN5107 D2 resonator. For the Electron Spin Echo (ESE) detected EPR experiments, a Hahn echo pulse sequence with pulses of 24 ns and 48 ns and a pulse separation of 300 ns was employed. The g values are determined by reading the magnetic field as indicated by the arrows in Figure S1 from the spectrum and using the resonance condition

$$h\nu = g\mu_B B \qquad (1)$$

with h Planck constant, μ_B the Bohr magneton, ν the microwave frequency and B the magnetic field.

The three-pulse ESEEM[1] experiments were carried out with pulses of 40 ns length. The time between the first two pulses was fixed at 200 ns. A mono-exponential background was subtracted from the modulation pattern. The resulting modulations were multiplied with a Hamming window function, zero-filled to 2048 points and Fourier transformed into frequency domain. The spectra in the right columns of Figures S2 and S3 are displayed as magnitude ESEEM spectra. The HYSCORE experiments were performed with 90 degree pulses of 16 ns length and an inversion pulse of 32 ns. The time between the first two pulses was fixed at 128 ns.

Pulsed EPR spectra:

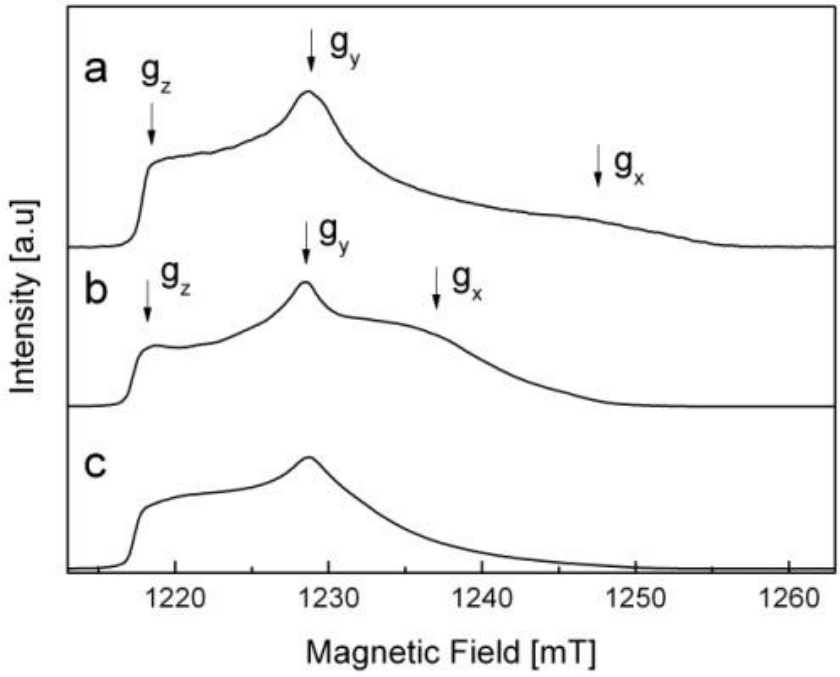

Figure A.1. Q-Band ESE detected EPR spectra (T = 30 K) of frozen solutions of Zn-reduced Cp_2TiCl_2 in THF, ν_{mw} = 34.117 GHz (a) without H_2O, (g_x, g_y, g_z) = (1.955, 1.983, 2.001), (b) with 10 eq. H_2O, (g_x, g_y, g_z) = (1.971, 1.985, 2.002) and (c) with 100 eq. H_2O. In the latter sample, the g_x and g_y values become essentially equal.

ESEEM spectra:

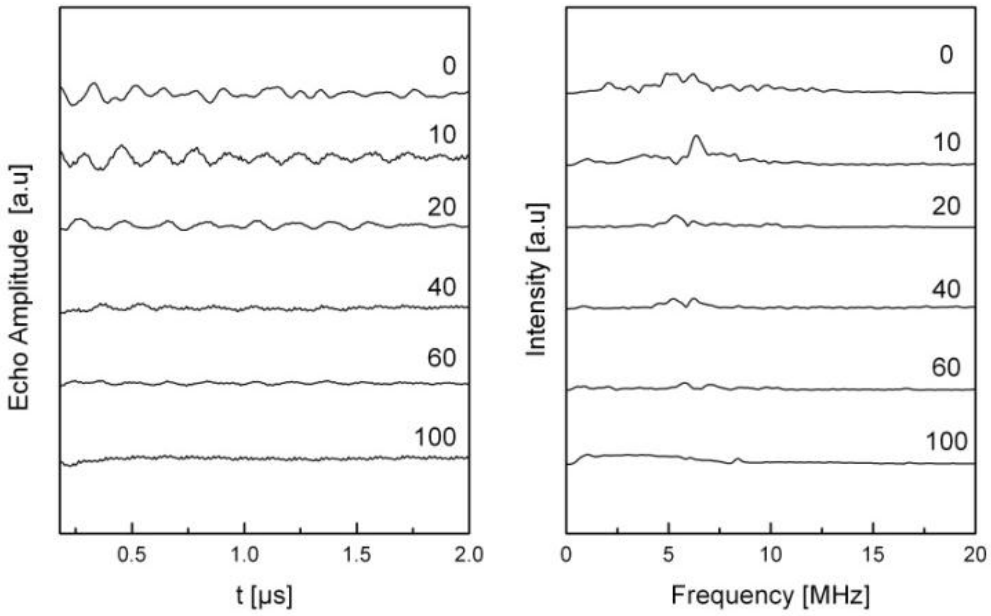

Figure A.2. Normalized Q-Band 3-pulse modulation patterns and ESEEM spectra (T = 30 K) of Cp_2TiCl in THF with different added molar equivalents of H_2O (indicated in figure) recorded at the g_y canonical orientation.

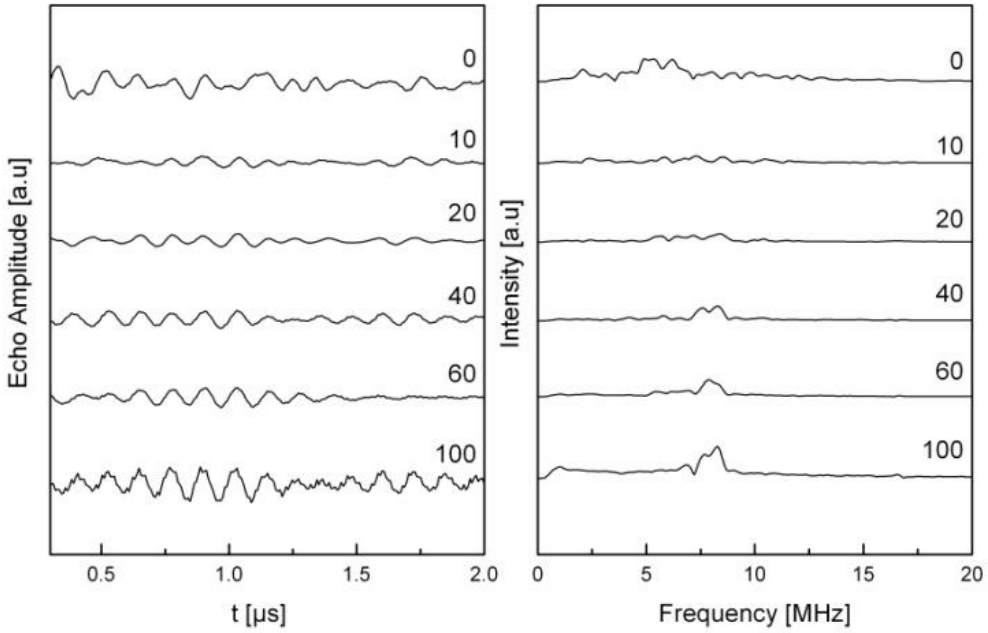

Figure A.3. Normalized Q-Band 3-pulse modulation patterns and ESEEM spectra (T = 30 K) of Cp_2TiCl in THF with different added molar equivalents of D_2O (indicated in figure) recorded at the g_y canonical orientation.

Cyclic Voltammetry:Materials: THF was distilled over potassium under an atmosphere of argon. The distilled water was degased and kept under an atmosphere of argon. Tetrabutylammoniumhexafluorophosphate, Bu_4NPF_6, and Tetrabutylammoniumiodide, Bu_4NI, were commercially available in electrochemical grade from Aldrich and were stored in a glovebox under an atmosphere of argon.

Apparatus.:All handling of chemicals and the cyclic voltammetric experiments were performed in a glovebox under an atmosphere of argon. The cyclic voltammograms were recorded by a 600D Electrochemical Analyzer/Workstation (CH-Instruments). The working electrode was a glassy carbon disk of diameter 1 mm. The electrode surface was polished using 0.25 µm diamond paste (Struers A/S), followed by cleaning in an ethanol bath. The counter electrode consisted of a platinum coil melted into glass, while a Ag/AgI electrode (silver wire immersed in a Pyrex tube containing 0.2 M Bu_4NPF_6 + 0.02 M Bu_4NI in THF) separated from the main solution by a ceramic frit served as the reference electrode. All potentials were reported against the Fc^+/Fc redox couple, the potential of which is equal to 0.52 V vs. SCE in 0.2 M Bu_4NPF_6/THF.[2]

Procedure. In the cyclic voltammetric experiments 0.77 g of Bu_4NPF_6 (2.0 mmol) and a small magnetic bar were added to the electrochemical cell. 9 mL of freshly distilled THF, 1 mL of the appropriate standard solution containing the zinc-reducedCp_2TiCl_2 and the appropriate amount of water were added to the cell and the solution was stirred for 10 min. At the end of each series of experiments a small amount of ferrocene was added and the potential of the Fc^+/Fc redox couple was measured.

Cyclovoltammograms with higher sweeprates.

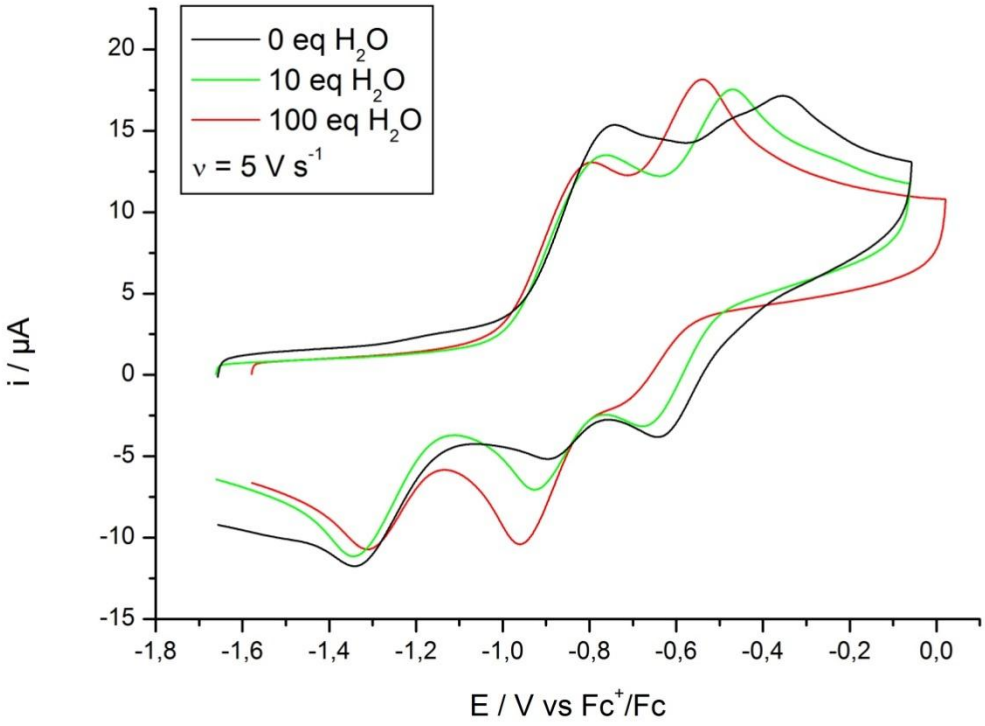

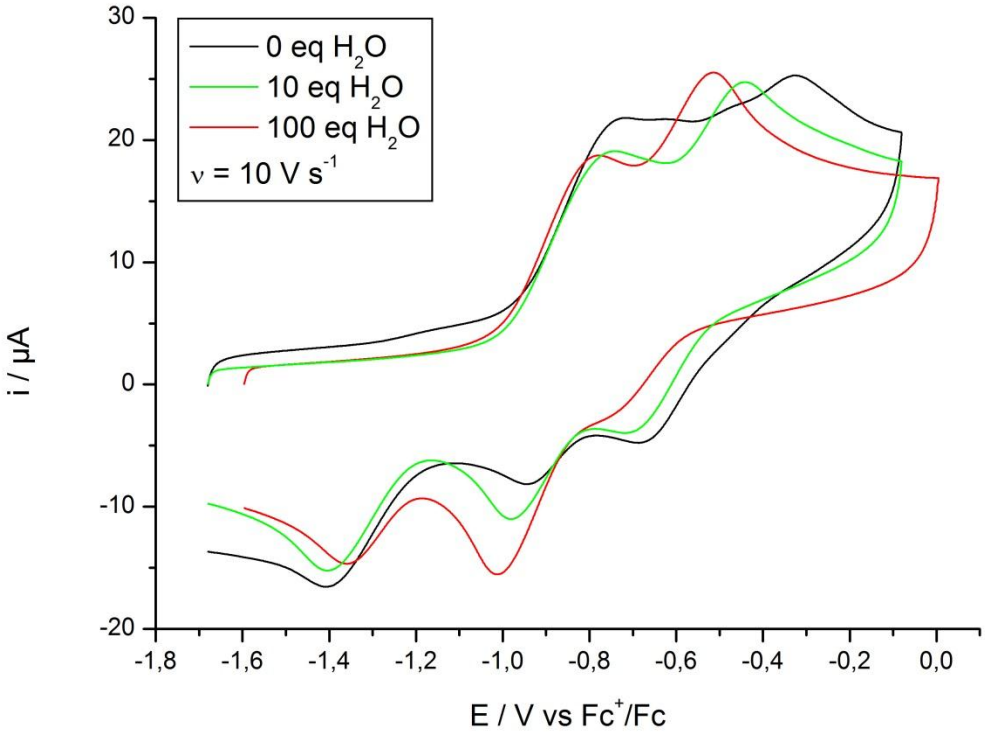

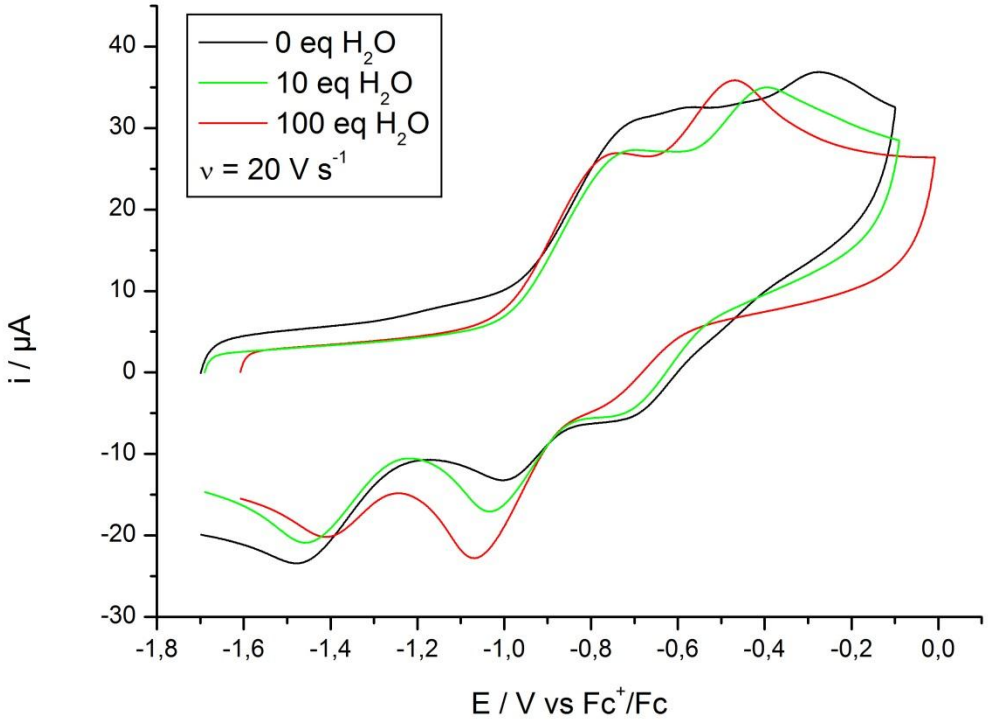
0 eq H2O
10 eq H2O
100 eq H2O
ν = 20 V s-1
i / µA
E / V vs Fc+/Fc

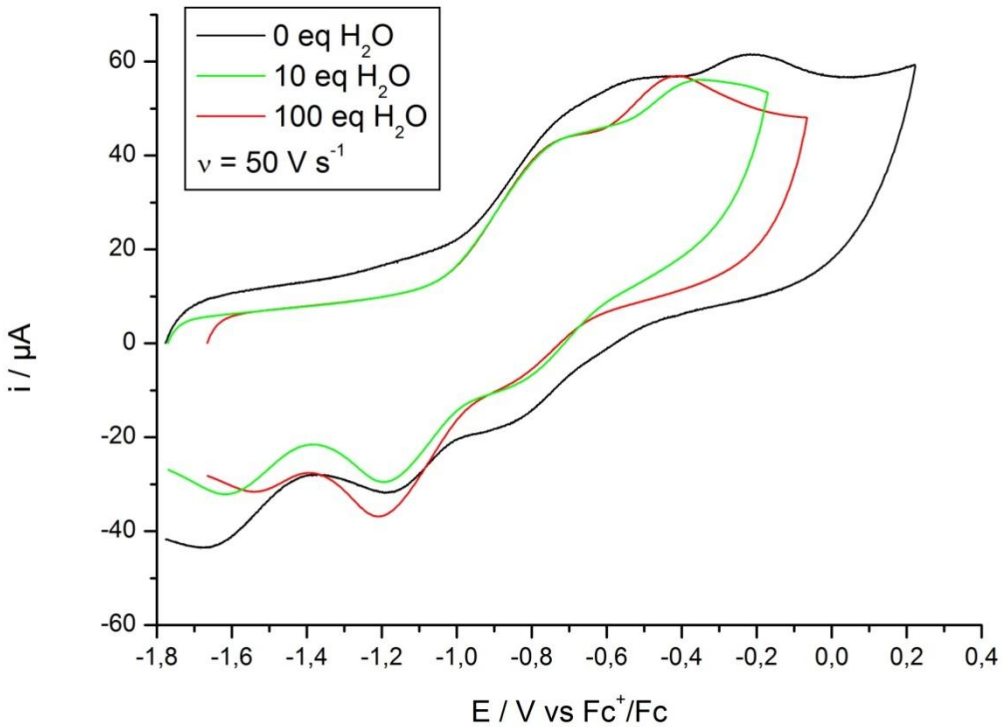
0 eq H2O
10 eq H2O
100 eq H2O
ν = 50 V s-1
i / µA
E / V vs Fc+/Fc

Computational procedures:

The anionic species were optimized with BP86/TZVP using COSMO in combination with ε=7.6.

B3LYP-d/TZVPP energies and BP86/TZVP zero point vibratinal energies:

	ZPVE	E	E+ZPVE
	au	au	au
H	0,000000	-0,496808	-0,496808
Cl^-	0,000000	-460,319744	-460,319744
2a	0,187950	-1773,123679	-1772,935729
2b	0,189136	-1773,133460	-1772,944324
3a	0,188732	-1312,752768	-1312,564036
3b	0,212854	-1389,216323	-1389,003469
Cp_2TiCl	0,164946	-1696,679194	-1696,514248
THF_2*H_2O	0,252382	-541,284638	-541,032256
$Cp_2TiCl(H_2O*THF_2)$	0,419443	-2237,993710	-2237,574267
H_2O	0,020611	-76,438839	-76,418229
$ZnCl_4^{2-}$	0,003327	-3620,474940	-3620,471613
$ZnCl_2$	0,001908	-2699,790872	-2699,788964
$Cp_2Ti(H_2O*THF_2)$	0,418952	-1777,623090	-1777,204139
$Cp_2Ti(H_2O*THF_2)_2$	0,673006	-2318,940928	-2318,267923
THF	0,113230	-232,414093	-232,300863
4	0,534214	-2010,065419	-2009,531205
5	0,293849	-2004,971868	-2004,678019
6	0,292744	-1544,578019	-1544,285275
7	0,547834	-2085,918164	-2085,370329
2b*THF	0,304693	-2005,562844	-2005,258151
3a*THF	0,303692	-1545,188801	-1544,885110
3b*3THF	0,558083	-2086,510490	-2085,952408
Cp_2Ti	0,163827	-1236,269764	-1236,105937
$THF*H_2O$	0,136965	-308,8621976	-308,725232

Structural analysis of selected Structures:

Structural features of **2b***2THF:

The H-O distance of the water Protons and the THF Oxygens are 1.75 Å and 1.82 Å respectively. The distance of the α-Protons to the Chloride are 2.71 Å and 2.73 Å. The distance of the Ti to the Water Oxygen is 2.24 Å.

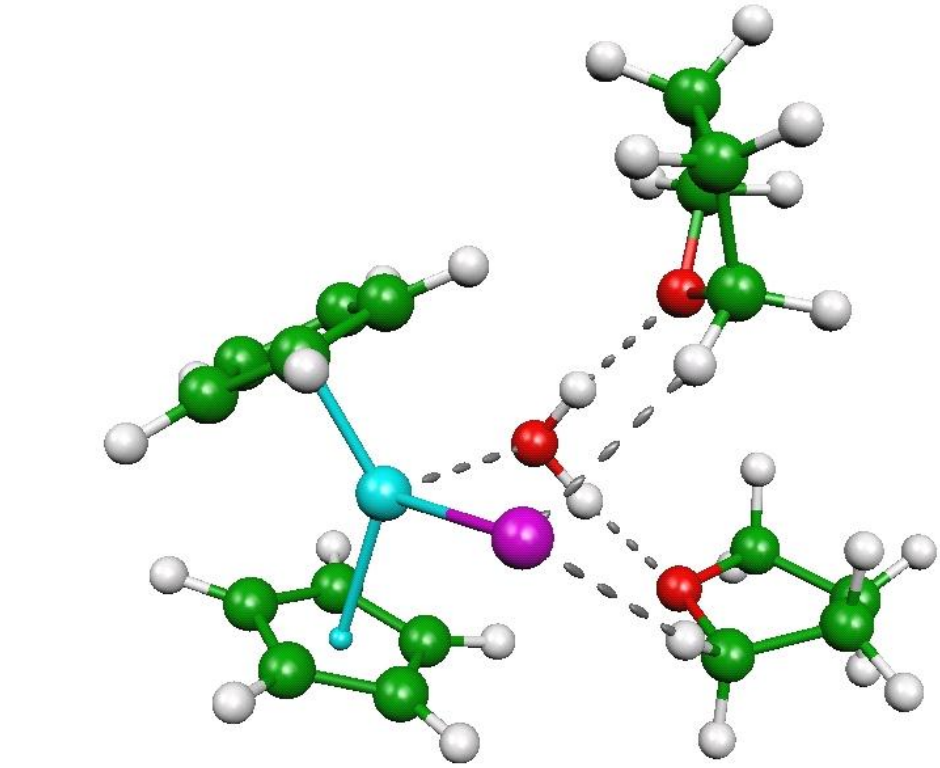

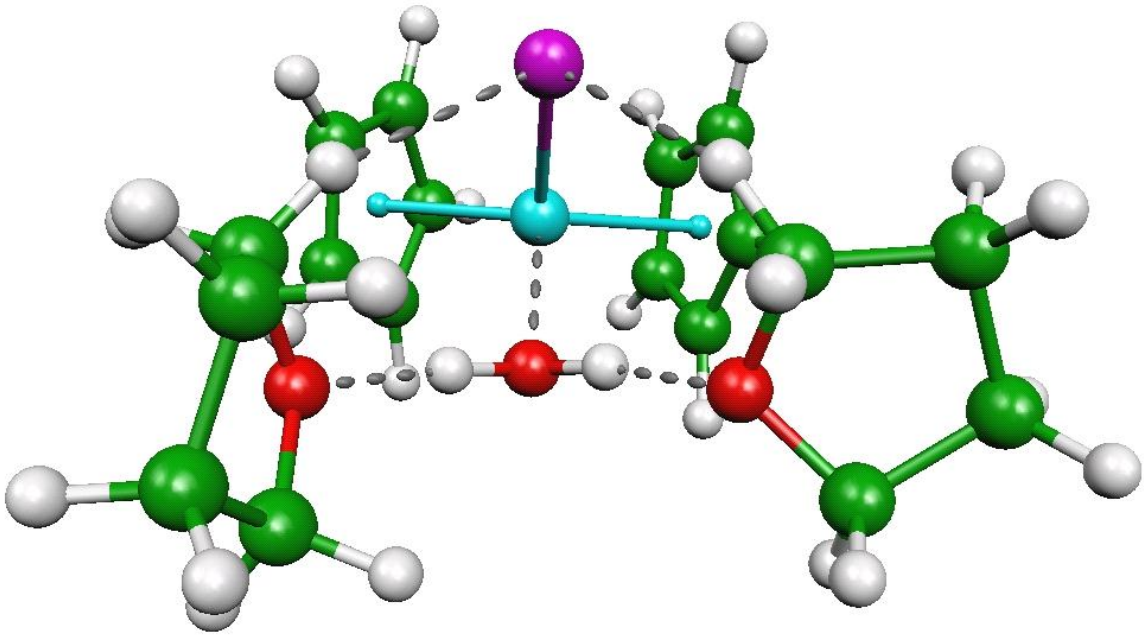

Structural features of **2b***THF:

The H-O distance of the water Proton and the THF Oxygen is 1.75 Å. The distance of the Ti to the Water Oxygen is 2.27 Å. The distance of the α-Protons to the Chloride is 3.16 Å, wich is significantly longer than in **2b***2THF. The distance of the second proton of water to the chloride is 2.16 Å.

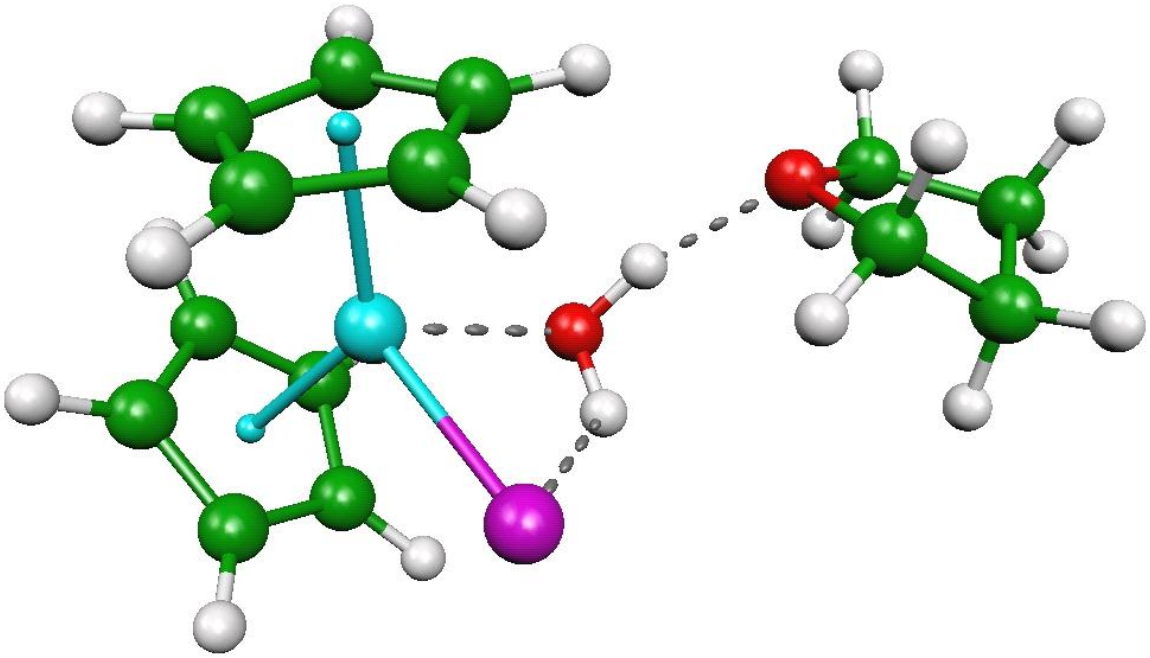

BP86/TZVP structures:

2a

25

C	2.1509734	0.6829834	0.0048631	C	-0.6203716	-1.2754417	1.1376258
C	1.9407194	0.8671078	-1.3870143	C	-0.4995047	-0.0886772	1.9168394
C	1.1671253	2.0438435	-1.5664767	C	-1.5732920	0.7846846	1.5729689
C	0.8891847	2.5980135	-0.2849714	H	-2.1453865	-1.8542743	-0.3980936
C	1.5149091	1.7625307	0.6848669	H	0.0345756	-2.1415681	1.1794707
Cl	-1.0974368	0.0705033	-2.5126202	H	0.2742261	0.1076610	2.6523831
Ti	-0.2037195	0.5012004	-0.3594691	H	-1.7545519	1.7724799	1.9887222
H	2.2658698	0.1961544	-2.1776896	H	2.7086487	-0.1271241	0.4673318
H	0.8010140	2.4200991	-2.5166337	H	-3.2493805	0.5365722	0.0954217
H	0.3343998	3.5107574	-0.0857772	H	-3.3273394	0.7271172	-2.3001619
H	1.5133513	1.9290510	1.7572803	O	-4.2266589	0.9823285	-2.0010697
C	-2.3759901	0.1280613	0.6031287	H	-4.8213091	0.4390886	-2.5434341
C	-1.7895120	-1.1376748	0.3358870				

2b

25

C	1.9574854	1.3010304	0.2226314	C	-0.4833669	-1.1967080	1.7002257
C	1.8694328	1.1223770	-1.1862812	C	-0.4587919	0.1104971	2.2450463
C	0.8030687	1.9141937	-1.6727312	C	-1.5863382	0.8243365	1.7394327
C	0.2135967	2.5951403	-0.5713357	H	-1.9328959	-2.1500308	0.2620874
C	0.9466529	2.2339060	0.5973695	H	0.2355290	-1.9845201	1.9133089
Cl	-1.4908842	-0.1529727	-2.2370767	H	0.2924947	0.4992279	2.9262787
Ti	-0.1641534	0.2901447	-0.1466883	H	-1.8393192	1.8575024	1.9616782
H	2.4731660	0.4393574	-1.7765713	H	2.6842707	0.8376034	0.8842800
H	0.4485585	1.9434671	-2.6975082	H	-3.1955501	0.2131346	0.3125638
H	-0.6242845	3.2848267	-0.6211566	O	0.7621430	-1.5566493	-1.1518542
H	0.7707896	2.6139345	1.5987669	H	0.0720637	-1.4952906	-1.8750038
C	-2.3091910	-0.0397509	0.8853794	H	0.5837573	-2.3876862	-0.6794406
C	-1.6250426	-1.2881105	0.8473502				

3a

24

C	2.1218041	1.1567893	0.2147232	C	-0.2435855	-1.4740014	1.7228620
C	2.0284630	0.8586907	-1.1722070	C	-0.2486666	-0.1714338	2.2794848
C	0.9086588	1.5562553	-1.7051570	C	-1.3662344	0.5398388	1.7467494
C	0.2990651	2.2922095	-0.6528357	H	-1.6732627	-2.4591026	0.2983785
C	1.0613218	2.0575946	0.5303614	H	0.4702373	-2.2632461	1.9464738
Ti	0.0808362	0.0199874	-0.0747328	H	0.4725857	0.2158575	2.9941024
H	2.7059213	0.2088653	-1.7234668	H	-1.6445367	1.5626242	1.9860424
H	0.5699339	1.5384077	-2.7395860	H	2.8895841	0.8011618	0.8965315
H	-0.5611832	2.9496623	-0.7452853	H	-2.9656464	-0.0769009	0.3090631
H	0.8816398	2.5102368	1.5007724	H	0.4943907	-1.2647840	-2.5703839
C	-2.0580608	-0.3186128	0.8569413	O	0.0228209	-1.3630388	-1.7241332
C	-1.3600673	-1.5655801	0.8355806	H	-0.4775352	-2.1977494	-1.7553541

$ZnCl_2$

3

Zn	-3.9073878	0.8480934	-0.0000012
Cl	-1.7691266	0.8480653	0.0000006
Cl	-6.0456465	0.8480653	0.0000006

3b

27

C	1.8570661	1.4267782	0.4315617	C	-1.5595069	0.7323172	1.7574452
C	2.0182352	0.9689306	-0.8957580	H	-1.8310054	-2.2848223	0.3294388
C	1.0309863	1.5986490	-1.7028716	H	0.4084740	-1.9867372	1.8355318
C	0.2687138	2.4782029	-0.8709191	H	0.3736995	0.5005170	2.8669265
C	0.7827453	2.3678668	0.4461408	H	-1.8742791	1.7384665	2.0195152
Ti	-0.1713615	0.2709966	-0.1624732	H	2.4623158	1.1331601	1.2848665
H	2.7475061	0.2401212	-1.2378996	H	-3.2501082	0.0142894	0.4945567
H	0.9254086	1.4679818	-2.7780652	O	0.4991389	-1.4941743	-1.4016968
H	-0.5263176	3.1485840	-1.1887057	H	-0.1420864	-1.7812403	-2.0775097
H	0.4333874	2.9202229	1.3133315	H	0.9025663	-2.2947479	-1.0250387
C	-2.2781744	-0.1773647	0.9459113	O	-1.5792611	0.1287227	-1.9686619
C	-1.5309434	-1.3851554	0.8611593	H	-1.4903917	0.8200093	-2.6493237
C	-0.3478250	-1.2289333	1.6466441	H	-2.5320801	0.0567090	-1.7800366
C	-0.3729489	0.0777094	2.2013954				

Cp_2TiCl

21

C	2.0609489	0.4205010	-0.0930967	C	-1.5364444	-1.0208505	0.1891920
C	1.6870953	0.7105244	-1.4303413	C	-0.5744174	-0.9938997	1.2312971
C	1.2057506	2.0597908	-1.4678128	C	-0.8049859	0.1745704	2.0229169
C	1.3153344	2.6040049	-0.1466623	C	-1.9100494	0.8727821	1.4720918
C	1.8315123	1.5888672	0.6989954	H	-1.6331312	-1.7916485	-0.5729004
Ti	-0.2641205	0.8941600	-0.1740632	H	0.1955293	-1.7404727	1.4068751
H	1.7562710	0.0295210	-2.2763418	H	-0.2403641	0.4687840	2.9036394
H	0.8697671	2.5951961	-2.3549145	H	-2.3407621	1.7950853	1.8569582
H	1.0520557	3.6158990	0.1550455	H	2.4661372	-0.5221982	0.2649013
H	2.0323444	1.6868468	1.7625330	H	-3.2095469	0.4037052	-0.3072483
C	-2.3584923	0.1454674	0.3216506				

H_2O

3

O	-2.3437162	1.8132964	-0.0705527
H	-1.3733924	1.8587832	-0.0705527

H	-2.6247392	2.7431483	-0.0705527

THF

13

C	-0.0018887	0.0360658	0.1135673
O	1.2652492	0.1368274	-0.5525637
C	1.8695088	1.3196702	-0.0137394
C	0.7352078	2.3582665	0.0551002
C	-0.5356877	1.4829671	0.2457003
H	-0.6405744	-0.6237139	-0.4877437
H	0.1331481	-0.4211704	1.1138662
H	2.2755298	1.1150156	0.9979967
H	2.7000261	1.6009060	-0.6739669
H	0.8826559	3.0785286	0.8713959
H	0.6783745	2.9232274	-0.8851108
H	-1.0103564	1.6453869	1.2230846
H	-1.2837647	1.7041515	-0.5268931

THF_2*H_2O

29

C	0.3721943	-3.4723499	-0.0045886	H	3.5453852	-5.0558842	2.2684252
O	1.2149474	-2.9521537	1.0502443	O	4.3909630	-5.5844582	3.8759088
C	1.9814076	-1.8298404	0.5258647	C	5.6286300	-6.2451535	3.4911869
C	1.6602555	-1.7319161	-0.9769980	C	3.5142227	-6.5829580	4.4404533
C	1.1002414	-3.1287809	-1.3018226	C	5.3538227	-7.7669806	3.5046833
H	0.2530447	-4.5492484	0.1739600	H	5.8957122	-5.8677408	2.4940383
H	-0.6222972	-2.9896337	0.0384724	H	6.4241248	-5.9629208	4.2002148
H	1.7031483	-0.9187735	1.0782495	C	3.8212285	-7.8540527	3.6525952
H	3.0446678	-2.0457076	0.7114456	H	3.7296987	-6.7122771	5.5185647
H	0.8957579	-0.9625348	-1.1619110	H	2.4861628	-6.2155981	4.3249442
H	2.5459041	-1.4774100	-1.5739326	H	5.8504526	-8.2421688	4.3632216
H	0.4375091	-3.1329038	-2.1779352	H	5.7154487	-8.2602414	2.5931839
H	1.9158993	-3.8459758	-1.4729997	H	3.4922949	-8.7682226	4.1654039
H	2.4485615	-4.3198722	1.4313971	H	3.3308868	-7.8010717	2.6702823
O	3.1277399	-5.0296990	1.3783311				

$ZnCl_4^{2-}$

5

Zn	-2.0215685	-0.8806856	-0.1639877
Cl	-0.9909597	0.0135779	-2.0576972
Cl	-1.5255938	-3.1560901	-0.0102525
Cl	-4.3319329	-0.6014830	-0.3357719
Cl	-1.2467231	0.2216228	1.7424229

$Cp_2Ti(H_2O*THF_2)$

50

C	1.8912618	0.1605328	-0.5882300	C	-0.5195420	3.5005280	-4.5072067
C	1.5123614	1.0661192	-1.6110226	C	-1.1459352	5.2518545	-2.9938812
C	1.4061372	2.3627312	-1.0347784	C	-0.9008736	4.7439133	-5.3099519
C	1.7222984	2.2649024	0.3521607	H	0.5544623	3.2719253	-4.5878832
C	2.0342459	0.9030292	0.6205084	H	-1.0991300	2.6061355	-4.7738240
Ti	-0.2513923	1.0348129	0.0015725	C	-0.6664985	5.8795530	-4.2986126
H	1.3188083	0.8059988	-2.6489272	H	-2.2378289	5.3453610	-2.8732269
H	1.1162125	3.2666443	-1.5640906	H	-0.6493599	5.6451734	-2.0969659
H	1.7640358	3.0850856	1.0637705	H	-1.9586887	4.7055565	-5.6085738
H	2.3391565	0.5006774	1.5819579	H	-0.2953417	4.8490781	-6.2188153
C	-2.2958180	0.0418180	0.6482352	H	-1.2197041	6.7940735	-4.5468993
C	-1.3087795	-0.9849593	0.5797097	H	0.4020312	6.1318440	-4.2367793
C	-0.3492941	-0.7186759	1.5957753	O	-4.1135229	2.0330350	-1.3683779
C	-0.7297174	0.4764119	2.2738480	C	-4.8208522	1.4994870	-2.5350174
C	-1.9372924	0.9389384	1.6928859	C	-5.0186644	2.8876657	-0.5899280
H	-1.3120933	-1.8393214	-0.0917818	C	-6.3006392	1.7171453	-2.2366486
H	0.5200052	-1.3290397	1.8216567	H	-4.4987081	2.0573780	-3.4297503
H	-0.1979944	0.9423806	3.0991609	H	-4.5351732	0.4450303	-2.6458341
H	-2.4799649	1.8345434	1.9858027	C	-6.2803581	3.0333979	-1.4400853
H	2.0576655	-0.9065933	-0.7087610	H	-5.2227958	2.3808744	0.3660024
H	-3.1663875	0.1381932	0.0047272	H	-4.5062717	3.8388736	-0.3909808
O	-1.4908935	2.1013276	-1.2541115	H	-6.6961765	0.8957201	-1.6217556
H	-1.2003306	2.7524494	-1.9782128	H	-6.9034787	1.7801800	-3.1513196
H	-2.5064062	2.0725115	-1.2657984	H	-7.1776394	3.1745332	-0.8246705
O	-0.8052656	3.8313833	-3.1055401	H	-6.1950720	3.8941038	-2.1194438

$Cp_2TiCl(H_2O*THF_2)$

51

C	1.7296032	0.7323841	0.3563030
C	2.1203265	0.6821498	-1.0118553
C	1.1771582	1.4117460	-1.7727428
C	0.1877288	1.9230159	-0.8896477
C	0.5464286	1.5223841	0.4314939
Cl	-0.6580475	-0.7194553	-3.1561810
Ti	-0.0313938	-0.4498397	-0.7433007
H	2.9723806	0.1389672	-1.4122658
H	1.1641901	1.5063264	-2.8530596
H	-0.6707642	2.5255207	-1.1726042
H	0.0137501	1.7851328	1.3398577
C	-2.3512035	-1.0272797	-0.4600648
C	-1.5602183	-2.2060799	-0.3365949
C	-0.7688423	-2.0906884	0.8452370
C	-1.0547299	-0.8359671	1.4315170
C	-2.0313416	-0.1785050	0.6235986
H	-1.5468725	-3.0351415	-1.0366585
H	-0.0446750	-2.8141238	1.2086275
H	-0.5982810	-0.4385607	2.3336444
H	-2.4456136	0.8104592	0.8009372
H	2.2540617	0.2738976	1.1902129
H	-3.0273316	-0.7993253	-1.2775183
O	1.3475302	-2.1432177	-1.2249373
H	2.0501754	-1.9231693	-1.8987345
H	0.8728029	-2.9120037	-1.6326278
O	0.3247401	-4.4344963	-2.4718356
C	-0.5378642	-4.3949698	-3.6351192
C	0.2151532	-5.7736886	-1.9510613
C	-1.7695655	-5.2409920	-3.2596782
H	-0.7506933	-3.3366347	-3.8363566
H	0.0006088	-4.8376171	-4.4938513
C	-1.2697021	-6.1516416	-2.1006525
H	0.8598759	-6.4505195	-2.5431944
H	0.5772676	-5.7585620	-0.9153133
H	-2.1316132	-5.8208573	-4.1190835
H	-2.5939492	-4.5987045	-2.9237865
H	-1.3924858	-7.2205616	-2.3210637
H	-1.8192801	-5.9379978	-1.1744104
O	3.3110362	-1.7168008	-3.0869819
C	4.2158820	-2.8412999	-3.2821362
C	2.8751774	-1.2066736	-4.3857238
C	4.4813601	-2.9187594	-4.7893323
H	5.1234276	-2.6624678	-2.6872616
H	3.7204551	-3.7523998	-2.9079650
C	3.1951790	-2.3175470	-5.3820812
H	1.8063793	-0.9623928	-4.3008586
H	3.4473296	-0.2895512	-4.6091141
H	4.6742626	-3.9466841	-5.1244701
H	5.3516451	-2.3028091	-5.0614061
H	2.3870837	-3.0638804	-5.3945755
H	3.3285446	-1.9377523	-6.4037865

$THF*H_2O$

16

C	0.9803142	-3.8670851	0.9616329
O	2.4245618	-3.8415930	1.0739371
C	2.9080853	-2.5388608	0.6311839
C	1.6807205	-1.7547492	0.1336532
C	0.6489284	-2.8641861	-0.1401734
H	0.6893355	-4.9009752	0.7333659
H	0.5276890	-3.5709535	1.9259659
H	3.4147018	-2.0440431	1.4739551
H	3.6432237	-2.7167407	-0.1684397
H	1.3106513	-1.0756695	0.9160790
H	1.9070246	-1.1525228	-0.7559474
H	-0.3884781	-2.5064324	-0.0930799
H	0.8177832	-3.3206288	-1.1263371
H	3.0794599	-5.1350946	-0.0293297
O	3.3202865	-5.7490004	-0.7646934
H	3.8608140	-6.4348377	-0.3413941

$Cp_2Ti(H_2O*THF_2)_2$

79

C	1.1520412	0.4080997	1.0452388
C	1.4943809	0.3148295	-0.3245712
C	0.5745797	1.1051088	-1.0653129
C	-0.3320080	1.7109182	-0.1429294
C	0.0294560	1.2790644	1.1589459
Ti	-0.7241193	-0.6283577	-0.1008657
H	2.2945513	-0.2927470	-0.7391120
H	0.5478415	1.2086759	-2.1466653
H	-1.1406369	2.3932139	-0.3892175
H	-0.4586733	1.5670192	2.0853524
C	-2.8907600	-1.4134287	0.6425388
C	-2.0758088	-2.5312487	0.3177210
C	-0.9857335	-2.5674995	1.2397076
C	-1.1314543	-1.4636300	2.1186192
C	-2.3033975	-0.7446823	1.7426265
H	-2.2377615	-3.2217270	-0.5055272
H	-0.1975121	-3.3141470	1.2752655
H	-0.4696107	-1.2116288	2.9419078
H	-2.6858636	0.1497158	2.2265106
H	1.6636445	-0.0839408	1.8677549
H	-3.7853012	-1.0982755	0.1116435
O	0.2004404	-1.9511578	-1.5997385
H	-0.3249980	-2.7201543	-1.9549178
H	1.1351918	-2.2748490	-1.4810276
O	-1.9757493	-0.3156896	-1.8869042
H	-1.5688187	0.1046283	-2.6937238
H	-2.8939303	0.0616791	-1.8021730
O	-1.1503106	-4.1137088	-2.6008928
C	-0.7604979	-5.5048677	-2.3722588
C	-2.0267253	-4.0395752	-3.7604751
C	-1.3859910	-6.3154419	-3.5128470
H	0.3373718	-5.5623293	-2.3517073
H	-1.1511466	-5.8060546	-1.3876589
C	-2.5886348	-5.4482788	-3.9246232
H	-2.7807876	-3.2692142	-3.5531709
H	-1.4373844	-3.7364846	-4.6437791
H	-1.6742664	-7.3248453	-3.1932716
H	-0.6815331	-6.4139046	-4.3517023
H	-3.4363844	-5.6072593	-3.2419436
H	-2.9293823	-5.6487976	-4.9486255
O	-0.9611161	0.8748850	-4.1375600
C	-0.3040410	0.1418068	-5.2096130
C	-1.3667654	2.1929319	-4.6249586
C	0.1513815	1.2089197	-6.2001548
H	0.5112596	-0.4388651	-4.7587609
H	-1.0269959	-0.5532774	-5.6717095
C	-0.9969513	2.2293998	-6.1118700
H	-2.4440991	2.3171268	-4.4435091
H	-0.8181895	2.9504041	-4.0434199
H	0.2918477	0.8102195	-7.2131633
H	1.0998754	1.6595162	-5.8725657
H	-1.8452632	1.9039375	-6.7315959
H	-0.7039880	3.2344708	-6.4407183
O	-4.5276654	0.6427676	-1.7350704
C	-5.6147396	0.0953939	-2.5449171
C	-4.9915311	1.8354804	-1.0341946
C	-6.7377342	1.1327127	-2.4937108
H	-5.2306980	-0.0870846	-3.5583957
H	-5.9243072	-0.8653313	-2.1023702
C	-6.5151731	1.7923779	-1.1219214
H	-4.6025876	1.7954639	-0.0077169
H	-4.5816638	2.7275009	-1.5376336
H	-7.7301380	0.6750785	-2.5937916
H	-6.6210587	1.8723904	-3.2994795
H	-6.9314679	1.1671451	-0.3184082
H	-6.9659583	2.7902263	-1.0473885
O	2.7787867	-2.8211945	-1.3858184
C	3.6866194	-2.8645055	-2.5307876
C	3.4146340	-3.4487680	-0.2321951
C	4.8539371	-3.7565433	-2.1051178
H	3.1304755	-3.2510005	-3.3963431
H	4.0162049	-1.8356671	-2.7491232
C	4.8979515	-3.5378569	-0.5830375
H	3.2014054	-2.8284426	0.6488975
H	2.9729451	-4.4483997	-0.0814101
H	5.7908681	-3.4806843	-2.6054930
H	4.6420772	-4.8109143	-2.3361466
H	5.4101514	-2.5950200	-0.3410620
H	5.4054565	-4.3501664	-0.0472593

4

63

C	2.5751730	-1.2039069	1.1354797	H	3.0311955	4.1066465	0.2388563
C	2.5884505	-0.5682554	-0.1274020	H	0.6439996	6.5863142	-1.5121036
C	2.4755514	0.8323303	0.0770174	H	1.5773134	6.3537802	-3.0077846
C	2.4240670	1.0705097	1.4856848	H	2.9528535	6.7142491	-0.6792265
C	2.4901587	-0.1876266	2.1342632	H	3.4767696	5.4044110	-1.7629884
Ti	0.4376172	-0.0683170	0.9096257	O	-2.3441568	3.3434151	1.2526888
H	2.6474090	-1.0676785	-1.0905790	C	-3.5778385	3.6033459	0.5144771
H	2.4459317	1.5946179	-0.6973731	C	-2.2523385	4.2593280	2.3920521
H	2.3650645	2.0379137	1.9760533	C	-4.4515693	4.4186107	1.4633638
H	2.4926863	-0.3475055	3.2079418	H	-3.3339443	4.1695917	-0.4003026
C	-1.7911561	-0.9290930	1.2647059	H	-4.0096971	2.6340325	0.2308752
C	-0.8445911	-1.9198695	1.6582936	C	-3.4058783	5.2499265	2.2262642
C	-0.1361049	-1.4078937	2.7806719	H	-2.3492281	3.6663708	3.3154416
C	-0.6248189	-0.0984255	3.0623433	H	-1.2607967	4.7327392	2.3751254
C	-1.6598596	0.1812800	2.1332285	H	-4.9987600	3.7563646	2.1500852
H	-0.7277399	-2.9107122	1.2287521	H	-5.1835014	5.0371985	0.9286299
H	0.6249483	-1.9396884	3.3425864	H	-3.7741436	5.6209047	3.1910300
H	-0.2886988	0.5528273	3.8645575	H	-3.0915326	6.1165053	1.6262233
H	-2.2246023	1.1082866	2.0704218	C	-0.2078214	-2.0141030	-1.6605904
H	2.6414322	-2.2735784	1.3159786	O	-0.1682738	-0.6229188	-1.1937011
H	-2.4833580	-1.0019890	0.4305041	C	-0.3441773	0.2831995	-2.3369187
O	-0.2762951	1.9025067	0.2364556	C	-0.8297116	-0.6025591	-3.4788507
H	0.3396160	2.6020697	-0.1255622	C	-0.1294152	-1.9382446	-3.1821630
H	-1.0404221	2.3951038	0.6501190	H	0.6285515	-2.5504853	-1.1942364
O	1.2758649	3.8510278	-0.8493743	H	-1.1554904	-2.4591242	-1.3196408
C	0.8512310	4.4986411	-2.0913649	H	-1.0478400	1.0633963	-2.0295596
C	2.2058690	4.7262880	-0.1367773	H	0.6318624	0.7439371	-2.5594332
C	1.3727414	5.9335819	-2.0149311	H	-1.9225435	-0.7209573	-3.4416556
H	1.2961020	3.9473868	-2.9355380	H	-0.5646644	-0.1894832	-4.4605528
H	-0.2436250	4.4305470	-2.1577900	H	-0.6172319	-2.7964905	-3.6611404
C	2.6388503	5.7769845	-1.1558642	H	0.9175393	-1.9099304	-3.5182370
H	1.6791159	5.1824556	0.7182337				

2b*THF

38

C	1.7765093	1.5601411	-0.8520794	H	-0.7790636	1.3676837	2.2672376
C	0.9597680	1.4124822	-2.0112873	H	2.8015203	1.2174082	-0.7460102
C	-0.3232870	1.9629412	-1.7259995	H	-2.7884548	0.2112345	0.8687195
C	-0.3061602	2.4267373	-0.3903960	O	1.5575994	-1.4025397	-1.1982462
C	0.9925038	2.1790550	0.1500781	H	0.9825131	-1.5569213	-1.9927846
Cl	-1.1063936	-1.1221134	-2.3186666	H	1.6455886	-2.3134854	-0.8002662
Ti	0.0131319	0.0223376	-0.3542046	O	1.7162140	-4.0307995	-0.4844998
H	1.2526032	0.9453942	-2.9464048	C	0.6753793	-4.7509234	-1.2125497
H	-1.1744107	1.9701946	-2.3994260	C	3.0048449	-4.6770867	-0.7175772
H	-1.1415513	2.8806135	0.1360109	C	1.4123334	-5.5368564	-2.2926782
H	1.3193474	2.4125956	1.1596146	H	0.1519532	-5.4218792	-0.5099968
C	-1.8327574	-0.2412640	1.1175507	H	-0.0372760	-4.0077384	-1.5976072
C	-1.4260749	-1.5666605	0.7978991	C	2.7165320	-5.9184742	-1.5707987
C	-0.1201108	-1.7668188	1.3052231	H	3.6548951	-3.9579997	-1.2413258
C	0.3022263	-0.5673857	1.9435555	H	3.4536663	-4.9144544	0.2577347
C	-0.7697613	0.3668257	1.8476372	H	1.6192538	-4.8936285	-3.1609123
H	-1.9977837	-2.2748441	0.2076707	H	0.8421300	-6.4086707	-2.6395161
H	0.4755764	-2.6691267	1.1920842	H	3.5398369	-6.1466178	-2.2603729
H	1.2541986	-0.4062194	2.4421850	H	2.5549264	-6.7990224	-0.9314689

5

37

C	1.9296934	1.3159059	-0.8687296	H	-1.2249711	1.4866887	1.9095863
C	1.2656318	1.0280311	-2.0878545	H	2.9359395	1.0053814	-0.6048700
C	-0.0541739	1.5416065	-2.0018695	H	-2.7762911	-0.3955744	0.7667066
C	-0.2161768	2.1350594	-0.7255161	O	1.5107904	-1.4167540	-0.7217494
C	1.0171469	1.9963913	-0.0219524	H	1.4391185	-2.3672719	-0.4407345
Cl	-1.4589586	-1.1586785	-1.8761544	O	1.3729051	-4.1419757	-0.3227923
Ti	0.1315360	-0.2419297	-0.3184020	C	0.4725154	-4.5906672	-1.3766334
H	1.6701252	0.4483184	-2.9111054	C	2.6862131	-4.7407929	-0.5339194
H	-0.8234550	1.4453867	-2.7599644	C	1.3822207	-4.9652351	-2.5419950
H	-1.1200096	2.6103875	-0.3556719	H	-0.0990474	-5.4639965	-1.0141977
H	1.2272601	2.3634606	0.9781182	H	-0.2190526	-3.7647547	-1.5923180
C	-1.7827856	-0.5437423	1.1779309	C	2.5853041	-5.5885287	-1.8121283
C	-1.0572558	-1.7750909	1.1765313	H	3.4129294	-3.9197907	-0.6374229
C	0.2044965	-1.5403964	1.7611292	H	2.9483966	-5.3353197	0.3544255
C	0.2912616	-0.1597344	2.0862556	H	1.6809374	-4.0599215	-3.0901189
C	-0.9625488	0.4439112	1.7601326	H	0.9024401	-5.6567608	-3.2474359
H	-1.4091453	-2.7151297	0.7653051	H	3.5103988	-5.5573262	-2.4027856
H	0.9965604	-2.2734671	1.8781596	H	2.3773294	-6.6401312	-1.5643425
H	1.1421673	0.3334939	2.5472988				

3a*THF

37

C	1.9253719	-0.0425903	-0.2165994	H	2.0022319	-1.1163661	-0.0684016
C	1.7235617	0.6106298	-1.4582111	H	-3.0451393	0.0458441	-0.7398385
C	1.6809642	2.0150169	-1.2055396	O	-1.1681831	2.4132798	-1.4214688
C	1.8612757	2.2243776	0.1953968	H	-0.8192891	3.0896279	-2.1474364
C	2.0113753	0.9516078	0.8020165	H	-2.1374309	2.4730641	-1.3957555
Ti	-0.1788228	1.0914241	-0.1429941	O	-0.3412008	4.0368055	-3.1628469
H	1.6303007	0.1260207	-2.4269576	C	-0.4776486	3.7434326	-4.6032466
H	1.5472719	2.7924500	-1.9536067	C	-0.4325907	5.4906273	-2.9416854
H	1.8959653	3.1836229	0.7057922	C	-0.8888356	5.0649487	-5.2463479
H	2.1669125	0.7674814	1.8615595	H	0.5007106	3.3909028	-4.9609613
C	-2.3346115	0.0714137	0.0841470	H	-1.2173796	2.9398853	-4.7180093
C	-1.3366735	-0.9085966	0.3400440	C	-0.2362055	6.1074352	-4.3212884
C	-0.6365245	-0.5079221	1.5158288	H	-1.4269842	5.7193312	-2.5262066
C	-1.1802354	0.7311214	1.9661738	H	0.3402410	5.7611637	-2.2114092
C	-2.2384900	1.0784433	1.0829738	H	-1.9828939	5.1762621	-5.2444517
H	-1.1719655	-1.8196782	-0.2286417	H	-0.5415215	5.1403144	-6.2842280
H	0.1615643	-1.0633857	1.9986653	H	-0.7032809	7.0970990	-4.3989439
H	-0.8741344	1.2858002	2.8489240	H	0.8341455	6.2151111	-4.5481263
H	-2.8607365	1.9675781	1.1645694				

Cp_2Ti

21

C	2.0609489	0.4205010	-0.0930967	C	-1.5364444	-1.0208505	0.1891920
C	1.6870953	0.7105244	-1.4303413	C	-0.5744174	-0.9938997	1.2312971
C	1.2057506	2.0597908	-1.4678128	C	-0.8049859	0.1745704	2.0229169
C	1.3153344	2.6040049	-0.1466623	C	-1.9100494	0.8727821	1.4720918
C	1.8315123	1.5888672	0.6989954	H	-1.6331312	-1.7916485	-0.5729004
Ti	-0.2641205	0.8941600	-0.1740632	H	0.1955293	-1.7404727	1.4068751
H	1.7562710	0.0295210	-2.2763418	H	-0.2403641	0.4687840	2.9036394
H	0.8697671	2.5951961	-2.3549145	H	-2.3407621	1.7950853	1.8569582
H	1.0520557	3.6158990	0.1550455	H	2.4661372	-0.5221982	0.2649013
H	2.0323444	1.6868468	1.7625330	H	-3.2095469	0.4037052	-0.3072483
C	-2.3584923	0.1454674	0.3216506				

6

36

C	1.8634255	-0.0522667	-0.1483224	H	-2.8321366	2.1334338	0.8805960
C	1.8049400	0.5802572	-1.4265116	H	1.8712249	-1.1235095	0.0316908
C	1.8622850	1.9855981	-1.2291377	H	-2.9650529	0.2131846	-0.9858326
C	1.9180777	2.2268940	0.1693599	O	-0.9272852	2.3404880	-1.3920999
C	1.9332383	0.9664250	0.8390376	H	-0.5373502	2.9897237	-2.0821275
Ti	-0.1721520	1.1714232	-0.2445801	O	0.0055225	3.9986404	-3.1605206
H	1.7384251	0.0735366	-2.3874138	C	-0.3691461	3.7063484	-4.5536247
H	1.8099301	2.7427250	-2.0071873	C	-0.2342563	5.4232925	-2.8828853
H	1.9533941	3.2041455	0.6471097	C	-1.1216824	4.9394188	-5.0456215
H	2.0043003	0.8171576	1.9126732	H	0.5589286	3.5350335	-5.1202104
C	-2.3376523	0.1952142	-0.0991205	H	-0.9692918	2.7863756	-4.5546969
C	-1.3883310	-0.8218033	0.2426357	C	-0.4540131	6.0716913	-4.2464743
C	-0.7742513	-0.4530790	1.4693527	H	-1.1257486	5.5047287	-2.2406558
C	-1.2745787	0.8232482	1.8416723	H	0.6403521	5.8074983	-2.3418641
C	-2.2678614	1.2051007	0.8825939	H	-2.1906768	4.8675909	-4.7974706
H	-1.2122143	-1.7434095	-0.3081796	H	-1.0311836	5.0717869	-6.1310921
H	-0.0241492	-1.0263950	2.0058296	H	-1.0771348	6.9722840	-4.1787317
H	-0.9959547	1.3838463	2.7315394	H	0.5066061	6.3538679	-4.7010710

3b*3THF

66

C	1.5525692	1.2783568	0.3375971	C	-0.1418381	-6.0523587	-3.1726275
C	1.6984548	1.1973478	-1.0673857	H	1.5368642	-4.7600699	-2.6331018
C	0.5866061	1.8477815	-1.6696651	H	0.3810310	-5.0214367	-1.2858923
C	-0.2429580	2.3574761	-0.6254664	H	0.3381619	-5.2421928	-5.1406510
C	0.3567559	2.0040003	0.6107003	H	-1.3131937	-5.8939242	-5.0407625
Ti	-0.3350619	-0.0040103	-0.5116614	H	0.5625586	-6.8800424	-3.3239741
H	2.5275868	0.7288974	-1.5932552	H	-1.0300413	-6.4473182	-2.6583262
H	0.3927539	1.9295263	-2.7357915	O	-1.3500403	1.3934331	-4.4495020
H	-1.1598590	2.9257929	-0.7525232	C	-0.8178547	0.7127391	-5.6226825
H	-0.0237251	2.2502306	1.5976319	C	-1.9901365	2.6444014	-4.8600202
C	-2.2368836	-1.0994447	0.5175624	C	-0.6962839	1.7948499	-6.6909788
C	-1.2960206	-2.0833853	0.1145522	H	0.1363735	0.2532439	-5.3330434
C	-0.1043931	-1.8997943	0.8816954	H	-1.5207940	-0.0807786	-5.9311125
C	-0.3203396	-0.7952771	1.7466859	C	-1.9229087	2.6736035	-6.3901390
C	-1.6334030	-0.2918611	1.5109726	H	-3.0182204	2.6546034	-4.4706060
H	-1.4499810	-2.8327690	-0.6573747	H	-1.4283626	3.4753631	-4.4054187
H	0.7927520	-2.5116065	0.8404120	H	-0.7043931	1.3832029	-7.7083998
H	0.3880377	-0.4063837	2.4719303	H	0.2347030	2.3652917	-6.5581119
H	-2.0952641	0.5498019	2.0197486	H	-2.8285296	2.2287946	-6.8278991
H	2.2407097	0.8757498	1.0756648	H	-1.8249534	3.6945331	-6.7801640
H	-3.2303907	-0.9566911	0.1001311	O	-4.4996869	0.4320595	-1.6393459
O	0.5384020	-1.2567315	-2.1563508	C	-5.4953768	-0.3643340	-2.3576662
H	0.1862152	-2.1793533	-2.3665633	C	-5.1556581	1.5579560	-0.9809730
H	1.5050644	-1.3409000	-2.1242953	C	-6.7976557	0.4351189	-2.2908592
O	-1.8433534	0.1066124	-2.0930187	H	-5.1314252	-0.5282420	-3.3815966
H	-1.6384139	0.5808636	-2.9468192	H	-5.5851040	-1.3384166	-1.8505836
H	-2.8108458	0.2579339	-1.9004845	C	-6.6422552	1.2119715	-0.9721501
O	-0.2789011	-3.7158579	-2.7644342	H	-4.7161130	1.6644587	0.0199496
C	-1.0238483	-3.9877878	-3.9964679	H	-4.9563924	2.4761274	-1.5592238
C	0.4745843	-4.9077530	-2.3740847	H	-7.6829698	-0.2131268	-2.3047027
C	-0.5375312	-5.3526844	-4.4843245	H	-6.8717148	1.1302578	-3.1401184
H	-2.0964497	-3.9956970	-3.7473064	H	-6.8848154	0.5704853	-0.1123004
H	-0.8267836	-3.1699309	-4.7030715	H	-7.2781654	2.1050419	-0.9229372

7

65

C	1.7994491	0.7642167	-0.1006704	H	1.3891222	-4.2955790	-2.2307430
C	1.7878533	0.7633613	-1.5190910	H	0.2544617	-5.1786280	-1.1584359
C	0.8128010	1.6888879	-1.9484548	H	0.5739920	-4.5852638	-4.9627089
C	0.2551279	2.3153528	-0.7888007	H	-0.7343873	-5.7703155	-5.1935543
C	0.8715490	1.7590607	0.3472727	H	1.2644439	-6.3933408	-3.4428677
Ti	-0.3794786	-0.0519098	-0.7396817	H	-0.4151369	-6.6773821	-2.9315147
H	2.3567016	0.0953628	-2.1570354	O	-1.7903141	1.6225708	-4.2190581
H	0.5255574	1.8853053	-2.9769692	C	-1.2639640	0.7092082	-5.2320872
H	-0.5290007	3.0667418	-0.7838728	C	-1.9537944	2.9595820	-4.7937238
H	0.6701456	2.0263583	1.3802604	C	-0.6864290	1.6118853	-6.3176442
C	-2.2977233	-0.8354150	0.5563223	H	-0.5326104	0.0564065	-4.7369420
C	-1.6024756	-1.9828057	0.1059373	H	-2.0948898	0.0949263	-5.6182573
C	-0.3114841	-1.9729776	0.7012477	C	-1.6532410	2.8089139	-6.2867758
C	-0.2185685	-0.8231774	1.5305151	H	-2.9766121	3.3022971	-4.5848893
C	-1.4406941	-0.1045017	1.4236100	H	-1.2413022	3.6363866	-4.2957141
H	-1.9645802	-2.7272598	-0.5973239	H	-0.6507194	1.1175346	-7.2968616
H	0.4689902	-2.7138082	0.5516629	H	0.3345407	1.9284710	-6.0573085
H	0.6309836	-0.5515077	2.1486971	H	-2.5710799	2.5746775	-6.8454398
H	-1.6866037	0.8224361	1.9339450	H	-1.2198073	3.7216864	-6.7145165
H	2.4490698	0.1634853	0.5297479	O	-4.6471786	0.4128910	-1.4212433
H	-3.3048674	-0.5484085	0.2641501	C	-5.4337995	-0.4893946	-2.2685139
O	0.0086100	-1.2033628	-2.1305593	C	-5.4842541	1.5343148	-0.9919891
H	-0.2645786	-2.1604301	-2.1983183	C	-6.7735999	0.2125476	-2.4959075
O	-2.0349037	0.8592921	-1.6946632	H	-4.8698937	-0.6715335	-3.1938151
H	-1.9054570	1.1790004	-2.6430658	H	-5.5525672	-1.4405784	-1.7267364
H	-3.0070342	0.6235666	-1.5907175	C	-6.9188078	1.0748419	-1.2300614
O	-0.6362736	-3.8419341	-2.4861815	H	-5.2479200	1.7422087	0.0598917
C	-1.2073614	-4.1471894	-3.7956049	H	-5.2331771	2.4196322	-1.5995550
C	0.4164504	-4.8122777	-2.1816027	H	-7.5970585	-0.5012044	-2.6244658
C	-0.2388565	-5.1261469	-4.4558593	H	-6.7321598	0.8492253	-3.3917914
H	-2.2018686	-4.5990813	-3.6447329	H	-7.2759875	0.4690834	-0.3845439
H	-1.3245280	-3.2005590	-4.3410612	H	-7.6089307	1.9176152	-1.3631034
C	0.3019708	-5.9047056	-3.2448680				

B. Additional Results on Radical 4-exo Cyclizations via Template Catalysis Study (Chapter 6)

Cyclic Voltammetry:

Materials. THF was distilled over potassium under an atmosphere of argon. Tetrabutylammoniumhexafluorophosphate, Bu_4NPF_6, and Tetrabutylammoniumiodide, Bu_4NI, were commercially available from Aldrich and were stored in a glovebox under an atmosphere of argon and used as received.

Apparatus. All handling of chemicals and the cyclic voltammetric experiments were performed in a glovebox under an atmosphere of argon. The working electrode was a glassy carbon disk of diameter 1 mm. The electrode surface was polished using 0.25 µm diamond paste (Struers A/S), followed by cleaning in an ethanol bath. The counter electrode consisted of a platinum coil melted into glass, while a Ag/AgI electrode (silver wire immersed in a Pyrex tube containing 0.2 M Bu_4NPF_6 + 0.02 M Bu_4NI in THF) separated from the main solution by a ceramic frit served as the reference electrode. All potentials were reported against the Fc^+/Fc redox couple, the potential of which is equal to 0.52 V vs. SCE in 0.2 M Bu_4NPF_6/THF.[S1]

Procedure. In the cyclic voltammetric experiments 0.77 g of Bu_4NPF_6 (2.0 mmol) and a small magnetic bar were added to the electrochemical cell. 9 mL of freshly distilled THF and 1 mL of the appropriate standard solution (20 mM; 0.1 mmol complex / 5 mL THF 0.2 mmol Mn/Zn) containing the compound of interest were added to the cell and the solution was stirred for 30 s. At the end of each series of experiments a small amount of ferrocene was added and the potential of the Fc^+/Fc redox couple was measured.

Additional Cyclovoltammogramms:

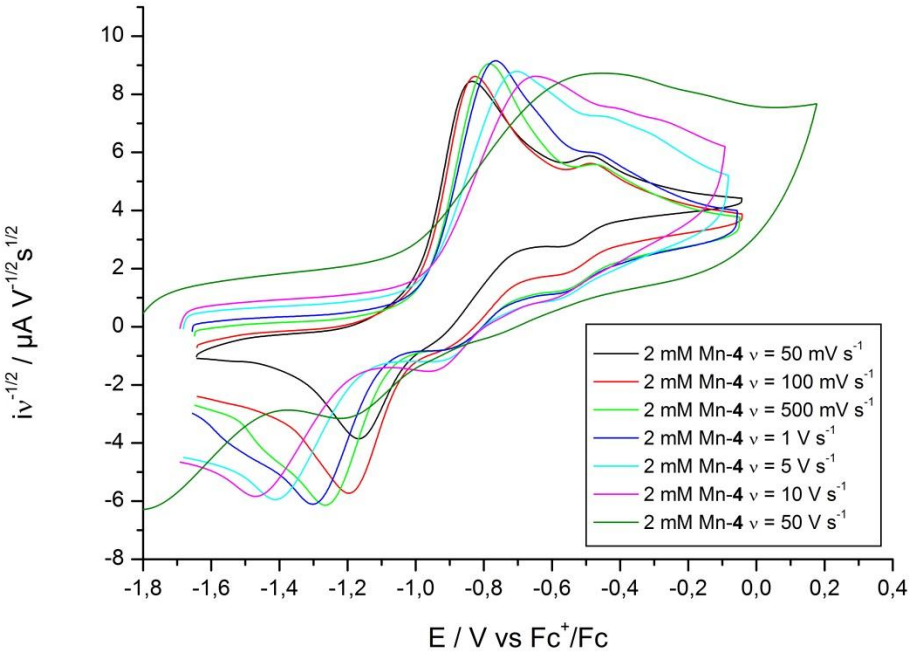

Figure B.1. CV of Mn-reduced **4** recorded in 0.2 M $TBAPF_6$/THF.

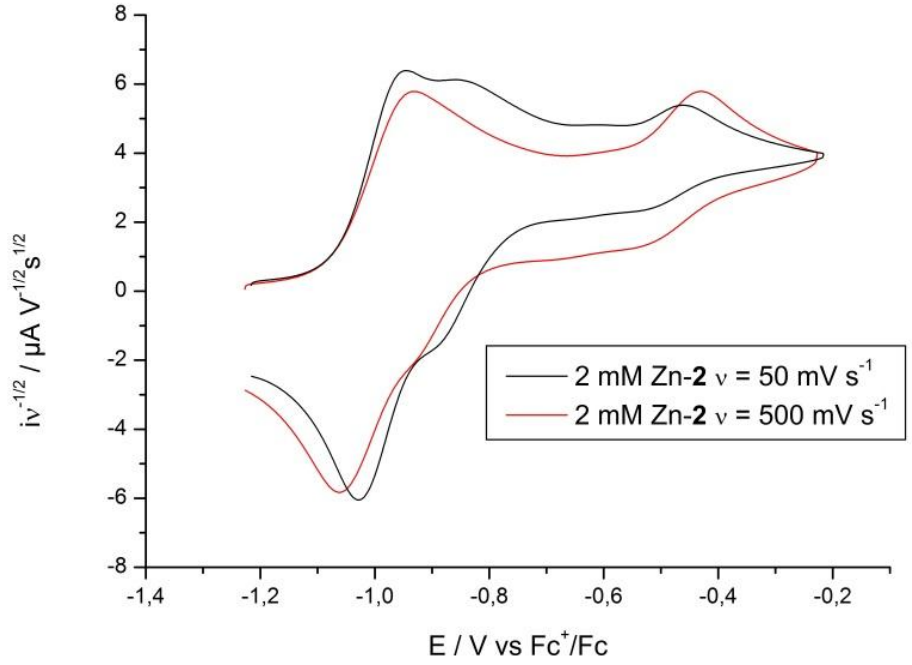

Figure B.2. CV of Zn-reduced **2** recorded at ν = 50 and 500 mV s^{-1} in 0.2 M $TBAPF_6$/THF.

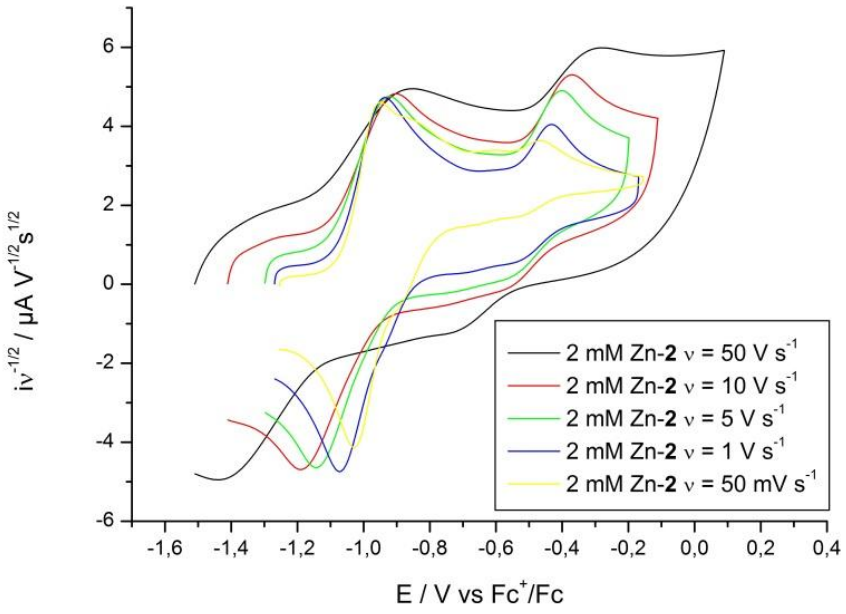

Figure B.3. CV of Zn-reduced **2** recorded in 0.2 M $TBAPF_6$/THF.

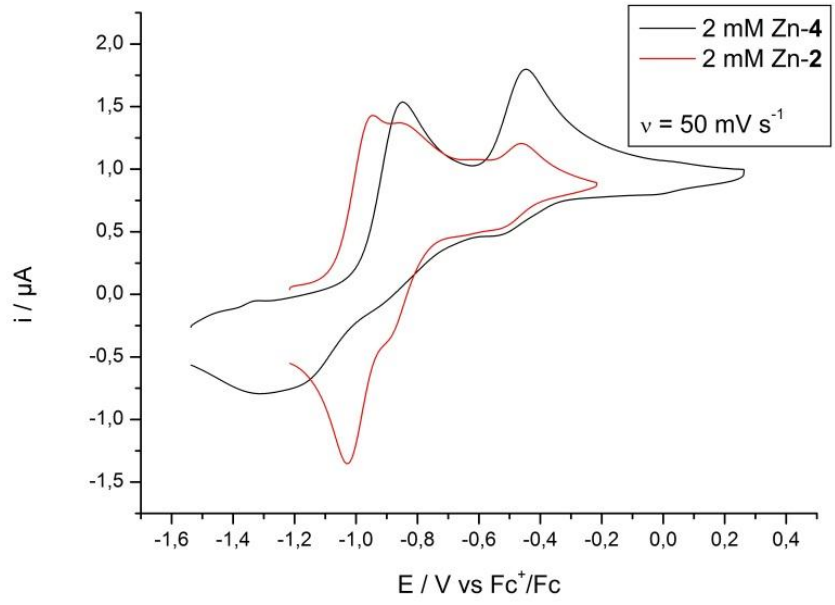

Figure B.4. CV of Zn-reduced **2** and **4** recorded at ν = 50 mV s^{-1} in 0.2 M $TBAPF_6$/THF.

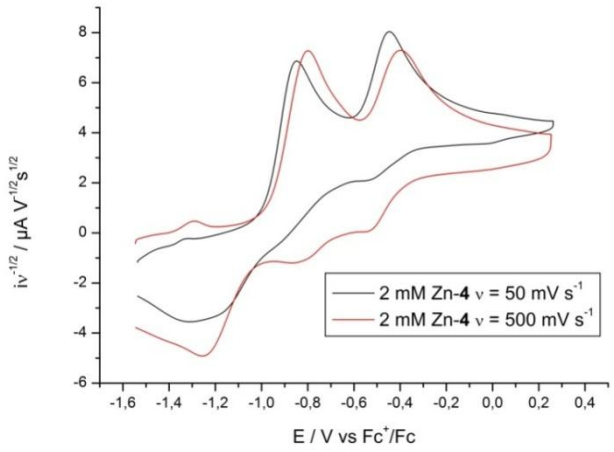

Figure B.5. CV of Zn-reduced **4** recorded at ν = 50 and 500 mV s^{-1} in 0.2 M $TBAPF_6$/THF.

Computational Details:

The geometry optimizations were carried out within the framework of DFT with the BP86/TZVP method (Becke-Perdew gradient corrected exchange and correlation density functional[S2] combined with a polarized split-valence basis set of triple-zeta quality[S3]) using the RI-approximation (resolution of identity) within the TURBOMOLE program package.[S4] The stationary points on the potential energy surface were characterized by analyzing the Hessian matrix.[S5] The energies were corrected for the zero point vibrational energy (ZPVE).[S5] Solvation effects were estimated by single point calculations at the gas phase structure using the COSMO model.[S6]

[S1] a) R. J. Enemærke, J. Larsen, T. Skrydstrup, K. Daasbjerg, *J. Am. Chem. Soc.* **2004**, *126*, 7853-7864; b) K. Daasbjerg, H. Svith, S. Grimme, M. Gerenkamp, C. Mück-Lichtenfeld, A. Gansäuer, A. Barchuk, F. Keller, *Angew. Chem.* **2006**, *118*, 2095-2098; *Angew. Chem. Int. Ed.* **2006**, *45*, 2041-2044.

[S2] a) A. D. Becke, *Phys. Rev. A* **1988**, *38*, 3098-3100. b) J. P. Perdew, *Phys. Rev. B,* **1986**, *33*, 8822-8824.

[S3] a) K. Eichkorn, F. Weigend, O. Treutler, R. Ahlrichs, *Theor. Chem. Acc.* **1997**, *97*, 119-124. b) A. Schäfer, C. Huber, R. Ahlrichs, *J. Chem. Phys*. **1994**, *100*, 5829-5835.

[S4] a) R. Ahlrichs, M. Bär, H.-P. Baron, R. Bauernschmitt, S. Böcker, M. Ehrig, K. Eichkorn, S. Elliott, F. Furche, F. Haase, M Häser, H. Horn, C. Huber, U. Huniar, C. Kölmel, M. Kollwitz, C. Ochsenfeld, H. Öhm, A. Schäfer, U. Schneider, O. Treutler, M. von Arnim, F. Weigand, P. Weis, H. Weiss, *Turbomole 5*, Institut für Physikal. Chemie, Universität Karlsruhe, **2002**. b) M. Häser, R. Ahlrichs, *J. Comput. Chem.* **1989**, *10*, 104-111. c) O. Treutler, R. Ahlrichs, *J. Chem. Phys.* **1995**, *102*, 346-354.

[S5] P. Deglmann, F. Furche, R. Ahlrichs, *Chem. Phys. Lett*. **2002**, *362*, 511-518.

[S6] A. Klamt, G. Schüürmann, *J. Chem. Soc., Perkin Trans. 2* **1993**, 799-805.

Optimized geometries:

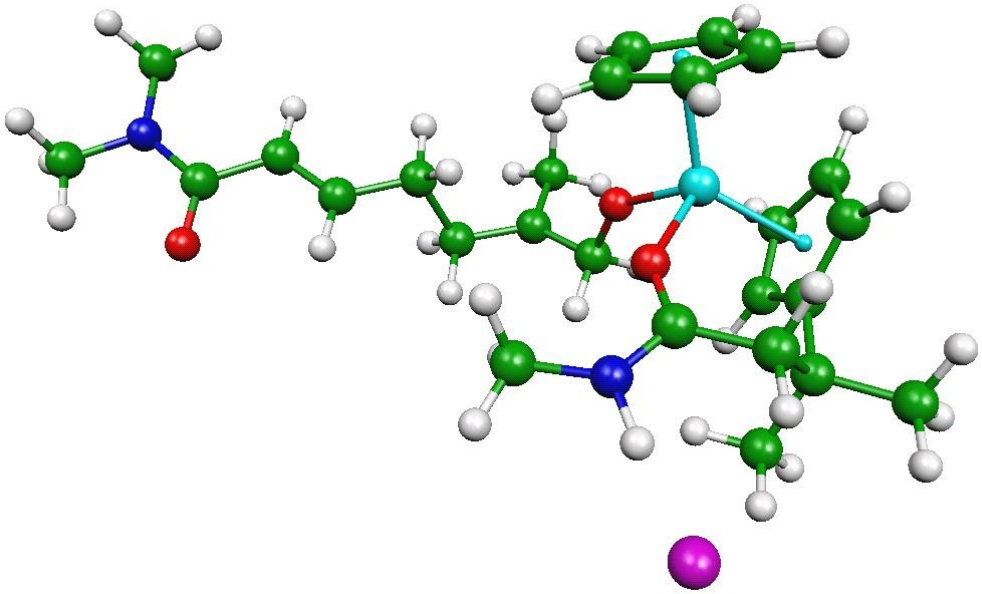

12

71

Ti	1.4146833	-1.5773547	0.4864667	C	1.3844863	0.3392010	-1.9726742
C	2.9871820	-3.3108620	-0.0091687	H	1.6154831	3.8487942	-0.2645110
C	1.7758497	-3.9669107	0.3520405	H	0.4039043	2.6010067	0.0940594
C	2.7552071	-2.6072175	-1.2155810	C	-0.4223339	4.4821519	-0.4914346
H	3.9249634	-3.3555513	0.5353286	H	3.6638888	2.1978411	-1.1494618
C	0.8013312	-3.7139647	-0.6585429	H	3.4271468	3.0716958	-2.6710784
H	1.6362111	-4.6023866	1.2220028	H	3.8354401	1.3329559	-2.6806546
C	1.4085206	-2.8472138	-1.6074208	H	2.0217647	-0.3167691	-2.5963891
H	3.4752393	-1.9852142	-1.7411356	H	0.3348380	0.1915207	-2.2849899
H	0.9219241	-2.4420286	-2.4890359	O	1.4961580	-0.0708455	-0.5967278
C	3.1735776	-1.0996983	2.1021217	H	-1.4497370	4.1782188	-0.7232679
C	2.3320292	-2.0748422	2.7229229	C	-0.2242128	5.7730342	-0.1774592
C	2.4302665	0.1039414	1.9854946	H	0.7869973	6.1211549	0.0414889
H	4.2154675	-1.2332216	1.8248301	C	-1.3743248	6.7287201	-0.1698910
C	1.0663865	-1.4872008	2.9262548	O	-2.4911034	6.3881732	-0.5828579
H	2.6150342	-3.0907017	2.9808127	N	-1.1423833	8.0098690	0.3025969
C	1.1254825	-0.1365664	2.4636116	C	0.1110296	8.5058104	0.8564231
H	2.7768246	1.0188046	1.5168614	H	0.6904327	9.0853216	0.1157979
H	0.1926966	-1.9764090	3.3476042	H	-0.1114715	9.1699511	1.7054644
H	0.2972503	0.5650315	2.4472407	H	0.7328995	7.6897795	1.2354874
C	-0.5943906	-4.3084459	-0.7079254	C	-2.2124918	8.9956198	0.1997160
C	-1.3954474	-3.8781225	0.5549694	H	-1.8916553	9.8490813	-0.4205824
H	-2.3797926	-4.3762937	0.5536381	H	-3.0812508	8.5131056	-0.2588312
H	-0.8458249	-4.1738897	1.4635006	H	-2.4875259	9.3738843	1.1977475
C	-1.6056185	-2.3910918	0.5797938	C	-0.4848092	-5.8510957	-0.6948844
O	-0.5962960	-1.5780557	0.5940584	H	-0.0013226	-6.2173553	0.2223073
N	-2.8371955	-1.9402614	0.5514738	H	-1.4907376	-6.2904730	-0.7509393
C	-3.1800018	-0.5265876	0.5077234	H	0.0997645	-6.2064100	-1.5557932
H	-2.9826028	-0.0405915	1.4748190	C	-1.3623841	-3.8752447	-1.9708315
H	-2.6045330	0.0011477	-0.2657677	H	-2.3973336	-4.2434423	-1.9174669
H	1.0278753	3.6903017	-2.7041097	H	-1.4119197	-2.7807077	-2.0683778
C	0.7707646	2.8550476	-2.0304420	H	-0.8864786	-4.2782019	-2.8769094
C	1.7878105	1.7662661	-2.1522206	H	-4.2502530	-0.4521413	0.2840335
H	-0.2208400	2.4854177	-2.3390258	H	-3.6478602	-2.6941551	0.4055968
C	0.6437522	3.4388294	-0.5813800	Cl	-4.8107899	-4.0192927	-0.0097636
C	3.2418762	2.1085847	-2.1708953				

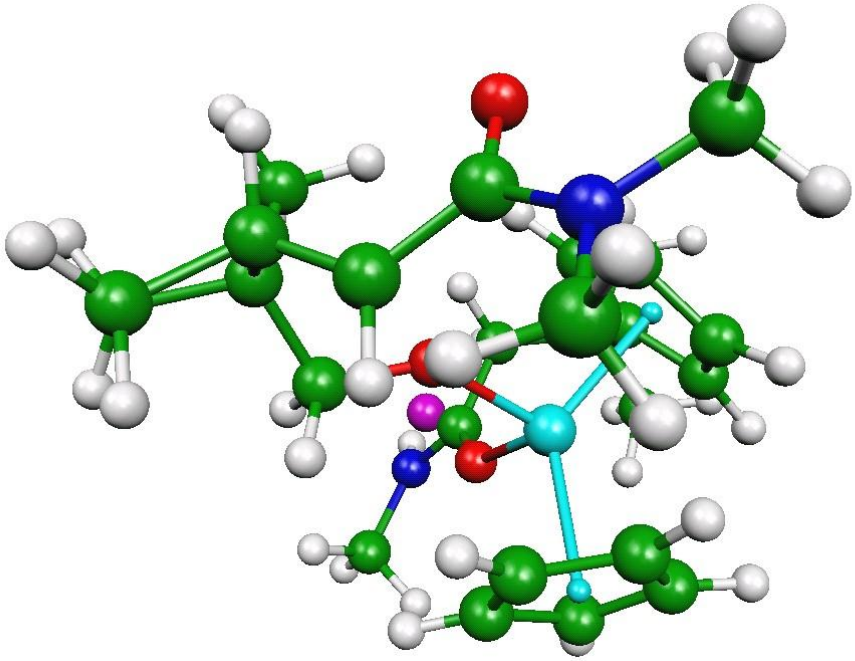

12P*cis*

71

C	0.5506206	1.9816353	-2.7501035
C	0.5511562	3.5508982	-2.3528564
Ti	-0.6454764	-0.1759185	0.7694361
C	0.5304147	0.3692596	2.7941732
C	0.3993505	-1.0502133	2.7851115
C	1.3788277	0.7415808	1.7180055
H	0.0857310	1.0423573	3.5208716
C	1.1704480	-1.5658622	1.7061144
H	-0.1778485	-1.6433999	3.4877471
C	1.7583706	-0.4442015	1.0457020
H	1.6523562	1.7504717	1.4134829
H	2.3677992	-0.4804696	0.1480582
C	-2.2561747	1.2335755	1.9076671
C	-2.5117563	-0.0923201	2.3695240
C	-2.5936041	1.2834334	0.5293516
H	-1.9107639	2.0693464	2.5082803
C	-2.9592393	-0.8566068	1.2702805
H	-2.3773710	-0.4508475	3.3853158
C	-3.0072476	-0.0072288	0.1274045
H	-2.4985244	2.1546868	-0.1119002
H	-3.1907401	-1.9172248	1.2836091
H	-3.2766466	-0.3115714	-0.8793705
C	1.4008969	-3.0191194	1.3427904
C	1.2113965	-3.2136730	-0.1822324
H	1.8860957	-2.5375120	-0.7322878
H	1.4733844	-4.2467361	-0.4700847
C	-0.1952428	-2.9449257	-0.6434227
O	-0.8604997	-1.8892275	-0.2799457
N	-0.7469148	-3.8322763	-1.4365091
C	-2.0982691	-3.7180273	-1.9605966
H	-2.3290778	-4.6540218	-2.4821209
H	-2.8312958	-3.5595747	-1.1562481
H	0.7944538	2.3915699	-4.9144083
C	0.0028022	2.3958555	-4.1528003
H	-0.8450740	1.8079081	-4.5348124
C	-0.3180051	3.8131889	-3.6190047
C	1.9266110	1.3345898	-2.7152872
C	-0.4903450	1.1415001	-2.0018784
H	-1.3816277	3.9343469	-3.3649166
H	-0.0146205	4.6662221	-4.2403890
H	2.3135861	1.3090094	-1.6882220
H	2.6384243	1.9003300	-3.3338061
H	1.8849218	0.3032377	-3.1026532
H	-0.6505877	0.2087175	-2.5807809
H	-1.4639438	1.6719956	-1.9797013
O	-0.0693099	0.7987808	-0.7055120
C	0.0407223	4.0262059	-1.0608336
H	-1.0415797	4.0988235	-0.9296515
C	0.9342196	4.2995744	0.0627411
O	2.0728667	3.7865462	0.1064669
N	0.4723089	5.1075532	1.0955443
C	-0.7577729	5.8838986	1.0576306
H	-1.5170550	5.4872272	1.7542920
H	-0.5454582	6.9255366	1.3488703
H	-1.1755070	5.9023785	0.0462185
C	1.3104491	5.3046685	2.2697820
H	0.7731714	5.0080851	3.1862811
H	2.2131977	4.6957121	2.1569263
H	1.5989594	6.3645126	2.3681426
C	0.4590562	-3.9698199	2.1048855
H	-0.5990318	-3.7140049	1.9456341
H	0.6085021	-4.9999667	1.7523353
H	0.6589187	-3.9435413	3.1861675
C	2.8662370	-3.3800714	1.6881088
H	3.0618543	-4.4305092	1.4288007
H	3.5754123	-2.7497281	1.1330053
H	3.0564547	-3.2437199	2.7625305
H	-2.1787564	-2.8804300	-2.6697171
H	1.5872390	3.8964917	-2.4839891
H	-0.2075405	-4.8072453	-1.5806427
Cl	0.6305100	-6.3862740	-1.5681144

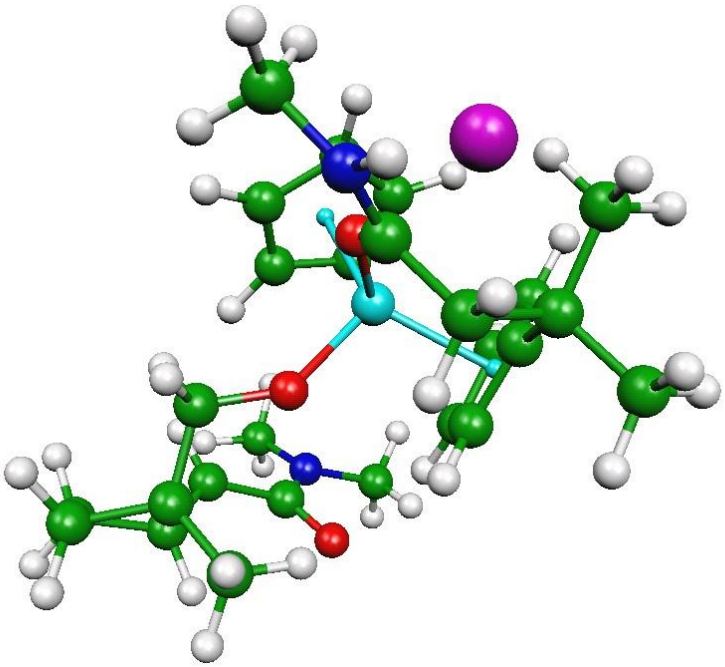

12TS*cis*

71

C	0.6531683	1.8808920	-2.8342022
C	0.5439484	3.9060881	-2.2730374
Ti	-0.5464035	-0.2054008	0.7086390
C	0.7138120	0.3115962	2.6920586
C	0.5457496	-1.1019876	2.6950332
C	1.5231613	0.6618107	1.5779302
H	0.3140179	0.9987953	3.4310953
C	1.2713038	-1.6423534	1.5940621
H	-0.0208970	-1.6771975	3.4212289
C	1.8580289	-0.5399330	0.9061292
H	1.7949623	1.6689438	1.2609910
H	2.4315897	-0.5994964	-0.0136041
C	-1.9755468	1.3688164	1.8652969
C	-2.3441786	0.0784145	2.3527991
C	-2.3363089	1.4330899	0.4955741
H	-1.5312205	2.1750565	2.4401324
C	-2.9006865	-0.6485301	1.2777476
H	-2.2156421	-0.2817420	3.3690167
C	-2.8891167	0.1831834	0.1232963
H	-2.1627197	2.2829825	-0.1582050
H	-3.2305133	-1.6820108	1.3117268
H	-3.2162339	-0.1058942	-0.8709608
C	1.4547859	-3.1020780	1.2295097
C	1.1143289	-3.3111333	-0.2692621
H	1.7220243	-2.6311550	-0.8881055
H	1.3521092	-4.3455187	-0.5719057
C	-0.3358974	-3.0553554	-0.5732254
O	-0.9493747	-1.9776105	-0.1856358
N	-0.9836219	-3.9791886	-1.2429969
C	-2.3914151	-3.8836733	-1.5935411
H	-3.0205435	-3.7430752	-0.7021624
H	-2.5734654	-3.0428153	-2.2790624
H	1.0210150	2.5943340	-4.8525644
C	0.1872539	2.5244987	-4.1393683
H	-0.6298780	1.9784893	-4.6391346
C	-0.2192278	3.9090541	-3.5926675
C	2.0694035	1.4161372	-2.7015961
C	-0.3942386	1.0711696	-2.1112321
H	-1.3018016	3.9612575	-3.4016565
H	0.0400061	4.7569442	-4.2462502
H	2.3643890	1.3582358	-1.6461371
H	2.7650091	2.0845213	-3.2278199
H	2.1876557	0.4052950	-3.1401682
H	-0.6283614	0.1866026	-2.7501818
H	-1.3383980	1.6483888	-2.0385396
O	0.0337615	0.6110051	-0.8603507
H	1.6325000	3.9990379	-2.3301300
C	-0.0356607	4.2831743	-1.0733830
H	-1.1181971	4.4282387	-1.0390301
C	0.7584041	4.4037082	0.1611303
O	1.8591224	3.8314508	0.2875902
N	0.2261280	5.1563563	1.2030754
C	-0.9085071	6.0615913	1.0846014
H	-1.7521883	5.7407116	1.7196621
H	-0.6122852	7.0750892	1.4038609
H	-1.2482905	6.1283841	0.0471398
C	0.9599246	5.2411678	2.4582510
H	0.2903703	5.0295623	3.3080713
H	1.7779121	4.5143872	2.4336085
H	1.3853994	6.2496692	2.5996777
C	0.5829672	-4.0345778	2.0907434
H	-0.4832268	-3.7695134	2.0334928
H	0.6869230	-5.0698554	1.7365592
H	0.8886092	-3.9975662	3.1467229
C	2.9427751	-3.4755727	1.4341243
H	3.0994179	-4.5326806	1.1756997
H	3.6010744	-2.8644202	0.8004429
H	3.2401935	-3.3236185	2.4818050
H	-2.6721585	-4.8208036	-2.0877453
H	-0.4635666	-4.9584288	-1.4129530
Cl	0.3894101	-6.5343038	-1.4549300

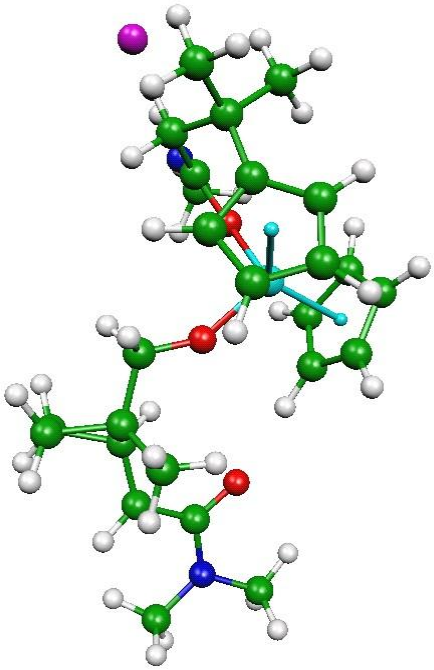

12P*trans*

71

Ti	-0.0015273	-0.6061603	1.2304497	C	1.6494377	1.0182116	-0.8315479
C	1.4651761	-1.1711392	3.0360385	H	1.0698713	2.0948806	-3.6454845
C	0.8406966	-2.3903182	2.6340751	H	1.4005491	3.8345161	-3.8086225
C	2.2839729	-0.7313164	1.9689041	C	0.6214934	3.1974478	-1.7718036
H	1.3471775	-0.6777781	3.9956857	H	1.6205291	3.0589430	1.0724231
C	1.2906331	-2.7206545	1.3272842	H	2.5472135	4.2526358	0.1340908
H	0.1590249	-2.9842012	3.2349767	H	3.3086512	2.7162120	0.6021566
C	2.1649742	-1.6731520	0.9133160	H	2.6186611	0.5742091	-0.5200180
H	2.8707979	0.1833285	1.9492452	H	1.3874328	0.5631125	-1.8062945
H	2.6638828	-1.6091465	-0.0493324	O	0.6322767	0.7150664	0.0837773
C	-0.9292947	0.8356933	2.9469631	H	-0.2944205	2.6088557	-1.6250990
C	-1.4583546	-0.4687985	3.1982905	C	0.3613728	4.6120704	-1.4589594
C	-1.4873836	1.3107593	1.7295024	H	1.0504270	5.3621765	-1.8522863
H	-0.2596745	1.3907191	3.5990619	C	-0.7068275	5.0047938	-0.5465430
C	-2.2799696	-0.8191991	2.1057117	O	-1.3076947	4.1520182	0.1441165
H	-1.2552038	-1.0849703	4.0687426	N	-1.0257124	6.3535919	-0.4471856
C	-2.2948833	0.2846698	1.1980514	C	-0.4128690	7.4134089	-1.2361059
H	-1.2685441	2.2580797	1.2400713	H	-1.1635395	8.1949082	-1.4245468
H	-2.7965902	-1.7652395	1.9701056	H	0.4419090	7.8830217	-0.7168491
H	-2.8040482	0.3116745	0.2398293	H	-0.0790316	7.0382047	-2.2093394
C	0.9690598	-3.9643725	0.5225821	C	-1.9702189	6.7802821	0.5761654
C	0.6006761	-3.5683010	-0.9276724	H	-2.7987156	7.3469112	0.1218117
H	1.4270564	-2.9979065	-1.3829881	H	-2.3654591	5.8884100	1.0725365
H	0.4489030	-4.4714370	-1.5454018	H	-1.4756463	7.4259701	1.3222793
C	-0.6485206	-2.7312432	-1.0091020	C	-0.1818840	-4.7788790	1.1420778
O	-0.8605619	-1.7179132	-0.2294408	H	-1.0925467	-4.1740784	1.2633597
N	-1.5395564	-3.0726589	-1.9107122	H	-0.4296074	-5.6250276	0.4861116
C	-2.7967531	-2.3675419	-2.1065851	H	0.0990295	-5.1781723	2.1277480
H	-3.3897490	-2.3387044	-1.1805402	C	2.2380898	-4.8493085	0.4679675
H	-2.6229209	-1.3327341	-2.4356282	H	2.0324976	-5.7571453	-0.1171353
H	3.3366683	3.6588535	-2.2384070	H	3.0772432	-4.3185446	-0.0042127
C	2.7182257	2.7527084	-2.3107922	H	2.5481572	-5.1481082	1.4798370
C	1.8795797	2.5274817	-1.0162231	H	-3.3596360	-2.9046120	-2.8784559
H	3.3642996	1.9209323	-2.6308256	H	-1.3884373	-4.0445891	-2.4406976
C	1.4104083	2.9891870	-3.1073534	Cl	-1.1160427	-5.7144325	-3.0712422
C	2.3633957	3.1775177	0.2710432				

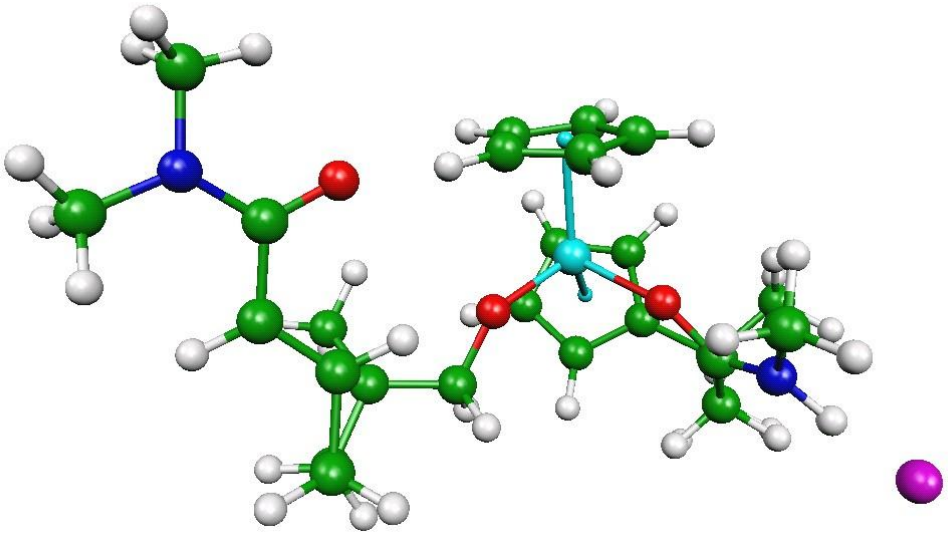

12TS*trans*

71

C	2.1768069	2.4433386	-0.6651398	C	2.3757682	3.1175471	0.6531290
C	0.7579106	3.4291825	-1.8984188	C	1.7856089	0.9851216	-0.6413636
Ti	-0.1107831	-0.6372397	1.2048842	H	1.6688823	2.2916213	-3.5185630
C	1.1364664	-1.2473475	3.1528338	H	2.1255164	4.0038527	-3.5332764
C	0.5281434	-2.4478317	2.6752465	H	1.5524494	2.8876446	1.3426970
C	2.0807613	-0.8264215	2.1866492	H	2.4423614	4.2086046	0.5397112
H	0.9264731	-0.7549909	4.0971155	H	3.3209986	2.7788190	1.1242581
C	1.1106511	-2.7843687	1.4239256	H	2.6864567	0.4165030	-0.3035419
H	-0.2316563	-3.0251858	3.1926413	H	1.5809920	0.6351140	-1.6719003
C	2.0539750	-1.7595639	1.1174911	O	0.6762875	0.6912546	0.1605630
H	2.6918515	0.0708085	2.2397306	H	-0.0229033	2.6764179	-1.7576031
H	2.6603859	-1.7075875	0.2177165	C	0.4477545	4.7193897	-1.5111338
C	-1.1949783	0.8245470	2.8071535	H	1.1165454	5.5299847	-1.8069372
C	-1.7607937	-0.4734378	3.0069880	C	-0.7017634	5.0003284	-0.6369112
C	-1.6190209	1.2999568	1.5367596	O	-1.3324847	4.0843256	-0.0703496
H	-0.5906644	1.3750767	3.5238462	N	-1.0665337	6.3269857	-0.4534815
C	-2.4681800	-0.8209953	1.8360146	C	-0.4423952	7.4635395	-1.1177906
H	-1.6573097	-1.0865141	3.8969451	H	-1.2038365	8.2400380	-1.2821324
C	-2.3779238	0.2795077	0.9287191	H	0.3705680	7.9091271	-0.5163662
H	-1.3436378	2.2427287	1.0664072	H	-0.0471920	7.1799960	-2.0990026
H	-2.9789597	-1.7619252	1.6512721	C	-2.1069535	6.6461762	0.5148507
H	-2.7849995	0.3086426	-0.0770310	H	-2.9361907	7.1860532	0.0292800
C	0.8476475	-4.0143621	0.5780939	H	-2.4824300	5.7082829	0.9360302
C	0.6599171	-3.6006982	-0.9013884	H	-1.7063632	7.2803286	1.3242361
H	1.5503580	-3.0550046	-1.2549931	C	-0.3896961	-4.7971184	1.0555291
H	0.5527780	-4.4956281	-1.5402504	H	-1.2905467	-4.1663980	1.0754710
C	-0.5449489	-2.7241762	-1.1201867	H	-0.5843122	-5.6334265	0.3697597
O	-0.8175290	-1.7111502	-0.3583467	H	-0.2356035	-5.2080896	2.0640906
N	-1.3314436	-3.0282811	-2.1259299	C	2.0886065	-4.9361292	0.6620989
C	-2.5337620	-2.2812794	-2.4619241	H	1.9258406	-5.8343188	0.0493089
H	-3.2373182	-2.2516595	-1.6168115	H	2.9914719	-4.4279347	0.2940702
H	-2.2909968	-1.2464138	-2.7434521	H	2.2714379	-5.2493702	1.7002290
H	3.6238725	3.7240269	-1.6437361	H	-3.0103266	-2.7866099	-3.3095884
C	3.0304952	2.8263899	-1.8707104	H	-1.1461979	-3.9994710	-2.6480425
H	3.7314142	2.0373366	-2.1956154	Cl	-0.8456667	-5.6673480	-3.2652594
C	1.9047619	3.1510222	-2.8751117				

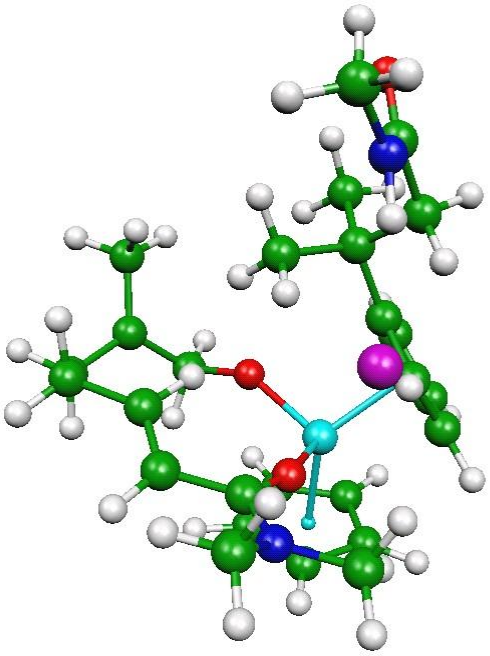

13

71

C	1.5627124	-2.6609022	2.4534368	H	1.0964324	2.1614060	3.4278331
C	0.7229197	0.1853816	2.7203153	C	0.7904577	2.1000518	1.2273896
Ti	1.7361634	-0.1536968	-0.9484954	O	1.0925109	1.3953882	0.2063288
C	3.6655350	1.3651021	-0.7992448	N	0.4647427	3.3956428	1.0718810
C	3.9491064	0.2205282	-0.0049934	H	4.2826293	-1.9174872	-0.5936193
C	3.5639299	0.9577161	-2.1473580	C	-1.9003309	-1.4779559	-0.9123353
H	3.5061984	2.3718618	-0.4260904	C	-3.1812673	-0.8269380	-1.5467488
C	4.0620208	-0.8936007	-0.8785125	H	-3.0156191	0.2524404	-1.6634350
H	4.0570908	0.2078871	1.0759219	H	-3.3473685	-1.2633642	-2.5434168
C	3.8077929	-0.4483429	-2.1967125	C	-4.4521477	-1.0448489	-0.7226870
H	3.3544017	1.5994950	-2.9974379	N	-4.8855170	0.0733582	-0.0792283
H	3.8453927	-1.0643425	-3.0888481	H	-4.2868590	0.9188536	-0.0912725
C	0.5431413	0.6914603	-2.8100912	C	-6.0523658	0.0682323	0.7842816
C	-0.5072455	0.5174849	-1.8743108	H	-6.7425252	0.8783249	0.5056812
C	1.0289260	-0.6043218	-3.1595172	H	-6.5574508	-0.8987416	0.6704718
H	0.8778552	1.6407422	-3.2186144	O	-5.0233771	-2.1457006	-0.6624054
C	-0.7174614	-0.8784772	-1.6642943	C	-0.2990592	4.1408966	2.0797741
H	-1.0833928	1.3105273	-1.3850559	H	0.0602691	5.1786406	2.1097164
C	0.2659440	-1.5611271	-2.4306114	H	-1.3618484	4.1042689	1.7811195
H	1.7700831	-0.8320501	-3.9180721	H	-0.1944059	3.6907489	3.0700576
H	0.4056367	-2.6378000	-2.4726901	C	0.3793644	3.9773999	-0.2713984
O	1.5377076	-1.5975293	0.2275391	H	1.0712479	3.4628018	-0.9436306
C	2.2575031	-2.4527067	1.1413052	H	-0.6588412	3.8586816	-0.6328138
H	2.3781686	-3.4254033	0.6283358	H	0.6418321	5.0419946	-0.2051155
H	3.2626562	-2.0359818	1.3321847	C	-1.9473004	-3.0061853	-1.0840278
C	0.4676362	-3.6687810	2.5771691	H	-2.8674519	-3.3960019	-0.6293371
H	0.5819334	-4.2713059	3.4956124	H	-1.9604132	-3.2904945	-2.1473770
H	-0.5326998	-3.2005477	2.6451233	H	-1.0788399	-3.4846415	-0.6051390
H	0.4373446	-4.3502703	1.7159383	C	-1.8425489	-1.1323283	0.5889307
C	1.9083738	-1.8099389	3.6412958	H	-1.8684027	-0.0441090	0.7509214
H	1.9584668	-2.4398036	4.5471611	H	-2.7059062	-1.5755891	1.1060791
H	2.9051863	-1.3603078	3.5036802	H	-0.9278767	-1.5547235	1.0224349
C	0.8925851	-0.6528163	3.9372057	H	0.4783549	-0.3747065	1.8170350
H	-0.0778289	-1.1061297	4.2039287	H	-5.7690429	0.2033373	1.8407617
H	1.2319313	-0.0681728	4.8056663	Cl	-2.7245810	2.5639404	0.0564138
C	0.8775632	1.5105209	2.5790615				

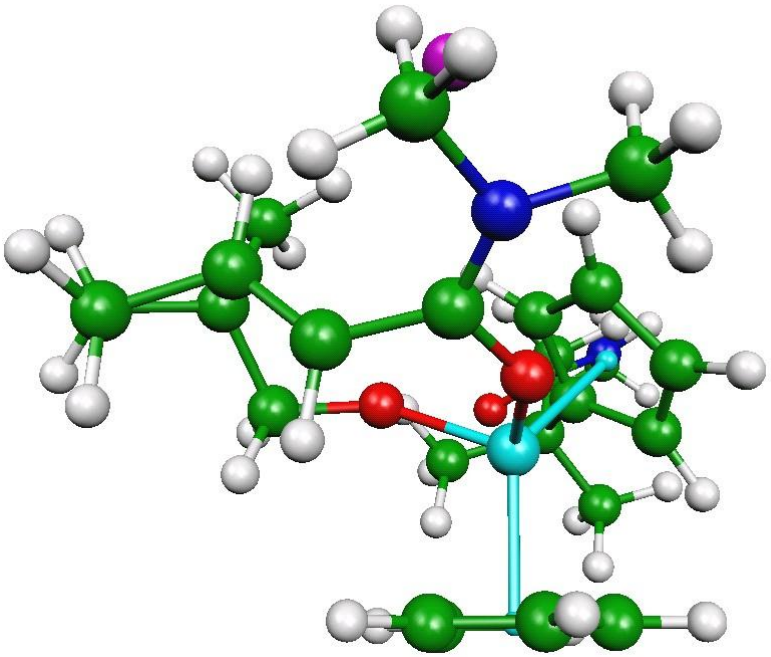

13T

71

C	1.9413798	1.8127818	2.1756949	H	3.5258834	-0.9421099	1.3118780
C	3.6886477	1.1816464	1.2181861	C	3.1849563	-0.3944875	-0.7291958
Ti	0.2949359	-1.2504758	-0.0317960	O	2.1339827	-1.1264801	-0.9282061
C	1.3629340	-3.4776415	0.3023647	N	3.9570372	-0.0830633	-1.7802896
C	1.3151523	-2.8588297	1.5784189	H	-0.4189466	-2.2230015	2.8414625
C	0.0372969	-3.6680351	-0.1492932	C	-3.2794379	-0.2138790	0.1632105
H	2.2628383	-3.7044891	-0.2606726	C	-4.0179210	1.0279463	-0.4486169
C	-0.0471199	-2.6820208	1.9295532	H	-3.4434753	1.9360023	-0.2086420
H	2.1713501	-2.5613289	2.1763780	H	-4.0127150	0.9321061	-1.5458035
C	-0.8416623	-3.1746690	0.8633804	C	-5.4440035	1.2540012	0.0566398
H	-0.2583431	-4.1216531	-1.0904899	N	-6.3819668	1.3859105	-0.9364480
H	-1.9250919	-3.2076770	0.8424476	H	-6.0726532	1.3298339	-1.9012723
C	-0.1351972	0.2095418	-1.9004225	C	-7.7817388	1.6762093	-0.6659436
C	-1.0556875	0.6458369	-0.9282865	H	-8.4357645	0.8881865	-1.0683129
C	-0.5065024	-1.1194593	-2.2747275	H	-7.9004164	1.7193733	0.4231059
H	0.7139923	0.8122616	-2.2349888	O	-5.7362902	1.3302831	1.2533405
C	-2.0113287	-0.3820262	-0.6737095	C	5.1385681	0.7719017	-1.6643494
H	-0.9862650	1.6013071	-0.4172430	H	5.8735877	0.4528833	-2.4163921
C	-1.6607134	-1.4743667	-1.5326107	H	4.8297461	1.8151100	-1.8485254
H	0.0025867	-1.7501563	-2.9991655	H	5.5727961	0.6760555	-0.6641240
H	-2.1994391	-2.4142616	-1.6113649	C	3.4658556	-0.2557900	-3.1484899
O	0.5875540	0.0608265	1.2130507	H	2.6778969	-1.0128537	-3.1631924
C	1.1531252	0.5433852	2.4033774	H	3.0673231	0.7157549	-3.4881758
H	0.3256924	0.7749047	3.1112369	H	4.3009871	-0.5743259	-3.7873862
H	1.7845848	-0.2277398	2.8885759	C	-4.2010393	-1.4421614	0.0493254
C	1.2641932	2.8997073	1.4084501	H	-5.1082807	-1.2875514	0.6489463
H	0.1808237	2.9274484	1.6259865	H	-4.5039452	-1.6283519	-0.9921590
H	1.6912701	3.8839399	1.6455902	H	-3.7142234	-2.3518244	0.4273457
H	1.3772918	2.7632285	0.3081985	C	-2.9419256	0.0524424	1.6457696
C	2.9839457	2.1355452	3.2450882	H	-2.2354231	0.8888296	1.7422414
H	3.1743923	3.2171905	3.2695084	H	-3.8543320	0.3039119	2.2008851
H	2.6971707	1.8260533	4.2648320	H	-2.4754351	-0.8351073	2.0972367
C	4.1790301	1.3581233	2.6556457	H	3.7370652	2.0460266	0.5450983
H	5.1448666	1.8827949	2.7229601	H	-8.0791311	2.6433562	-1.0985842
H	4.3063289	0.3757337	3.1354739	Cl	2.3114010	2.7537078	-1.8984957
C	3.5748520	-0.0739634	0.6464848				

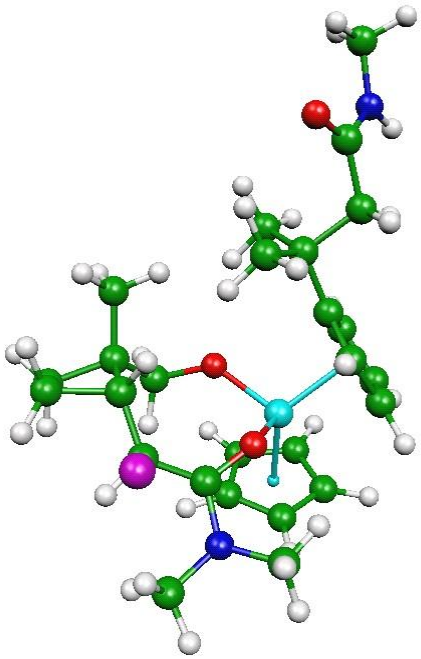

13P

71

Ti	0.5112035	-1.5773495	0.2397586	H	3.7002357	1.9254495	0.2502684
C	2.6503286	-2.8008267	0.0082457	C	2.5780020	0.4050970	-0.7223872
C	2.6979207	-2.0741286	1.2323115	O	1.4476129	-0.2462619	-0.8947599
C	1.6397639	-3.7756842	0.1157861	N	3.6659684	-0.0619134	-1.4353882
H	3.2768066	-2.6148482	-0.8571474	H	1.4923814	-2.2764259	3.1059986
C	1.7215291	-2.6188894	2.1015810	C	-2.8775794	0.1933073	-0.2608792
H	3.3731920	-1.2520446	1.4491166	C	-4.1865085	-0.1183091	-1.0735515
C	1.0421251	-3.6495354	1.4083672	H	-3.9636839	-0.0330438	-2.1483535
H	1.3612821	-4.4905005	-0.6524715	H	-4.4775735	-1.1640457	-0.8841726
H	0.2338772	-4.2566203	1.8061193	C	-5.3560237	0.8212732	-0.7761690
C	-0.5988890	-2.4518848	-1.7095330	N	-6.4749318	0.2000404	-0.2747662
C	-1.0954410	-1.1206184	-1.6704611	H	-6.4465847	-0.8040578	-0.1334344
C	-1.1302454	-3.1396585	-0.5856624	C	-7.6977584	0.9197913	0.0449740
H	0.0542213	-2.8663605	-2.4732395	H	-7.9426612	0.8374702	1.1148691
C	-1.9494373	-0.9767434	-0.5457267	H	-7.5265720	1.9743771	-0.2017847
H	-0.8322630	-0.3341515	-2.3709452	O	-5.3122861	2.0365214	-0.9777397
C	-1.9201172	-2.2184119	0.1541795	C	4.9577834	0.6216829	-1.3520837
H	-0.9981399	-4.1897361	-0.3493826	H	5.6913830	0.0331724	-1.9172436
H	-2.4452745	-2.4410784	1.0793340	H	4.8816935	1.6407837	-1.7732229
O	0.1066142	-0.3548164	1.5916324	H	5.2985705	0.6770844	-0.3096258
C	0.9414543	0.3793020	2.4847220	C	3.4201137	-0.7087535	-2.7268052
H	0.5501189	0.2442350	3.5127355	H	2.4395591	-1.1913063	-2.7193653
H	1.9761695	-0.0018314	2.4671713	H	3.4376366	0.0469150	-3.5312302
C	0.9740578	1.8684254	2.1544129	H	4.2018524	-1.4572501	-2.9221042
C	-0.3986348	2.5098158	2.3779836	C	-3.2221747	0.2597056	1.2400736
H	-0.6970846	2.3977590	3.4331525	H	-3.8034718	1.1662760	1.4583072
H	-0.3865610	3.5836990	2.1461966	H	-3.8271166	-0.6062846	1.5516252
H	-1.1685082	2.0428652	1.7562237	H	-2.3082465	0.2682446	1.8466156
C	2.0720897	2.7219358	2.8611920	C	-2.2620104	1.5155570	-0.7541976
H	1.7712951	3.2591077	3.7723572	H	-2.1244982	1.5065283	-1.8447811
H	2.9751099	2.1299228	3.0783919	H	-2.9248071	2.3574806	-0.5219213
C	2.2268389	3.5307184	1.5451710	H	-1.2796484	1.6794749	-0.2953288
H	1.5882560	4.4215764	1.5207896	H	0.8386280	2.5901822	0.0113210
H	3.2365699	3.8257855	1.2350424	H	-8.5469484	0.5451077	-0.5461690
C	1.5998175	2.3343539	0.7605264	Cl	2.8865096	3.2008436	-2.0331966
C	2.6921122	1.5492343	0.0965517				

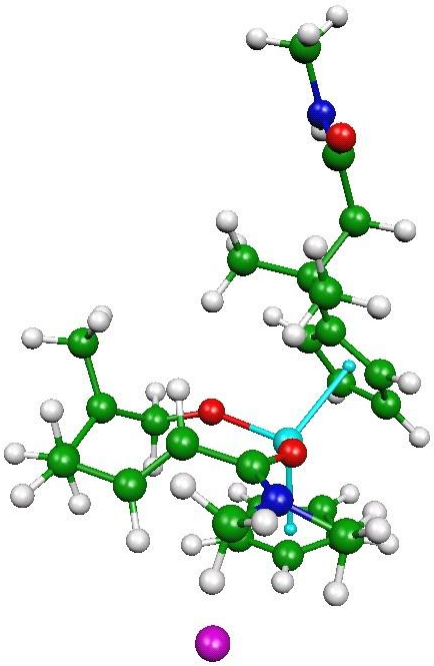

14

71

Ti	0.5853817	-1.4929203	0.2308806	C	1.2796562	2.0316644	-0.0440617
C	2.2493380	-2.9137787	-0.7950548	H	0.2719826	2.1607951	0.3643624
C	2.9483491	-1.7354318	-0.4185954	C	1.3466895	1.1559574	-1.2344275
C	1.8060673	-3.5647995	0.3925351	O	0.8363733	-0.0260902	-1.1486811
H	2.1095694	-3.2743459	-1.8107394	N	1.8273481	1.5812399	-2.4028725
C	2.8960270	-1.6365329	0.9880368	H	3.3382151	-0.8235509	1.5560639
H	3.4540259	-0.9917786	-1.0478735	C	-2.8301717	0.1148608	-0.5111769
C	2.1845132	-2.7616234	1.4982375	C	-4.2875280	-0.4076199	-0.7852886
H	1.2758489	-4.5107063	0.4447860	H	-4.3129080	-0.8685667	-1.7849639
H	1.9745497	-2.9771950	2.5430581	H	-4.5152001	-1.2028430	-0.0581521
C	-0.8636958	-3.0985572	-0.8988607	C	-5.3729810	0.6690410	-0.7537873
C	-1.3437884	-1.8791513	-1.4127103	N	-6.3435663	0.4736578	0.1983560
C	-1.1398569	-3.1138961	0.5058313	H	-6.2753065	-0.3435972	0.7955280
H	-0.3717090	-3.8803892	-1.4684486	O	-5.3904400	1.6333782	-1.5230558
C	-1.9773195	-1.1400642	-0.3578451	C	2.4465411	2.8980992	-2.5857189
H	-1.2379816	-1.5469313	-2.4413158	H	2.0373641	3.6120380	-1.8659370
C	-1.8439038	-1.9198552	0.8159046	H	3.5338557	2.7805766	-2.4284936
H	-0.9380307	-3.9263835	1.1977555	H	2.2324847	3.2373891	-3.6082727
H	-2.1680490	-1.6319725	1.8114938	C	2.1177985	0.6312113	-3.4799627
O	0.3863959	-0.4657281	1.7565033	H	1.5563701	-0.2924582	-3.3202833
C	0.9186116	-0.1349068	3.0504850	H	1.8361929	1.0813788	-4.4413138
H	0.2466444	-0.6062383	3.7942034	H	3.2030126	0.4294622	-3.4493274
H	1.9206089	-0.5828325	3.1649975	C	-2.8202888	0.9461618	0.7856912
C	0.9887765	1.3388562	3.2974136	H	-3.3816706	1.8803034	0.6438556
C	-0.2551760	2.0827559	3.6615092	H	-3.2787751	0.4026631	1.6255251
H	-0.0462454	2.8815624	4.3933074	H	-1.7902669	1.1927088	1.0751507
H	-0.7224512	2.5843871	2.7919299	C	-2.3641708	0.9889503	-1.6898218
H	-1.0203832	1.4148673	4.0837650	H	-2.3545391	0.4221615	-2.6318960
C	2.2673015	2.1017812	3.1398470	H	-3.0538812	1.8308256	-1.8248868
H	2.4537852	2.6791294	4.0656640	H	-1.3515716	1.3715710	-1.5136835
H	3.1192809	1.4160600	3.0161326	C	-7.4767644	1.3707314	0.3642033
C	2.2795695	3.1354487	1.9602033	H	-8.4290728	0.8425635	0.2063330
H	1.3763686	3.7621027	2.0310127	H	-7.4823694	1.8263948	1.3659504
H	3.1492040	3.7951422	2.0974747	H	-7.3766908	2.1622704	-0.3878534
C	2.3623943	2.4591081	0.6249171	Cl	4.8632447	0.9226313	-1.2773888
H	3.3572049	2.2070367	0.2181275				

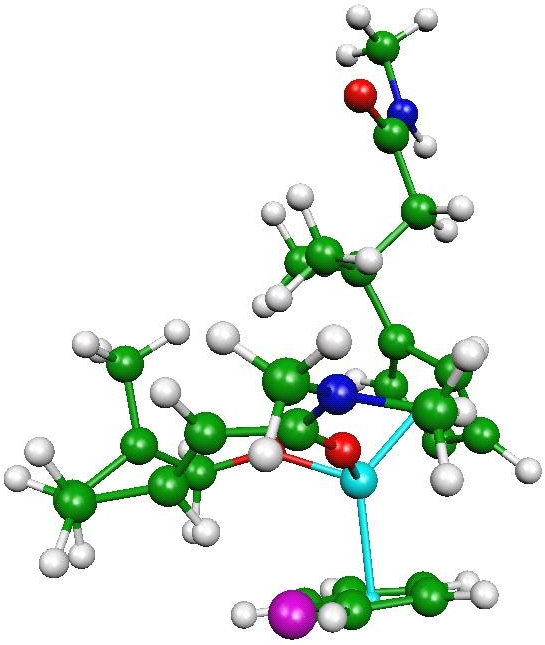

14T

71

C	1.1870813	0.9814708	3.0938791	C	1.7255235	2.2303288	0.2661416
C	2.3321478	1.6332481	1.3445624	H	1.5850394	3.3109102	0.2711337
Ti	0.7390725	-1.5024271	-0.0044751	C	1.3380116	1.5013264	-0.9276693
C	2.5045909	-2.4984857	-1.3415336	O	1.0576883	0.2419791	-0.8956880
C	3.1471185	-1.5296712	-0.5223244	N	1.1529981	2.1671733	-2.0976455
C	1.9931146	-3.5264361	-0.5045793	H	3.3781232	-1.4225868	1.6897629
H	2.4451110	-2.4611465	-2.4260435	C	-2.8281896	0.0270380	0.0093677
C	2.9890744	-1.9431618	0.8199427	C	-4.1176828	-0.1674304	-0.8664519
H	3.6245217	-0.6030408	-0.8801432	H	-3.8597630	0.0155770	-1.9209095
C	2.2583528	-3.1678847	0.8425157	H	-4.4352124	-1.2195934	-0.7894168
H	1.4830348	-4.4251314	-0.8362632	C	-5.2762075	0.7671308	-0.5180373
H	1.9757869	-3.7350568	1.7260947	N	-6.4168240	0.1306110	-0.0931161
C	-0.6735257	-2.6296288	-1.6133469	H	-6.4099851	-0.8821889	-0.0346438
C	-1.2699542	-1.3498551	-1.6031980	O	-5.2048643	1.9947706	-0.6174622
C	-0.9100630	-3.2193857	-0.3304835	C	1.7078897	3.5151158	-2.2753767
H	-0.1568713	-3.0863801	-2.4518252	H	2.8105689	3.4515006	-2.2325365
C	-1.9145906	-1.1385378	-0.3451461	H	1.3833577	3.8870389	-3.2541958
H	-1.2410716	-0.6393252	-2.4245123	H	1.3299444	4.2043861	-1.5112469
C	-1.6789882	-2.3013736	0.4290897	C	1.0925481	1.3871679	-3.3353889
H	-0.6398071	-4.2224099	-0.0162252	H	0.5849763	0.4370810	-3.1537852
H	-1.9845526	-2.4516939	1.4600788	H	0.5468225	1.9618928	-4.0947766
O	0.4197333	-0.8768259	1.7117135	H	2.1251061	1.1869626	-3.6726995
C	0.9913674	-0.5090351	2.9550505	C	-3.2151092	-0.0194065	1.4987857
H	0.3002425	-0.8685383	3.7497523	H	-3.8194448	0.8596753	1.7627127
H	1.9547789	-1.0265266	3.1108417	H	-3.8029108	-0.9186216	1.7394755
C	-0.0375486	1.8315236	3.2205725	H	-2.3176736	-0.0233736	2.1318258
H	-0.4926948	1.7023256	4.2233266	C	-2.1662963	1.3796604	-0.3161157
H	0.1910241	2.9008752	3.1071494	H	-1.8597655	1.4330485	-1.3702580
H	-0.8001525	1.5642328	2.4779011	H	-2.8714586	2.2004100	-0.1349876
C	2.4796454	1.5267235	3.6856629	H	-1.2687137	1.5223796	0.3003038
H	2.3352557	2.0896725	4.6225096	C	-7.6329765	0.8456142	0.2613965
H	3.1911561	0.7125441	3.8931295	H	-8.4762018	0.5357017	-0.3739475
C	2.9637019	2.3874527	2.4994144	H	-7.9008201	0.6811723	1.3161759
H	2.5547475	3.4069614	2.5593477	H	-7.4388841	1.9132973	0.1045542
H	4.0574615	2.4730850	2.3983388	Cl	4.3297309	1.4301298	-1.7440018
H	2.6993998	0.6185399	1.1967530				

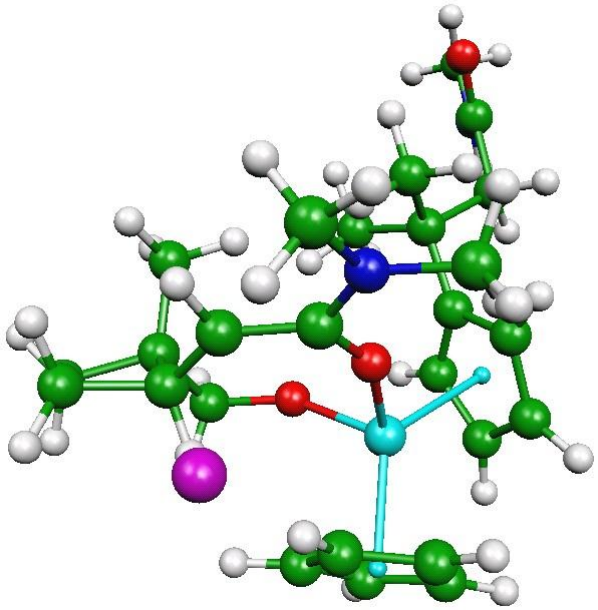

14P

71

Ti	0.6003590	-1.5329611	0.0899248	C	2.2808335	1.9201950	-0.1170438
C	2.4028905	-2.6637734	-1.1073893	H	2.5458278	2.9531949	-0.3287464
C	3.0236703	-1.7376298	-0.2208365	C	1.5782435	1.2278533	-1.1382739
C	1.7577838	-3.6566884	-0.3297706	O	0.9775080	0.0800585	-0.9695517
H	2.4338570	-2.6167706	-2.1927711	N	1.4838667	1.7878147	-2.3865170
C	2.7296704	-2.1495559	1.0986464	H	3.0633622	-1.6575791	2.0067123
H	3.6051147	-0.8583943	-0.5157478	C	-2.9309552	0.1360146	-0.0826438
C	1.9219632	-3.3206342	1.0408386	C	-4.3449828	-0.2386100	-0.6568793
H	1.2125557	-4.5133659	-0.7132313	H	-4.2630501	-0.3524043	-1.7486521
H	1.5284624	-3.8716380	1.8911270	H	-4.6352679	-1.2202706	-0.2497951
C	-0.8907454	-2.7779728	-1.3770207	C	-5.4379142	0.7963692	-0.3921955
C	-1.4490560	-1.4889713	-1.5244029	N	-6.4624606	0.3568819	0.4105442
C	-1.1322518	-3.1951354	-0.0299343	H	-6.4193483	-0.5904891	0.7708110
H	-0.4054178	-3.3534853	-2.1593533	O	-5.4141464	1.9350943	-0.8664340
C	-2.0645828	-1.0970554	-0.2989025	C	2.2196186	3.0059989	-2.7289709
H	-1.4135867	-0.8924700	-2.4313747	H	3.2794324	2.8928444	-2.4464923
C	-1.8534537	-2.1592214	0.6172574	H	2.1467201	3.1570140	-3.8120415
H	-0.8875759	-4.1593670	0.4046130	H	1.7886422	3.8894484	-2.2312892
H	-2.1449740	-2.1652807	1.6634427	C	0.8495021	1.0788784	-3.4883091
O	0.3233421	-0.6405653	1.6855123	H	0.3568035	0.1829315	-3.1049680
C	0.9300785	0.0289552	2.7648191	H	0.1040865	1.7250310	-3.9774083
H	0.1934464	0.0930134	3.5905303	H	1.6017221	0.7807491	-4.2377185
H	1.7899827	-0.5568822	3.1415731	C	-3.0599096	0.4584391	1.4177864
C	1.4205025	1.4400766	2.4051652	H	-3.6280501	1.3883566	1.5609892
C	0.2778134	2.4227088	2.1738298	H	-3.5840969	-0.3421740	1.9619281
H	-0.3482257	2.5058840	3.0767756	H	-2.0685921	0.5819647	1.8718151
H	0.6595794	3.4270479	1.9383846	C	-2.3629254	1.3542293	-0.8355084
H	-0.3625426	2.1063891	1.3400526	H	-2.3108837	1.1656592	-1.9175104
C	2.4972833	2.0038230	3.3902434	H	-3.0097623	2.2282234	-0.6920785
H	2.1680660	2.8236694	4.0436366	H	-1.3489249	1.5837876	-0.4829962
H	2.9447883	1.2171957	4.0164023	C	-7.5992604	1.1918208	0.7656323
C	3.3898135	2.3783500	2.1773796	H	-8.5450952	0.7377355	0.4340672
H	3.2797691	3.4350311	1.8940583	H	-7.6466932	1.3636871	1.8517962
H	4.4593771	2.1440994	2.2284400	H	-7.4655757	2.1543551	0.2577340
C	2.5362995	1.4532968	1.2694947	Cl	4.7310567	1.3102269	-1.0540121
H	2.9918211	0.4563563	1.2437162				

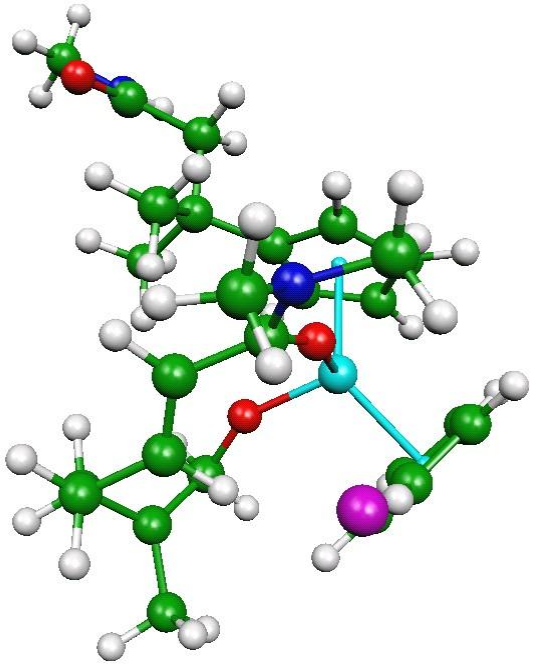

15

71

Ti	0.7437911	-1.1202576	-0.8327322	C	-2.8335812	0.1397570	-0.0658788
C	2.6846656	-1.3027585	-2.2768712	C	-4.1601717	0.3513938	-0.8800509
C	3.1822937	-1.0634583	-0.9618678	H	-3.9668042	1.0773703	-1.6848443
C	2.0473467	-2.5659695	-2.2924529	H	-4.4282576	-0.6016475	-1.3633140
H	2.7895688	-0.6230191	-3.1183762	C	-5.3363619	0.8853628	-0.0624859
C	2.8268114	-2.1770413	-0.1688573	N	-6.4248563	0.0491364	-0.0122112
H	3.7049106	-0.1473768	-0.6363466	H	-6.3736282	-0.8381184	-0.5014822
C	2.0963302	-3.0990087	-0.9726206	C	-7.6496464	0.3910062	0.6942793
H	1.5946119	-3.0426168	-3.1562292	H	-7.8557571	-0.3230085	1.5060534
H	1.6809625	-4.0517001	-0.6517565	H	-7.5080795	1.3896298	1.1242946
C	-0.5643858	-1.0584306	-2.8556244	O	-5.3216477	1.9822070	0.5022950
C	-1.1844633	-0.0265144	-2.1141591	C	2.0909578	4.2781061	-0.2042958
C	-0.8544038	-2.2906078	-2.1904290	H	3.1819075	4.1320379	-0.1015870
H	0.0062769	-0.9341007	-3.7712064	H	1.8585063	5.1532943	-0.8241453
C	-1.8906724	-0.5946424	-1.0101392	H	1.6512278	4.4183927	0.7879374
H	-1.1202726	1.0330365	-2.3452099	C	1.8833456	2.9721760	-2.2774961
C	-1.6703458	-1.9937504	-1.0676437	H	1.2999104	2.1723822	-2.7424370
H	-0.5869338	-3.2877500	-2.5245473	H	1.6654961	3.9277569	-2.7706703
H	-2.0282673	-2.7254417	-0.3489571	H	2.9608231	2.7363898	-2.3466164
O	0.3433930	-1.4852374	0.9307921	C	-3.1275349	-0.7072155	1.1860809
C	0.5072340	-2.3057183	2.0941393	H	-3.7705986	-0.1481484	1.8801115
C	1.2244526	-1.6359523	3.2254839	H	-3.6403585	-1.6485916	0.9363435
C	0.6499219	-0.3941098	3.8369345	H	-2.1908457	-0.9533892	1.7044035
H	-0.3724824	-0.2312009	3.4638394	C	-2.2512791	1.4973280	0.3672600
H	0.5839203	-0.5153747	4.9351710	H	-1.9987394	2.1241465	-0.5002108
C	1.4824724	0.9025712	3.5638546	H	-2.9853214	2.0496335	0.9671756
H	0.9530662	1.7679401	3.9906564	H	-1.3375824	1.3406358	0.9560372
H	2.4519187	0.8198743	4.0825425	C	2.5500088	-2.1341658	3.7039478
C	1.7095980	1.0671607	2.0993220	H	2.6206026	-2.0914763	4.8044175
H	2.3472326	0.3197431	1.6220647	H	2.7408832	-3.1718083	3.3926113
C	1.1841617	2.0150475	1.3140402	H	3.3958680	-1.5234117	3.3276811
H	0.5953273	2.8373173	1.7286461	H	-8.5109976	0.4124984	0.0099103
C	1.3542970	1.9542804	-0.1515167	H	1.0315362	-3.2365116	1.8131350
O	1.1694638	0.8464002	-0.7712064	H	-0.5181341	-2.5902313	2.4137637
N	1.5393491	3.0848608	-0.8582305	Cl	4.4944984	1.9152566	-0.1392732
H	3.0465702	-2.2904923	0.8881575				

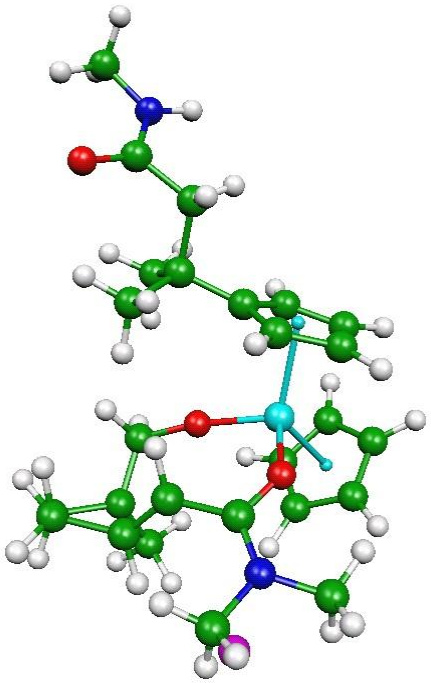

15T

71

C	1.5528477	2.2146278	1.7341030	C	-3.1134935	0.2613523	-0.2043307
C	2.0455505	2.5406365	-0.2497978	C	-4.4739584	-0.1744986	-0.8615669
Ti	0.3599272	-1.3682048	0.2372374	H	-4.3438948	-0.1955509	-1.9546173
C	2.4204637	-2.7199316	0.4564433	H	-4.7014134	-1.2046877	-0.5451073
C	2.4792219	-1.6353713	1.3750916	C	-5.6560479	0.7485001	-0.5606963
C	1.3509377	-3.5635067	0.8144988	N	-6.7121348	0.1376547	0.0692917
H	3.0759681	-2.8451284	-0.3993596	H	-6.6381808	-0.8505275	0.2868448
C	1.4446370	-1.8341546	2.3277513	C	-7.9412668	0.8393198	0.4064780
H	3.2093306	-0.8220567	1.3123806	H	-8.1170735	0.8367599	1.4927994
C	0.7252530	-3.0051692	1.9731764	H	-7.8280234	1.8749490	0.0650141
H	1.0613279	-4.4754116	0.3019117	O	-5.6729012	1.9436485	-0.8661036
H	-0.1255824	-3.4200486	2.5067944	C	3.9226039	1.5871539	-2.7173755
C	-0.8578845	-2.4771575	-1.5365184	H	4.7373541	1.7226669	-1.9860830
C	-1.3933596	-1.1509128	-1.6011208	H	4.3313206	1.4550798	-3.7291832
C	-1.2996132	-3.0563357	-0.3279827	H	3.2532764	2.4528222	-2.7024972
H	-0.2347755	-2.9469713	-2.2926454	C	3.8991995	-0.8746739	-2.6013513
C	-2.1730213	-0.9113311	-0.4474030	H	3.2110470	-1.7182346	-2.5037821
H	-1.2194382	-0.4512038	-2.4128950	H	4.3174702	-0.8530966	-3.6164374
C	-2.0429509	-2.0685023	0.3818976	H	4.7103889	-0.9462242	-1.8561978
H	-1.1182923	-4.0699740	0.0092979	C	-3.3374974	0.5018654	1.3014900
H	-2.5094180	-2.2124029	1.3533441	H	-3.9817801	1.3791192	1.4531469
O	0.1497711	0.2899708	0.9670274	H	-3.8255546	-0.3585464	1.7833677
C	0.2153328	1.4978669	1.6981633	H	-2.3847425	0.6807572	1.8152488
C	1.4504341	3.7406222	1.6402437	C	-2.6050042	1.5495502	-0.8765414
H	0.5951737	4.1749360	2.1860957	H	-2.4721315	1.4103715	-1.9592699
H	2.3672928	4.1945938	2.0411906	H	-3.3323555	2.3590812	-0.7409485
C	1.3904753	3.8723249	0.1091419	H	-1.6398480	1.8482324	-0.4477566
H	0.3544148	3.9019881	-0.2613958	C	2.6541093	1.6306793	2.5606932
H	1.9150429	4.7479161	-0.3043395	H	2.3603660	0.6921820	3.0497900
H	3.1265273	2.4426134	-0.0735035	H	3.5623239	1.4040069	1.9509709
C	1.4714803	1.6567346	-1.1528572	H	2.9700737	2.3423274	3.3421696
H	0.4013916	1.7317286	-1.3659657	H	-8.8086806	0.3869369	-0.0971696
C	2.0770099	0.3997913	-1.5991399	H	-0.0774912	1.2780204	2.7472346
O	1.4794873	-0.7220184	-1.3365136	H	-0.5559442	2.1784442	1.2922683
N	3.1793555	0.3773367	-2.3590235	Cl	5.0711984	0.6270694	0.3671554
H	1.2071470	-1.1819878	3.1633313				

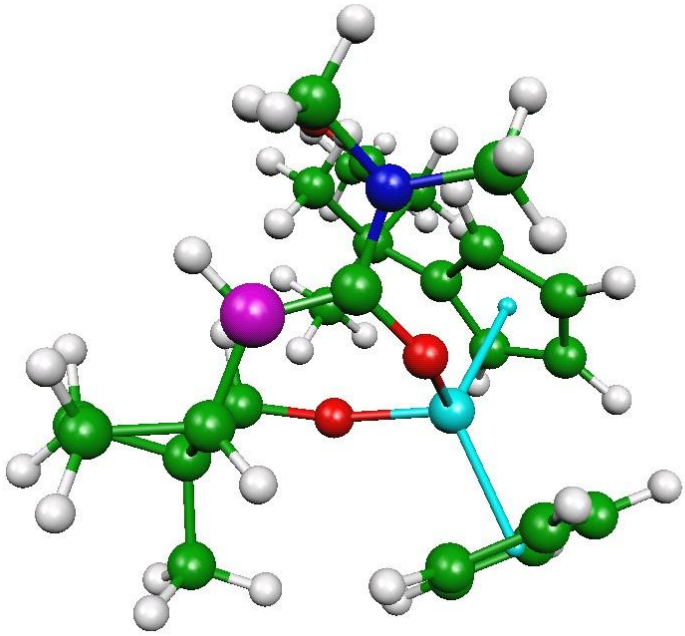

15P

71

Ti	0.5009085	-1.5666967	-0.0795832	N	1.3990291	1.5606194	-2.2769886
C	2.5371873	-2.9385907	-0.5984476	H	1.3149672	-2.9578322	2.5198288
C	2.6077775	-2.4950831	0.7536302	C	-2.9093033	0.3648171	0.0856818
C	1.4409827	-3.8128015	-0.7185549	C	-4.2951847	0.1930999	-0.6396285
H	3.1880177	-2.6060398	-1.4015173	H	-4.1829921	0.5085914	-1.6884301
C	1.5536307	-3.1078024	1.4710441	H	-4.5543599	-0.8772454	-0.6512019
H	3.3336774	-1.7907101	1.1449001	C	-5.4391167	1.0110442	-0.0381888
C	0.8066658	-3.9004806	0.5591723	N	-6.4935442	0.2634690	0.4262721
H	1.1204608	-4.3088358	-1.6299022	H	-6.4405849	-0.7464894	0.3466002
H	-0.0645494	-4.5003326	0.8066446	C	-7.6879198	0.8594583	1.0048880
C	-0.7339911	-1.8040469	-2.1283695	H	-7.8250994	0.5446235	2.0504489
C	-1.1832793	-0.5196292	-1.6863596	H	-7.5553193	1.9473851	0.9738672
C	-1.2770013	-2.7694874	-1.2486842	O	-5.4298870	2.2432179	0.0183069
H	-0.1268730	-2.0020416	-3.0075514	C	1.5097484	3.0068616	-2.4778683
C	-2.0101355	-0.6859778	-0.5519718	H	2.5686865	3.3198731	-2.4414361
H	-0.9241603	0.4276732	-2.1498903	H	1.0793909	3.2488368	-3.4575929
C	-1.9988650	-2.0799108	-0.2367066	H	0.9362150	3.5467182	-1.7131203
H	-1.1765839	-3.8458319	-1.3298770	C	1.5605966	0.7732477	-3.5006762
H	-2.5148118	-2.5505435	0.5969266	H	1.5136993	-0.2913610	-3.2608246
O	0.2873845	-0.4925363	1.3759214	H	0.7659473	1.0279450	-4.2166115
C	0.4443649	0.6771695	2.1526235	H	2.5417651	0.9903262	-3.9571318
H	0.0052453	1.5281031	1.6012735	C	-3.1005752	0.1090666	1.5936097
H	-0.1326975	0.5570916	3.0903473	H	-3.7232428	0.8993817	2.0358730
C	1.8976902	0.9962900	2.4822385	H	-3.5990870	-0.8539577	1.7816339
C	2.1848281	2.4459141	2.9857197	H	-2.1367512	0.0943459	2.1148979
H	1.4265239	3.1614898	2.6324687	C	-2.3802099	1.7896029	-0.1578034
H	2.3100670	2.5730869	4.0705852	H	-2.2972161	2.0039381	-1.2329013
C	3.4558939	2.4657211	2.0949428	H	-3.0712373	2.5277045	0.2664538
H	3.6833990	3.3806342	1.5355209	H	-1.3870062	1.9209972	0.2912974
H	4.3582706	2.1654738	2.6418438	C	2.4948562	-0.0332279	3.4440242
C	2.8686948	1.2928978	1.2510108	H	3.5557755	0.1734002	3.6453913
H	3.5591230	0.4687003	1.0280147	H	1.9605227	-0.0079125	4.4075855
C	2.2762253	1.7980095	-0.0241575	H	2.4195364	-1.0514694	3.0440950
H	2.1891523	2.8759060	-0.1325984	H	-8.5860747	0.5896710	0.4293391
C	1.7825015	0.9981737	-1.0778842	Cl	4.6111411	2.1895611	-1.2669879
O	1.7417853	-0.3138043	-0.9919522				

Spindensities of the optimized structures:

12	**12P*cis***	**12TS*cis***	**12P*trans***	**12TS*trans***	**13**	**13T**
36c -0.07812	2c -0.13564	2c -0.13854	40c -0.12259	2c -0.12431	26c -0.07876	2c -0.10002
32c -0.07496	49c -0.07087	37c -0.03222	50c -0.06889	37c -0.02981	30c -0.06826	26c -0.02711
37c -0.03015	48h -0.05058	49h -0.02713	49h -0.05208	49h -0.02613	23c -0.04939	37h -0.02596
35c 0.03836	1c 0.09266	43h 0.04375	52n 0.07796	51o 0.04372	3ti 0.04898	27h 0.03515
41h 0.06503	50o 0.10626	48c 0.45999	51o 0.10526	48c 0.42546	28h 0.05644	36c 0.44380
33c 0.93801	47c 0.92205	1c 0.54102	48c 0.92334	1c 0.56523	1c 0.94784	1c 0.50696

13P	14	**14T**	**14P**	15	**15T**	**15P**
35c -0.04089	25c -0.08073	2c -0.12452	35c -0.04749	64c -0.09051	2c -0.11204	31c -0.04474
37h -0.01365	29c -0.07776	30c -0.03448	38h -0.02238	23c -0.07357	32h -0.02602	34h -0.01659
59h 0.01171	21c -0.04676	23c -0.02886	55c -0.01150	21c -0.05480	64c -0.02267	32h 0.01166
40n 0.11937	1ti 0.04510	71cl 0.08373	41n 0.12299	25h 0.03917	3ti 0.04699	37n 0.11707
71cl 0.35496	27h 0.05959	37c 0.32780	71cl 0.30305	67h 0.06428	31c 0.46157	71cl 0.35135
36c 0.37035	24c 0.95203	1c 0.61061	37c 0.45590	22c 0.96566	1c 0.48438	33c 0.39749

	Cosmo	kcal/mol
	ε=∞	10
13	0	0
13T	14,4	14,6
13P	10,7	11,1
15	0	0
15T	13,5	13
15P	7,6	6,9
14	0	0
14T	10	10,4
14P	0,7	0

	Energy	ZPVE
	au	au
12	-2659,2909	0,5763
12TS*cis*	-2659,2739	0,576
12TS*trans*	-2659,2733	0,5756
12P*cis*	-2659,2873	0,5771
12P*trans*	-2659,2893	0,5778

	Energy	ZPVE
	au	au
13P	-2659,2566	0,5816
14P	-2659,2724	0,5808
15P	-2659,2568	0,5804
13T	-2659,2447	0,5773
14T	-2659,2441	0,578
15T	-2659,2409	0,5774
13	-2659,2708	0,5797
14	-2659,2625	0,5788
15	-2659,258	0,5783

Cosmo	Energy
ε=10	au
12	-2659,33311
12TS*cis*	-2659,31197
12TS*trans*	-2659,31183
12P*cis*	-2659,3254
12P*trans*	-2659,3273

	Energy
	au
13P	-2659,29219
14P	-2659,30514
15P	-2659,29119
13	-2659,30789
14	-2659,30305
15	-2659,30001
13T	-2659,28234
14T	-2659,28579
15T	-2659,27849

Cosmo	Energy
ε=∞	au
12	-2659,34194
12TS*cis*	-2659,31981
12TS*trans*	-2659,31982
12P*cis*	-2659,33331
12P*trans*	-2659,33511

	Energy
	au
13P	-2659,30057
14P	-2659,31258
15P	-2659,29905
13T	-2659,29047
14T	-2659,29502
15T	-2659,28668
13	-2659,31571
14	-2659,31171
15	-2659,30906

C. Additional Results on an Unusal Case of Facile Non-Degenerate P-C Bond Making and Breaking Study (Chapter 7)

EPR experiments

CW-EPR spectra were recorded on a Bruker ESP 300E EPR spectrometer equipped with a 4102ST X-band CW resonator and an Oxford ESR900 helium gas-flow cryostat. The CW-EPR measurements on liquid solutions were carried out at 150 K. The modulation amplitude amounted to 50 μT and the microwave frequency was 9.42 GHz. The microwave power was 0.63 mW.

Computational Methods

All the DFT calculations were employed using the ORCA program package with the scalar relativistic, all-electron ZORA approach and empirical Van der Waals correction. The RI-BP86 method in combination of TZVP basis set was used for geometry optimizations, in which a one-center relativistic correction was applied. The final single point energies were computed using the hybrid B3LYP density functional with the basis set of triple-ζ quality including high angular momentum polarization functions (def2-TZVPP). The density fitting and chain of sphere (RIJCOSX) approximation has been employed in single point calculations.

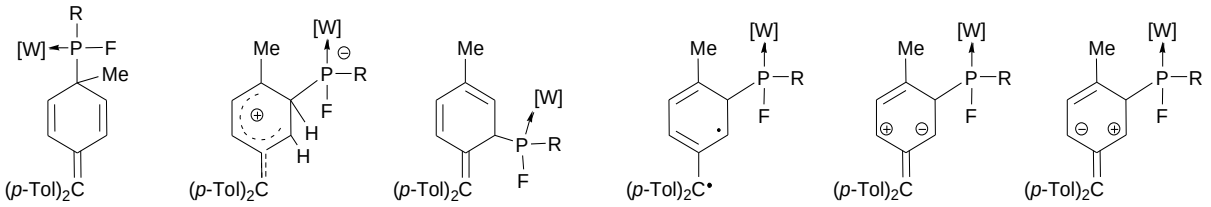

Scheme C.1. Schematic structures of various isomers.

Table C.1. The calculated relative energies (kcal/mol) for combined singlet diradicals **4**+**5**, **6, 7** and **12**; their corresponding structures are shown in Figures S1-S4 and Tables S1-S4.

Molecule	Relative energy (kcal/mol)
singlet diradicals **4**+**5**	0
6	-13.9
7	-38.5
12	-19.2

From the aspect of thermal stability, complex **7** was obtained.

Table C.2. The calculated relative energies (kcal/mol) for combined singlet diradicals **9**+**5**, **10a**-**d**, **11** and P-C atropisomers of **10a,c**; their corresponding structures are shown in Figures S5-S12 and Tables S5-S12.

Molecule	Relative energy (kcal/mol)
singlet diradicals **9**+**5**	0
10a *(s-trans)*	-12.7
10a' *(s-cis)*	-9.2
10b, **10d'** or **10d''**	≥ 31.5
10c	-12.8
10c' (P-C atropisomer)	-6.8
10d (singlet)	21.2
10d (triplet)	9.0
11	-19.4

Structures **10b**, **10d**, **10d'** and **10d''** are geometrically identical. The electronic configuration of **10b**, **10d'** and **10d"** are closed shell solutions (spin restricted methodology) of **10d**, which are at least 31.5 kcal/mol higher in energy than **5**+**9**. Consequently, the intermediates **10b''**, **10d', 10d** and **10d''** are too high in energy and should be ruled out as candidates for the observed intermediates.

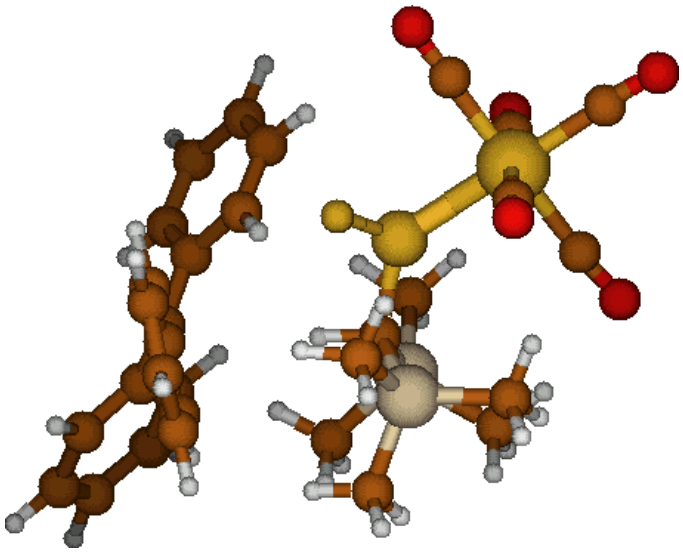

Figure C.1. The optimized molecular structure of combined singlet diradicals **4**+**5.**

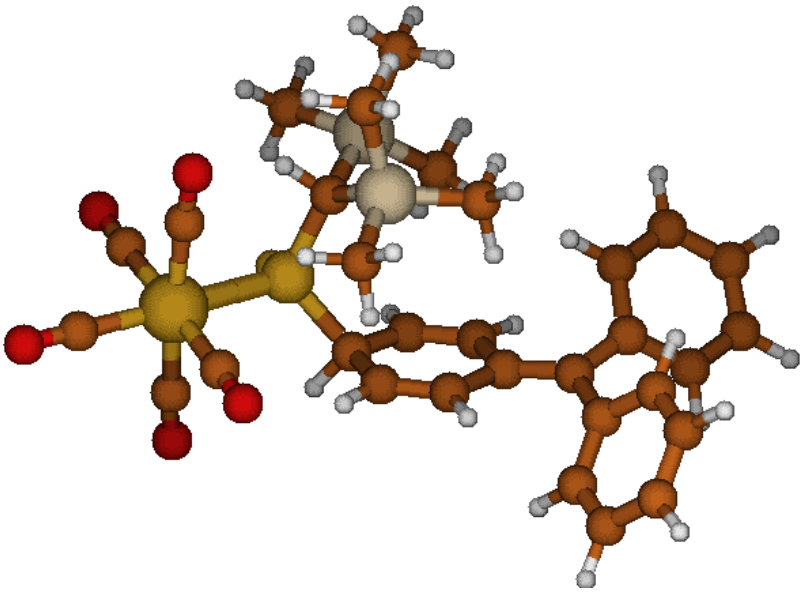

Figure C.2. The optimized molecular structure of **6**.

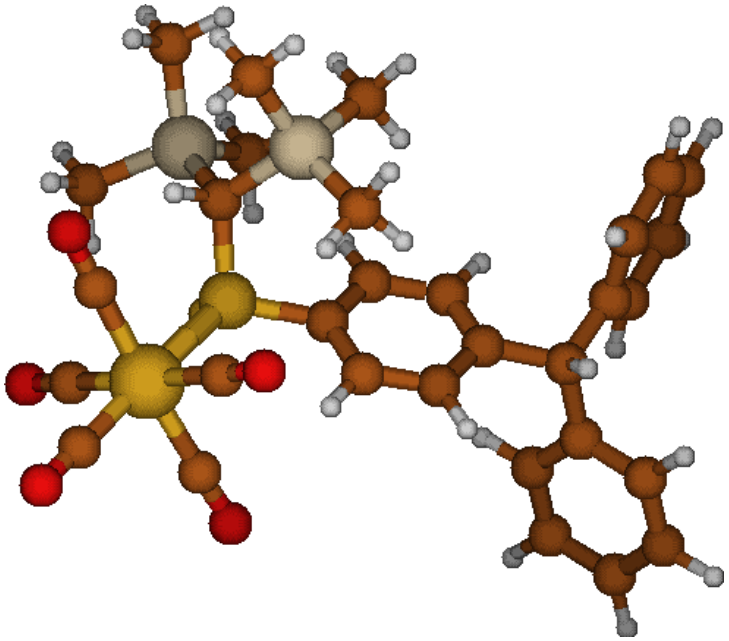

Figure C.3. The optimized molecular structure of **7**.

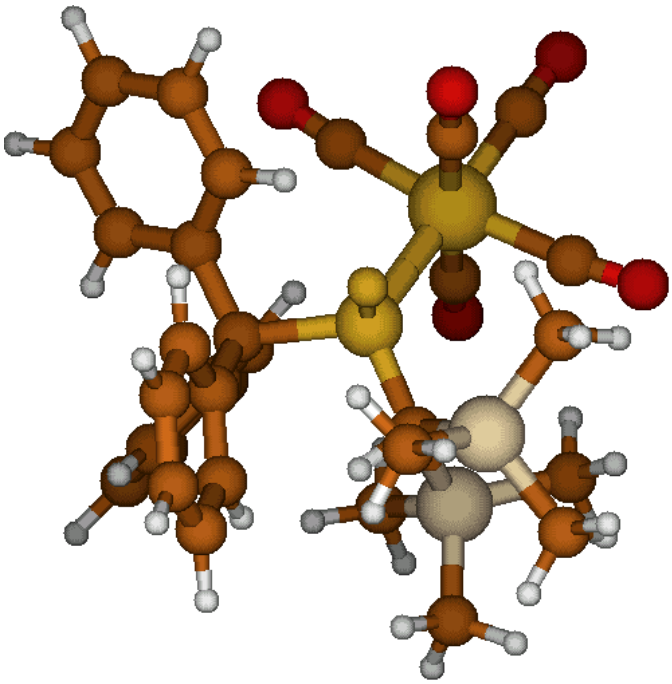

Figure C.4. The optimized molecular structure of complex **12**.

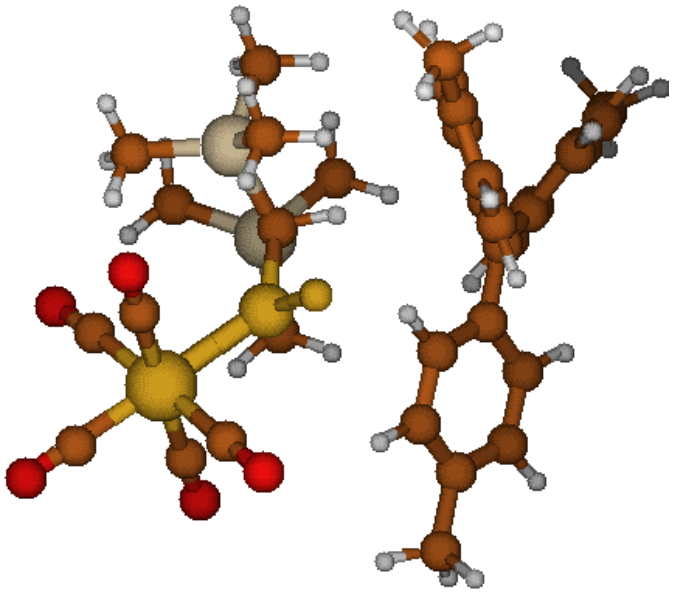

Figure C.5. The optimized molecular structure of combined singlet diradicals **5**+**9**.

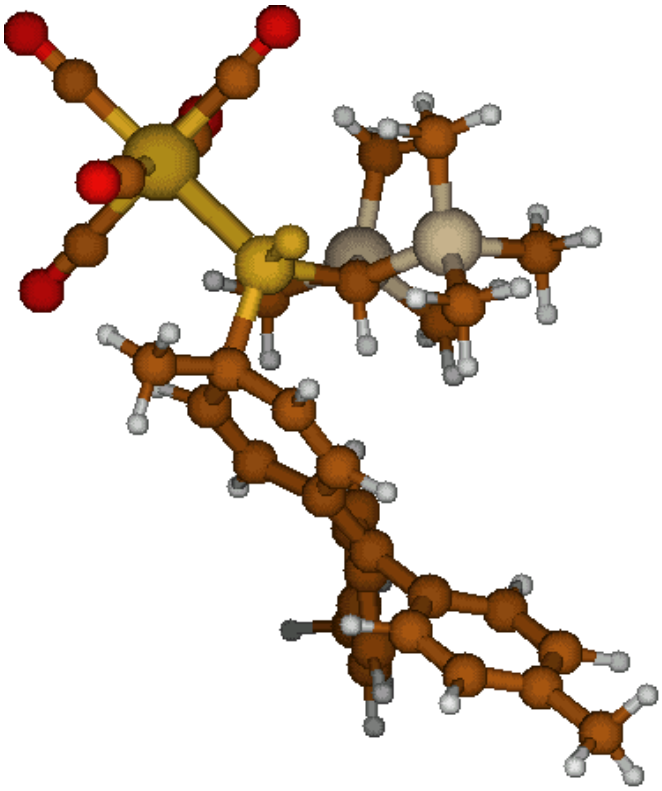

Figure C.6. The optimized molecular structure of **10a** *(s-trans)*.

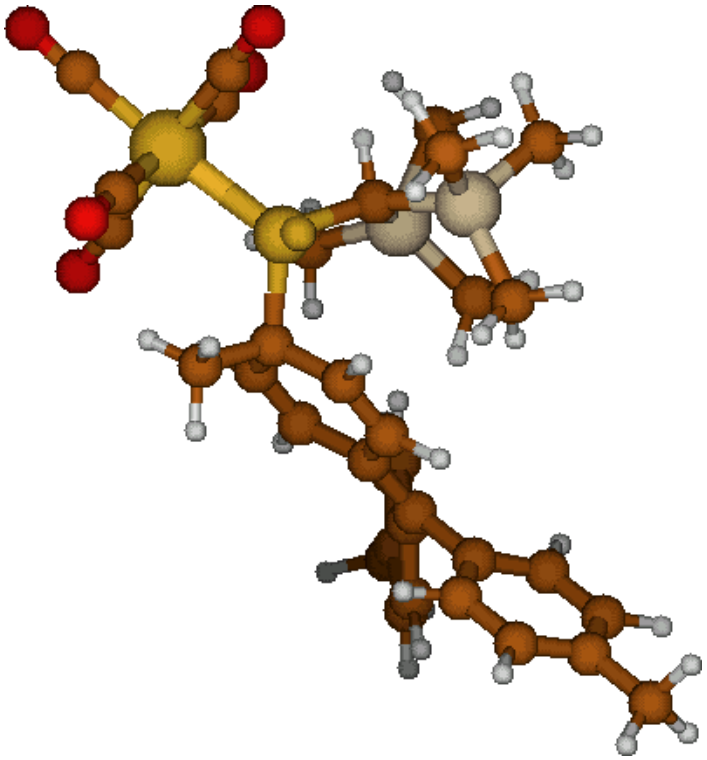

Figure C.7. The optimized molecular structure of **10a'** (*s-cis*).

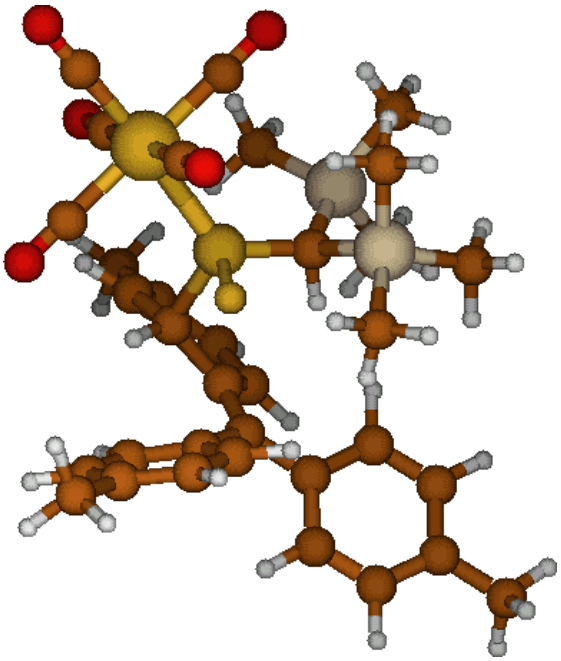

Figure C.8. The optimized molecular structure of **10c** *(s-trans)*.

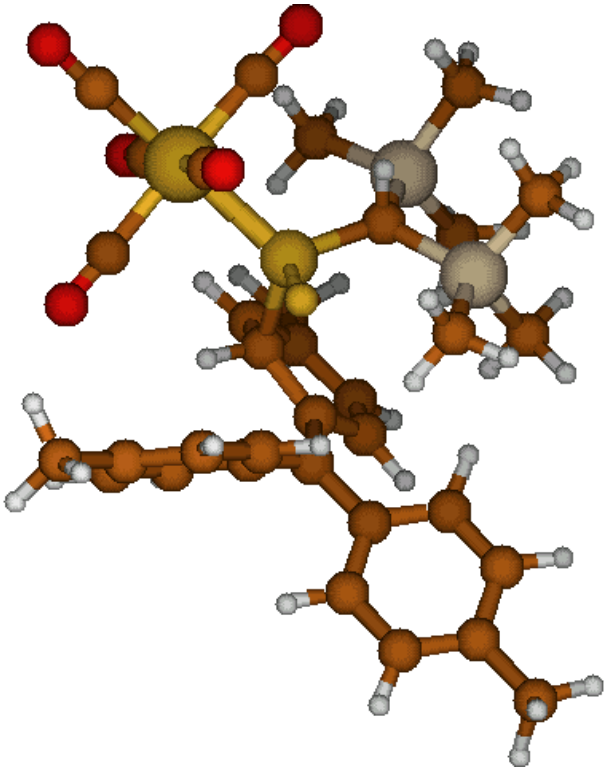

Figure C.9. The optimized molecular structure of **10c'** *(s-cis).*

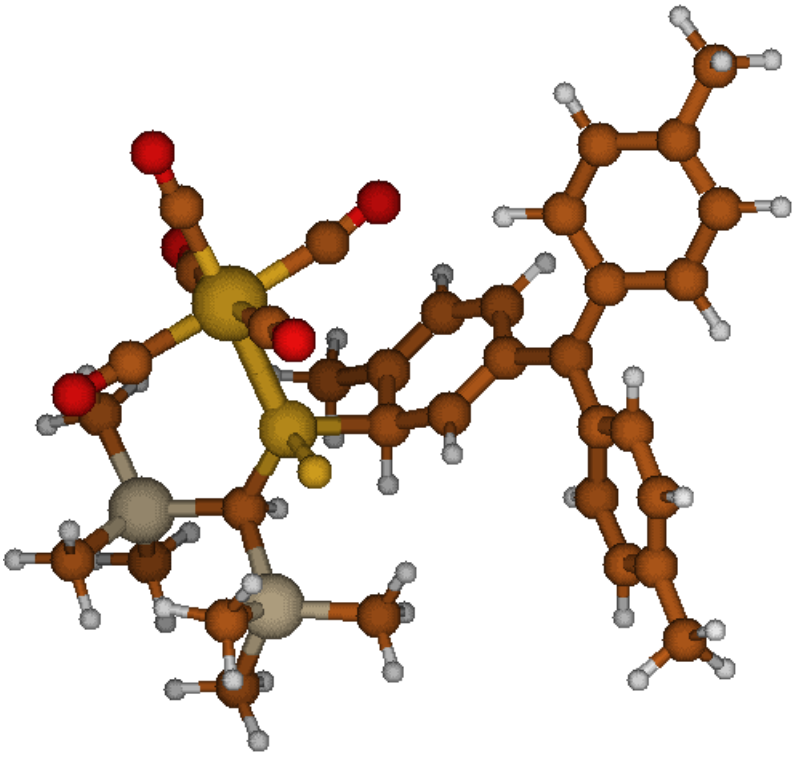

Figure C.10. The optimized molecular structure of **10d** (singlet state).

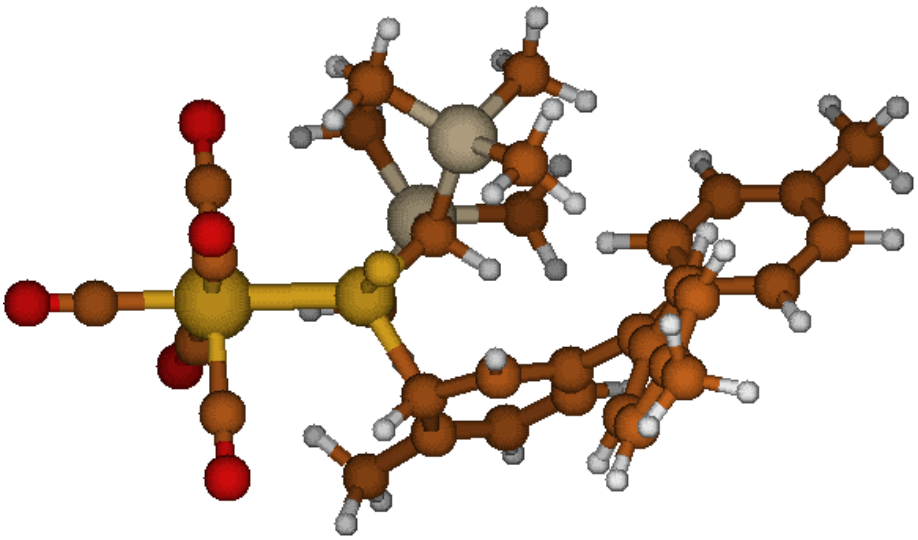

Figure C.11: The optimized molecular structure of **10d** (triplet state).

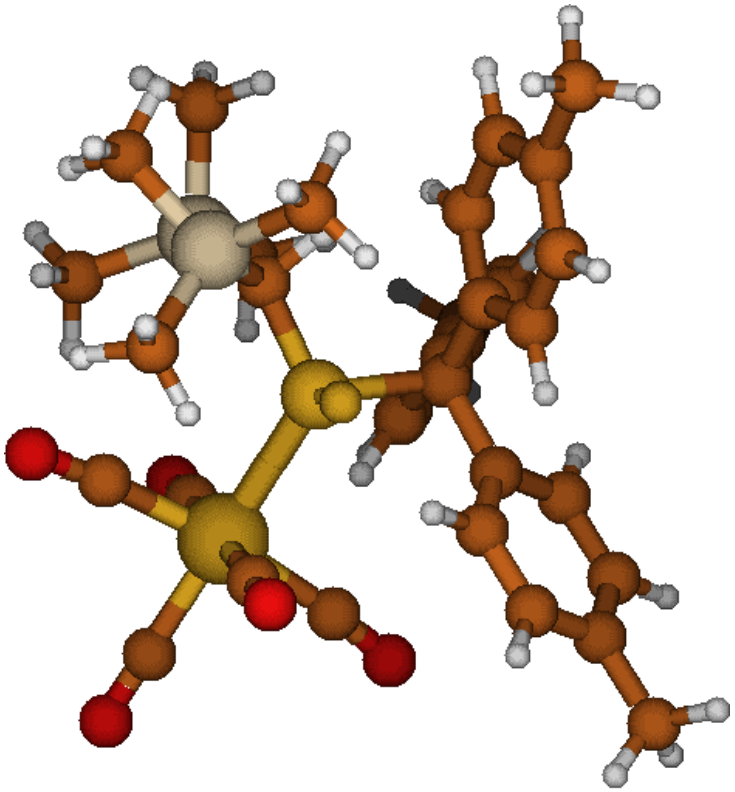

Figure C.12: The optimized molecular structure of **11**.

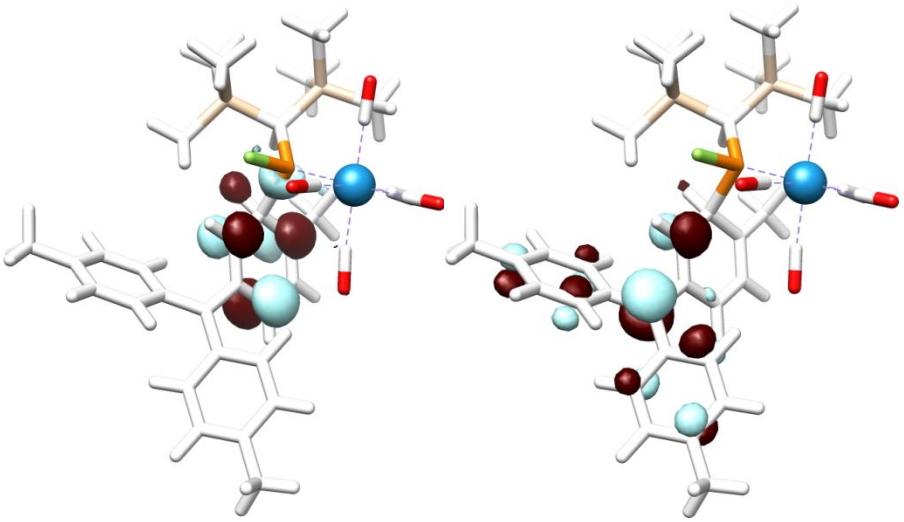

10d (singlet)

Figure C.13. SOMOs of **10d** (singlet state).

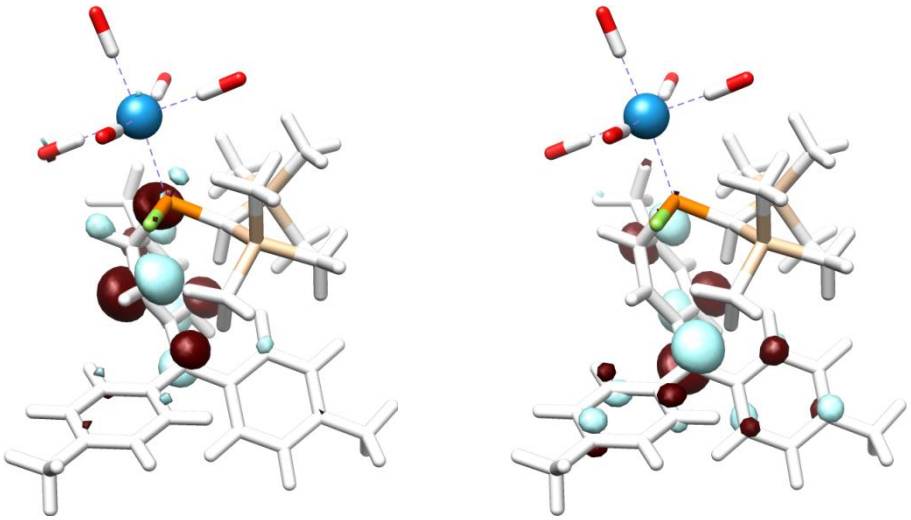

10d (triplet)

Figure C.14. SOMOs of **10d** (triplet state).

Table C.3. The optimized cartesian coordinates of combined singlet diradicals **4**+**5**.

C	-0.857350	-1.633761	-0.591027	H	-2.156741	-3.961535	1.492936
C	-1.107768	-4.695603	-1.303984	H	-3.536820	-3.506679	0.465046
C	0.845919	-3.717732	0.866641	H	-3.518609	-3.051404	2.184266
C	1.396352	-3.093483	-2.101080	C	0.734283	1.971459	1.285631
C	-3.317250	-0.173783	0.648749	C	-0.310530	2.642707	0.532030
C	-0.951617	-1.083409	2.392713	C	-0.941590	3.821415	1.012188
C	-2.890007	-3.167025	1.285507	C	-0.755218	2.139199	-0.717541
C	-4.595490	-2.334116	-5.090217	C	-1.961345	4.437588	0.293868
C	-1.862538	-2.983041	-4.478661	C	-1.778942	2.754027	-1.430282
C	-3.971302	-3.123399	-2.436655	C	-2.395071	3.907200	-0.929596
C	-4.630948	-0.371800	-2.939835	C	0.810431	2.117460	2.737477
C	-2.599102	-0.245571	-5.008275	C	-0.355124	2.237742	3.533581
F	-0.153221	-0.507560	-2.894275	C	2.060148	2.121666	3.403769
O	-5.342618	-2.728842	-5.883369	C	-0.273786	2.357956	4.918038
O	-1.064731	-3.698951	-4.912059	C	2.138852	2.250553	4.788108
O	-4.419557	-3.935974	-1.744098	C	0.973346	2.368630	5.555904
O	-5.406394	0.374979	-2.518379	C	1.714788	1.125304	0.609439
O	-2.239931	0.571436	-5.741848	C	2.233824	-0.032145	1.242840
P	-1.528424	-0.941953	-2.116693	C	2.189007	1.423141	-0.692007
Si	0.059697	-3.312332	-0.800136	C	3.171378	-0.842813	0.609356
Si	-2.040575	-1.527175	0.926852	C	3.126489	0.609622	-1.322596
W	-3.262490	-1.695705	-3.712038	C	3.626090	-0.528700	-0.677677
H	-0.045122	-0.924281	-0.319987	H	-0.600849	4.257197	1.951322
H	-0.541455	-5.640885	-1.348411	H	-0.286970	1.242196	-1.116706
H	-1.537356	-4.523665	-2.300953	H	-2.418899	5.348066	0.685169
H	-1.935784	-4.827472	-0.594010	H	-2.105826	2.319755	-2.376641
H	0.088654	-3.910939	1.641567	H	-1.329129	2.204421	3.044840
H	1.483401	-2.887523	1.206703	H	2.971074	2.038596	2.809957
H	1.474828	-4.618710	0.774878	H	-1.189452	2.432160	5.507494
H	2.040688	-3.987001	-2.145770	H	3.116430	2.266509	5.273329
H	2.025336	-2.220572	-1.867513	H	1.871552	-0.290006	2.238078
H	0.960532	-2.938409	-3.099615	H	1.820849	2.318267	-1.193512
H	-3.921897	-0.030686	1.559581	H	3.545888	-1.732911	1.118033
H	-4.008003	-0.418083	-0.173200	H	3.477558	0.868686	-2.322669
H	-2.829657	0.783498	0.403084	H	-3.199084	4.389974	-1.486715
H	-0.458050	-0.113220	2.240133	H	1.035990	2.465447	6.640887
H	-0.172175	-1.841942	2.556946	H	4.357727	-1.167188	-1.174535
H	-1.556991	-1.010462	3.310837				

Table C.4. The optimized cartesian coordinates of complex **6**.

C	-0.608773	6.229772	10.213409	H	-2.651065	6.248627	5.683961
C	-0.740550	5.140779	9.203645	C	-3.846070	9.009154	6.473294
H	-0.010754	5.109287	8.395067	H	-3.082357	9.735011	6.151672
C	-1.710801	4.203700	9.260123	H	-4.681212	9.558916	6.924143
H	-1.758707	3.451206	8.473435	H	-4.220664	8.505723	5.566513
C	-2.738486	4.186326	10.294540	C	-4.414851	6.636483	8.388738
C	-2.592747	5.204116	11.325136	H	-5.037320	7.218059	9.086124
H	-3.279555	5.178754	12.171249	H	-3.975343	5.793095	8.940394
C	-1.607071	6.125793	11.313232	H	-5.076867	6.220454	7.612000
H	-1.497603	6.819345	12.145272	C	-3.861323	8.371452	11.676261
C	-3.781903	3.274947	10.294077	H	-3.099007	8.189380	12.445948
C	-3.777308	2.075113	9.429945	H	-4.198662	7.395811	11.300680
C	-2.633950	1.260962	9.308826	H	-4.716262	8.873199	12.160137
H	-1.736528	1.528259	9.868650	C	-4.756800	10.199247	9.433775
C	-2.648856	0.119253	8.506319	H	-5.406638	9.424713	9.001250
H	-1.754972	-0.502701	8.433604	H	-4.486754	10.906054	8.635066
C	-3.809005	-0.235343	7.809528	H	-5.344080	10.751431	10.186582
H	-3.821132	-1.128281	7.182559	C	-2.314167	10.964521	11.038673
C	-4.957657	0.555305	7.931251	H	-3.009373	11.570822	11.642809
H	-5.867957	0.283359	7.394066	H	-1.909412	11.615050	10.246542
C	-4.944780	1.691426	8.740320	H	-1.477973	10.654159	11.679577
H	-5.842654	2.302578	8.844849	C	3.176479	9.055359	7.068704
C	-4.972003	3.445621	11.154033	C	2.605283	7.565847	9.537726
C	-5.596857	4.699344	11.307811	C	1.433790	6.791047	7.008128
H	-5.196953	5.555389	10.764214	C	0.296233	9.423360	6.732883
C	-6.729881	4.844536	12.109171	C	1.622259	10.282555	9.140223
H	-7.201291	5.824143	12.206042	F	-0.270494	8.685934	10.959583
C	-7.267418	3.737236	12.773655	O	4.130307	9.366732	6.489317
H	-8.153557	3.849541	13.400384	O	3.191394	7.011311	10.368575
C	-6.669085	2.481122	12.617900	O	1.417681	5.823066	6.370729
H	-7.084541	1.610928	13.129041	O	-0.430393	9.933630	5.985589
C	-5.541617	2.335278	11.810122	O	1.681312	11.280910	9.719426
H	-5.080942	1.354580	11.682098	P	-0.492180	7.987507	9.491762
C	-2.107989	8.652585	8.979022	Si	-3.083951	7.704312	7.602789
H	-1.776603	9.541321	8.403391	Si	-3.235789	9.495285	10.304109
C	-1.997789	6.669021	6.467823	W	1.514451	8.520545	8.091958
H	-1.498112	5.832554	6.968599	H	0.415315	6.214944	10.644484
H	-1.237828	7.284460	5.965121				

Table C.5. The optimized cartesian coordinates of complex **7**.

C	-1.622688	6.279610	9.843394	H	-2.569209	6.565755	6.775698
C	-1.214912	5.089546	9.226031	H	-4.333245	6.438535	6.605244
H	-0.401874	5.102438	8.501774	C	-4.283133	9.494173	6.836556
C	-1.861518	3.890712	9.518203	H	-3.461859	9.603460	6.109491
H	-1.538645	2.966528	9.034117	H	-4.510295	10.489979	7.242197
C	-2.922223	3.849027	10.433959	H	-5.170309	9.138274	6.287726
C	-3.311485	5.036530	11.068273	C	-5.240121	8.049086	9.394463
H	-4.132322	5.016191	11.786869	H	-5.466918	8.974732	9.943090
C	-2.668001	6.239050	10.778175	H	-5.033497	7.254132	10.125957
H	-2.986324	7.154577	11.276018	H	-6.145871	7.758968	8.836286
C	-3.570278	2.506509	10.747316	C	-3.253976	9.601678	11.951362
H	-3.689271	1.984275	9.781722	H	-2.478477	8.982570	12.426502
C	-2.666465	1.632316	11.608821	H	-4.155216	8.987545	11.801510
C	-1.770995	2.179108	12.536800	H	-3.515271	10.411834	12.652048
H	-1.673364	3.263445	12.614093	C	-3.951016	11.499553	9.633835
C	-0.995259	1.346795	13.350438	H	-4.906401	10.996686	9.426686
H	-0.298721	1.786922	14.066133	H	-3.607075	11.974480	8.701659
C	-1.104639	-0.042244	13.242129	H	-4.142529	12.301971	10.365769
H	-0.494376	-0.691615	13.871812	C	-1.084952	11.372748	10.626073
C	-1.995239	-0.596041	12.315426	H	-1.313969	12.228619	11.282381
H	-2.082978	-1.679730	12.220141	H	-0.704089	11.778509	9.674640
C	-2.770783	0.238025	11.507629	H	-0.281212	10.787251	11.093589
H	-3.471647	-0.191853	10.787887	C	2.879936	8.011552	6.884143
C	-4.966068	2.664081	11.336942	C	1.908546	6.365883	9.078541
C	-6.043187	2.916265	10.475291	C	0.345987	6.675990	6.621021
H	-5.865689	2.947285	9.397369	C	0.394116	9.517932	6.963172
C	-7.327234	3.130969	10.980522	C	1.990119	9.260853	9.336280
H	-8.156256	3.320323	10.296298	F	-0.474969	8.327745	10.959172
C	-7.549556	3.100781	12.361901	O	3.853440	8.046282	6.256504
H	-8.552051	3.266230	12.759790	O	2.312246	5.478337	9.701313
C	-6.481465	2.849487	13.227811	O	-0.129477	5.972319	5.831216
H	-6.647334	2.818522	14.306146	O	-0.086265	10.413157	6.403020
C	-5.197339	2.631297	12.717603	O	2.436136	10.012276	10.092352
H	-4.365583	2.424759	13.393301	P	-0.861077	7.879529	9.428269
C	-2.244199	9.000987	9.015077	Si	-3.813594	8.254162	8.178241
H	-1.830959	9.627475	8.203325	Si	-2.634313	10.344175	10.337316
C	-3.518364	6.596946	7.331960	W	1.183964	7.942152	7.985321
H	-3.523229	5.757364	8.041038				

Table C.6. The optimized cartesian coordinates of **12**.

C	12.185687	10.329643	11.768561	H	10.155098	4.204340	11.852934
C	12.904701	9.838104	13.029416	H	10.836114	4.443697	13.482402
C	12.193366	9.276038	14.111314	H	11.694983	3.433127	12.294737
H	11.104380	9.256799	14.090617	C	13.500860	6.069852	13.058317
C	12.848312	8.780352	15.239953	H	14.147085	5.179583	13.131998
H	12.260845	8.362875	16.059525	H	13.070867	6.259943	14.054148
C	14.241588	8.817196	15.317862	H	14.126024	6.937127	12.802608
C	14.964441	9.361544	14.254514	C	8.251506	8.834267	11.939979
H	16.054180	9.400330	14.295388	H	7.215854	8.573002	12.218183
C	14.305741	9.864967	13.130491	H	8.214930	9.366360	10.983074
H	14.896632	10.289237	12.321303	H	8.638976	9.533720	12.696765
C	13.059240	11.329017	10.965243	C	8.925826	6.398388	13.551170
C	14.118707	10.941015	10.123055	H	9.738867	6.614641	14.262826
H	14.362710	9.892692	9.986746	H	8.832306	5.306941	13.475053
C	14.897571	11.886575	9.450940	H	7.991244	6.791309	13.982769
H	15.699908	11.542860	8.796096	C	8.536940	6.172848	10.471478
C	14.651447	13.250294	9.609498	H	9.148550	5.283108	10.264488
C	13.619853	13.654860	10.459070	H	8.459333	6.749037	9.537896
H	13.411944	14.716128	10.605302	H	7.521192	5.835029	10.736144
C	12.836472	12.709143	11.122629	C	11.086018	8.813523	6.175342
H	12.033109	13.059387	11.768660	C	13.341330	8.385929	7.865692
C	10.834877	11.014302	12.039499	C	10.865368	6.833674	8.084314
C	9.998765	11.315776	10.954563	C	9.378526	9.228196	8.425870
H	10.287003	10.983198	9.961735	C	11.768526	10.818671	8.001391
C	8.824429	12.049496	11.109245	F	13.455890	8.177654	10.777130
H	8.196114	12.245555	10.239369	O	10.936499	8.806167	5.025213
C	8.459414	12.527003	12.369573	O	14.458460	8.151148	7.681861
C	9.304210	12.284630	13.454867	O	10.544683	5.733514	7.914209
H	9.058837	12.682999	14.440874	O	8.246987	9.467437	8.512496
C	10.482876	11.550343	13.289656	O	11.945161	11.943152	7.800956
H	11.144939	11.428178	14.144231	P	11.895263	8.690893	10.668141
C	11.122860	7.454635	11.751620	Si	12.137383	5.785937	11.793100
H	11.377267	7.792280	12.773668	Si	9.221639	7.227978	11.870099
C	12.856028	5.230777	10.145796	W	11.358459	8.810915	8.166563
H	13.638897	4.486032	10.369507	H	14.757236	8.427327	16.196581
H	13.320205	6.039202	9.566429	H	15.254414	13.988361	9.078425
H	12.101273	4.737318	9.518540	H	7.539357	13.098267	12.501361
C	11.087711	4.346205	12.417375				

Table C.7. The optimized cartesian coordinates of combined singlet diradicals **5**+**9**.

C	-0.843224	-1.625493	-0.587975	C	-0.315749	2.630650	0.527706
C	-1.101517	-4.684053	-1.305599	C	-0.966006	3.802574	0.998624
C	0.853871	-3.715046	0.870014	C	-0.760402	2.120852	-0.718764
C	1.408606	-3.089725	-2.095745	C	-1.994687	4.398282	0.278495
C	-3.305681	-0.165072	0.651687	C	-1.797193	2.715766	-1.426139
C	-0.943024	-1.075398	2.397325	C	-2.438817	3.868736	-0.946823
C	-2.878818	-3.158789	1.283825	C	0.809083	2.121242	2.733877
C	-4.595960	-2.300067	-5.085202	C	-0.351617	2.251332	3.534757
C	-1.861843	-2.965716	-4.476861	C	2.055752	2.119984	3.405818
C	-3.972290	-3.099785	-2.434629	C	-0.266606	2.371926	4.917633
C	-4.609337	-0.337508	-2.932264	C	2.132384	2.249353	4.788549
C	-2.586181	-0.225620	-5.002996	C	0.974752	2.373199	5.575160
F	-0.138130	-0.511794	-2.899864	C	-3.542252	4.526960	-1.729270
O	-5.347355	-2.688359	-5.877825	C	1.060958	2.471964	7.074792
O	-1.063937	-3.681956	-4.909780	C	1.713129	1.122270	0.611184
O	-4.424438	-3.911356	-1.743382	C	2.234504	-0.033394	1.244255
O	-5.373664	0.420391	-2.509131	C	2.180703	1.401168	-0.696435
O	-2.223388	0.591014	-5.735436	C	3.158875	-0.853458	0.606002
P	-1.513404	-0.931928	-2.113532	C	3.104338	0.574655	-1.327173
Si	0.069448	-3.305461	-0.796526	C	3.616031	-0.568359	-0.690958
Si	-2.028279	-1.518157	0.929005	C	4.631347	-1.448780	-1.368197
W	-3.256638	-1.673703	-3.708450	H	-0.635965	4.248799	1.936788
H	-0.031243	-0.915819	-0.315725	H	-0.284340	1.229569	-1.121278
H	-0.538219	-5.630720	-1.357823	H	-2.467212	5.303425	0.668181
H	-1.533658	-4.504287	-2.300090	H	-2.126567	2.266484	-2.366182
H	-1.927877	-4.817900	-0.594046	H	-1.328495	2.227738	3.051082
H	0.095966	-3.909561	1.643939	H	2.969158	2.035397	2.815815
H	1.489429	-2.883611	1.210531	H	-1.182287	2.456888	5.508063
H	1.483608	-4.615418	0.777702	H	3.111131	2.265362	5.274494
H	2.050027	-3.985157	-2.142566	H	-3.134805	5.281909	-2.423933
H	2.039835	-2.220200	-1.858851	H	-4.094877	3.790311	-2.330693
H	0.974236	-2.930119	-3.094104	H	-4.251105	5.041212	-1.063351
H	-3.906617	-0.020454	1.564770	H	0.195915	3.010738	7.488983
H	-3.999562	-0.411037	-0.167170	H	1.076303	1.468423	7.534221
H	-2.817813	0.791101	0.402650	H	1.980530	2.989106	7.387338
H	-0.451192	-0.104416	2.244310	H	1.878399	-0.289297	2.242275
H	-0.162126	-1.832492	2.561432	H	1.812533	2.290620	-1.208152
H	-1.549655	-1.004033	3.314689	H	3.527530	-1.747760	1.114377
H	-2.146187	-3.953600	1.492372	H	3.442782	0.819492	-2.336553
H	-3.523839	-3.497599	0.461650	H	5.656056	-1.084674	-1.179754
H	-3.509516	-3.043834	2.181235	H	4.571690	-2.481338	-0.993869
C	0.733458	1.971693	1.283720	H	4.480628	-1.463488	-2.457739

Table C.8. The optimized cartesian coordinates of complex **10a**.

C	11.297671	8.618618	11.765815	C	12.537475	11.474981	10.711001
H	11.671710	9.400166	12.455963	C	14.024200	10.063363	12.102526
C	11.428639	5.476645	11.727404	C	12.143009	12.131078	11.823873
H	11.471743	4.577002	12.363316	H	12.202220	11.820644	9.732362
H	12.251969	5.419241	11.002532	C	13.639735	10.750949	13.199497
H	10.480040	5.447203	11.170442	H	14.755958	9.259486	12.192647
C	10.225186	6.902744	14.141424	C	12.625568	11.799068	13.158342
H	9.219156	6.738012	13.729139	H	11.487487	12.996046	11.720313
H	10.191998	7.802114	14.773443	H	14.076089	10.490851	14.163677
H	10.469224	6.042261	14.786834	C	14.581186	10.409228	9.695162
C	13.212955	7.110073	13.674079	H	15.192564	9.495947	9.679611
H	13.324225	6.260263	14.367699	H	14.178796	10.584970	8.689258
H	13.290751	8.039875	14.259021	H	15.224154	11.259708	9.966296
H	14.046948	7.086563	12.958956	C	12.177126	12.448753	14.297693
C	9.283379	10.602464	10.400261	C	10.983536	13.317895	14.292886
H	8.241324	10.693812	10.053057	C	10.963521	14.509313	15.046143
H	9.935488	10.595268	9.517126	C	9.814679	12.977219	13.584011
H	9.534625	11.501017	10.984112	C	9.841360	15.335408	15.054391
C	8.731478	9.577416	13.171802	H	11.847107	14.783227	15.624556
H	9.492922	10.026076	13.828813	C	8.691898	13.801330	13.602659
H	8.285697	8.729477	13.708589	H	9.784996	12.036059	13.037129
H	7.946067	10.334808	13.015837	C	8.686370	15.001448	14.330167
C	8.543239	7.566048	10.843848	H	9.855719	16.259568	15.637174
H	8.428615	6.826953	11.652754	H	7.794947	13.502421	13.054710
H	9.083665	7.076333	10.021211	C	12.873328	12.318144	15.596624
H	7.539964	7.830114	10.475241	C	12.139376	12.121001	16.783568
C	11.534621	7.958985	5.906643	C	14.271338	12.434837	15.702372
C	13.774157	8.071016	7.577592	C	12.781588	12.006452	18.013831
C	11.524988	6.362415	8.282014	H	11.051474	12.057417	16.725618
C	9.735757	8.582709	7.941048	C	14.909568	12.329000	16.938917
C	11.910381	10.347024	7.453213	H	14.853646	12.629351	14.800415
F	13.543772	7.616265	10.608120	C	14.179628	12.103887	18.114489
O	11.422914	7.726281	4.776235	H	12.190586	11.841485	18.918097
O	14.894274	7.886432	7.355629	H	15.995363	12.435700	16.998128
O	11.366934	5.231957	8.469050	C	7.483705	15.907713	14.321267
O	8.586378	8.703772	7.866165	H	7.496797	16.565425	13.435452
O	11.963421	11.478093	7.200411	H	6.548749	15.328587	14.284752
P	12.383783	8.742857	10.306997	H	7.464170	16.551908	15.212443
Si	11.547555	7.011409	12.799979	C	14.868677	11.965135	19.446873
Si	9.460633	9.076248	11.497518	H	14.362945	12.563138	20.220855
W	11.765617	8.354508	7.866554	H	14.856889	10.916113	19.787314
C	13.454181	10.294672	10.739613	H	15.918002	12.287881	19.386680

Table C.9. The optimized cartesian coordinates of complex **10a'**.

C	10.841933	9.299121	11.481207	C	14.307430	8.238966	11.896459
H	10.381429	10.201052	11.026537	C	12.625730	6.487614	11.402352
C	11.166635	8.725588	14.546795	C	14.473193	7.712141	13.127100
H	11.433639	9.163291	15.522944	H	14.936917	9.070538	11.579910
H	11.809755	7.848912	14.383370	C	12.814470	5.972047	12.634793
H	10.125241	8.376669	14.612669	H	11.902904	6.032591	10.724574
C	10.186943	11.456457	13.553845	C	13.740843	6.547037	13.599900
H	9.133870	11.158202	13.630171	H	15.225071	8.146709	13.785715
H	10.276184	12.232403	12.778200	H	12.211663	5.118925	12.944677
H	10.479889	11.918062	14.512040	C	14.210441	7.251036	9.626135
C	13.100742	10.780391	13.252155	H	13.565061	6.857743	8.828664
H	13.023534	11.798983	13.665032	H	14.782000	8.106073	9.238014
H	13.569746	10.860347	12.261932	H	14.916675	6.467221	9.935612
H	13.777826	10.190195	13.884424	C	13.895963	6.039574	14.880287
C	9.552716	6.462139	12.382447	C	14.591497	6.792491	15.944128
H	8.562927	6.073307	12.677140	C	15.456165	6.131443	16.840170
H	10.183888	6.515721	13.279268	C	14.382281	8.171962	16.137399
H	10.005447	5.738184	11.691563	C	16.109032	6.827996	17.854297
C	8.510931	7.939235	9.886520	H	15.612341	5.057587	16.726388
H	9.051306	7.209431	9.268545	C	15.031669	8.863160	17.159470
H	8.483937	8.890967	9.332784	H	13.677676	8.692741	15.489184
H	7.471829	7.590349	10.007975	C	15.914344	8.207597	18.030620
C	8.002677	9.056025	12.639059	H	16.783586	6.294066	18.528103
H	7.786736	10.062258	12.248153	H	14.841086	9.930535	17.295528
H	8.291259	9.153669	13.695362	C	13.368424	4.714343	15.265355
H	7.067437	8.472962	12.597872	C	12.738133	4.531311	16.512542
C	13.385079	12.477999	7.667688	C	13.515140	3.587222	14.434126
C	13.441798	9.615345	7.389561	C	12.246662	3.284608	16.892526
C	10.975021	10.931579	8.175996	H	12.637843	5.386689	17.182508
C	12.334149	12.251235	10.313480	C	13.028861	2.339313	14.823073
C	14.797082	10.886584	9.630109	H	14.038384	3.698824	13.483260
F	11.365264	7.947211	9.203309	C	12.378057	2.166036	16.053668
O	13.655928	13.366291	6.974155	H	11.753261	3.170677	17.860878
O	13.742441	8.888421	6.541710	H	13.169077	1.476353	14.167573
O	9.874320	10.927215	7.817446	C	16.642539	8.960528	19.112804
O	11.995192	13.027293	11.105401	H	17.645631	9.265730	18.769044
O	15.874946	10.872661	10.058311	H	16.098524	9.872927	19.397953
P	12.133669	8.961877	10.237598	H	16.779303	8.337169	20.009191
Si	11.364042	10.024869	13.201121	C	11.825087	0.824898	16.459227
Si	9.287638	8.149245	11.590085	H	11.913312	0.669368	17.544987
W	12.901424	10.927921	8.870484	H	10.754506	0.749568	16.202865
C	13.380959	7.663664	10.874062	H	12.347872	0.006435	15.942987

Table C.10. The optimized cartesian coordinates of complex **10c**.

C	11.133242	8.009621	11.764296	C	12.565240	11.075804	10.070205
H	11.785411	8.492621	12.514825	C	13.681046	9.791668	11.961693
C	10.120241	5.104270	11.213340	C	12.055482	11.969325	10.949055
H	10.052562	4.077549	11.608827	C	13.015898	10.720391	12.843982
H	10.611389	5.046395	10.229147	C	12.235219	11.733745	12.371516
H	9.099635	5.482973	11.063191	H	13.997208	9.506942	9.822104
C	10.427581	6.201828	14.140092	C	11.340963	13.215782	10.510277
H	9.437640	6.660849	14.253864	H	10.311687	13.224103	10.907745
H	11.130665	6.737863	14.799106	H	11.843809	14.117428	10.897658
H	10.367189	5.162705	14.504654	H	11.286534	13.279291	9.415077
C	12.858536	5.484597	12.585091	H	12.495602	11.257614	8.997984
H	12.803336	4.585567	13.221911	H	11.815847	12.459632	13.071992
H	13.506819	6.214988	13.093389	H	13.236851	10.671064	13.909534
H	13.326448	5.212598	11.630405	C	14.664823	8.920713	12.408020
C	9.025358	10.230643	10.850462	C	14.817120	8.559355	13.832022
H	8.215083	10.849334	11.271830	C	13.709249	8.343559	14.676145
H	8.662511	9.815050	9.899721	C	16.098922	8.352727	14.386138
H	9.880526	10.883561	10.632148	C	13.872821	7.957087	16.004900
C	9.612217	9.612032	13.805025	H	12.701506	8.460546	14.277575
H	10.408314	10.372714	13.806384	C	16.258429	7.974502	15.716153
H	9.869257	8.844067	14.550306	H	16.974707	8.498005	13.752616
H	8.671962	10.092250	14.121387	C	15.149158	7.765975	16.552638
C	7.965909	7.685728	12.059560	H	12.992504	7.784552	16.628862
H	8.079095	6.810698	12.712844	H	17.264884	7.834388	16.118124
H	7.747778	7.326728	11.044555	C	15.652431	8.327611	11.479256
H	7.083143	8.250409	12.405407	C	16.022670	6.974503	11.571755
C	10.566888	7.955058	5.932176	C	16.296762	9.120836	10.511200
C	11.772532	6.222028	7.867628	C	16.966164	6.429440	10.703303
C	9.274540	7.489176	8.450101	H	15.546602	6.346021	12.324367
C	10.419914	10.086957	7.832644	C	17.243431	8.573218	9.648162
C	12.958478	8.825841	7.293470	H	16.056256	10.184506	10.456975
F	13.199520	7.189047	10.287316	C	17.587437	7.214023	9.720111
O	10.265974	7.829170	4.819497	H	17.226977	5.371484	10.784676
O	12.136676	5.124432	7.862521	H	17.736123	9.211611	8.911157
O	8.222397	7.091499	8.730795	C	15.330041	7.331160	17.983021
O	10.019855	11.171655	7.753875	H	15.775025	6.323835	18.035953
O	14.005904	9.208680	6.979206	H	16.007759	8.012823	18.521230
P	12.018439	8.315859	10.205385	H	14.368346	7.307165	18.515168
Si	11.122093	6.182917	12.379580	C	18.579946	6.613953	8.759634
Si	9.434956	8.869603	12.080347	H	19.083753	5.741410	9.201068
W	11.109577	8.161712	7.865569	H	18.074437	6.274669	7.839484
C	13.204571	9.804946	10.522125	H	19.342690	7.349352	8.463198

Table C.11. The optimized cartesian coordinates of complex **10c'**.

C	11.025661	8.424062	11.694447	C	14.431431	7.952827	10.818225
H	10.226695	9.145741	11.421020	C	13.161155	5.752393	10.557437
C	12.703370	8.429478	14.431126	C	14.927480	7.551188	12.009531
H	13.498571	9.032821	14.899015	C	13.690336	5.428233	11.864452
H	13.153106	7.503274	14.051297	C	14.514525	6.266561	12.549094
H	11.983192	8.160258	15.217244	H	13.588988	7.203628	9.003682
C	10.517119	10.485900	13.887468	C	15.921776	8.368451	12.781716
H	9.802758	9.864731	14.445269	H	15.492189	8.660806	13.754780
H	9.957969	11.071289	13.141874	H	16.834460	7.786842	12.991602
H	10.969290	11.196299	14.599440	H	16.200682	9.281083	12.236923
C	13.175801	10.703180	12.479345	H	14.779307	8.883370	10.369995
H	13.527770	11.249703	13.371309	H	14.950419	5.938930	13.495481
H	12.768523	11.443367	11.779100	H	13.512805	4.428582	12.256876
H	14.045281	10.223216	12.014631	C	12.594207	4.788389	9.743300
C	9.311902	5.787154	11.062357	C	12.187431	3.451073	10.228677
H	8.682482	5.031151	11.561462	C	11.538203	3.252671	11.461377
H	10.114206	5.267943	10.523922	C	12.413177	2.313552	9.423537
H	8.695409	6.318148	10.322158	C	11.155649	1.978964	11.880285
C	8.417637	7.773312	13.144980	H	11.309579	4.115717	12.082865
H	8.000942	8.558718	12.494674	C	12.038765	1.042935	9.850779
H	8.616882	8.218935	14.129849	H	12.897667	2.440472	8.454485
H	7.639178	7.004019	13.279658	C	11.401036	0.849349	11.087394
C	10.797250	5.962983	13.739442	H	10.643963	1.857126	12.838191
H	10.769456	6.492018	14.702133	H	12.241194	0.179620	9.212057
H	11.847828	5.732475	13.513157	C	12.421667	4.983911	8.281978
H	10.252229	5.012376	13.863832	C	11.180995	4.742373	7.670795
C	11.921546	11.897210	7.293493	C	13.512685	5.314132	7.460486
C	10.175933	9.690021	7.747965	C	11.028397	4.870795	6.291257
C	10.899268	11.385434	9.951755	H	10.330309	4.464528	8.294980
C	13.738543	10.988600	9.283402	C	13.359847	5.424915	6.079210
C	12.991641	9.199741	7.210166	H	14.493899	5.464216	7.916204
F	10.834641	7.259922	9.275690	C	12.112590	5.218360	5.471527
O	11.901058	12.799058	6.564593	H	10.050672	4.695968	5.836081
O	9.178668	9.344736	7.277048	H	14.222232	5.679443	5.459601
O	10.278001	11.964372	10.742869	C	10.974257	-0.525814	11.529322
O	14.771259	11.381944	9.635888	H	10.157941	-0.908525	10.894380
O	13.600551	8.577364	6.446746	H	11.806899	-1.242901	11.452782
P	11.825859	8.285174	10.054528	H	10.618861	-0.516006	12.569726
Si	11.890502	9.471422	13.085013	C	11.941945	5.388464	3.984658
Si	9.949434	6.964529	12.385088	H	11.041355	4.869476	3.625452
W	11.949212	10.328895	8.561897	H	11.840188	6.455579	3.724569
C	13.378422	7.183370	10.083694	H	12.814030	5.000795	3.436459

Table C.12. The optimized cartesian coordinates of complex **10d** (singlet state).

C	14.829595	9.983363	13.653465	C	14.289181	7.053898	8.229719
C	14.623967	10.318108	14.977917	C	16.139726	9.475344	8.332914
C	14.790473	9.299467	15.979310	H	15.335646	6.849711	11.283741
C	15.100556	7.982962	15.605938	H	18.525202	5.607467	7.966600
C	15.268450	7.598631	14.289721	H	18.666361	7.299341	8.491604
C	15.145854	8.611025	13.200774	H	17.215504	6.758464	7.607374
C	14.141524	11.647392	15.360499	H	15.148802	4.764645	9.015964
C	14.529556	12.231690	16.629304	H	15.458676	4.302153	10.707138
C	13.679761	13.132815	17.324173	H	16.490384	3.665159	9.411018
C	14.052846	13.677177	18.545820	H	18.845745	4.336659	10.621408
C	15.290344	13.363497	19.138925	H	18.050884	4.927146	12.092758
C	16.134711	12.470295	18.461074	H	19.332152	5.893528	11.323492
C	15.769638	11.915018	17.238472	H	13.046646	9.743673	9.391567
C	15.701075	13.987703	20.445229	H	13.983735	10.043054	10.874946
C	15.509668	6.174541	13.900936	H	12.982077	8.574818	10.726289
P	16.712888	8.596083	12.034818	H	13.646231	6.345051	8.773707
C	16.118851	7.416781	10.739715	H	15.025913	6.476687	7.653052
Si	15.081638	8.326306	9.378506	H	13.653536	7.600292	7.512551
C	13.649513	9.261371	10.179175	H	17.046474	8.969337	7.970713
C	13.270519	12.381018	14.450683	H	16.444914	10.370988	8.890424
C	13.314873	13.793084	14.365805	H	15.561552	9.797192	7.450767
C	12.485488	14.491451	13.491527	H	10.790257	11.877265	12.133222
C	11.566884	13.823981	12.667619	H	9.626651	14.271680	11.824806
C	11.509471	12.420266	12.751579	H	10.747559	15.660743	11.876831
C	12.341179	11.714786	13.610993	H	10.964172	14.372518	10.665815
C	10.679620	14.575876	11.711985	H	12.705663	13.372778	16.896708
W	18.983470	8.821764	13.095657	H	16.453984	11.243440	16.723536
C	19.809965	8.409089	11.275965	H	13.368229	14.351882	19.065978
O	20.299086	8.209132	10.242965	H	17.103267	12.215966	18.898295
F	16.428821	10.030128	11.292892	H	14.616664	9.548491	17.024625
C	18.909544	10.818372	12.619377	H	14.700211	10.745867	12.887461
O	18.876442	11.950327	12.392080	H	15.184309	7.217287	16.381703
C	18.222162	9.286156	14.938660	H	14.396023	8.274020	12.451808
O	17.908748	9.544454	16.023407	H	16.519057	13.423180	20.915784
C	20.828340	9.105440	13.854200	H	14.854876	14.033678	21.148182
O	21.895395	9.266102	14.279046	H	16.053122	15.022521	20.292460
C	19.025622	6.901645	13.783110	H	15.546142	5.518309	14.781357
O	19.056756	5.852740	14.276943	H	14.714067	5.813734	13.221772
Si	17.161695	5.980920	9.997928	H	16.459352	6.057799	13.347759
C	17.959116	6.466176	8.363442	H	12.556982	15.580341	13.434904
C	15.939367	4.558651	9.747998	H	14.033177	14.333805	14.982779
C	18.471653	5.243520	11.127118	H	12.273283	10.627831	13.663663

Table C.13. The optimized cartesian coordinates of complex **10d** (triplet state).

C	11.104103	8.673059	11.908317	C	12.787011	11.280351	10.537915
H	11.645062	9.413592	12.527806	C	14.089179	9.781863	12.053403
C	10.634696	5.594435	12.072607	C	12.449418	12.019402	11.654043
H	10.619180	4.709138	12.729059	C	13.698895	10.530009	13.169571
H	11.387898	5.418606	11.289363	C	12.829162	11.647306	12.957063
H	9.650788	5.673735	11.587016	H	14.177781	9.754078	9.897082
C	9.755539	7.371049	14.432680	C	12.471256	11.728312	9.149083
H	8.748105	7.620426	14.073848	H	11.957125	12.699674	9.149117
H	10.080134	8.150852	15.139474	H	13.392787	11.812132	8.547196
H	9.690350	6.424192	14.995319	H	11.829602	10.996718	8.631154
C	12.688753	6.959894	13.972514	C	14.144327	10.173355	14.505868
H	12.587762	6.211855	14.776630	C	13.251701	10.382963	15.638594
H	12.972392	7.914868	14.441708	C	11.847776	10.293382	15.491413
H	13.507259	6.650285	13.309933	C	13.743769	10.654903	16.939123
C	9.314494	10.798131	10.320177	C	10.989625	10.469509	16.571397
H	8.370003	11.356366	10.437421	H	11.430284	10.056255	14.514281
H	9.315253	10.367432	9.312931	C	12.879742	10.833241	18.013806
H	10.141532	11.517367	10.395950	H	14.821221	10.738908	17.085745
C	9.111681	10.482723	13.285011	C	11.484546	10.745382	17.855434
H	9.898141	11.247683	13.393587	H	9.910837	10.381945	16.418043
H	9.112944	9.862196	14.190424	H	13.290916	11.054359	19.001994
H	8.142329	11.004771	13.228386	C	15.439301	9.538072	14.705162
C	8.024555	8.249966	11.399745	C	15.637058	8.569647	15.719988
H	8.099447	7.373978	12.059510	C	16.547828	9.844574	13.880687
H	8.033735	7.885188	10.362796	C	16.868860	7.950620	15.895742
H	7.044713	8.723827	11.576152	H	14.792380	8.288813	16.349749
C	11.485669	6.850086	6.280965	C	17.779666	9.224300	14.068239
C	12.853465	6.010243	8.545966	H	16.427551	10.593187	13.096549
C	10.041922	6.629271	8.757757	C	17.968000	8.267103	15.077942
C	10.507638	9.166642	7.443766	H	16.983286	7.190925	16.673022
C	13.344009	8.698685	7.519845	H	18.621083	9.489367	13.423440
F	13.267651	7.330192	11.023401	C	10.558471	10.951013	19.024235
O	11.373609	6.377565	5.227956	H	10.854176	10.325278	19.881331
O	13.486780	5.062900	8.733370	H	10.581364	11.999374	19.366223
O	9.103468	6.029022	9.073509	H	9.521062	10.704879	18.755946
O	9.840129	9.976088	6.948824	C	19.305449	7.610953	15.294064
O	14.277125	9.301729	7.188912	H	19.813848	8.035037	16.176809
P	12.206735	8.459004	10.476678	H	19.193457	6.530239	15.472866
Si	11.045167	7.129670	13.073193	H	19.964506	7.755553	14.425888
Si	9.391791	9.512459	11.689493	H	11.899820	12.953517	11.510337
W	11.693076	7.649357	8.115016	H	12.531864	12.255123	13.810401
C	13.484477	9.981677	10.724860	H	14.744900	8.924943	12.192111

Table C.14. The optimized cartesian coordinates of complex **11**.

C	12.190188	10.334644	11.773437	H	7.118767	13.804002	13.508484
C	12.907055	9.837234	13.031432	C	11.121172	7.462387	11.753447
C	12.201670	9.271199	14.112928	H	11.375654	7.802427	12.775054
H	11.112371	9.260913	14.103882	C	12.859914	5.238349	10.152362
C	12.861529	8.752536	15.227960	H	13.652818	4.505977	10.380976
H	12.276077	8.329714	16.047889	H	13.312375	6.047807	9.565521
C	14.257652	8.757801	15.311677	H	12.110604	4.730516	9.530123
C	14.965612	9.322555	14.242125	C	11.087833	4.350868	12.416428
H	16.057307	9.351259	14.277435	H	10.152548	4.213462	11.855406
C	14.308942	9.850453	13.131462	H	10.841087	4.441609	13.483322
H	14.902213	10.281952	12.327697	H	11.693756	3.438271	12.285042
C	13.062245	11.330034	10.967641	C	13.495086	6.077817	13.067643
C	14.128069	10.945445	10.133037	H	14.158557	5.198925	13.123919
H	14.381717	9.898198	10.004075	H	13.059984	6.240269	14.066163
C	14.897458	11.890418	9.451876	H	14.101816	6.963034	12.828875
H	15.701703	11.545857	8.797640	C	8.251072	8.848182	11.946069
C	14.652513	13.261481	9.579737	H	7.216679	8.586709	12.228669
C	13.607300	13.650927	10.426941	H	8.211843	9.378228	10.988250
H	13.385583	14.713532	10.552451	H	8.642668	9.549090	12.699362
C	12.830519	12.710781	11.102493	C	8.925219	6.413660	13.557292
H	12.020017	13.065532	11.737376	H	9.724317	6.657314	14.276106
C	10.837562	11.012420	12.042386	H	8.860508	5.319559	13.488742
C	10.005337	11.324245	10.956723	H	7.975917	6.785240	13.975190
H	10.302064	11.009460	9.960410	C	8.528516	6.186839	10.478613
C	8.827744	12.047720	11.112402	H	9.136267	5.294723	10.271000
H	8.205848	12.252207	10.238172	H	8.452857	6.763354	9.545025
C	8.430344	12.514679	12.372493	H	7.511523	5.853404	10.743962
C	9.286445	12.263186	13.451018	C	11.090241	8.819421	6.177797
H	9.031323	12.655753	14.438380	C	13.345761	8.388217	7.870396
C	10.472356	11.540407	13.290451	C	10.866629	6.842641	8.094115
H	11.129281	11.421918	14.149705	C	9.386399	9.244438	8.430968
C	14.976535	8.159292	16.491239	C	11.785336	10.824439	8.002778
H	14.280224	7.949312	17.315947	F	13.456656	8.178569	10.778814
H	15.764892	8.833036	16.861920	O	10.939983	8.810498	5.027401
H	15.463788	7.211000	16.208395	O	14.463132	8.151612	7.689857
C	15.490707	14.279388	8.852465	O	10.545191	5.741193	7.933148
H	16.321723	14.629397	9.488369	O	8.255820	9.487609	8.520787
H	14.892933	15.160921	8.576688	O	11.969666	11.947490	7.800309
H	15.928658	13.852109	7.938594	P	11.897921	8.699111	10.671422
C	7.133902	13.257880	12.554031	Si	12.135334	5.794649	11.797082
H	6.281168	12.558301	12.551809	Si	9.220195	7.240930	11.874901
H	6.968929	13.974960	11.735347	W	11.363867	8.818633	8.168221

9 Bibliography

(1) E.J. Corey, X. M. C. In *The Logic of Chemical Synthesis*; Wiley: New York, 1989.

(2) Enders, D.; Hoffmann, R. W. *Chem. Unserer Zeit* **1985**, *19*, 177.

(3) E., F. *Ber. d. Deutsch. Chem. Ges* **1894**, *27*, 2985.

(4) Yang, D. *Accounts Chem. Res.* **2004**, *37*, 497.

(5) Jose´ Justicia, J. L. O.-L. p., Araceli G. Campan˜a, J. Enrique Oltra, Juan M. Cuerva, Elena Bun˜ uel, Diego J. Ca´rdenas *Journal of the American Chemical Socitey* **2005**, *127*, 14911.

(6) Justicia, J.; Rosales, A.; Bunuel, E.; Oller-Lopez, J. L.; Valdivia, N.; Haidour, A.; Oltra, J. E.; Barrero, A. F.; Cardenas, D. J.; Cuerva, J. M. *Chem.-Eur. J.* **2004**, *10*, 1778.

(7) Jana, S.; Guin, C.; Roy, S. C. *Tetrahedron Lett.* **2004**, *45*, 6575.

(8) J. M. Cuerva, J. J., J. L. Oller-López, B. Bazdi and J. E. Oltra *Mini-Reviews in Organic Chemistry* **2006**, *3*, 23.

(9) Ziegler, F. E.; Sarpong, M. A. *Tetrahedron* **2003**, *59*, 9013.

(10) Paterson, I.; Berrisford, D. J. *Angew. Chem.-Int. Edit. Engl.* **1992**, *31*, 1179.

(11) Jacobsen, E. N. *Accounts Chem. Res.* **2000**, *33*, 421.

(12) Nugent, W. A. *J. Am. Chem. Soc.* **1992**, *114*, 2768.

(13) Tokunaga, M.; Larrow, J. F.; Kakiuchi, F.; Jacobsen, E. N. *Science* **1997**, *277*, 936.

(14) Katsuki, T.; Sharpless, K. B. *J. Am. Chem. Soc.* **1980**, *102*, 5974.

(15) Zhang, W.; Loebach, J. L.; Wilson, S. R.; Jacobsen, E. N. *J. Am. Chem. Soc.* **1990**, *112*, 2801.

(16) Irie, R.; Noda, K.; Ito, Y.; Matsumoto, N.; Katsuki, T. *Tetrahedron Lett.* **1990**, *31*, 7345.

(17) Gansauer, A.; Narayan, S. *Adv. Synth. Catal.* **2002**, *344*, 465.

(18) Gansauer, A.; Fan, C. A.; Keller, F.; Karbaum, P. *Chem.-Eur. J.* **2007**, *13*, 8084.

(19) Nugent, W. A.; Rajanbabu, T. V. *J. Am. Chem. Soc.* **1988**, *110*, 8561.

(20) Rajanbabu, T. V.; Nugent, W. A. *J. Am. Chem. Soc.* **1989**, *111*, 4525.

(21) Rajanbabu, T. V.; Nugent, W. A.; Beattie, M. S. *J. Am. Chem. Soc.* **1990**, *112*, 6408.

(22) Rajanbabu, T. V.; Nugent, W. A. *J. Am. Chem. Soc.* **1994**, *116*, 986.

(23) Samsel, E. G.; Srinivasan, K.; Kochi, J. K. *J. Am. Chem. Soc.* **1985**, *107*, 7606.

(24) Shaik, S.; Kumar, D.; de Visser, S. P.; Altun, A.; Thiel, W. *Chem. Rev.* **2005**, *105*, 2279.

(25) Brown, H. C.; Ikegami, S.; Kawakami, J. H. *J. Org. Chem.* **1970**, *35*, 3243.

(26) Barluenga, J.; Florez, J.; Yus, M. *J. Chem. Soc.-Chem. Commun.* **1982**, 1153.

(27) Barluenga, J.; Fananas, F. J.; Villamana, J.; Yus, M. *J. Chem. Soc.-Perkin Trans. 1* **1984**, 2685.

(28) Benkeser, R. A.; Rappa, A.; Wolsieffer, L. A. *J. Org. Chem.* **1986**, *51*, 3391.

(29) Bartmann, E. *Angew. Chem.-Int. Edit. Engl.* **1986**, *25*, 653.

(30) Cohen, T.; Jeong, I. H.; Mudryk, B.; Bhupathy, M.; Awad, M. M. A. *J. Org. Chem.* **1990**, *55*, 1528.

(31) Dorigo, A. E.; Houk, K. N.; Cohen, T. *J. Am. Chem. Soc.* **1989**, *111*, 8976.

(32) P. Renaud, M. S. In *Radicals in organic synthesis*; Wiley-VCH: Weinheim, 2001; Vol. Vol. 2.

(33) McCarroll, A. J.; Walton, J. C. *Angew. Chem.-Int. Edit.* **2001**, *40*, 2225.

(34) Lewis, F. M.; Mayo, F. R.; Hulse, W. F. *J. Am. Chem. Soc.* **1945**, *67*, 1701.

(35) Mayo, F. R.; Walling, C.; Lewis, F. M.; Hulse, W. F. *J. Am. Chem. Soc.* **1948**, *70*, 1523.

(36) Mayo, F. R.; Lewis, F. M.; Walling, C. *Discussions of the Faraday Society* **1947**, *2*, 285.

(37) Hart, D. J. *Science* **1984**, *223*, 883.

(38) Giese, B. *Angew. Chem.-Int. Edit. Engl.* **1985**, *24*, 553.
(39) Gomberg, M. *Berichte Der Deutschen Chemischen Gesellschaft* **1900**, *33*, 3150.
(40) C., W. *Ber. Chem. Gesell.* **1879**, *12*, 522.
(41) L. MICHAELIS, M. P. S., S. GRANICK *J. Am. Chem. Soc.* **1939**, *61*, 1981.
(42) Kharasch, M. S.; Kuderna, B. M.; Urry, W. *J. Org. Chem.* **1948**, *13*, 895.
(43) Kharasch, M. S.; Jensen, E. V.; Urry, W. H. *J. Am. Chem. Soc.* **1947**, *69*, 1100.
(44) Kharasch, M. S.; Urry, W. H.; Jensen, E. V. *J. Am. Chem. Soc.* **1945**, *67*, 1626.
(45) Spellmeyer, D. C.; Houk, K. N. *J. Org. Chem.* **1987**, *52*, 959.
(46) Beckwith, A. L. J. *Tetrahedron* **1981**, *37*, 3073.
(47) Porter, N. A.; Magnin, D. R.; Wright, B. T. *J. Am. Chem. Soc.* **1986**, *108*, 2787.
(48) Stork, G. *Bull. Chem. Soc. Jpn.* **1988**, *61*, 149.
(49) Ouertani, M.; Collin, J.; Kagan, H. B. *Tetrahedron* **1985**, *41*, 3689.
(50) Girard, P.; Namy, J. L.; Kagan, H. B. *J. Am. Chem. Soc.* **1980**, *102*, 2693.
(51) Molander, G. A.; Wolfe, C. N. *J. Org. Chem.* **1998**, *63*, 9031.
(52) Miyabe, H.; Torieda, M.; Kiguchi, T.; Naito, T. *Synlett* **1997**, 580.
(53) Sturino, C. F.; Fallis, A. G. *J. Am. Chem. Soc.* **1994**, *116*, 7447.
(54) Fukuzawa, S.; Nakanishi, A.; Fujinami, T.; Sakai, S. *J. Chem. Soc.-Perkin Trans. 1* **1988**, 1669.
(55) Molander, G. A. *Chem. Rev.* **1992**, *92*, 29.
(56) Kagan, H. B. *Tetrahedron* **2003**, *59*, 10351.
(57) Rowlands, G. J. *Tetrahedron* **2009**, *65*, 8603.
(58) Souppe, J.; Danon, L.; Namy, J. L.; Kagan, H. B. *J. Organomet. Chem.* **1983**, *250*, 227.
(59) Kagan, H. B.; Namy, J. L.; Girard, P. *Tetrahedron* **1981**, *37*, 175.
(60) Suginome, H.; Yamada, S. *Tetrahedron Lett.* **1987**, *28*, 3963.
(61) Stork, G.; Sher, P. M.; Chen, H. L. *J. Am. Chem. Soc.* **1986**, *108*, 6384.
(62) Curran, D. P.; Rakiewicz, D. M. *J. Am. Chem. Soc.* **1985**, *107*, 1448.
(63) Curran, D. P.; Rakiewicz, D. M. *Tetrahedron* **1985**, *41*, 3943.
(64) Fevig, T. L.; Elliott, R. L.; Curran, D. P. *J. Am. Chem. Soc.* **1988**, *110*, 5064.
(65) Curran, D. P.; Chen, M. H. *Tetrahedron Lett.* **1985**, *26*, 4991.
(66) Corey, E. J.; Ghosh, A. K. *Tetrahedron Lett.* **1988**, *29*, 3205.
(67) Baguley, P. A.; Walton, J. C. *Angew. Chem.-Int. Edit.* **1998**, *37*, 3073.
(68) Studer, A.; Amrein, S. *Synthesis* **2002**, 835.
(69) Ollivier, C.; Renaud, P. *Chem. Rev.* **2001**, *101*, 3415.
(70) Renaud, P.; Gerster, M. *Angew. Chem.-Int. Edit.* **1998**, *37*, 2563.
(71) Sibi, M. P.; Manyem, S.; Zimmerman, J. *Chem. Rev.* **2003**, *103*, 3263.
(72) Gansauer, A.; Bluhm, H. *Chem. Rev.* **2000**, *100*, 2771.
(73) Gansauer, A.; Pierobon, M.; Bluhm, H. *Angew. Chem.-Int. Edit.* **1998**, *37*, 101.
(74) Yang, X. M.; Stern, C. L.; Marks, T. J. *J. Am. Chem. Soc.* **1994**, *116*, 10015.
(75) Shapiro, P. J.; Cotter, W. D.; Schaefer, W. P.; Labinger, J. A.; Bercaw, J. E. *J. Am. Chem. Soc.* **1994**, *116*, 4623.
(76) Coates, G. W.; Waymouth, R. M. *Science* **1995**, *267*, 217.
(77) Xu, G. X. *Macromolecules* **1998**, *31*, 2395.
(78) Xu, G. X.; Ruckenstein, E. *Macromolecules* **1998**, *31*, 4724.
(79) Kaminsky, W.; Kulper, K.; Brintzinger, H. H.; Wild, F. *Angew. Chem.-Int. Edit. Engl.* **1985**, *24*, 507.
(80) Jordan, R. F.; Bajgur, C. S.; Willett, R.; Scott, B. *J. Am. Chem. Soc.* **1986**, *108*, 7410.
(81) Kim, H. J.; Maria, L. C. D. *Eur. Polym. J.* **1994**, *30*, 1295.
(82) Ewen, J. A.; Jones, R. L.; Razavi, A.; Ferrara, J. D. *J. Am. Chem. Soc.* **1988**, *110*, 6255.
(83) Ewen, J. A. *J. Am. Chem. Soc.* **1984**, *106*, 6355.
(84) Erker, G.; Nolte, R.; Tsay, Y. H.; Kruger, C. *Angew. Chem.-Int. Edit. Engl.* **1989**, *28*, 628.
(85) Okuda, J. *Chem. Berichte* **1990**, *123*, 1649.

(86) Miyatake, T.; Mizunuma, K.; Seki, Y.; Kakugo, M. *Makromolekulare Chemie-Rapid Communications* **1989**, *10*, 349.
(87) Sernetz, F. G.; Mulhaupt, R.; Fokken, S.; Okuda, J. *Macromolecules* **1997**, *30*, 1562.
(88) Grassi, A.; Lamberti, C.; Zambelli, A.; Mingozzi, I. *Macromolecules* **1997**, *30*, 1884.
(89) Ishihara, N.; Kuramoto, M.; Uoi, M. *Macromolecules* **1988**, *21*, 3356.
(90) Pellecchia, C.; Longo, P.; Grassi, A.; Ammendola, P.; Zambelli, A. *Makromolekulare Chemie-Rapid Communications* **1987**, *8*, 277.
(91) Soga, K.; Nakatani, H.; Monoi, T. *Macromolecules* **1990**, *23*, 953.
(92) Zambelli, A.; Oliva, L.; Pellecchia, C. *Macromolecules* **1989**, *22*, 2129.
(93) Longo, P.; Proto, A.; Oliva, L. *Macromol. Rapid Commun.* **1994**, *15*, 151.
(94) Ready, T. E.; Day, R. O.; Chien, J. C. W.; Rausch, M. D. *Macromolecules* **1993**, *26*, 5822.
(95) Flores, J. C.; Chien, J. C. W.; Rausch, M. D. *Organometallics* **1994**, *13*, 4140.
(96) Foster, P.; Chien, J. C. W.; Rausch, M. D. *Organometallics* **1996**, *15*, 2404.
(97) Asandei, A. D.; Moran, I. W. *J. Am. Chem. Soc.* **2004**, *126*, 15932.
(98) Mahanthappa, M. K.; Waymouth, R. M. *J. Am. Chem. Soc.* **2001**, *123*, 12093.
(99) Bohm, L. L. *Angew. Chem.-Int. Edit.* **2003**, *42*, 5010.
(100) Knecht, E.; Hibbert, E. *Berichte Der Deutschen Chemischen Gesellschaft* **1903**, *36*, 1549.
(101) Knecht, E. *Berichte Der Deutschen Chemischen Gesellschaft* **1903**, *36*, 166.
(102) Black, I. A.; Hirst, E. L.; Macbeth, A. K. *Journal of the Chemical Society* **1922**, *121*, 2527.
(103) Vantamel.Ee; Schwartz, M. A. *J. Am. Chem. Soc.* **1965**, *87*, 3277.
(104) Ammeter, J. H. O., N.; Bucher, R. *Helv. Chim. Acta* **1975**, *58*, 671.
(105) Prout, K. C., T. S.; Forder, S. R.; Critchley, B.; Denton, B.; Rees, G. V. *Acta Crystallogr. Sect. B* **1974**, *30*, 2290.
(106) Petersen, J. L.; Dahl, L. F. *J. Am. Chem. Soc.* **1974**, *96*, 2248.
(107) Petersen, J. L.; Dahl, L. F. *J. Am. Chem. Soc.* **1975**, *97*, 6416.
(108) Petersen, J. L.; Lichtenberger, D. L.; Fenske, R. F.; Dahl, L. F. *J. Am. Chem. Soc.* **1975**, *97*, 6433.
(109) Gansauer, A.; Lauterbach, T.; Bluhm, H.; Noltemeyer, M. *Angew. Chem.-Int. Edit.* **1999**, *38*, 2909.
(110) Cesarotti, E.; Kagan, H. B.; Goddard, R.; Kruger, C. *J. Organomet. Chem.* **1978**, *162*, 297.
(111) Wild, F.; Zsolnai, L.; Huttner, G.; Brintzinger, H. H. *J. Organomet. Chem.* **1982**, *232*, 233.
(112) Collins, S.; Kuntz, B. A.; Taylor, N. J.; Ward, D. G. *J. Organomet. Chem.* **1988**, *342*, 21.
(113) Halterman, R. L. *Chem. Rev.* **1992**, *92*, 965.
(114) Cesarotti, E.; Ugo, R.; Kagan, H. B. *Angew. Chem.-Int. Edit. Engl.* **1979**, *18*, 779.
(115) Cesarotti, E.; Ugo, R.; Vitiello, R. *Journal of Molecular Catalysis* **1981**, *12*, 63.
(116) Colletti, S. L.; Halterman, R. L. *Tetrahedron Lett.* **1992**, *33*, 1005.
(117) Collins, S.; Kuntz, B. A.; Hong, Y. *J. Org. Chem.* **1989**, *54*, 4154.
(118) Martin, H. A.; Jellinek, F. *J. Organomet. Chem.* **1967**, *8*, 115.
(119) Coutts, R. S. P.; Wailes, P. C. *Aust. J. Chem.* **1967**, *20*, 1579.
(120) Nöth, H., Hartwimmer, R. *Chem. Ber.* **1960**, *93*, 2238.
(121) Noth, H.; Voitlander, J.; Nussbaum, M. *Naturwissenschaften* **1960**, *47*, 57.
(122) Nöth, H., Hartwimmer, R. *Chem. Ber.* **1960**, *93*, 2246.
(123) Martin, R. L.; Winter, G. *Journal of the Chemical Society* **1965**, 4709.
(124) Reid, A. F.; Wailes, P. C. *Aust. J. Chem.* **1965**, *18*, 9.
(125) Giddings, S. A.; Best, R. J. *J. Am. Chem. Soc.* **1961**, *83*, 2393.

(126) Druce, P. M.; Kingston, B. M.; Lappert, M. F.; Spalding, T. R.; Srivasta.Rc *Journal of the Chemical Society a -Inorganic Physical Theoretical* **1969**, 2106.
(127) Salzmann, J. J. *Helvetica Chimica Acta* **1968**, *51*, 526.
(128) Reid, A. F.; Scaife, D. E.; Wailes, P. C. *Spectrochimica Acta* **1964**, *20*, 1257.
(129) Corbin, D. R.; Atwood, J. L.; Stucky, G. D. *Inorg. Chem.* **1986**, *25*, 98.
(130) Coutts, R. W., P. C. *Inorg. Nucl. Chem. Letters* **1967**, *3*, 1.
(131) McMurry, J. E. *Chem. Rev.* **1989**, *89*, 1513.
(132) Furstner, A.; Bogdanovic, B. *Angew. Chem.-Int. Edit. Engl.* **1996**, *35*, 2442.
(133) R., F. *Liebigs Ann.* **1859**, *110*, 23.
(134) Raubenheimer, H. G.; Seebach, D. *Chimia* **1986**, *40*, 12.
(135) Handa, Y.; Inanaga, J. *Tetrahedron Lett.* **1987**, *28*, 5717.
(136) Barden, M. C.; Schwartz, J. *J. Am. Chem. Soc.* **1996**, *118*, 5484.
(137) Mukaiyama, T.; Kagayama, A.; Shiina, I. *Chem. Lett.* **1998**, 1107.
(138) Matsubara, S.; Hashimoto, Y.; Okano, T.; Utimoto, K. *Synlett* **1999**, 1411.
(139) Gansauer, A. *Chem. Commun.* **1997**, 457.
(140) Gansauer, A.; Moschioni, M.; Bauer, D. *Eur. J. Org. Chem.* **1998**, 1923.
(141) Gansauer, A.; Bauer, D. *J. Org. Chem.* **1998**, *63*, 2070.
(142) Corey, E. J.; Zheng, G. Z. *Tetrahedron Lett.* **1997**, *38*, 2045.
(143) Dunlap, M. S.; Nicholas, K. M. *Synth. Commun.* **1999**, *29*, 1097.
(144) Azizi, N.; Saidi, M. R. *Org. Lett.* **2005**, *7*, 3649.
(145) Daasbjerg, K.; Svith, H.; Grimme, S.; Gerenkamp, M.; Muck-Lichtenfeld, C.; Gansauer, A.; Barchuk, A.; Keller, F. *Angew. Chem.-Int. Edit.* **2006**, *45*, 2041.
(146) Kochi, J. K.; Singleto.Dm; Andrews, L. J. *Tetrahedron* **1968**, *24*, 3503.
(147) Hardouin, C.; Doris, E.; Rousseau, B.; Mioskowski, C. *Org. Lett.* **2002**, *4*, 1151.
(148) Hardouin, C.; Doris, E.; Rousseau, B.; Mioskowski, C. *J. Org. Chem.* **2002**, *67*, 6571.
(149) Gansauer, A.; Bluhm, H.; Pierobon, M. *J. Am. Chem. Soc.* **1998**, *120*, 12849.
(150) Barrero, A. F.; Rosales, A.; Cuerva, J. M.; Oltra, J. E. *Org. Lett.* **2003**, *5*, 1935.
(151) Gansauer, A.; Barchuk, A.; Fielenbach, D. *Synthesis* **2004**, 2567.
(152) Chakraborty, T. K.; Das, S. *Tetrahedron Lett.* **2002**, *43*, 2313.
(153) Hardouin, C.; Chevallier, F.; Rousseau, B.; Doris, E. *J. Org. Chem.* **2001**, *66*, 1046.
(154) Gansauer, A.; Bluhm, H.; Lauterbach, T. *Adv. Synth. Catal.* **2001**, *343*, 785.
(155) Gansauer, A.; Bluhm, H.; Pierobon, M.; Keller, M. *Organometallics* **2001**, *20*, 914.
(156) Gansauer, A.; Franke, D.; Lauterbach, T.; Nieger, M. *J. Am. Chem. Soc.* **2005**, *127*, 11622.
(157) Dotz, K. H.; da Silva, E. G. *Tetrahedron* **2000**, *56*, 8291.
(158) Gansauer, A.; Bluhm, H.; Rinker, B.; Narayan, S.; Schick, M.; Lauterbach, T.; Pierobon, M. *Chem.-Eur. J.* **2003**, *9*, 531.
(159) Giese, B. *Angew. Chem.-Int. Edit.* **1989**, *28*, 969.
(160) Baldwin, J. E. *J. Chem. Soc.-Chem. Commun.* **1976**, 734.
(161) Clive, D. L. J.; Magnuson, S. R. *Tetrahedron Lett.* **1995**, *36*, 15.
(162) Clive, D. L. J.; Magnuson, S. R.; Manning, H. W.; Mayhew, D. L. *J. Org. Chem.* **1996**, *61*, 2095.
(163) Maiti, G.; Roy, S. C. *J. Chem. Soc.-Perkin Trans. 1* **1996**, 403.
(164) Mandal, P. K.; Maiti, G.; Roy, S. C. *J. Org. Chem.* **1998**, *63*, 2829.
(165) Gansauer, A.; Pierobon, M.; Bluhm, H. *Synthesis* **2001**, 2500.
(166) Gansauer, A.; Pierobon, M. *Synlett* **2000**, 1357.
(167) Gansauer, A.; Pierobon, M.; Bluhm, H. *Angew. Chem.-Int. Edit.* **2002**, *41*, 3206.
(168) Justicia, J.; Oltra, J. E.; Cuerva, J. M. *J. Org. Chem.* **2005**, *70*, 8265.
(169) In *Radicals in Organic Synthesis*; P. Renaud, M. S., Ed.; Wiley-VCH: Weinheim, 2001.
(170) Smith, D. M.; Nicolaides, A.; Golding, B. T.; Radom, L. *J. Am. Chem. Soc.* **1998**, *120*, 10223.

(171) Gansauer, A.; Lauterbach, T.; Geich-Gimbel, D. *Chem.-Eur. J.* **2004**, *10*, 4983.
(172) Newcomb, M.; Choi, S. Y.; Horner, J. H. *J. Org. Chem.* **1999**, *64*, 1225.
(173) Park, S. U.; Varick, T. R.; Newcomb, M. *Tetrahedron Lett.* **1990**, *31*, 2975.
(174) Bowry, V. W.; Lusztyk, J.; Ingold, K. U. *J. Am. Chem. Soc.* **1991**, *113*, 5687.
(175) Beesley, R. M.; Ingold, C. K.; Thorpe, J. F. *Journal of the Chemical Society* **1915**, *107*, 1080.
(176) Ingold, C. K. *Journal of the Chemical Society* **1921**, *119*, 305.
(177) Allinger, N. L.; Zalkow, V. *J. Org. Chem.* **1960**, *25*, 701.
(178) P. Piccardi, P. M., M. Modena, E. Santoro *J. Chem. Soc. Perkin Trans. 1* **1973**, 982.
(179) Simmons, H. E.; Smith, R. D. *J. Am. Chem. Soc.* **1958**, *80*, 5322.
(180) Hegedus, L. S. In *Transition Metals in the Synthesis of Complex Organic Molecules*; 2nd Ed. ed.; Books, U. S., Ed. 1999.
(181) C. H. Schiesser, L. M. W. *Tetrahedron* **1998**, *52*, 13265.
(182) Rossi, R. A.; Pierini, A. B.; Penenory, A. B. *Chem. Rev.* **2003**, *103*, 71.
(183) Weinges, K.; Schmidbauer, S. B.; Schick, H. *Chem. Berichte* **1994**, *127*, 1305.
(184) Johnston, D.; McCusker, C. M.; Procter, D. J. *Tetrahedron Lett.* **1999**, *40*, 4913.
(185) Johnston, D.; McCusker, C. F.; Muir, K.; Procter, D. J. *J. Chem. Soc.-Perkin Trans. 1* **2000**, 681.
(186) Hutton, T. K.; Muir, K.; Procter, D. J. *Org. Lett.* **2002**, *4*, 2345.
(187) Johnston, D.; Francon, N.; Edmonds, D. J.; Procter, D. J. *Org. Lett.* **2001**, *3*, 2001.
(188) Jung, M. E.; Trifunovich, I. D.; Lensen, N. *Tetrahedron Lett.* **1992**, *33*, 6719.
(189) Jung, M. E.; Kiankarimi, M. *J. Org. Chem.* **1995**, *60*, 7013.
(190) Ogura, K.; Sumitani, N.; Kayano, A.; Iguchi, H.; Fujita, M. *Chem. Lett.* **1992**, 1487.
(191) David, H.; Afonso, C.; Bonin, M.; Doisneau, G.; Guillerez, M. G.; Guibe, F. *Tetrahedron Lett.* **1999**, *40*, 8557.
(192) Bezzenine-Lafollee, S.; Guibe, F.; Villar, H.; Zriba, R. *Tetrahedron* **2004**, *60*, 6931.
(193) Villar, H.; Guibe, F.; Aroulanda, C.; Lesot, P. *Tetrahedron: Asymmetry* **2002**, *13*, 1465.
(194) Zriba, R.; Bezzenine-Lafollee, S.; Guibe, F.; Guillerez, M. G. *Synlett* **2005**, 2362.
(195) Cuerva, J. M.; Campana, A. G.; Justicia, J.; Rosales, A.; Oller-Lopez, J. L.; Robles, R.; Cardenas, D. J.; Bunuel, E.; Oltra, J. E. *Angew. Chem.-Int. Edit.* **2006**, *45*, 5522.
(196) Paradas, M.; Campana, A. G.; Jimenez, T.; Robles, R.; Oltra, J. E.; Bunuel, E.; Justicia, J.; Cardenas, D. J.; Cuerva, J. M. *J. Am. Chem. Soc.* **2010**, *132*, 12748.
(197) Barrero, A. F.; Oltra, J. E.; Cuerva, J. M.; Rosales, A. *J. Org. Chem.* **2002**, *67*, 2566.
(198) Campana, A. G.; Estevez, R. E.; Fuentes, N.; Robles, R.; Cuerva, J. M.; Bunuel, E.; Cardenas, D.; Oltra, J. E. *Org. Lett.* **2007**, *9*, 2195.
(199) Jimenez, T.; Campana, A. G.; Bazdi, B.; Paradas, M.; Arraez-Roman, D.; Segura-Carretero, A.; Fernandez-Gutierrez, A.; Oltra, J. E.; Robles, R.; Justicia, J.; Cuerva, J. M. *Eur. J. Org. Chem.* **2010**, 4288.
(200) House, H. O.; 2nd ed ed.; Benjamin, W. A., Ed. MenloPark, CA, 1972.
(201) Spiegel, D. A.; Wiberg, K. B.; Schacherer, L. N.; Medeiros, M. R.; Wood, J. L. *J. Am. Chem. Soc.* **2005**, *127*, 12513.
(202) Pozzi, D.; Scanlan, E. M.; Renaud, P. *J. Am. Chem. Soc.* **2005**, *127*, 14204.
(203) Roschenthaler, G. V.; Sauerbrey, K.; Schmutzler, R. *Chem. Ber.-Recl.* **1978**, *111*, 3105.
(204) Bartlett, P. A.; Carruthers, N. I.; Winter, B. M.; Long, K. P. *J. Org. Chem.* **1982**, *47*, 1284.
(205) Boisdon, M. T.; Barrans, J. *J. Chem. Soc.-Chem. Commun.* **1988**, 615.
(206) Bauer, S.; Marinetti, A.; Ricard, L.; Mathey, F. *Angew. Chem.-Int. Edit. Engl.* **1990**, *29*, 1166.
(207) Streubel, R.; Kusenberg, A.; Jeske, J.; Jones, P. G. *Angew. Chem.-Int. Edit. Engl.* **1995**, *33*, 2427.

(208) Streubel, R.; Ostrowski, A.; Wilkens, H.; Ruthe, F.; Jeske, J.; Jones, P. G. *Angew. Chem.-Int. Edit. Engl.* **1997**, *36*, 378.

(209) Ozbolat, A.; von Frantzius, G.; Perez, J. M.; Nieger, M.; Streubel, R. *Angew. Chem.-Int. Edit.* **2007**, *46*, 9327.

(210) Bode, M.; Schnakenburg, G.; Jones, P. G.; Streubel, R. *Organometallics* **2008**, *27*, 2664.

(211) Helten, H.; Perez, J. M.; Daniels, J.; Streubel, R. *Organometallics* **2009**, *28*, 1221.

(212) Anders Lund, M. S., Shigetaka Shimada In *Principles and Applications of ESR Spectroscopy*; Springer Dordrecht Heidelberg London New York, 2011.

(213) John A. Weil, J. R. B. In *ELECTRON PARAMAGNETIC RESONANCE*; Second Edition ed.; John Wiley & Sons, Inc., Hoboken: New Jersey, 2007.

(214) Gareth R. Eaton, S. S. E., David P. Barr, Ralph T. Weber In *Quantitative EPR*; Springer-Verlag: Wien, 2010.

(215) van Gastel, M. *Photosynth. Res.* **2009**, *102*, 367.

(216) Schweiger, A. *Angew. Chem.-Int. Edit. Engl.* **1991**, *30*, 265.

(217) In *ELECTRON PARAMAGNETIC RESONANCE A Practitioner's Toolkit*; Marina Brustolon, E. G., Ed.; John Wiley & Sons, Inc., Hoboken: New Jersey, 2009.

(218) In *High Resolution EPR*; Graeme Hanson, L. B., Ed.; Springer Dordrecht Heidelberg London New York, 2009; Vol. 28.

(219) Arroyo, C. M.; Kramer, J. H.; Leiboff, R. H.; Mergner, G. W.; Dickens, B. F.; Weglicki, W. B. *Free Radic. Biol. Med.* **1987**, *3*, 313.

(220) Tsai, P.; Elas, M.; Parasca, A. D.; Barth, E. D.; Mailer, C.; Halpern, H. J.; Rosen, G. M. *J. Chem. Soc.-Perkin Trans. 2* **2001**, 875.

(221) Clement, J. L.; Barbati, S.; Frejaville, C.; Rockenbauer, A.; Tordo, P. *J. Chem. Soc.-Perkin Trans. 2* **2001**, 1471.

(222) Reszka, K. J.; McCormick, M. L.; Buettner, G. R.; Hart, C. M.; Britigan, B. E. *Nitric Oxide-Biol. Chem.* **2006**, *15*, 133.

(223) Alvarez, M. N.; Peluffo, G.; Folkes, L.; Wardman, P.; Radi, R. *Free Radic. Biol. Med.* **2007**, *43*, 1523.

(224) Samuni, A.; Krishna, C. M.; Riesz, P.; Finkelstein, E.; Russo, A. *Free Radic. Biol. Med.* **1989**, *6*, 141.

(225) Migita, C. T.; Migita, K. *Chem. Lett.* **2003**, *32*, 466.

(226) Zhao, H. T.; Joseph, J.; Zhang, H.; Karoui, H.; Kalyanaraman, B. *Free Radic. Biol. Med.* **2001**, *31*, 599.

(227) Abragam, A.; Pryce, M. H. L. *Proceedings of the Royal Society of London Series a-Mathematical and Physical Sciences* **1951**, *205*, 135.

(228) Slichter, C. P. In *Principles of magnetic resonance*; 3rd. edn. ed.; Springer: Berlin, 1996.

(229) Schweiger, A. *Appl. Magn. Reson.* **1993**, *5*, 229.

(230) Hahn, E. L. *Physical Review* **1950**, *80*, 580.

(231) Blume, R. J. *Physical Review* **1958**, *109*, 1867.

(232) Feher, G. *Physical Review* **1956**, *103*, 834.

(233) Davies, E. R. *Phys. Lett. A* **1974**, *A 47*, 1.

(234) Gemperle, C.; Schweiger, A. *Chem. Rev.* **1991**, *91*, 1481.

(235) Schweiger, A. *J. Chem. Soc.-Faraday Trans.* **1995**, *91*, 177.

(236) Mims, W. B. *Physical Review B-Solid State* **1972**, *5*, 2409.

(237) Schweiger, A.; Stoll, S.; Calle, C.; Mitrikas, G. *J. Magn. Reson.* **2005**, *177*, 93.

(238) Hofer, P.; Grupp, A.; Nebenfuhr, H.; Mehring, M. *Chem. Phys. Lett.* **1986**, *132*, 279.

(239) Vinck, E.; Van Doorslaer, S. *Phys. Chem. Chem. Phys.* **2004**, *6*, 5324.

(240) Hofer, P. *J. Magn. Reson. Ser. A* **1994**, *111*, 77.

(241) Liesum, L.; Schweiger, A. *J. Chem. Phys.* **2001**, *114*, 9478.

(242) Jeschke, G.; Rakhmatullin, R.; Schweiger, A. *J. Magn. Reson.* **1998**, *131*, 261.
(243) Jeschke, G.; Schweiger, A. *Mol. Phys.* **1996**, *88*, 355.
(244) Jeschke, G.; Schweiger, A. *J. Chem. Phys.* **1996**, *105*, 2199.
(245) Hohenberg, P.; Kohn, W. *Phys. Rev. B* **1964**, *136*, B864.
(246) Kohn, W.; Sham, L. J. *Physical Review* **1965**, *140*, A1133.
(247) Yang, R. G. P. a. W.; Oxford Universty Press: New York, 1988.
(248) Sprik, M.; Hutter, J.; Parrinello, M. *J. Chem. Phys.* **1996**, *105*, 1142.
(249) Perdew, J. P.; Zunger, A. *Phys. Rev. B* **1981**, *23*, 5048.
(250) Perdew, J. P.; Yue, W. *Phys. Rev. B* **1986**, *33*, 8800.
(251) Becke, A. D. *Phys. Rev. A* **1988**, *38*, 3098.
(252) Becke, A. D. *J. Chem. Phys.* **1992**, *97*, 9173.
(253) C. Lee, W. Y. u. R. G. P. *Phys. Rev. B.* **1988**, *37*, 785.